

**TARGETING AKT/MTOR PATHWAY IN ORDER TO SENSITISE RECTAL  
TUMOUR CELLS TO IRRADIATION USING PATIENT DERIVED  
ORGANOIDS AS A MODEL**

by

**AGATA ANNA STODOLNA**



**UNIVERSITY OF  
BIRMINGHAM**

**A thesis submitted to the University of Birmingham for the degree of  
DOCTOR OF PHILOSOPHY**

Institute of Cancer and Genomic Sciences

Birmingham Medical School

College of Medical and Dental Sciences

University of Birmingham

January 2022

UNIVERSITY OF  
BIRMINGHAM

**University of Birmingham Research Archive**

**e-theses repository**

This unpublished thesis/dissertation is copyright of the author and/or third parties. The intellectual property rights of the author or third parties in respect of this work are as defined by The Copyright Designs and Patents Act 1988 or as modified by any successor legislation.

Any use made of information contained in this thesis/dissertation must be in accordance with that legislation and must be properly acknowledged. Further distribution or reproduction in any format is prohibited without the permission of the copyright holder.

## ABSTRACT

Treatment resistance is one of the key contributors to low overall survival rates in Colorectal cancer (CRC) patients. Although both resistance to chemotherapy and radiotherapy is observed in CRC patients, radioresistance of rectal cancer patients is a major issue in the clinic. 40% of patients with rectal cancer that receive neo-adjuvant radiotherapy will have no significant response to treatment, whereas only 10% of patients will have a complete pathological response (pathCR) to treatment. In order to understand pathCR radiosensitivity markers need to be defined. Studying radiotherapy with current models has been challenging due to the nature of the available models and their limitations to recapitulate the patients' tumour biology. The emerging new 3 dimensional (3D) organoid models show promise in regards to the modelling of cancer and patients' response with in vitro experiments that will be able to recapitulate tumour microenvironment. The aim of this study was to establish an organoid model for studying irradiation in rectal cancer patients and to identify radiosensitivity and radioresistance drivers in order to understand and tackle the problem of resistance to radiotherapy in clinical patients. Organoid lines were established and characterised for pathological and molecular features. The organoids were subjected to short-course radiotherapy (25Gy dose delivered in 5 fractions over the course of 5 days) and the response to the treatment was measured. Furthermore, the changes caused by the irradiation were investigated by performing whole genome sequencing, DNA methylation arrays, total RNA

sequencing, and single-cell sequencing on irradiated and control organoids. Lastly, combination drug and radiotherapy assays were performed using organoids with mTOR and Akt inhibitors in order to sensitise cells to irradiation. The results revealed that irradiation causes changes on a genome-wide scale and disrupts the mTOR/PIK3CA signalling pathway. Combination therapy showed that Rapamycin is not effective in sensitising cells to irradiation, whereas AZD2014 was able to sensitise certain organoid lines to irradiation; the same was found to be the case for MK-2206. In conclusion, the results showed organoids pose as representative models for modelling radiotherapy response, and that blocking mTOR via dual inhibition of mTORC1 and mTORC2 as well as inhibition of Akt can sensitise cells to irradiation. Finally it was found that, in order to sensitise resistant lines, the dual inhibition of mTOR/Akt might be required.

## DEDICATION

I dedicate this thesis to my daughter, Sophie, who has been my inspiration and motivation.

## ACKNOWLEDGEMENTS

I would like to acknowledge and thank all the people that contributed to this thesis, either directly or indirectly. For their help and support, I am beyond grateful.

First and foremost, I would like to thank my supervisors Professor Andrew Beggs and Professor Jean-Baptiste Cazier for guiding and supporting me throughout my PhD, as well as Cancer Research UK for providing the funding that made this all possible. I would like to thank every member of the Beggs lab for their support, with special acknowledgements to Mohammed Elasrag for helping me with Whole Genome Sequencing analysis, as well as Oliver Pickles, Joao Silva, Joanne Stockdon, Louise Tee, Kasun Wanigasooriya, Celina Whalley, and Rachel Wheat. I would also like to express my appreciation to Dr Regina Andrijes that has helped greatly with establishing the organoid culture in our laboratory.

I am extremely grateful to the Centre for Computational Biology, University of Birmingham, for supporting me with data analysis tasks, and in particular I would like to thank Grigorios Papatzikas, who performed the RNA sequencing analysis presented in this thesis.

I would also like to thank Professor Christopher Yau for helping me with the single-cell data analysis presented in this thesis.

I would like to thank all of my dear friends that supported me through the last few years, with special thanks to Sam Benkwitz-Bedford.

Finally, I would like to thank my beloved husband that stood by me and supported me throughout all these years.

## TABLE OF CONTENTS

1.	INTRODUCTION.....	1
1.1.	Colorectal Cancer Overview.....	1
1.2.	Colorectal cancer classification.....	2
1.3.	Molecular genetics of colorectal cancer.....	6
1.3.1.	The Adenoma-Carcinoma sequence.....	7
1.3.2.	Adenomatous polyposis coli (APC).....	9
1.3.3.	K-ras (KRAS).....	13
1.3.4.	TP53.....	14
1.3.5.	TGF- $\beta$ signalling pathway and SMAD4/2.....	15
1.3.6.	Phosphoinositide 3-kinases (PI3Ks) and <i>PIK3CA</i> .....	18
1.3.7.	Mammalian Target of Rapamycin (mTOR).....	20
1.3.8.	F-box and WD repeat domain-containing 7 ( <i>FBXW7</i> ).....	22
1.4.	Epigenetics of CRC.....	23
1.4.1.	Aberrant methylation in CRC.....	24
1.4.2.	CpG Island methylator phenotype.....	26
1.5.	Colorectal cancer treatment.....	27
1.6.	DNA damage repair (DDR).....	33
1.7.	Treatment resistance.....	36
1.8.	Models to study colorectal cancer.....	39
1.8.1.	Cancer cell lines.....	40
1.8.2.	Murine patient derived xenograft models.....	42
1.8.3.	Organoids.....	43
1.9.	Rationale.....	50
2.	MATERIALS AND METHODS.....	53
2.1.	Ethical approval and patient recruitment.....	53
2.2.	Cell culture.....	53

2.2.1.	Cell culture reagents.....	53
2.2.2.	Culturing and passaging.....	54
2.2.3.	Conditioned media for organoid culture.....	55
2.3.	Organoid culture.....	57
2.3.1.	Organoid culture reagents.....	57
2.3.2.	Organoid derivation and maintenance.....	60
2.3.3.	Organoid Assays.....	63
2.4.	Haematoxylin and Eosin (H&E) staining.....	72
2.5.	Immunohistochemistry (IHC).....	73
2.6.	Light microscopy.....	74
2.7.	Nucleic acid extraction.....	75
2.7.1.	Sample disruption and homogenisation.....	75
2.7.2.	Nucleic acid extraction.....	75
2.8.	Nucleic acid quantification and quality control.....	76
2.8.1.	2.6.1 Qubit™.....	76
2.8.2.	TapeStation.....	77
2.9.	Sequencing.....	77
2.9.1.	DNA Sequencing.....	78
2.9.2.	RNA Sequencing.....	85
2.9.3.	Chromium single cell 3' sequencing.....	89
2.10.	Methylation array.....	96
2.10.1.	Bisulfite DNA conversion.....	97
2.10.2.	450k Arrays.....	98
2.11.	Data analysis.....	100
2.11.1.	Panel Sequencing.....	100
2.11.2.	Whole Genome Sequencing.....	101
2.11.3.	RNA Sequencing.....	101
2.11.4.	Single-cell sequencing.....	103
2.11.5.	Methylation array.....	103
2.12.	Protein analysis.....	104
2.12.1.	Protein extraction.....	104

2.12.2.	Protein quantification .....	105
3.	RESULTS CHAPTER 1: METHOD DEVELOPMENT – ESTABLISHING HUMAN COLORECTAL ORGANOID CULTURES .....	106
3.1.	Introduction.....	106
3.2.	Aims and Methods.....	107
3.2.1.	Patient recruitment.....	108
3.2.2.	Method outline .....	108
3.3.	Results .....	110
3.3.1.	Protocol modifications: sample collection and initial washing .....	110
3.3.2.	Sample dissociation.....	111
3.3.3.	Culturing Media.....	115
3.3.4.	Normal tissue – trouble shooting .....	116
3.3.5.	Passaging.....	118
3.3.6.	Freezing.....	120
3.3.7.	Matrigel.....	121
3.4.	Protocol summary.....	121
3.5.	Discussion .....	124
4.	RESULTS CHAPTER 2: CHARACTERISATION OF ESTABLISHED ORGANOID LINES FOR MODELLING IRRADIATION RESPONSE .....	127
4.1.	Introduction.....	127
4.2.	Aims and methods.....	130
4.3.	Results .....	131
4.3.1.	Establishing lines for the disease modelling .....	131
4.3.2.	Characterisation of organoid lines .....	134
4.3.3.	Mutational profile .....	142
4.3.4.	Irradiating organoids.....	146
4.3.5.	Measuring organoids’ viability after irradiation treatment.....	150
4.4.	Discussion .....	153
4.4.1.	Organoid pathology .....	153

4.4.2.	Genomic characterisation of organoids .....	155
4.4.3.	Organoid irradiation .....	157
4.5.	Conclusions .....	159
5.	RESULTS CHAPTER 3: EFFECTS OF IRRADIATION TREATMENT ON COLORECTAL ORGANIDS AND THEIR GENOMICS .....	160
5.1.	Introduction.....	160
5.2.	Aims and Methods.....	164
5.3.	Results .....	167
5.3.1.	Irradiation response .....	167
5.3.2.	Whole genome sequencing .....	172
5.3.3.	Methylation array results.....	175
5.3.4.	Total RNA Sequencing .....	179
5.4.	Single-cell sequencing.....	197
5.4.1.	Short term effects of irradiation.....	197
5.4.2.	Long term effects of irradiation .....	199
5.5.	Discussion .....	201
5.5.1.	Irradiation response .....	201
5.5.2.	Irradiation causes changes to DNA .....	203
5.5.3.	Short-course radiotherapy causes cell cycle arrest .....	204
5.5.4.	<i>PI3K</i> genes are upregulated in patients that do not respond to radiotherapy .....	205
5.5.5.	Irradiated organoids overexpress <i>SMAD7</i> .....	206
5.5.6.	Single-cell sequencing reveals mTOR as potential driver of radioresistance.....	208
5.6.	Conclusions.....	209
6.	RESULTS CHAPTER 4: SENSITISING CELLS TO IRRADIATION WITH MTOR AND AKT INHIBITORS .....	210
6.1.	Introduction.....	210
6.2.	Aims and methods.....	211

6.3.	Results .....	212
6.3.1.	Targeting mTOR .....	212
6.3.2.	Targeting Akt .....	226
6.4.	Discussion .....	229
6.4.1.	Inhibition of mTORC1 is not sufficient to sensitise cells to irradiation 230	
6.4.2.	Dual inhibition of mTORC1 and mTORC2 results in partial sensitisation of cells to irradiation.....	232
6.4.3.	Inhibition of Akt partially sensitises cells to irradiation .....	234
6.5.	Conclusions.....	235
7.	DISCUSSION AND CONCLUSIONS .....	236
7.1.	Organoids pose as a good model for studying irradiation and modelling patients' response to treatment.....	236
7.2.	mTOR/Akt pathway plays a key role in driving radioresistance ...	237
7.3.	Radiosensitivity markers.....	238
7.4.	Study limitations .....	239
7.5.	Future direction.....	240
7.6.	Final Conclusions .....	241
8.	BIBLIOGRAPHY .....	243
9.	APPENDIX A .....	I
10.	APPENDIX B .....	I
11.	APPENDIX C .....	I
12.	APPENDIX D .....	I
13.	APPENDIX E .....	I

## LIST OF ILLUSTRATIONS

Figure 1.1 - Identification of consensus subtypes. ....	4
Figure 1.2 - The Adenoma-Carcinoma Sequence.....	8
Figure 1.3 - Wnt signalling. ....	11
Figure 1.4 - APC gene schematic and distribution of mutation hotspots. ....	13
Figure 1.5 - TGF- $\beta$ signalling. ....	16
Figure 1.6 - mTOR downstream and upstream effectors. ....	22
Figure 1.7 - Methylation at CpG islands.....	25
Figure 1.8 - Colorectal cancer stages. ....	28
Figure 1.9 - Tumour control probability and normal tissue complication probability curves. ....	33
Figure 1.10 - DNA damage repair pathways.....	34
Figure 1.11 - Organoid derivation processes and culturing niche factors.....	46
Figure 1.12 - Organoids applications in basic and translational research. ....	49
Figure 2.1 - Experimental plate layout for drug assays. ....	68
Figure 2.2 - Luciferase reaction.....	69
Figure 2.3 - The Principal for the 10x Chromium Single Cell Sequencing.....	90
Figure 2.4 - 450k methylation array chemistry. ....	97
Figure 3.1 - Outline of the protocol for organoids derivation. ....	109
Figure 3.2 - Visual crypt inspection post digestion. ....	113
Figure 3.3 - Castro-Viejo surgical scissors fragmentation. ....	115
Figure 3.4 - Organoids at different stages of culture. ....	118

Figure 3.5 - Mechanical disruption. ....	119
Figure 3.6 - Organoids derivation steps. ....	123
Figure 4.1 - Summary of murine based pre-clinical models for studying tumour and normal tissue response to irradiation used in radiobiology research.....	128
Figure 4.2 - H&E staining of original tumour tissue sections. ....	136
Figure 4.3 - Immunohistochemistry of original tumour sections. ....	137
Figure 4.4 - Organoid lines' morphology. ....	139
Figure 4.5 - Immunohistochemistry stains of organoids. ....	141
Figure 4.6 - The results of the panel sequencing. ....	143
Figure 4.7 - Organoids ready for the irradiation experiment.....	147
Figure 4.8 - Schematic of irradiation delivery with IBL 437C irradiator.....	148
Figure 4.9 - Irradiation method schematic.....	150
Figure 4.10 - Irradiation effect on organoid lines. ....	151
Figure 4.11 - Irradiation response. ....	153
Figure 5.1 - Experimental plan schematic. ....	165
Figure 5.2 - Organoid response to irradiation.....	168
Figure 5.3 - Organoid irradiation response.....	170
Figure 5.4 - Copy number variations (CNVs) scatter plot for irradiated samples. ....	172
Figure 5.5 - Heatmap representing significant differentially methylated genes between irradiated and control organoids. ....	177
Figure 5.6 - Heatmap representing methylation across all samples.....	178
Figure 5.7 - PCA plot for retrospective RNASeq data. ....	181
Figure 5.8 - Overlap of significant pathways. ....	183

Figure 5.9 - Visual representation of differentially expressed genes in the top 5 significantly enriched pathways.....	185
Figure 5.10 - Visual representation of differentially significant genes for remaining pathways.....	187
Figure 5.11 - Differential expression comparison for individual genes from the mTOR pathway. ....	188
Figure 5.12 - Differential expression comparison for the remaining individual genes from mTOR pathway. ....	189
Figure 5.13 - Gene Set Enrichment Analysis and enrichment scored. ....	190
Figure 5.14 - mTOR signalling pathway in responders vs. non-responders....	191
Figure 5.15 - Principal Component Analysis plot for organoid RNASeq data..	192
Figure 5.16 - Differentially expressed gene in Colon Cancer Pathway. ....	193
Figure 5.17 - Differential expression of irradiated and control organoids. ....	196
Figure 5.18 - t-SNE plots of single-cell sequencing data for short-term irradiation effects exploration.....	198
Figure 5.19 - UMAP representing difference in cell populations between control and irradiated organoid cells. ....	200
Figure 5.20 - Differential Pathway Analysis results for S292064IRR organoid line. ....	201
Figure 6.1 - Comparison of chemotherapy with combination therapy on organoids. ....	214
Figure 6.2 - Everolimus and Rapamycin kill curves.....	216
Figure 6.3 - Approach comparison of sensitising cells to irradiation with Rapamycin.....	219
Figure 6.4 - Sensitising cells to irradiation with Rapamycin and Everolimus...	221
Figure 6.5 - AZD2014 Kill curve. ....	223
Figure 6.6 - Sensitising cells to irradiation with AZD2014. ....	225

Figure 6.7 - MK-2206 Kill curve.....	227
Figure 6.8 - Sensitising cells to irradiation with MK-2206.....	229

## LIST OF TABLES

Table 1.1 - The CMS Classification.....	5
Table 1.2 - CRIS types and their functional and phenotypic characteristics.....	6
Table 2.1 - Lab Made Organoid Culture Media A.....	58
Table 2.2 - Lab Made Organoid Culture Media B.....	59
Table 2.3 - List of therapeutic agents and their targets. ....	66
Table 2.4 - Concentrations for Rapamycin and Everolimus. ....	67
Table 2.5 - Concentrations for AZD2014 and MK-2206. ....	67
Table 2.6 - List of genes for the targeted panel sequencing. ....	79
Table 2.7 - Fragmentation, end-repair and A-tailing program. ....	80
Table 2.8 - Target enrichment program.....	81
Table 2.9 - PCR amplification program. ....	83
Table 2.10 - cDNA synthesis program. ....	86
Table 2.11 - Adapter ligation program.....	87
Table 2.12 - PCR amplification program. ....	88
Table 2.13 - Samples viability and cell counts.....	91
Table 2.14 - Post GEM barcoding incubation.....	92
Table 2.15 - cDNA library construction program. ....	93
Table 2.16 - Fragmentation, end repair and A-tailing program.....	94
Table 2.17 - Indexing program. ....	95
Table 4.1 - Summary of patients' tumour information.....	133

Table 5.1 - Summarised irradiation response information for organoids. ....	171
Table 5.2 - Top 10 SNVs in irradiated organoids. ....	174
Table 5.3 - Highlighted SNVs. ....	174
Table 5.4 - List of all significant differentially methylated regions in treated and control organoids. ....	176
Table 5.5 - GSEA for differentially methylated regions in irradiated organoids. ....	179
Table 5.6 - List of top 10 enriched pathways. ....	181
Table 5.7 - Selected differentially expressed genes. ....	184
Table 5.8 - List of genes upregulated in irradiated organoids. ....	194
Table 5.9 - List of genes upregulated in control organoids. ....	195
Table 5.10 - Top 10 enriched pathways for organoid RNA experiment. ....	197

## LIST OF DEFINITIONS/ABBREVIATIONS

2D	-	Two Dimensional
3D	-	Three Dimensional
APC	-	Adenomatous Polyposis Coli
ASCs	-	Adult Stem Cells
ATP	-	Adenosine Triphosphate
cDNA	-	Complementary DNA
CIMP	-	CpG Island Methylatorphenotype
CIN	-	Chromosomal Instability
CMS	-	Consensus on Molecular Subtypes of colorectal cancer
CNVs	-	Copy Number Variations
CRC	-	Colorectal Cancer
CRIS	-	Colorectal Cancer Intrinsic Subtypes
CSCs	-	Cancer Stem Cells
DDR	-	DNA Damage Repair

DMEM	-	Dullbecco's Modified Eagle Medium
dMMR	-	Deficient MMR
DMSO	-	Dimethyl Sulfoxide
DNA	-	Deoxyribonucleic Acid
ECM	-	Extracellular Matrix
EDTA	-	Ethylenediaminetetraacetic Acid
EGFR	-	Epidermal Growth Factor
EMT	-	Epithelial-Mesenchymal Transition
FAP	-	Familial Adenomatous Polyposis
FBS	-	Foetal Bovine Serum
FBXW7	-	F-Box and WD repeat domain-containing 7
FFPE	-	Formalin Fixed Paraffin Embedded
GDB	-	Gentle Dissociation Buffer
GSEA	-	Gene Set Enrichment Analysis
GTP	-	Guanosine Triphosphate
H&E	-	Haematoxylin and Eosin

HPTM	-	Histone Post-translational Modification
IHC	-	Immunohistochemistry
LOH	-	Loss of Heterozygosity
MCR	-	Mutation Cluster Region
MMR	-	Mismatch Repair
MSI	-	Microsatellite Instability
MSS	-	Microsatellite Stable
mTOR	-	Mammalian Target of Rapamycin
mTORC	-	Mammalian Target of Rapamycin Complex
NGS	-	Next Generation Sequencing
OHS	-	Organoid Harvesting Solution
PBS	-	Phosphate Buffered Saline
PCA	-	Principal Component Analysis
PCR	-	Polymerase Chain Reaction
PDTX	-	Patient Derived Tumour Xenograft
PGE2	-	Prostaglandin E2

PI3K	-	Phosphoinositide 3-Kinase
pMMR	-	Proficient MMR
PSCs	-	Pluripotent Stem Cells
RNA	-	Ribonucleic Acid
SNVs	-	Single Nucleotide Variants
TME	-	Total Mesorectal Excision
TNM	-	Tumour Node-metastases
TRG	-	Tumour Regression Grade
TRS	-	Tumour Regression Score
TSG	-	Tumour Suppressor Gene
WGS	-	Whole Genome Sequencing

# 1. INTRODUCTION

## 1.1. Colorectal Cancer Overview

Colorectal cancer (CRC) is a major cause of cancer morbidity and mortality, with second highest cancer mortality rates across the world (Fearon, 2011, WHO, 2022). Additionally, it is the 3<sup>th</sup> most common type of cancer worldwide with around 1.93 million cases reported in 2020 (WHO, 2022). In United Kingdom alone it is estimated that around 42 000 people get diagnosed with CRC each year (Cancer Research UK, 2019). The causes of CRC have been studied in great detail and several lifestyle choices have been identified as risk factors contributing to the disease onset, such as diet rich in unsaturated fats, high alcohol consumption, smoking, and reduced physical activity (Kuipers et al. 2015). Moreover, along with the described risk factors, inherited genetic lesions and somatic mutations also play a crucial role as contributory agents (Fearon, 2011). Whereas many risk factors have been linked to CRC, also, there have been agents described to protect against CRC. As an example, some non-steroidal anti-inflammatory drugs including aspirin have been shown to have significant anti-carcinogenic effects in the gastrointestinal tract (Baron and Sandler, 2000). Oestrogen, calcium, and some statins have been shown to produce similar results (Poynter et al. 2005, Fearon, 2011).

## **1.2. Colorectal cancer classification**

Colorectal cancer can be categorised differently depending on different types of classification. Histologically, CRC classifies into three major subtypes: intestinal type adenocarcinoma, mucinous adenocarcinoma and signet-ring cell carcinoma. For many years the CRC classification was mainly based on microscopic morphology and clinical management of the disease proceeded based on acknowledging tumour as a homogenous (Jass, 2007). However, CRC is a complex disease and the heterogeneity of tumours presents itself both between patients but also inside the tumour itself (Molinari et al. 2018). Patients diagnosed with it can have a very different clinical course and response to treatment despite the tumours having similar histopathological features. The highly dynamic nature of the malignant cells and evolutionary pressure has resulted in gradual preference towards molecular characterisation over the classical pathological approach for the classification of colorectal cancer (Blanco-Calvo et al. 2015). It is known that mutations in colorectal cancer can be attributed by genomic instability, and three different profiles have been described: chromosomal instability (CIN), microsatellite instability (MSI) and CpG island methylator phenotype (CIMP) (The Cancer Genome Atlas Network, 2012). CIN is distinguished by changes in structure and number of chromosomes. This demonstrates itself as variations in chromosome numbers within cells from individual clones. CIN phenotype is a result of accelerated rate of gains and losses of chromosome parts (or whole). It is estimated that between 65% and 70% of sporadic colorectal tumours can be classified as CIN (Pino and Chung,

2010). On the other hand, tumours with MSI account for only 15% of sporadic CRC tumours. Microsatellites are a short tandem repeat sequences that can be found across the human genome. Due to their repetitive nature, these repeats are prone to replication errors, which can be repaired by the DNA mismatch repair (MMR) mechanism. Patients with defective MMR, classed as MMR deficient (dMMR), present with MSI phenotype. MSI can be furthered classified to high (MSI-H) and low (MSI-L), there is also a classification for microsatellite stable (MSS), which is also relates to proficient MMR (pMRR). MSI in sporadic patients have been linked to better prognosis in comparison to MSS tumours (Samowitz et al. 2001). Loss of function mutations of MMR pathway genes (MSH1, MSH2, MSH6, PMS2) results in the MSI phenotype in colorectal cancer patients. The mutations need to occur in both alleles to result in gene failure, and the germ-line mutations in MMR genes are common and have been linked to the hereditary disease – Lynch syndrome. 90% of patients that have developed colorectal cancer from being diagnosed before with lynch syndrome display a MSI phenotype. Additionally to MMR gene mutations, MSI in patients with sporadic CRC is often a result of epigenetic inactivation of the MLH1 gene (Kawakami, Zaanani and Sinicrope, 2015).

As methylation-caused silencing of mismatch repair genes, CIMP and MSI tend to appear together. Tumours are characterised on the basis of the genomic instability profile they are expressing. Despite identifying the different CRC tumour profiles, it has not been found to be reflective of the true tumour subtype, and the need of the more complex and thorough classification system has grown.

Therefore, The CRC Subtyping Consortium (CRCSC) was formed in order to create a framework that identified intrinsic subtypes of colorectal cancer. The CRCSC published their results in 2015 where they describe the consensus on molecular subtypes of colorectal cancer (CMS). In their framework four different subtypes were identified: CMS1, CMS2, CMS3 and CMS4 (Figure 1.1; Guinney et al. 2015).

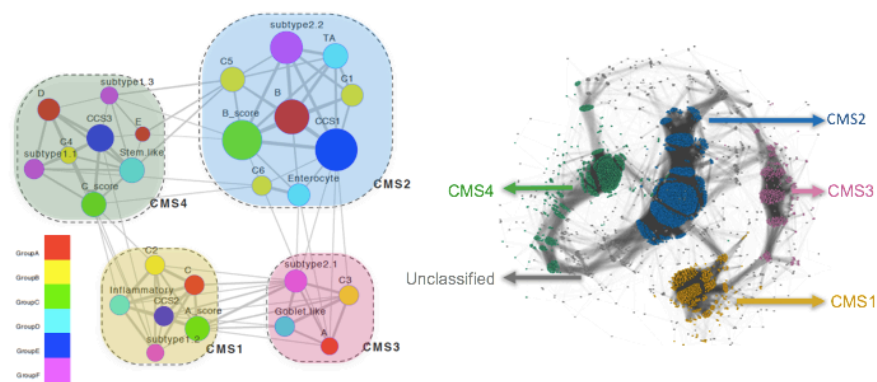


Figure 1.1 - Identification of consensus subtypes.

Graph on the right: Identified subtypes through 6 systems (each colour belongs to a different system/group), circled are consensus subtypes.

Graph on the left: Representation of each patient investigated by nodules. Nodules clustered in the consensus subtypes are colour-coded. Grey nodules are non-consensus patients.

(Figure adapted from Guinney et al. 2015).

Each of the consensus subtypes has been associated with individual characteristics and associated genes (Table 1.1). In addition, Guinney et al. (2015) identified an association between CMS groups and clinical variables. Tumours with CMS1 were found to be in females with right-sided lesions and present with a higher histopathological grade. On the other tumours the mainly

left-sided lesions were associated with CMS2 group. Finally, the CMS4 group characterised with tumours diagnosed at advanced stages (III and IV). Thus the CMS4-diagnosed patients have the worse overall and relapse-free survival rate. The best overall survival rate has been associated with CMS2, whereas CMS1 and CMS3 have intermediate survival rates (Guinney et al. 2015).

Table 1.1 - The CMS Classification

CMS1 (MSI Immune)	14%	MSI, high in CIMP, hypermutated profile BRAF mutation Immune infiltration and activation
CMS2	37%	High in somatic copy number alterations WNT and MYC activation
CMS3	13%	Mixed MSI status, low somatic copy number alterations, low in CIMP KRAS mutations metabolic deregulation
CMS4	23%	High in somatic copy number alterations Stromal infiltration, TGF- $\beta$ activation, angiogenesis

One of the disadvantages of the CMS classification system is the fact that genes characterising CMS4 have stromal origin, correlated with cancer-associated fibroblasts – a strong indicator of aggressive tumours (Calon et al. 2015; Isella et al. 2015). With such a strong signature from tumour stromal cells, it is speculated that more subtle gene signatures expressed by the cancer cells can be masked. For this reason, another molecular classification system has been developed – Colorectal Cancer Intrinsic Subtypes (CRIS). Using a large population of Patient-

Derived Xenograft (PDX) mouse models (515 samples from 244 patients) Isella et al. (2017) distinguished 5 colorectal cancer subtypes (CRIS-A, CRIS-B, CRIS-C, CRIS-D, and CRIS-E) that in addition to CMS classification gives a deeper analytical resolution to colorectal cancer classification. The summary of the CRIS profiles and individual characteristics are summarised in Table 1.2. CRIS can be used independently to predict the prognosis, especially CRIS-B has showed to have very poor prognosis. Finally, the authors showed that CRIS classification can predict response to certain therapeutic agents (Isella et al. 2017).

Table 1.2 - CRIS types and their functional and phenotypic characteristics

Classification type	Classification type characteristic
CRIS-A	Glycolytic and mucinous, enriched for MSI or KRAS mutations, BRAF mutated
CRIS-B	Associated with poor prognosis, increased TGF- $\beta$ pathway activity
CRIS-C	Elevated EGFR signalling; sensitive to EGFR inhibitors
CRIS-D	IGF2 gene overexpression and amplification, Wnt activation
CRIS-E	Rich in TP53 mutations, Paneth cell-like phenotype

### 1.3. Molecular genetics of colorectal cancer

As mentioned in Section 1.1, different agents contribute towards the initiation of colorectal cancer. Apart from lifestyle choices, a small group (5-10%) of CRC have tumours with a hereditary component (Kuipers et al. 2015). A few hereditary syndromes are known to lead to colorectal cancer, with the two most common syndromes being Familial Adenomatous Polyposis (FAP) and Hereditary Non-

polyposis Colorectal Cancer (HNPCC), also called Lynch syndrome (Lynch and Chapelle, 2003; Fearon, 2011). FAP is characterised with the presence of multiple adenomatous polyps (>100) and mutation in wnt signalling pathway genes, where in 90% of cases it is mutation in adenomatous polyposis coli (APC) gene (Vasen, Tomilson and Castells, 2015). HNPCC, however, present itself without extensive polyposis and with defects in genes such as MSH2, MLH1, PMS2, MSH6, and EPCAM. Mutations in these genes causes impaired mismatch repair which leads to genetic mutations, which tend to accumulate in microsatellite regions, giving rise to MSI. Other, less common, hereditary syndromes include serrated polyposis and polyposis associated with mutY DNA glycosylase (MUTYH) gene mutations (Kuipers et al. 2015). While only a small number of inherited colorectal cancers contribute to all CRC cases, they have helped greatly with understanding the events that lead to initiation of sporadic colorectal cancer and the concept adenoma-carcinoma sequence.

### **1.3.1. The Adenoma-Carcinoma sequence**

The adenoma-carcinoma sequence model suggests that the initiation of colorectal cancer occurs in a sequential manner with attributing specific genetic alterations. Wnt pathway activation initiates transformation of the normal epithelium into a small benign localised lesion termed a polyp. There are two main different types of polyps – hyperplastic and adenomatous. Although the majority of the colorectal polyps are hyperplastic, it is the latter type that is known

to be precursors of colorectal cancer. The key event of the mentioned polyp initiation is usually inactivating mutations in the *APC* gene. The polyp then becomes dysplastic with the loss of *APC* and a *KRAS* oncogene mutation results in intermediate adenoma. Further hits resulting in loss of another tumour suppressor gene (TSG), *SMAD4*, lead to late adenoma. Finally, the loss of *p53* leads to the carcinoma (Figure 1.2) (Fearon and Vogelstein, 1990; Fodde, Smits and Clevers 2001).

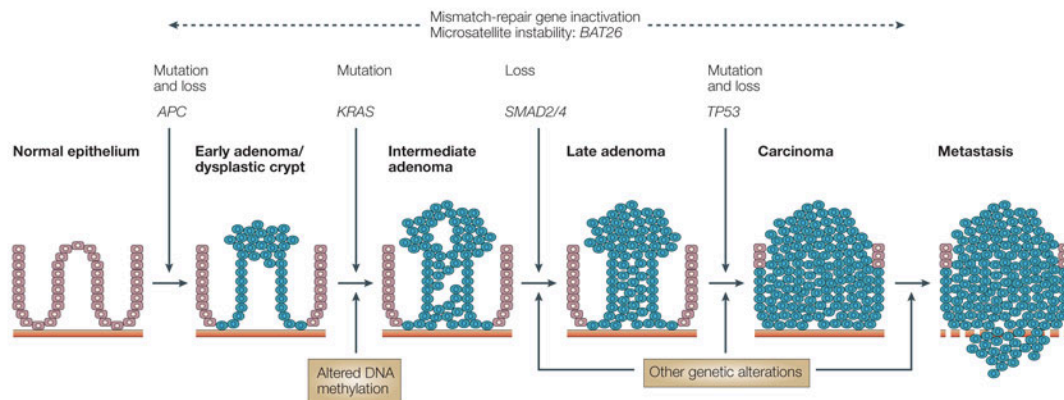


Figure 1.2 - The Adenoma-Carcinoma Sequence.

The transformation of normal epithelium into invasive carcinoma through sequential attribution of somatic mutations. Losses of tumour suppressor genes: *APC*, *SMAD2/4* and *TP53* along with mutation in oncogene *KRAS* is believed to be the main genetic events driving CRC initiation. Additionally, other genetic and epigenetic events are thought to occur and contribute to carcinogenesis.

Figure taken from Davies, Miller and Coleman (2005).

Drost et al. (2015) sequentially delivered the most frequent mutations into small intestinal organoids using the CRISPR-Cas9 method. The organoids were derived from leucine-rich repeat containing G-protein coupled receptor 5 positive (*Lgr5*<sup>+</sup>) intestinal stem cells that were recognised to be an origin of intestinal

neoplasia (Barker et al. 2009; Schepers et al. 2012). Drost et al. (2015) have shown that organoids with mutation in KRAS and loss in all APC, P53, and SMAD4 resulted in intestinal organoids with cancerous properties. Furthermore, they have investigated this *in vivo* by injecting mutated organoids (triple: KRAS<sup>G12D</sup>/APC<sup>KO</sup>/P53<sup>KO</sup>; Quadruple: KRAS<sup>G12D</sup>/APC<sup>KO</sup>/P53<sup>KO</sup> /SMAD4<sup>KO</sup>) into immunocompromised mice. They found that both triple- and quadruple-derived organoids were resulting in highly proliferative profiles, whereas the quadruple-derived organoids resulted in solid tumour masses that displayed features of invasive carcinoma.

Defining the adenoma-carcinoma sequence was very important for colorectal cancer research, as it gave insight into the molecular nature of the disease. Nevertheless, it has since then been understood that colorectal cancer has different paths of carcinogenesis and progression. The adenoma-carcinoma sequence, although seen in the majority of sporadic cancers, cannot be applied to every colorectal tumour.

### **1.3.2. Adenomatous polyposis coli (APC)**

APC belongs to a wide group of TSGs and it has been first characterised in patients with FAP. The APC gene, localised in chromosome 5q21, encodes 312 kDa protein that is involved in cell-to-cell adhesion, cell migration, apoptosis in the colonic crypts, and chromosomal segregation (Bodmer et al. 1987; Aoki and Taketo, 2007; Polakis, 2007). However, its most established role in cancer is that

APC is a negative regulator of  $\beta$ -catenin protein in  $\beta$ -catenin dependent Wnt signalling pathways (Fearon, 2011).

The glycoprotein Wnt binds to the *frizzled*, a transmembrane receptor, and the low-density lipoprotein receptor-related protein LRP5/6. This through Dishevelled protein inhibits glycogen synthase kinase 3 $\beta$  (GSK3 $\beta$ ) and Axin and as a result stabilises  $\beta$ -catenin in the cytoplasm and nucleus. When  $\beta$ -catenin enters nucleus it binds the transcription factors of the T-cell factor (TCF) and leads to gene transcription (Gao and Chen, 2009). APC can destabilise  $\beta$ -catenin and lead to its inactivation as it creates a complex with Axin and glycogen synthase kinase 3 $\beta$  (GSK3 $\beta$ ) via interactions with the 20 amino acid repeats or SAMP (Ser-Ala-Met-Pro) repeats. This complex then is able to bind with  $\beta$ -catenin. Casein kinase 1 (CK1) is also recruited to the complex and within GSK3 $\beta$  initiates phosphorylation of  $\beta$ -catenin. The phosphorylation of  $\beta$ -catenin leads to further degradation of the protein through the ubiquitin-proteasome pathway (Figure 1.3; Fodde, Smits and Clevers, 2001; Fearon, 2011).

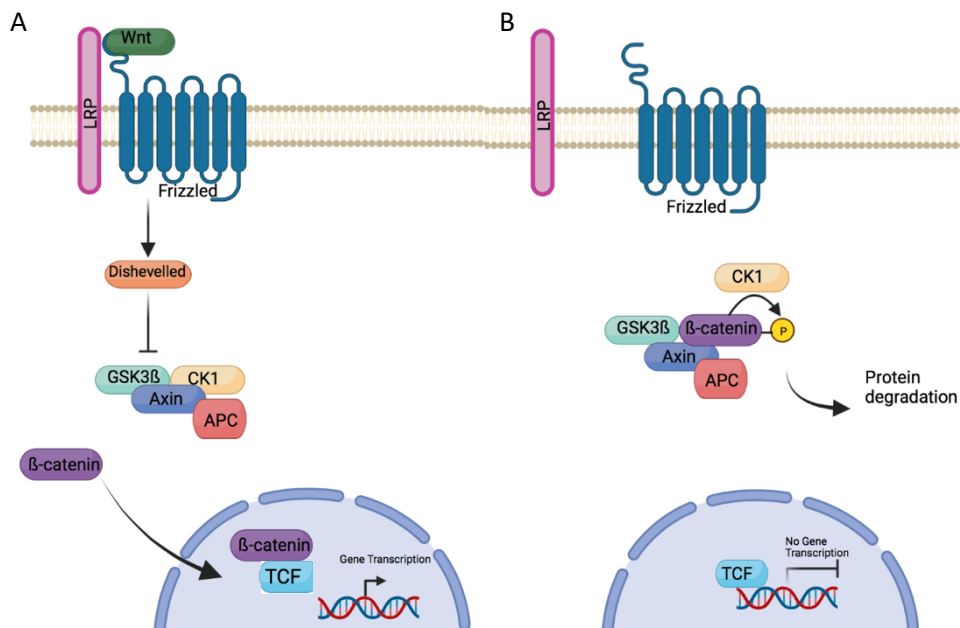


Figure 1.3 - Wnt signalling.

A) Wnt binds to Frizzled and LRP receptors which inhibits downstream complex of proteins (GSK3 $\beta$ /Axin/CK1/APC), which lets  $\beta$ -catenin enter the nucleus and bind TCF transcription factor and promote gene transcription.

B) In the absence of Wnt,  $\beta$ -catenin gets phosphorylated by the GSK3 $\beta$ /Axin/CK1/APC complex which leads to  $\beta$ -catenin degradation and subsequent switched off transcription of Wnt target genes.

Created with Biorender.com

T-cell factor 4 (TCF4) is the main transcription factor transducing  $\beta$ -catenin signals in colonic epithelium, making the Wnt signalling pathway – a major transduction pathway involved stabilising the intestinal microenvironment (Barker et al., 1999). Mutated APC cannot bind  $\beta$ -catenin, which as a result accumulates in a cell permanently stimulating the Wnt pathway. This leads to hyperproliferation in epithelium that often results in cancer.

The APC protein plays another important role in the formation of microtubules that are involved in chromosomal division. The C-terminus of the protein interacts

with the EB-1 protein, which is involved in regulation of microtubule dynamics. This interaction is thought to help APC localise to the kinetochore of metaphase chromosomes. Cells with APC mutations have been found to have accumulation of microtubules that unsuccessfully connected to kinetochores. These failed interactions between spindle microtubules and kinetochore lead to chromosomal instability (Fodde, Smits and Clever, 2001).

More than 90% of APC mutations are nonsense or frameshift mutations resulting in a truncated protein (Fearon, 2011). The germ-line APC mutations are mostly distributed in the 5' half of the gene with exception of two hot-spots at codons 1061 and 1309, whereas the somatic mutations in the APC gene are clustered in the mutation cluster region (MCR) located between codons 1281 and 1556, the region responsible for downregulation of the  $\beta$ -catenin, see Figure 1.4 (Christie et al. 2012).

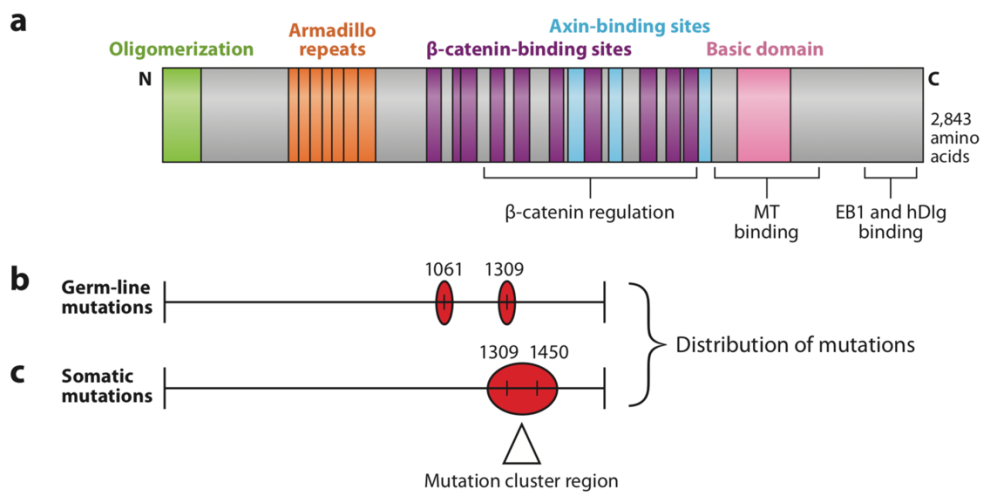


Figure 1.4 - APC gene schematic and distribution of mutation hotspots.

A) Schematic of APC gene and its domains;

B) Two mutational hotspots in germ-line mutations;

C) Mutation cluster region with highlighted two most common codons mutated caused by somatic lesions.

Taken from Fearon, 2011.

### 1.3.3. K-ras (KRAS)

There are three human *RAS* genes that play crucial role in cancer, *KRAS*, *NRAS* and *HRAS*. Genetic mutations of these genes are frequently found in different types of cancers including colorectal cancer, in which the most common Ras mutation is *KRAS* (Porru et al. 2018). *KRAS* is a gene encoding the 21kDa Ras protein that belongs to GTPases and is involved in RAS/MAPK signalling (Jancik et al. 2010). When activated, *KRAS* rapidly forms RAS-GTP complex resulting in engagement of downstream proteins that further regulate cellular pathways (Cox and Der, 2010). This protein plays a very important role in signal transduction of cell differentiation regulatory pathways. *KRAS* is located in chromosome

12p.12.1 and belongs to the oncogenes which means a single amino acid substitution can activate a mutation that contributes to carcinogenesis (Jancik et al. 2010).

Mutational hot spots of *KRAS* have been identified over the years and include glycine-12, glycine -13 and glycine-61. Mutations in these regions result in overstimulation of effectors leading to uncontrolled cell division and tumour growth (Waters and Der, 2018). Furthermore, all known *KRAS* carcinogenic mutations affect the domain responsible for GTP binding, resulting in decreased GTPase activity and constant stimulation of the Ras protein (Jiang et al. 2009). Approximately 40% of sporadic adenomas and carcinomas present themselves with an activated *KRAS* mutation. Moreover, the frequency of *KRAS* increases greatly depending on the size of the lesion. While only 10% of adenomas that are less than 1cm in size have a *KRAS* mutation, between 40 and 50% of adenomas larger than 1 cm show *KRAS* alterations (Vogelstein et al. 1988). Although *KRAS* has been found to be involved in the adenoma-carcinoma sequence and contributes to colorectal adenoma development, it is not essential for adenoma initiation (Fearon, 2011).

#### **1.3.4. TP53**

The *TP53* gene is located on the short arm of chromosome 17 and encodes the p53 protein often referred to as the “Guardian of the Genome” due to its important in regulation of cell proliferation. The p53 protein blocks cell proliferation when

DNA gets damaged and initiates apoptosis when DNA repair is not sufficient. It also plays a crucial role in restricting angiogenesis as p53 is a key transcriptional regulator of the proteins that are involved in cell cycle checkpoints G1/S and G2/M (Baker et al. 1989; Voudsen and Prives, 2009)

The main mechanism for inactivation of one allele of certain tumour suppressor genes including p53, is loss of heterozygosity (LOH), an allele imbalance resulted from the loss of the entire gene and surrounding chromosomal region. Different events can lead to LOH, such as direct deletion, mitotic recombination or even loss of an entire chromosome (Nichols et al. 2020). Thus, 70% of colorectal carcinomas show 17p LOH (Fearon, 2011). A second allele is usually inactivated by a missense mutation that occurs mainly at codons 175, 245, 248, 273, and 282 (Voudsen and Prives, 2009; Fearon, 2011). Very few carcinomas lack LOH of 17p but then present p53 mutations, whereas the majority of adenomas lack 17p LOH and p53 mutations (Baker et al. 1990). This suggests that loss of p53 through LOH and mutations is closely associated with the adenoma-carcinoma transformation.

#### **1.3.5. TGF- $\beta$ signalling pathway and SMAD4/2**

The transforming growth factor beta (TGF- $\beta$ ), encoded by *TGFB1*, is involved in cell growth, differentiation, apoptosis, and cellular homeostasis. TGF- $\beta$  binds to a type II receptor which activates trans-phosphorylates receptor I and initiates down-stream activation of receptor-associated SMAD proteins (R-SMADs) which

can then bind coSMAD – SMAD4 (Jung, Staudacher and Beauchamp, 2017). SMAD2 and SMAD3 (R-SMADs) can bind SMAD4. This complex then migrates to the nucleus (Figure 1.5) where they act as transcription factors that regulate the transcription of genes such cell-cycle checkpoint genes (p21, p27 and p15). Activation of checkpoint genes causes cell-cycle arrest, resulting in proliferation inhibition of epithelial cells (Massaguè, 2008).

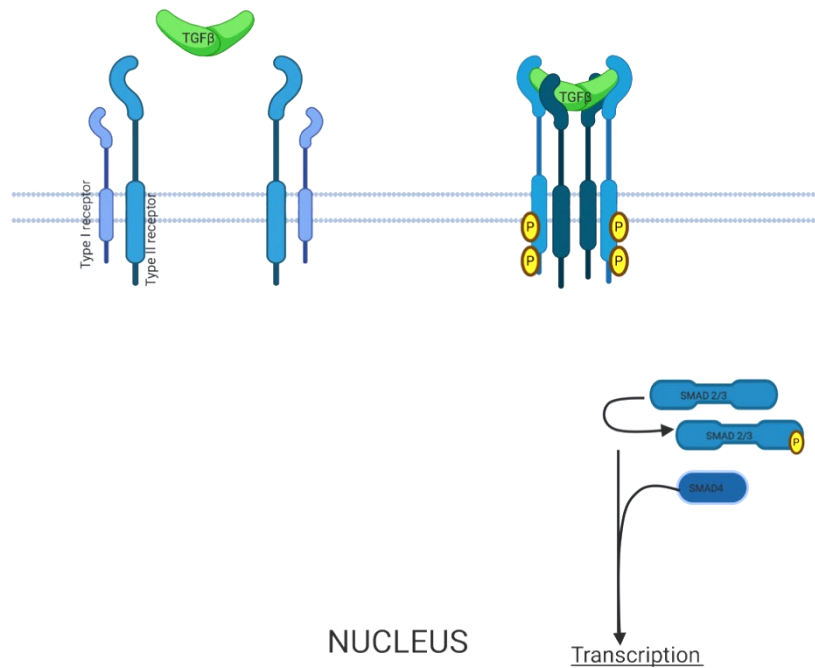


Figure 1.5 - TGF-β signalling.

TGF-β binds to TGF beta receptor type-2 (TGFB2) and promotes dimerization of TGFB2 with type 1 receptor (TGFB1). This results in transphosphorylation and activation of SMAD2 and SMAD3. With SMAD4 this leads to gene transcription which promotes cell survival and cell growth.

Created with BioRender.com

Around 70% of CRC cases present LOH of chromosome 18q, on which two tumour suppressor genes are located: *SMAD4* and *SMAD2*. These two genes are usually mutated in a group of CRCs along with LOH of 18q. Both genes act downstream of the TGF- $\beta$  receptor complex. Mutations inactivating either of the tumour suppressor genes result in regulation of cell-cycle and disruption of cellular homeostasis, leading to carcinogenesis (Nguyen and Duong, 2018).

The above description of TGF- $\beta$  explains its antioncogenic properties as a tumour suppressor gene; however, the TGF- $\beta$  can also have a role in tumour progression as pro-oncogenic. TGF- $\beta$  has been found to promote metastasis as it induces the epithelial-mesenchymal transition (EMT). It has been shown that TGF- $\beta$  along with Ras cooperate and induce the EMT, and what is more, Ras through its downstream effector pathway PI3K/Akt drives cancer cell growth by suppressing TGF- $\beta$ -induced apoptosis and proliferation arrest (Grusch et al. 2010; Saitoh et al. 2015).

TGF- $\beta$ , being bidirectional, acts as a tumour suppressor gene during early tumour development stages. During the later stages, it promotes metastasis and cancer cell invasion. Advanced tumours with high expression of TGF- $\beta$  have poor prognosis and are associated with aggressive cancer (Liu et al. 2018).

### 1.3.6. Phosphoinositide 3-kinases (PI3Ks) and *PIK3CA*

PI3Ks belong to a large family of lipid enzymes that phosphorylate phosphatidylinositols on plasma membranes and control signalling in key cellular processes such as cell survival, metabolism, and inflammation (Vanhaesebroeck et al. 2010). Enzymes from the family of PI3Ks are highly related to each other, yet they can be distinguished by substrate specificity. PI3Ks can be further divided into three different classes – I, II, and III. Class I consists of heterodimeric enzymes consisting of regulatory sub-unit and common p110 catalytic sub-unit. Class IA can be distinguished with enzymes p110 $\alpha$ , p110 $\beta$  and p110 $\delta$  sharing p85 as their regulatory subunit. Enzyme p110 $\gamma$ , however, belongs to class IB and consists of p101 and p84/p87 as its regulatory sub-units (Kaplan et al. 1987). One of the major downstream effectors of class I PI3Ks is Akt. Upon its activation Akt is phosphorylated by PDK1 on T308. This further activates the mammalian target of rapamycin complex 1 (mTORC1) and results in increased cell survival and protein synthesis. An important negative regulator of PI3K-Akt signalling is phosphatase and Tensin homolog (PTEN), a tumour suppressor with strong phosphatase activity (Martini et al. 2014). Class II consists of PI3K-C2 $\alpha$ , PI3K-C2 $\beta$  and PI3K-C2 $\gamma$  – high molecular mass monomers that are distinguished by their long N- and C-terminal domains (Falasca and Maffucci, 2012). Class III consists of only PI3K-C3, also known as vacuolar protein sorting 34 (Vps34). Classes II and III are largely involved in regulation of vesicular trafficking and are less characterised in comparison to class I (Martini et al. 2014).

Due to a strong association with pathways involved in cell survival and proliferation, it is indeed the class I of PI3Ks that has been strongly associated with cancer. Phosphatidylinositol-4,5-bisphosphate 3-kinase catalytic subunit, or p110 $\alpha$ , is encoded by the *PIK3CA* gene and it is known to be the most frequently deregulated in cancer from the PI3K family. *PIK3CA* mutations were identified across different types of cancers including CRC. Genetic lesions affecting *PIK3CA* mostly consist of missense mutations and they tend to cluster in two major hot spots: exon 9 of the helical domain at E542K and E545K, and exon 20 of the kinase domain at H1047R (Samuels et al. 2004; Martini et al. 2014). In CRC it has been found that mutations of *PIK3CA* are observed in higher frequencies on exon 9 than exon 20 (Barbi et al. 2010).

Between 15-25% of sporadic cancers have *PIK3CA* mutations and the majority result in over-activation of the Akt pathway. Several studies have shown that systematic use of aspirin after colorectal cancer diagnosis has been associated with improved clinical outcome and that there is a potential in regular aspirin use to reduce colorectal cancer incidence and morbidity (Rothwell et al. 2011; Drew, Cao and Chan, 2016;). It has been further shown that aspirin has beneficial effects on CRC patients with mutant *PIK3CA*, rather than with wild type carrying patients (Liao et al. 2012; Domingo et al. 2013; Frouws et al. 2017). Gu et al. (2017) further showed that the *PIK3CA* mutant cells treated with aspirin would decrease in viability, as opposed to wild type cells, suggesting aspirin induces cell cycle arrest which leads to apoptosis and consequently results in a reduction

of cell viability. In CRC the *PIK3CA* mutations have been shown to be more prevalent in women than in men (Benvenuti et al. 2008, Fearon, 2011).

### **1.3.7. Mammalian Target of Rapamycin (mTOR)**

Mammalian target of rapamycin (mTOR) is a large (289kDa) serine-threonine protein kinase that has been conserved through evolution. The N-terminal of mTOR consists of several different repeats that promote protein-protein interactions, whereas the C-terminal consists of a kinase domain that is related to the PI3K family. mTOR protein is a catalytic sub-unit of two functionally different protein complexes – mammalian target of rapamycin complex 1 (mTORC1) and complex 2 (mTORC2) (Liu and Sabatini, 2020). mTORC1 consists of five sub-units: mTOR, regulatory-associated protein of mTOR (Raptor), mammalian lethal with Sec13 protein 8 (mLST8), proline rich Akt substrate 40kDA (PRAS40), and DEP-domain-containing mTOR-interacting protein (Deptor). mTORC2 consists of six sub-units: mTOR, rapamycin-insensitive companion of mTOR (Rictor), mammalian stress-activated protein kinase interacting protein (mSIN1), protein observed with Rictor-1 (Protor-1), mLST8, and Deptor. The differences between the complexes result in substrate specificity and differences in downstream cell signalling (Figure 1.6 A). mTORC1 has been shown to play a key role in cell growth and proliferation through phosphorylation of p70 ribosomal s6 kinase 1 (S6K1) and eukaryotic initiation factor 4E (eIF4E) – binding protein 1 (4E-BP1) (Kim, Cook and Chen, 2017). It

promotes protein synthesis resulting in an increase in cell size and proliferation. mTORC1 also promotes other anabolic processes such as lipid synthesis and mitochondrial biosynthesis. However, mTORC1 has also been shown to decrease some catabolic processes like autophagy. The upstream activation of mTORC1 is driven by the Akt phosphorylating and inhibiting tuberous sclerosis 2 (TSC2), which then allows Ras homolog enriched in brain (Rheb) to activate mTORC1. mTORC2 regulates cell metabolism, survival and proliferation through its key substrate Akt, a positive downstream regulator of these processes. Although the upstream regulation of mTORC2 is not very clear, it is known that it responds to growth factor stimulation through PI3K pathway and ribosome association (Kim, Cook and Chen, 2017; Liu and Sabatini, 2020). Multiple upstream signals have an effect on mTOR signalling. Nutrient level, stress, energy or growth factor availability have been shown to activate both complexes through several pathways (see Figure 1.6 B)

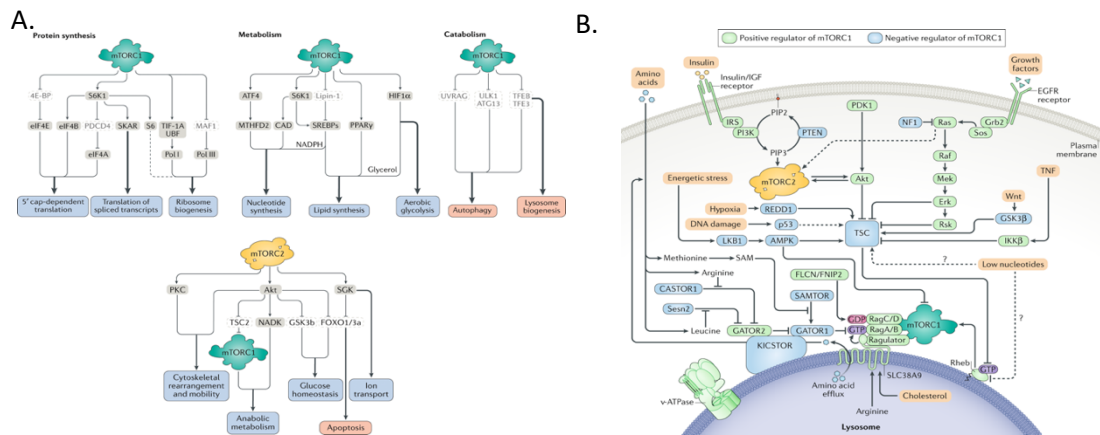


Figure 1.6 - mTOR downstream and upstream effectors.

A) A schematic of downstream signalling of both mTORC1 and mTORC2.

B) Upstream signalling of mTOR.

Figure adapted from Liu and Sabatini, 2020.

*mTOR* mutations in human cancers are rare. However, the deregulation of *mTOR* is not. This is due to activation of the pathway through upstream signalling in PI3K/Akt/mTOR pathways. More commonly the mutations of PIK3CA or another common lesion in CRC is inactivating mutation in *PTEN*, a negative regulator of PI3K, which will also lead to over-expression of *mTOR* (Kim, Cook and Chen, 2017).

### 1.3.8. F-box and WD repeat domain-containing 7 (*FBXW7*)

*FBXW7* is a tumour suppressor gene located on chromosome 4q that encodes a protein consisting of four sub-units that are involved in cell cycle regulation (Wang et al. 2012). Structurally, *FBXW7* is comprised of 40-amino acid F-box which

recruit the SKP1-Culin1-F-box (SCF) –E3 ubiquitin protein ligase complex (eight WD40 repeats responsible for binding substrates) and the D domain responsible for facilitating FBXW7 dimerization (Korphaisarn et al. 2017). SCF protein ubiquitin E3 ligase complexes negatively regulate the increased abundance of selected proteins through phosphorylation-dependent ubiquitination. Some of these proteins include cyclin E, c-Myc, c-Jun, mTOR, and NOTCH. These have all been found to play a role in cell proliferation, division, and survival (Cheng and Li, 2012; Li et al. 2015). Therefore, inactivating mutations of *FBXW7* lead to failed regulation of its targets and interfere with cellular homeostasis, which then leads to carcinogenesis (Li et al. 2015).

Studies have reported that *FBXW7* mutations occur in approximately 10-20% of CRC patients and are associated with worse overall survival (Korphaisarn et al. 2017, Tong et al. 2017). Interestingly, missense point mutations affecting substrate binding sites constitute 70% of *FBXW7* mutations (Korphaisarn et al. 2017). Furthermore, three arginine residues (R465, R479, and R505) have been identified as hotspots for the missense mutations (Tong et al. 2017).

#### **1.4. Epigenetics of CRC**

In addition to germline and somatic mutations in CRC, epigenetics plays an important role in the initiation and progression of carcinogenesis. Epigenetics refers to alterations in gene expression without changes in DNA sequence (Handy, Castro and Loscalzo, 2011). Epigenetic processes include histone post-

translational modifications (HPTMs), microRNA and non-coding RNA expression, nucleosome positioning, and DNA methylation. However, it is the aberrant DNA methylation that has been the main and best studied epigenetic mechanism deregulated in colorectal cancer (Lao and Grandy, 2011).

#### **1.4.1. Aberrant methylation in CRC**

DNA methylation is an enzymatic reaction in which methyl groups are added to the 5-position of cytosine bases. These 5-methylcytosines can be usually found in cytosine-phospho-guanine (CpG) dinucleotides at specific sites called CpG islands (Figure 1.7). Those CpG islands are usually located within the gene promoter 5' region (Moore, Le and Fan, 2012). The addition of the methyl groups is carried out by a special group of enzymes called DNA methyltransferases (Jin, Li and Robertson, 2011). DNA methylation is a natural genome-wide process and it is used for silencing genes that no longer need to be expressed in the cell and usually involves developmental genes (Hernando-Herraez et al. 2015). The aberrant DNA methylation can result in silencing of TSGs or wrongly activating oncogenes, consequently leading to carcinogenesis.

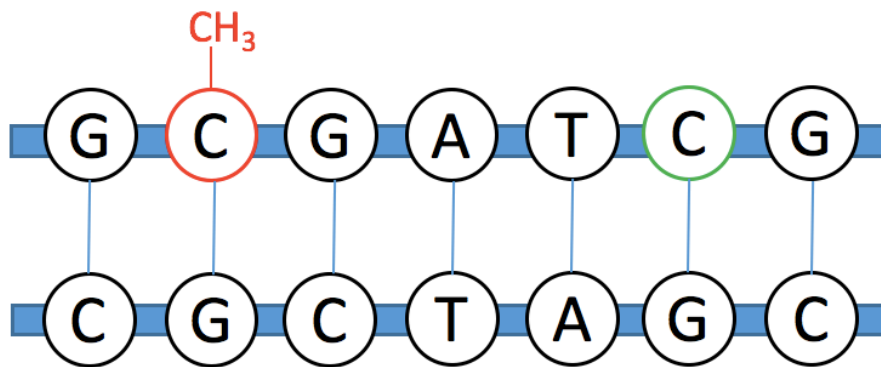


Figure 1.7 - Methylation at CpG islands.

In red a cytosine with methyl group added at CpG island site, and in green unmethylated cytosine at the CpG island site.

Two main systems involved in genome-wide methylations in CRC are the Methyl CpG binding domain (MBD) protein and polycomb complex genes. MBD-containing protein play a key role in interpretation of DNA methylation. 11 known proteins for this family have been identified. The methyl-CpG-binding protein 2 (MeCP2) was the first MBD-containing protein described, and subsequently through sequence homology more MBD proteins were later discovered: MBD1-MBD6. Later, four more MBD protein have been characterised: SEDTB1, SEDTB2, BAZ2A and BAZ2B. MBDs bind the DNA methylations and then direct the histone modification and chromatin organisation that results in transcriptional repression (Parry and Clarke, 2011).

Polycomb complex group proteins selectively facilitate repression of gene expression through polycomb repressive complexes (PRCs). PRCs are multisubunit complexes which regulate chromatin structure through catalysing the HPTMs (Levine, King and Kingston, 2004). There are two PRCs, PRC1 and PRC2, both of which induce specific covalent HPTMs that have been described in the literature as repressive marks (Wang et al., 2015). PRC1 facilitates monoubiquitination of lysine 119 on histone H2A (H2AK119Ub1) through RING1B E3 ligase, whereas EZH1/2 methyltransferase in PRC2 catalyses trimethylation of lysine 27 of histone 3 (H3K27me3) (Cao et al. 2002). Subunits of PRC1 and PRC2 complex, such as Bmi1, Ezh2, and Suz12, have been found overexpressed in colon cancers (Sauvageau and Sauvageau, 2010).

#### **1.4.2. CpG Island methylator phenotype**

Almost two decades ago an epigenetic phenotype that is characterised by numerous promoter region CpG islands were hypermethylated (Toyata et al. 1999). This study proposed two CIMP categories, CIMP- and CIMP+, and suggested methylation of CDKN2A, MINT1, MINT2, MINT31 and MLH1 as markers for the phenotype. Although some of the methylation detected was due to aging (majority of loci are methylated in colonic mucosa due to age progression), a specific subset of CRC samples presented a hypermethylated phenotype (Issa, 2002). MLH1 protein belongs to the MMR genes family and its mutation is often associated with MSI in hereditary CRCs. However, the lack of

expression of MLH1 in sporadic tumours have been observed frequently (Thibodeau et al. 1998), suggesting the MLH1 promoter region is hypermethylated. Due to the aberrant methylation in MLH1 a lot of MSI tumours overlap with CIMP. Therefore, CIMP has been divided into four different categories: CIMP+/MSI+, CIMP+/MSI-, CIMP-/MSI+ and CIMP-/MSI- (Issa, 2004). CIMP positive patients, especially CIMP+/MSI-, have been associated with poor prognosis (Lam et al. 2016).

### **1.5. Colorectal cancer treatment**

Pathologic staging is the first and one of the most important prognosis factors that a patient will get after diagnosis. Staging of CRC is done with the tumour-node-metastases (TNM) system, which identifies the invasion of the tumour based on three main aspects: invasion depth of the intestinal wall, lymph node involvement, and presence of distant metastatic sites (Wolpin and Mayer, 2008). The depth of tumour invasion is defined by the T stage (T1-T4), where T1 is an invasion of the submucosa and T4 means invasion into serosa or nearby structures (see Figure 1.8). Lymph node involvement is defined by the N stage and is divided into three categories – N0 (no lymph nodes involved), N1 (1-3 lymph nodes involved) and N2 (more than three lymph nodes involved). Lastly, M defines the absence or presence of distant sites of disease by M0 or M1, respectively (Greene, Stewart and Norton, 2002). Patient prognosis is associated with the tumour stage. The 5-year survival rate decreases with an increased

staging of colorectal cancer, where for stages 1, 2, and 3 the rates are 94%, 82%, and 67% respectively. Furthermore, metastatic or stage 4 tumours have an even more drastic decrease in 5-year survival rate as it is only 11% survive (Sagaert, Vanstapel and Verbeek, 2018).

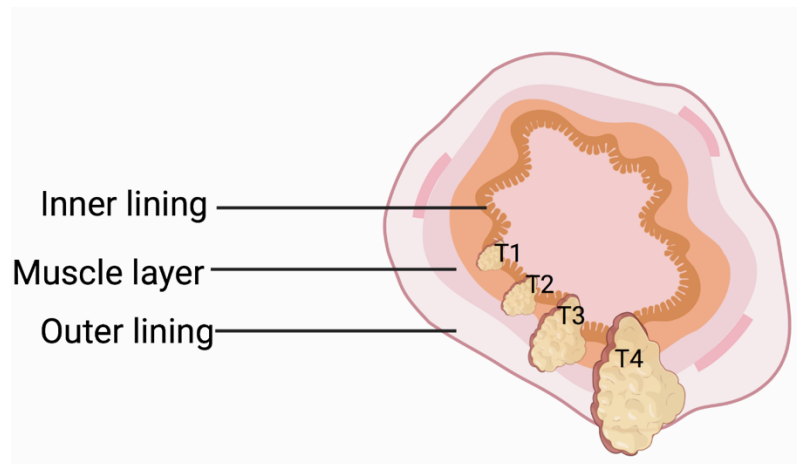


Figure 1.8 - Colorectal cancer stages.

The invasion of tumour into the intestine, at stage T1 invading only the inner intestinal lining, T2 invading the muscle layer, T3 invading muscle and also invading the outer lining, and lastly T4 invading all layers and nearby structures.

Created with Biorender.com

Treatment regimen will largely depend on the tumour stage and its location. Surgery is the most common treatment recommended to patients with CRC and often is combined with chemotherapy for colon tumours, radiotherapy or combination of both in case of rectal cancers. When receiving combined treatment patients can either get adjuvant treatment (additional treatment administered post-surgery) or neo-adjuvant treatment (treatment administered prior to surgery). Colon and sigmoid cancers are treated with adjuvant therapy

that consist of surgery followed by chemotherapy. In cases of more advanced disease resulting in tumour invasion and spread to lymphatic nodes, patients will receive chemotherapy before surgery (Feeney et al. 2019). Recent data from the FoxTROT clinical trial has showed that the outcome of neoadjuvant administration prior to surgery can be beneficial for all patients with colon cancer and pose a standardised treatment regimen (Seymour and Morton, 2019; Body et al. 2021). In this trial patients with T3 or T4, N0-2, and M0 colon cancers have been recruited and randomly assigned to the neoadjuvant chemotherapy (NAC) or control groups. Patients in the NAC group received 6 weeks of chemotherapy prior to surgery and 18 weeks of chemotherapy following surgery. Patients in the control group have had surgery followed by 24 weeks of chemotherapy administration. The initial short-term observations showed improved 2-year failure rate but the long-term effects are yet to be determined (Seymour and Morton, 2019).

Rectal cancer treatment, however, differs from colon/sigmoid cancer treatment due to its position in the body. The rectum is located in the narrow pelvis region and extends from the transitional mucosa of the anal dentate line to the sigmoid colon (Wolpin and Mayer, 2008). The pelvic structures surrounding the rectum limit access during surgery, resulting in a higher risk of local recurrence. To minimise this risk, neo-adjuvant radiotherapy is added to the treatment regimen as a standard for rectal cancer patients.

There is a variety of chemotherapeutic drugs that are used in the clinic for CRC treatment. The most commonly administered drugs are fluoropyrimidines – Fluorouracil (5FU) or Capecitabine (Xie, Chen and Fang, 2020). Fluorinated pyrimidines act as inhibitors of thymidylate synthetase, which is an enzyme limiting the synthesis of pyrimidine nucleotide which in turn is required for DNA replication (Vertessy and Toth, 2009). Often calcium folinate is administered in combination with 5FU in order to increase its cytotoxic activity (Vodenkova et al. 2020). Other cytotoxic drugs used for treatment of CRC are Oxaliplatin and Irinotecan. Both drugs' mechanisms focus on preventing DNA replication and transcription, the former through inhibition of DNA synthesis, whereas the latter achieves this via inhibition of topoisomerase I. When administered, Oxaliplatin or Irinotecan are often combined with 5FU and folic acid. Some patients can be offered more targeted drugs that are monoclonal antibodies. In CRC treatment Cetuximab and Panitumumab are used and their key mechanism is to inhibit the epidermal growth factor receptor (EGFR). These monoclonal antibodies are used in combination with standard chemotherapy, and most commonly in case of treating the metastatic disease (Xie, Chen and Fang, 2020).

Two types of radiotherapy regimens can be used for rectal cancer treatment, short-course radiotherapy or long-course radiochemotherapy. Short-course radiotherapy consists of total 25 Gray (Gy) administered in 5 fractions of 5 Gy, whereas long-course treatment consist of 45-50.4 Gy administered in 25-28 fractions with 1.8 Gy per fraction (Kim et al. 2016). A trail conducted by the Polish group compared short- course neoadjuvant radiotherapy with preoperative long-

course radio-chemotherapy for T3 or T4 stage rectal cancers and found no significant differences in disease-free survival, overall survival, late toxicity or local recurrence between those two regimens (Bujko et al. 2006). Another trial that also looked into comparison between those two neoadjuvant therapies also found no significant difference in the local recurrence rates, apart from the distant tumours, in which the long-course chemo-radiotherapy was more successful. There were no differences in late toxicity and the overall survival rates were similar- 74% for short-course radiotherapy and 70% for long-course chemo-radiotherapy (Ngan et al. 2012). Currently, both of the regimens are used and depending on the country, one is more preferable than the other, for example the long-course chemo-radiotherapy is more of a standard, whereas the short-course radiotherapy is being chosen more in Europe (Tseng et al. 2019). In the UK, patients with advanced rectal cancer will get short-course radiotherapy followed by surgery after one week from finishing the treatment, whereas patients with less advanced disease will receive neo-adjuvant long-course radiotherapy combined with chemotherapy. Until today there is no clear consensus about the interval between the end of long-course treatment and the surgery, hence it can range between 4 to 8 weeks. The response to the tumour is measured by the tumour regression grade (TRG) system which classifies the regressive changes after treatment (Kim et al. 2016).

Radiation therapy is often selected as part of the treatment for various type of cancers as it causes damage to cancer cells. The damage is deliver by direct mechanism of ionising photons and particles causing alterations to

macromolecules. Additionally, an indirect damage is also caused by the production of free radicals causing double strand breaks in the DNA and triggering programmed cell death via DNA damage repair (DDR) pathway (Galeaz, Totis and Bisio, 2021; Kocakavuk et al. 2021). Depending on the cell damage, the DDR pathway agents will send a signal about the cell's fate, i.e. deciding on the cell's death or survival (Huang and Zhou, 2020). Healthy cells surrounding the tumour are also affected by the irradiation, however due to the lack of accompanying genetic mutations the cell is most likely to recover with an appropriate irradiation dose. The increase in dose rises the probability of toxic effects in late-responding normal tissue cells (usually less sensitive to fraction doses) and therefore limits the dose of radiotherapy treatment. The balance of minimal late normal tissue complications and tumour control is key for a good therapeutic outcome. This can be quantified by plotting tumour control probability (TCP) and normal tissue complication probability (NTCP) against Radiation dose, as seen in Figure 1.9. The separation between the curves gives the size of the therapeutic index (Ray, Sibson and Kiltie, 2015).

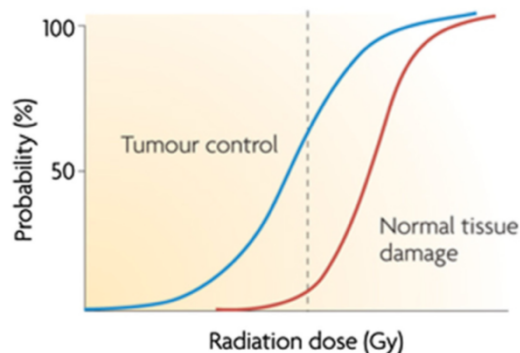


Figure 1.9 - Tumour control probability and normal tissue complication probability curves.

Response curves for Tumour control (blue) and Normal tissue damage (red). The dashed lines represent the optimal dose for minimal normal tissue damage and maximum tumour tissue damage.

Taken from Ray, Sibson and Kiltie, 2015.

## 1.6. DNA damage repair (DDR)

DNA, under influence of different agents, can be exposed to stress and be damaged leading to the accumulation of genetic lesions. The agents that can affect DNA integrity can be either endogenous (such as by-products of metabolic processes happening in cells), or exogenous. Examples of endogenous factors include mitochondrial respiration, and intracellular free radical oxygen species. Exogenous factors include exposure to UV light, ionising radiation (IR), thermal disruption, viruses, and mutagenic chemicals. It has been estimated that each day every cell in the human body can experience  $10^5$  spontaneous or induced DNA lesions (Ciccia and Elledge, 2010). As it is known, DNA damage and genetic lesions can directly alter the primary structure of DNA, directly affecting replication and transcription carrying the errors over. Therefore, cells must be

equipped with mechanisms that are able to repair the damage. Since the DNA can be damaged in different ways, there are multiple diverse and complex DNA damage repair mechanisms (see Figure 1.10; Chatterjee and Walker, 2017).

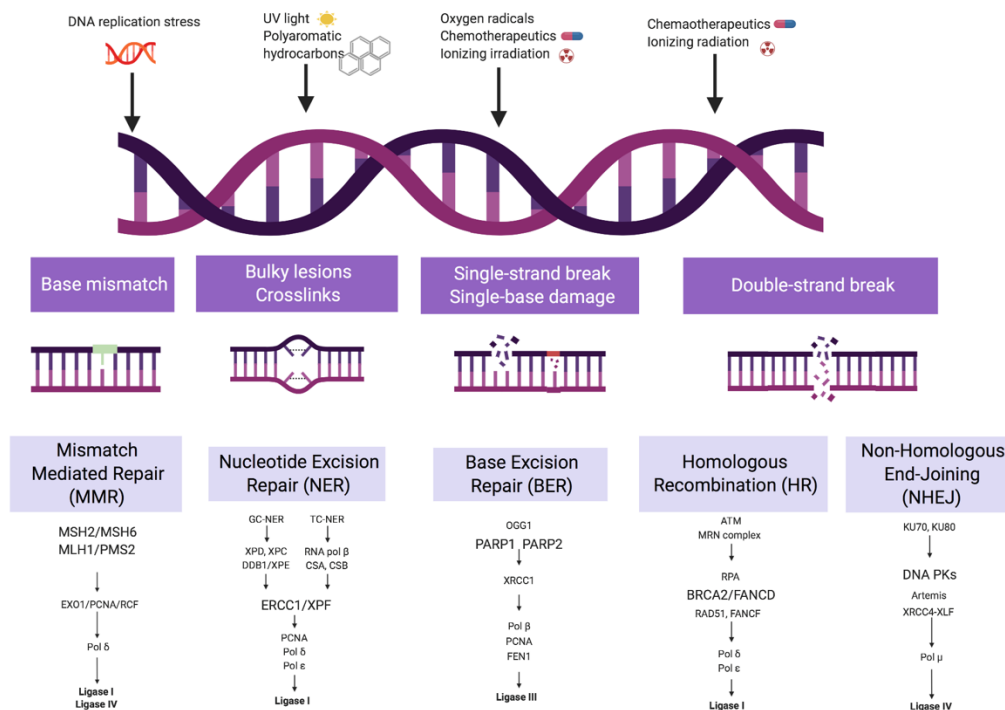


Figure 1.10 - DNA damage repair pathways.

An overview of DNA damage inducing agents, DNA damage types and their repair mechanisms  
Created with BioRender.com

MMR is based on correcting mismatched nucleotides in the otherwise complementary paired DNA strands. Usually, single base-base mismatches and small insertions/deletions are caused by replication errors. These type of lesions,

when detected, trigger a single-strand incision that is then proceeded upon nuclease, polymerase, and ligase enzymes (Jiricny, 2006).

Base excision repair is recruited for repair of single strand breaks. The Glycosylase enzyme is usually responsible for recognising the damage and mediating base removal prior to repair being completed by nuclease, polymerase, and ligase enzymes (Lindahl and Barnes, 2000).

Bulky DNA add-ons and cross-links are repaired by the nucleotide excision repair (NER) system, which is responsible for recognition of helix-distorting mutations. This type of lesions is characteristic for UV light-caused damage. The NER mechanism operates through two main pathways: transcription-coupled NER, and global-genome NER. The common mechanism for these pathways is the excision of the lesion as 22-30 base oligonucleotide producing single-stranded DNA that is proceeded by DNA polymerase and accompanying factors before acting ligation enzymes (Jackson and Bartek, 2009).

Lastly, the damage resulting in double strand breaks (DSBs) is mainly caused by ionizing radiation and chemotherapeutics and can be repaired via two main repair pathways: non-homologous end joining (NHEJ), and homologous repair (HR; San Filippo, Sung and Klein, 2008). The former pathway works through Ku proteins mediating activation of the protein kinase DNA-PKcs facilitating recruitment and activation of polymerases and DNA ligase IV (Jackson and Bartek, 2009). There is a possibility of a Ku-independent NHEJ called the MMEJ or alternative NHEJ pathway. Both result in error-prone repair, however these

can be operated in any cell cycle phase as oppose to homologous repair (McVey and Lee, 2008). HR is initiated by excision of the broken DNA and generating single strand DNA (ssDNA). This is further proceeded by Rad51 and BRCA2 proteins mediating strand invasion of the homologous template and leading to the repair. This pathway uses the template of sister-chromatid sequences in order to mediate accurate repair. Hence this pathway is restricted to the S and G<sub>2</sub> phases of the cell cycle (Jackson and Bartek, 2009; Fugger and West, 2016).

### **1.7. Treatment resistance**

5 year overall survival for CRC in UK is still relatively low – 58.4% (Bowel cancer survival statistics, 2022), despite the understanding of the molecular processes behind the disease and combined treatment regimens that include combination of surgery with chemo- or/and radiotherapy. It is believed that the resistance to the treatments plays a major problem in the clinical settings and contributes towards the continuing low overall survival rates (Buckley et al. 2020). Resistance to both, chemotherapy and radiotherapy, is often observed in patients with colorectal cancer. The treatment resistance can be either primary, in which case the tumour does not respond to the treatment from the beginning. However, the resistance to treatment can also be acquired, where cells after the exposure to treatment become resistant (Galeaz, Totis and Bisio, 2021). The resistance mechanisms arise through either genetic mutations that will directly interact or affect the drug target or through aberrations that will result in bypassing the drug

target through an upstream/downstream effector or a parallel pathway (Venkatesan et al. 2017).

Only around one third of patients is thought to respond to 5FU treatment as a single agent, and half of patients respond to it in a combination with oxaliplatin-based therapy (Weidlich et al. 2011; Virag et al. 2013). Furthermore, the EGFR targeted drugs (cetuximab and panitumumab) have also been shown to have limited efficiency due to the acquired resistance of cancer cells (Van Emburgh et al. 2014). This has been shown to be a result of the mutated *KRAS*, a downstream effector, causing bypass resistance mechanisms (Amado et al. 2008). Similarly to *KRAS*, an amplification of *MET* (a parallel pathway) resulting in the pathway bypass and contributing to treatment resistance (Bardelli et al. 2013).

In case of radioresistance, studies have shown that the gene dysregulation of oncogenes and tumour suppressor genes involved in different signalling pathways is ultimately responsible for the radiation resistance (Rich, 2007; Willers et al. 2013). However, radioresistance is not as straight forward and multiple biological mechanisms and genetic alterations contribute towards it, hence till today there is no solution for sensitising tumour cells to radiotherapy. What is more, the tumour heterogeneity and patient to patient tumour difference contributes to polymodality of the issue. Multiple pathways have been proposed to play a role in radioresistance, such as DNA damage repair pathways, apoptosis and alterations in cell cycle (Geng and Wang, 2016), additionally Buckley et al. (2020) proposed to extend this list to pathways involved to cancer

hallmarks. As tumour resistance to irradiation is one of the key problems in not only colorectal cancer but other types of cancer that include radiotherapy as part of their treatment, many studies have been undertaken to identify potential markers of radioresistance. Until today, many potential targets have been identified that could pose as such. For example, KRAS have been linked to radiotherapy resistance in multiple studies and multiple cancers (Grana et al. 2002, Jancik et al. 2010, Chakrabarti, 2015). The presence of oncogenic KRAS mutations is thought to convey the resistance to the treatment as it enhances the DNA repair capacity in the cancerous cells (Williams et al. 2016). Conversely, a study done on ovarian cancer cell line with mutant allele of KRAS showed a significant increased sensitivity to the treatment that involved radiation combined with cisplatin in comparison to the same line with wild type allele (Samouelieu et al. 2004). Specifically for CRC studies have looked to link distant metastasis to therapy resistance. As treatment resistance is closely related to distant metastasis. It was proposed to look at genes that contribute to metastasis and progression in order to identify potential biomarkers of radiation resistance. PRL-3 also known as PTP4A3 have been highlighted as metastasis associated gene as the protein expressed have been found in 100% of metastatic sites in CRC . What is more, the expression of PRL-3 correlated specifically with CRC despite the metastatic sites. Further studies showed as well that PRL-3 is a driver of tumour progression and has a causative role rather than being a consequence. Another marker of radioresistance that is also associated with tumour progression is survivin (also known as Birc5). Overexpression of this protein has

been linked to the cell death inhibition. Studies showed that cells could be radiosensitised by the inhibition of Survivin (Rodel et al. 2003; Pennati, Folini and Zaffaroni, 2008). Additionally, hypoxic environment has been linked to increased resistance to radiotherapy, consequently genes involved in the maintenance of the redox homeostasis and the protection against oxidative stress. Several transcription factors (TFs) have been proposed to be involved in radioresistance. A nuclear factor kappa B (NF- $\kappa$ B) responsible for controlling the immune system development, inflammation, cell growth and apoptosis. Another TF is STAT3 have been shown to be stimulated by the cytokines can drive the radioresistance through the inflammatory pathway (Galeaz, Totis and Bisio, 2021). Finally, both Akt and mTOR pathway have been also linked to radioresistance in a large number of different studies, due their main involvement in cell survival, stress responses and apoptosis regulation (Toulany and Rodemann, 2013; Sato et al. 2019).

Although several studies have linked multiple genetic alterations to have an inhibiting effect on radiotherapy effectiveness, currently we still don't have an effective and reliable marker that could be a target for radiotherapy sensitisation or patient stratification.

### **1.8. Models to study colorectal cancer**

In order to study complex diseases such as cancer an accurate model is essential. Many preclinical models have been developed over the years to be

able to study such complex diseases as cancer. Since many signalling pathways are evolutionary conserved across species, model organisms have posed as good models for studying signalling, development, and cancer. For the last one, mouse models have been especially utilised in laboratories across the world (Kim, Koo and Knoblich, 2020). In addition to animal models, cell lines have played a crucial part in studying cancer. Although, many biological discoveries have been possible thanks to 2D cultures and animal models, the limitations of such models have been limiting research. It has been shown that certain biological processes are specific to the human body and cannot be replicated in animal models. As an example, metabolism and brain and blood barrier differences have resulted in differences during drug efficacy testing (O-Brown, Pfau and Gu, 2018; Kim, Koo and Knoblich, 2020). When it comes to cell lines, despite them being human based the monolayer structure is not representative of the human body. With human-derived models comprised of cancer cell lines and patient-derived tumour xenografts (PDX) murine models, the need for a more accurate human cell-based model has been emerging over the years. This has led to the establishment of the first organoid cultures which have revolutionised the disease modelling field (Sachs and Clevers, 2014;).

### **1.8.1. Cancer cell lines**

Immortalised cell lines are derived from mutated cells of multicellular organisms – usually human or mice. Mutations in these cells gives them the ability to avoid

senescence and proliferate almost indefinitely. The first cell line, HeLa, was derived in 1951 from a cervical tumour and revolutionised the research industry (Lucey, Nelson-Rees and Hutchins, 2009). Since then cell culture and the cell line concept has grown. With over 3,600 cell lines available (ATCC), many research studies are performed on this kind of disease model. Cell lines can be studied with a wide variety of different laboratory techniques and used for studying cancerous cell biology as well as the reaction of cancer cells to certain drugs (Li et al. 2020).

Cell lines have many advantages. They are cost effective and relatively easy to maintain due to their mutation-acquired properties. Furthermore, in current days there are limited ethical issues linked to animal or human tissue sampling. Finally, a pure population of cells provides results that are easy to reproduce and therefore they can be used in high-throughput experiments (Kaur and Dufour, 2012; Li et al. 2020).

Although cell lines are widely used across research laboratories and contribute greatly to cancer studies, they have many disadvantages. Cell lines are homogenous and lack other types of cells that contribute to the tumour microenvironment. Additionally, the majority of cell lines are derived from tumours or cells that have acquired oncogenic potential in vitro. In cancer research this is not much of an issue, however it means that studying the normal counterpart is often impossible (Li et al. 2020). The main flaw of cell lines, however, is their lack of genetic and phenotypic stability. Over extended periods of time, serial passage

can cause genotypic variations and heterogeneity in cultures. As cancer is a highly heterogeneous and complex disease, it is argued that due to the mentioned drawbacks cell lines cannot fully represent the interactions and microenvironment of a tumour (Kaur and Dufour, 2012; Li et al. 2020).

### **1.8.2. Murine patient derived xenograft models**

In contrast to 2D cell lines, murine models have been widely used in cancer research for a long time, mainly due to them being able to replicate the tumour microenvironment. There are different ways scientists use mice to model cancer – from studying specific mouse strains, through allografts, to patient-derived xenografts and engineered mice (Kim, Koo and Knoblich, 2020). The only human-derived murine models are represented by patient-derived tumour xenograft (PDX) mice, firstly established in 1953. Patient tumour tissue is transplanted into immunocompromised mice. The tissue can be directly implanted either subcutaneously (into the layer of skin directly below dermis and epidermis), or orthotopically (directly into the organ of the transplanting tissue origin). The latter technique allows the study of patients' tumours in a close and more relevant environment for the transplanted tumour (Zhang et al. 2016). These are very useful in the study of malignancies in their original tumour environment, as they retain the heterogeneity and complexity of the tumours being studied, while also retaining genetic and phenotypic stability.

However, PDTX are labour-intensive, time-consuming, and can be problematic due to ethical issues (John et al. 2011). What is more, genetic manipulation cannot be carried out and high-throughput screening is inefficient and expensive (Li et al. 2020). Furthermore, because the tumours are grown in different species it has been argued that the models do not entirely mimic the tumour-host interactions as these might differ across species. Additionally, mice used for xenografts are immunocompromised, which means the tumour interactions with the immune system, which play a very important role in the study of cancer, are completely lacking in these models. It has been also argued that murine models cannot represent the human physiological processes as they are profoundly different, as the metabolism of mice differs to that of humans. Lastly, mice in laboratories are inbred which reduces genetic diversity, which is essential for studying disease onset, treatment response, and patient diversity (Kim, Koo and Knoblich, 2020).

### **1.8.3. Organoids**

As the need for a more accurate human-based model increased, there have been several attempts to create new models. Prior to establishing organoid cultures, different attempts to introduce a three-dimensional (3D) model have been made, such as spheroid cultures, human cells bio-printing, and 'organ-on-chip' technology. Although, all of these can be considered to be useful models, organoids have been found to be superior due to their specific properties.

Organoids are characterised with the ability to self-organise into 3D structures that maintain their self-renewing properties while also allowing stem cell differentiation (Lancaster and Knoblich, 2014). Organoids are grown *in vitro* and can be derived from either pluripotent stem cells (PSCs) or adult stem cells (ASCs), and are able to self-organise into native tissue specific microanatomy (Kretzschmar and Clevers, 2016). A fundamental discovery in the establishment of organoid cultures was the identification of Lgr5 as a specific marker gene for intestinal stem cells, which enabled the characterisation and purification of these stem cells (Barker et al. 2007). Later discoveries of importance included the definition of niche factors that are essential for the organoid culture medium. It was noted that the epidermal growth factor (EGF), Noggin, R-spondin, and Wnt are essential to maintain the stem cell population in culture along with defining the extracellular matrix that would allow three dimensional growth (Kretzschmar and Clevers, 2016). With those findings, in 2009 a successful derivation of organoid cultures established from intestinal mouse ASCs has been described by Sato and his colleagues (Sato et al. 2009). Inspired by murine studies, human organoids have also been derived with few modifications to culture media due to the differences between mice and human biology (Sato et al. 2009; Sato et al. 2011). As mentioned in the organoid definition, 3D structures can be generated with either ASCs or PSCs (see Figure 1.11). Human PSC-derived organoids are established by controlled differentiation protocols, designed to mimic developmental processes for the tissue of interest (Kim, Koo and Knoblich, 2020). Cultures generated this way cannot be passaged and expanded as ASC-derived

organoids. However, they can be cultured and maintained for long periods of time (McCauley and Wells, 2017). Since organoid cultures have become possible, many different types of organoids have been grown from a variety of organs such as the liver, stomach, lungs, oesophagus, pancreas, brain, and more (Karthaus et al. 2014; Bartfeld et al. 2015; Huch et al. 2015; Linnemann et al. 2015; Schlaermann et al. 2016; Turco et al. 2017; Lee et al. 2018; Loomans et al. 2018; Sachs et al. 2019).

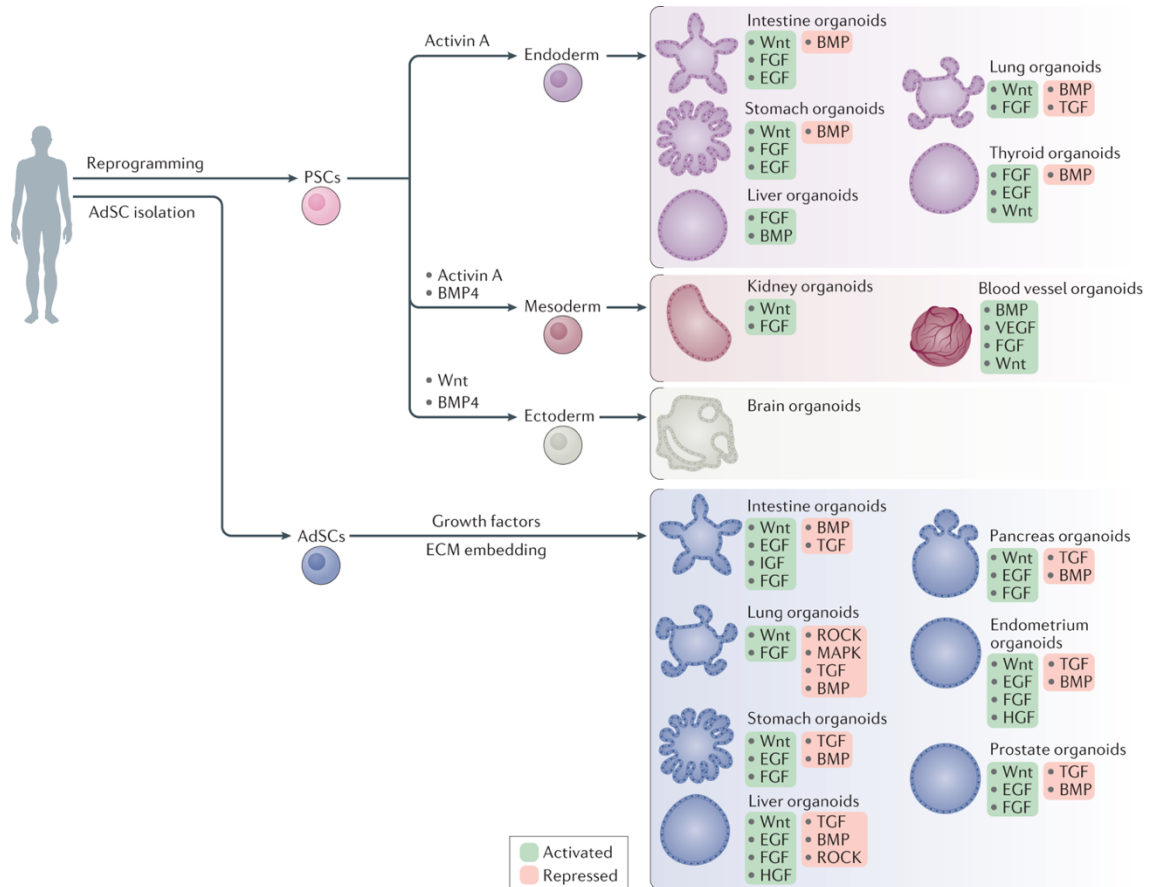


Figure 1.11 - Organoid derivation processes and culturing niche factors.

Two different ways to derive human organoids. Organoids generated from pluripotent stem cells (PSCs) are derived by first directing the germ-layer specification followed by culturing cells in specific niche factors that will allow maturation and differentiation of cells into desired types. For adult stem cell (ASC) derived organoids, stem cells from specific tissue population are required for establishing cultured. These cells are embedded in extracellular matrix and cultured under specific conditions.

Taken from Kim, Koo and Knoblich, 2020.

Very quickly organoids have become very popular in cancer research due to their unique properties and advantages that would tackle the problems of previously available models (described above) for the disease. The organoids' abilities to self-organise into 3D structures and to be generated from little amounts of tissue such as biopsies which can then be cultured indefinitely, give them a superior advantage over the other models. In contrast to cell lines, organoids have been

shown to be both genetically and phenotypically stable (Li et al. 2020). Furthermore, organoids are highly heterogeneous and maintain their 3D structure, replicating tissue and tumour more accurately – sometimes even almost identically (Kim, Koo and Knoblich, 2020). As organoids can be derived from patient tissue, they represent human biology as opposed to human-based murine systems. Furthermore, although more expensive than cell line cultures, organoids are relatively cheap and can be established rapidly and expanded easily and used for high-throughput analyses. Finally, organoids pose as a great tool for genetic engineering. Due to these advantages, which tackle the main disadvantages of cell lines and murine models, organoids have become a promising new model for studying human biology and complex human diseases such as cancer.

Organoids can be a multimodal model with which different aspects of human biology can be studied and all applications developed for cell cultures can be applied to them. What is more, organoids can also be utilised in translational studies, as seen in Figure 1.12 (Kretzschmar and Clevers, 2016; Clevers, 2016; Young and Reed, 2016). Examples of organoids being utilised in a wide range of research subjects show their potential and accessibility. For example, they have been used in infectious diseases research, where scientists used them to model pathogen and host interactions such as with the zika virus (ZIKV) and cerebral organoids (Garcez et al. 2016). Organoids have also been co-cultured with bacteria to deepen the understanding of the human intestinal microbiome (Puschhof et al. 2021), or to study infection with helicobacter pylori (Shlaermann

et al. 2016). Additionally, during the recent SARS-COVID-19 pandemic they have also been utilised to study the virus (Kim, Koo and Knoblich, 2020). In addition to this, organoids have been used to study cystic fibrosis and the Clevers laboratory used the CRISPR/Cas9 method to genetically engineer organoids that can then be further used for cystic fibrosis treatment (Schwank et al. 2013). Finally, organoids have been widely utilised in the study of different types of cancer and more and more studies have utilised organoids as their disease model (Drost and Clevers, 2018).

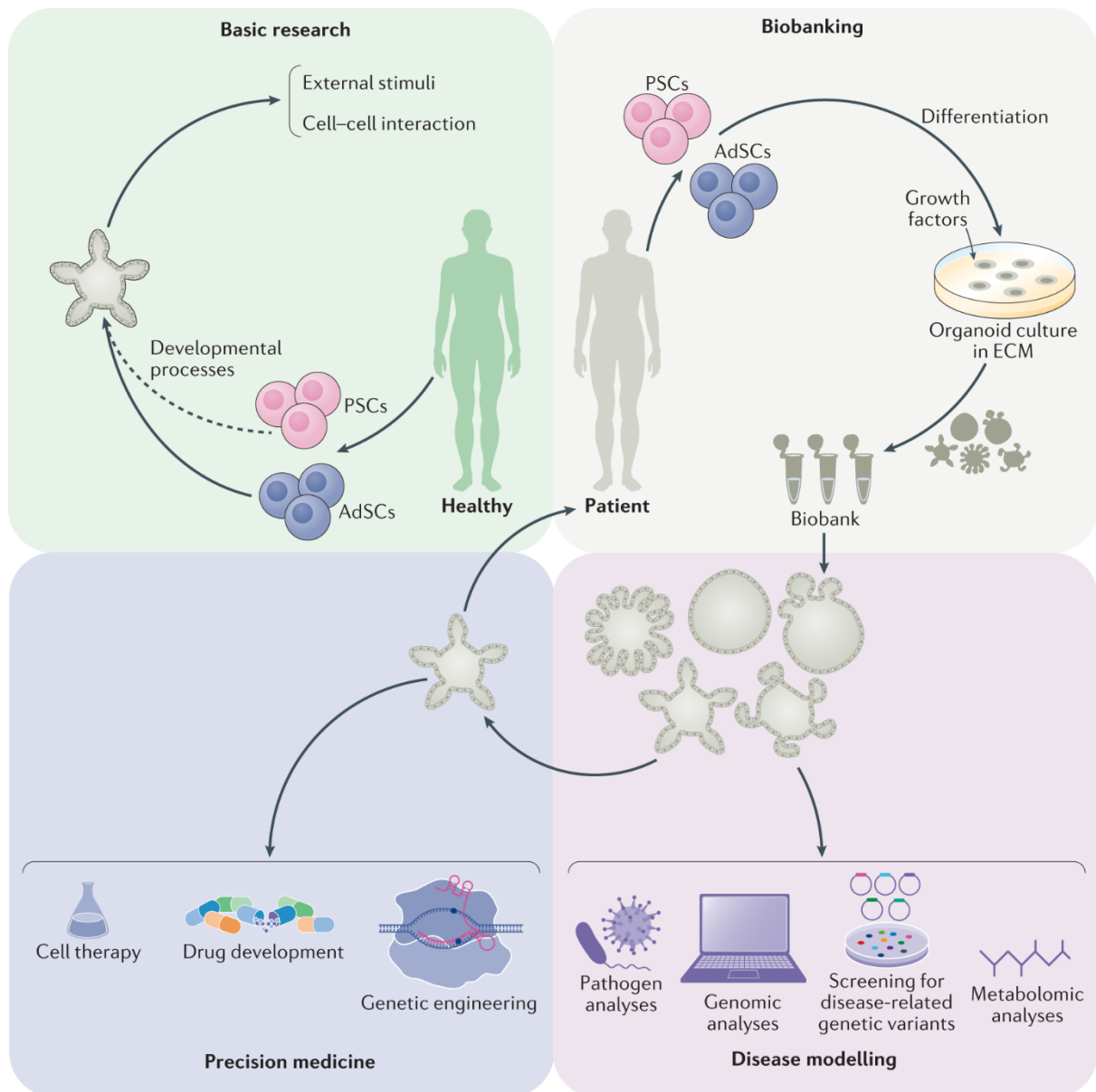


Figure 1.12 - Organoids applications in basic and translational research.

Organoids can be used in research for studying cell biology; can be used for biobanking and translation research.

Taken from Kim, Koo and Knoblich, 2020.

Other advantages of culturing organoids as a disease model are that they form efficiently and self-renew, they can expand long-term, and most importantly stay genetically stable. Moreover, cell types from the native system are observed in

the cultures, closely replicating the microenvironment conditions (Sachs and Clevers, 2014; Young and Reed, 2016). Lastly, organoids have been shown to be easy to manipulate genetically. Many papers have successfully used CRISP/Cas9 gene editing method to manipulate organoids (Drost et al. 2015; Matano et al. 2015).

Although, organoids have a lot of advantages and can be used efficiently in research, they also have some limitations and disadvantages. The main limitation of organoid cultures is the fact that the microenvironment is sometimes lacking, and there is no stroma interaction that is a very important component in tumour signalling. Furthermore, organoid cultures have been limited to tissues with only epithelial origin. Lastly, due to the model and methods being relatively new and still being rapidly developed and modified, there might be slight variations in culture and derivation protocols between different research groups. Nevertheless, the amount of advantages makes organoids suitable and promising for the study of cancer.

### **1.9. Rationale**

As described in above sections, CRC is a heterogenous disease in which molecular traits can play crucial roles in patients' prognosis and treatment response. Particularly, in rectal cancer resistance to radiotherapy has been observed. Only a small proportion of patients presenting with late stages of rectal cancer undergoing neo-adjuvant therapy will have pathological complete

response (pathCR), whereas more patients will not respond to radiation (Lorimer et al. 2017; Sanchez-Perez et al. 2017). Samples from two cohorts of patients (responders and non-responders) have previously been sequenced to screen for potential response markers. Two potential markers for radiosensitivity have been identified: *FBXW7* and *PIK3CA*, which have been significantly enriched in patients with pathological complete response in comparison to patients without pathCR (Stockton et al. 2021). *FBXW7* has been shown to play a role in the double-strand break repair pathway (Zhang et al. 2016). Additionally, Koyama et al. (2018) have increased response to radiotherapy by blocking the Akt pathway, which could suggest that *PIK3CA* can also play the role of a radiosensitivity marker. Finding a radiosensitivity marker for rectal cancer could help with patient stratification and potentially finding new targeted therapies, improving the treatment and overall survival of patients.

Furthermore, the pursuit for the ideal model for translation research continues and there has been no ideal model for studying tumour radiosensitivity and radioresistance. Consequently, establishing such a model is necessary for studying tumour response to irradiation. As organoids have been emerging as models to closely replicate patients' tumour environments, we have decided to utilise them for modelling rectal cancer response to radiotherapy treatment. The main aim of this study is to establish an organoid-based model for studying radiosensitivity and validating inactivating mutations of *FBXW7* and *PIK3CA* as potential markers of good response to radiotherapy. In order to achieve the aim following objectives were set:

1. Establish an organoid culture and patient-derived colorectal cancer organoids for modelling irradiation response (Chapter 3)
2. Model and characterise the response of patient-derived organoids to short course radiotherapy treatment (Chapter 4)
3. Identify and validate the markers of radiosensitivity (Chapter 5)
4. Based on the identified markers, use targeted chemotherapy to investigate if cells can be sensitised to radiotherapy (Chapter 6)

Hypothesis: Patient-derived colorectal cancer organoids can be developed and used to study radiosensitivity and to evaluate the role of inactivating mutations in FBXW7 and PIK3CA as radiosensitivity markers.

## **2. MATERIALS AND METHODS**

### **2.1. Ethical approval and patient recruitment**

All human material (tissue and blood) and matching anonymised clinical data used in this study have been obtained under ethical approval from the Human Biomaterials Resource Centre (HBRC) Birmingham BioBank (project approval code: 17-287).

Patients were identified and recruited prospectively before undergoing surgery at the Queen Elizabeth Hospital, Birmingham. Tissue from consenting patients that underwent tumour (colorectal adenocarcinoma) resection have been sampled by the pathologist and a matching set of tumour and normal healthy tissue were then transferred to the Biobank where they were anonymised and catalogued. Anonymised samples were then released to the laboratory on the same day as the patient's surgery and stored at 4°C until being processed.

### **2.2. Cell culture**

#### **2.2.1. Cell culture reagents**

L-WRN cells (CRL-3276, ATCC, USA) culture medium: Dulbecco's Modified Eagle Medium (DMEM; Life Technologies, USA) supplemented with 10% Foetal

Bovine Serum (FBS, Life Technologies, USA), 0.5mg/ml G-418 (Gibco, USA) and 0.5mg/ml hygromycin (Life Technologies, USA).

Cultrex HA-R-Spondin1-Fc 293T Cells (Bio-technie, USA) culture medium: DMEM supplemented with 10% FBS, 300µg/ml Zeocin (Thermo Fisher Scientific, USA).

L-Wnt-3A cell (CRL-2647, ATCC, USA) culture medium: DMEM supplemented with 10% FBS and 0.4mg/ml G-418.

### **2.2.2. Culturing and passaging**

Cultrex HA-R-Spondin1-Fc 293T cells and L-Wnt-3A cells were cultured by Dr Regina Andrijes at the Berditchevski laboratory. L-WRN cells were cultured in our laboratory.

All cells were cultured in their culture media (see Section 2.2.1) in T75 flasks and passaged when approximately 80% confluence was achieved. To passage cells, culture media was aspirated and cells were washed with 10ml of phosphate buffered saline (PBS) in order to remove any residual culture media. Cells were then covered with 2ml of 0.25% Trypsin with 1mM EDTA (Life Technologies, USA) and were incubated for 2-3 minutes at 37°C. Cultrex HA-R-Spondin1-Fc 293T Cells were trypsinised with 0.25% Trypsin-EDTA diluted with PBS 1:3. Once the cells were detached from the bottom of the flask, 8ml of the appropriate culture media was added to the cell suspension in order to stop the activity of

Trypsin-EDTA. The cell suspension was collected and transferred to a sterile 15ml falcon tube and centrifuged at 200xg for 5 minutes at room temperature. The supernatant was removed and cell pellet was resuspended in 2ml of L-WRN culture media. Cells were then transferred to a new, sterile T75 flask and topped up with 13ml of L-WRN culture media. Cells were cultured at 37°C, 5% CO<sub>2</sub> in a cell culture designated incubator (New Brunswick Galaxy, Eppendorf, Germany).

### **2.2.3. Conditioned media for organoid culture**

Cultrex HA-R-Spondin1-Fc 293T and L-Wnt-3A conditioned media were collected by Dr Regina Andrijes at the Berditchevski laboratory and supplemented to the Beggs laboratory. L-WRN media was collected at the Beggs laboratory.

#### **2.2.3.1. L-WRN conditioned media protocol**

Cells were split 1:10 and seeded in T150 flasks. Cells were then suspended in 25ml of L-WRN culture medium without G-418 and Hygromycin B. Cells were cultured for 3-4 days. The media was removed and rinsed with L-WRN culture medium without G148 and Hygromycin B. 25ml of fresh L-WRN culture media lacking antibiotics was added to the flask and incubated for 24 hours. The media was aspirated, transferred to a 50ml falcon tube and then centrifuged at 2000xg for 5 minutes. The supernatant was filtered through a 0.22µM filter into a 1L sterile bottle and stored at 4°C. The cells were resuspended in 25ml of L-WRN culture

medium without G-418 and Hygromycin B. This was repeated for collecting batches 2, 3, and 4. After the 4<sup>th</sup> collection an equal volume of Advanced DMEM/F12 supplemented with 1xGlutaMax and 8% FBS was added to the combined batches. The conditioned media was stored at 4°C.

#### **2.2.3.2. Cultrex HA-R-Spondin1-Fc 293T conditioned media protocol**

Cells were cultured in T75 containing 15ml of Cultrex HA-R-Spondin1-Fc 293T medium. When cells reached 80% confluence, they were split 1:5 across five T75 flasks; one flask was cultured with 15ml of standard culture media, whereas the remaining 4 contained 15ml of culture media, each without Zeocin. Cells were incubated for 3 days and then trypsinised with 1:3 diluted Trypsin -EDTA in PBS. DMEM with 10% FBS was added to neutralise cells and centrifuged at 200xg for 5 minutes. The supernatant was discarded and the cell pellets were resuspended in 10ml of culture media and distributed across 10 T75 flasks, each containing 20ml of Advanced DMEM/F12 supplemented with 1xGlutaMax and 8% FBS. The medium was harvested after 7 days and pooled together and centrifuged at 1000xg for 10 minutes. The supernatant was filtered through a 0.22µM filter. The conditioned media was stored at 4°C.

### **2.2.3.3. L-Wnt-3A conditioned media protocol**

Cells were cultured in T75 flask containing 10ml of L-Wnt-3A culture medium. Cells were passaged over 10 T75 flasks. 9 of the flasks contained 10ml of DMEM/F12 supplemented with 1xGlutaMax and 8% FBS, and 1 flask contained the L-Wnt-3A culture media. Media from the 9 flasks was harvested after 4 days and centrifuged at 1000xg for 5 minutes. The supernatant was pooled and filtered through a 0.22 $\mu$ M filter and stored at 4°C. The cells were cultured in 10ml of DMEM/F12 supplemented with 1xGlutaMax and 8% FBS for 3 days. The media was collected, pooled, and centrifuged at 1000xg for 5 minutes. The supernatant was filtered through a 0.22 $\mu$ M filter. Two batches of filtered conditioned media were combined together with a 1:1 ratio, and stored at 4°C.

## **2.3. Organoid culture**

### **2.3.1. Organoid culture reagents**

#### **2.3.1.1. Basal culture medium**

Advanced DMEM/F12 supplemented with 2mM GlutaMAX 100 (Life Technologies, USA), 10mM HEPES (Gibco, USA), 100U/ml penicillin/100 mg/ml streptomycin (Gibco, USA), 10 $\mu$ M Rho kinase inhibitor Y-27632 (Tocris, UK).

### 2.3.1.2. Human colorectal organoid culture matrix and medium

Organoids were initially cultured in media made in-house at the Beggs laboratory which contained a blend of niche factors essential for organoid culture. Two different blends of reagents were used for organoid protocols, one with 2 conditioned media (R-spondin and Wnt) and with recombinant Noggin (see Table 2.1) and another blend containing a L-WRN conditioned media containing Wnt, R-spondin and Noggin expressed by cells (see Table 2.2). These two media were used in the method development stage of establishing organoids (Chapter 3).

Table 2.1 - Lab Made Organoid Culture Media A.

Reagent name	Supplier	Solvent	Final Concentration / Volume
Advanced DMEM F12	Gibco, USA	N/A	
HEPES	Gibco, USA	N/A	10mM
GlutaMAX-1	Gibco, USA	N/A	2mM
B27 supplement	Gibco, USA	N/A	1x
N-Acetylcysteine	Sigma-Aldrich, USA	Distilled water	1mM
Recombinant Noggin	Peprtech, UK	PBS/BSA (1%)	100ng/ml
Recombinant EGF	Gibco, USA	PBS/BSA (1%)	50ng/ml
R-spondin			10ml conditioning media
Wnt			35ml conditioning media
Recombinant FGF10	Peprtech, UK	PBS/BSA (1%)	100ng/ml
A-83-01	Sigma-Aldrich, USA	DMSO	500nM
SB202190	Tocris, UK	DMSO	10mM
Nicotinamide	Sigma-Aldrich, USA	Distilled water	10mM
Gastrin I	Sigma-Aldrich, USA	PBS/BSA (1%)	10nM

Table 2.2 - Lab Made Organoid Culture Media B.

Reagent name	Supplier	Solvent	Final Concentration / Volume
Advanced DMEM F12	Gibco, USA	N/A	
HEPES	Gibco, USA	N/A	10mM
GlutaMAX-1	Gibco, USA	N/A	2mM
B27 supplement	Gibco, USA	N/A	1x
N-Acetylcysteine	Sigma-Aldrich, USA	Distilled water	1mM
Recombinant EGF	Gibco, USA	PBS/BSA (1%)	50ng/ml
Recombinant FGF10	Peprtech, UK	PBS/BSA (1%)	100ng/ml
A-83-01	Sigma-Aldrich, USA	DMSO	50 nM
SB202190	Tocris, UK	DMSO	10mM
Nicotinamide	Sigma-Aldrich, USA	Distilled water	10mM
Gastrin I	Sigma-Aldrich, USA	PBS/BSA (1%)	10nM
Wnt			
R-spondin		}	35ml of L-WRN conditioned media
Noggin			

The organoid culture media was later substituted for a commercially available human intestinal organoid culture media – Human IntestiCult (StemCell Technologies, Canada). This media was used as organoid culture media for all of the experiments in this thesis.

Cultured organoids were laid on plates suspended in 100% Matrigel Basement Membrane Matrix Growth Factor Reduced, Phenol Red Free (Corning, USA).

#### **2.3.1.3. Chelation buffer**

Distilled water with 5.6mmol/l  $\text{Na}_2\text{HPO}_4$ , 8mmol/l  $\text{KH}_2\text{PO}_4$ , 96.2mmol/l sucrose, 54.9mmol/l D-sorbitol, 0.5mmol/l DL-dithiothreitol).

#### **2.3.1.4. Tumour dissociation buffer**

Advanced DMEM/F-12 supplemented with 2.5% FBS, 0.1mg/ml Primocin (Invivogen), 75U/ml collagenase IX (Sigma-Aldrich, USA) and 125 $\mu\text{g}/\text{ml}$  dispase II (Invitrogen).

#### **2.3.1.5. Freezing culture medium**

Advanced DMEM/F12 supplemented with 10% DMSO, 10% FBS and 0.1mg/ml Primocin.

### **2.3.2. Organoid derivation and maintenance**

#### **2.3.2.1. Cell harvesting for establishing patient derived organoids**

Tumour and normal tissue derived from the patient was kept in Roswell Park Memorial Institute (RPMI) with 0.1mg/ml Primocin until processed (no longer than

24 hours). Any residue fat was removed from the tissue and the sample was cut into 1cm pieces. Then the tissue pieces were transferred to a fresh 50ml tube containing ice cold Dulbecco's Phosphate Buffered Saline without magnesium and chloride (PBS0, Sigma-Aldrich, USA) and washed by vigorous shaking. The pieces of tissue were transferred to a new 50ml tube containing ice cold PBS0. This process was repeated until the supernatant was almost clear. Tissue pieces were transferred to a sterile 5ml tube containing Tumour Dissociation Buffer (for tumour tissue) or Gentle Dissociation Buffer (for normal tissue; STEMCell Technologies, Canada) and chopped further into smaller pieces using Castro-Viejo scissors. Tissue was further incubated at 37°C for 30 minutes (normal tissue) or 1 hour (tumour tissue). In order to remove leftover non-digested tissue pieces, the samples were passed through a 70um filter. The cell suspension was centrifuged at 200xg for 5 minutes and the supernatant was removed and discarded. The cell pellet was resuspended in thawed Matrigel. 50µl of the cell suspension was plated into 1 well of a pre-warmed 24-well cell culture plate and let to polymerise in a CO<sub>2</sub> incubator (37°C, 5% CO<sub>2</sub>) for 10 to 15 minutes. After making sure the Matrigel solidified, 500µl of human organoid media with 0.1mg/ml Primocin was added into a single well. Plates were incubated at CO<sub>2</sub> incubator (37°C, 5% CO<sub>2</sub>).

### **2.3.2.2. Passaging of organoids**

Approximately 7 days after seeding the plate, organoids are ready for passaging. Media was removed and 500µl of ice cold PBS0 was added into each well. Matrigel was disrupted and PBS0-organoid suspension was transferred to a 15ml falcon tube, then centrifuged at 400xg for 5minutes. Supernatant was carefully removed and organoids were resuspended in 1ml of TrypLE (Life Technologies, USA) and incubated in a water bath at 37°C for 3 minutes. Organoids were further broken down with pipetting up and down 3 to 5 times using a P1000 pipette and tip with P10 tip on top. Then 2ml of ice cold PBS0 were added to the suspension and centrifuged at 200xg for 5 minutes. The supernatant was carefully removed and the pellet was resuspended in Matrigel. 50µl of Matrigel containing digested organoids was plated into one well of a pre-heated 24-well cell culture plate and left in the incubator to polymerise. 500µl of organoid culture media was added to each well and plates were incubated in a CO<sub>2</sub> incubator (37°C, 5% CO<sub>2</sub>).

### **2.3.2.3. Cryopreservation of organoids**

2 to 3 days after passaging, media was removed and Matrigel was disrupted with Cultrex® Organoid Harvesting Solution (OHS; Trevigen, USA). The suspension was transferred into a 15ml falcon tube with 4ml of ice cold PBS0. Tubes were centrifuged at 150xg for 10 minutes at 4°C. Supernatant was carefully removed and organoids were re-suspended in 1ml of freezing culture media. 1ml of the

suspension was transferred into a labelled cryovial. Cryovial was placed in Mr. Frosty (Thermo Fisher Scientific, USA) and stored at -80°C. Frozen organoids for long term storage were transferred into liquid nitrogen storage.

When needed, cryopreserved organoids were thawed at 37°C and immediately transferred to 15ml falcon tube with 5ml of pre-warmed basal medium or Human IntestiCult medium. Organoids were centrifuged at 300xg for 5 minutes and the supernatant was discarded. The organoid pellet was resuspended in Matrigel and plated on a 24-well plate. Organoids were cultured in human organoids medium with 0.1mg/ml Primocin in a CO<sub>2</sub> incubator (37°C, 5% CO<sub>2</sub>).

#### **2.3.2.4. Mycoplasma screening**

All derived lines were frequently screened for the presence of mycoplasma with an EZ-PCR Mycoplasma Test Kit (Biological Industries, Israel) using the manufacturer's instructions.

#### **2.3.3. Organoid Assays**

##### **2.3.3.1. Plating organoids for irradiation and drug screening assays**

Organoids used for irradiation and drug screen experiments were always processed and plated 3 days after their last passage. At least 24h prior to the experiment each well of a 96-well clear bottom plate was laid with 40µl of Matrigel

and incubated at 37°C to polymerise. On the day of the experiment, one well of each line would be sacrificed for estimating the organoid count. This was done by aspirating the media from the well and resuspending the organoid culture in ice cold PBS0. Organoids were then transferred into a sterile 15ml falcon tube and centrifuged at 400xg for 5 minutes. The supernatant was carefully removed and discarded. The organoids were resuspended with 1ml of TrypLE Express and incubated at 37°C for 3 minutes. In order to dissociate organoids into single cells, additional mechanical disruption was performed using a P1000 pipette and tip with P10 tip placed on top of it. Once organoids were dissociated they were washed with PBS0 and centrifuged at 200xg for 5 minutes. Pelleted cells were resuspended in 1ml of PBS0. 50µl of the cell suspension was mixed with equal volume of Trypan Blue. 10µl of the Trypan Blue-cell mixture was applied onto the chambers of counting slides and cell were counted using an automated haemocytometer (TC20 Automated Cell Counter, Bio-Rad, USA). The average of two readings was recorded as a cell count for each well. As wells were always plated from a homogenous cell population, it was considered that the remaining wells plated from the same population would have a similar organoid count. For plating, 3 day old organoids were collected into 15ml falcon tubes and Matrigel was dissociated by incubating organoids in OHS on ice for 30 minutes followed by 400xg centrifugation. The supernatant was removed and discarded and the organoids were resuspended in an appropriate volume of Human IntestiCult. 100µl (for drug or combination assay) or 150µl (for irradiation assay) of the organoid suspension was plated onto each Matrigel covered well of a 96-well

plate; approximately 10 000 cells were plated per well using cell count from the well sacrifice. Plated organoids were used for drug, irradiation screening, or combination of drug and irradiation screening.

#### **2.3.3.2. Irradiation of organoids**

Organoids were exposed to 5Gy every day for 5 days, resulting in a total dose of 25Gy. The first dose was delivered to organoids that have been passaged 3 days prior to the experiment. Organoids were irradiated in their plates; either clear bottom 96-well plates for the viability experiments, or 24-well plates for irradiation effect sequencing experiments or for lysate extraction. Plates with their covers were secured with parafilm for transporting them to the radiation source, and kept that way for the duration of the irradiation process. The culture media was replaced every 2 days during the course of the radiation treatment. For the drug combination treatment see Section 2.3.3.3. Organoids for single-cell sequencing experiments were irradiated with an IBL 437C irradiator (CIS Bio International, France), a gamma irradiator that utilises a caesium source. The remaining experiments that involved irradiation of organoids were performed with an X-ray source irradiator CellRad (Precision X-ray, USA).

### 2.3.3.3. Drug screening of organoids

All used chemotherapeutic agents were resuspended in DMSO (Cell Signalling Technology, USA) to stock concentration of 20mM or 10mM and stored in -20°C. The list of all the drugs used in this thesis are listed in the Table 2.3. To prepare appropriate concentrations, stock solutions were diluted into working solutions using DMSO. Lists of dilutions for Rapamycin and Everolimus, and for AZD2014 and M-2206 can be found in Table 2.4 and Table 2.5 respectively. The working concentrations were diluted 1:500 with Human IntestiCult media resulting in twice the desired final concentration. Then, 100µl of drug-media suspension was added to each 96-well plate well containing plated organoids for the assay. Each drug concentration was tested in triplicate per line and control was Human IntestiCult media with 0.1% DMSO vehicle.

Table 2.3 - List of therapeutic agents and their targets.

<b>DRUG NAME</b>	<b>SUPPLIER</b>	<b>TARGET</b>	<b>SOLVENT</b>	<b>STOCK</b>
<b>RAPAMYCIN</b>	Sigma-Aldrich	mTORC1	DMSO	20mM
<b>EVEROLIMUS</b>	Adooq Bioscience	mTORC1	DMSO	20mM
<b>AZD2014</b>	Cayman Chemical	mTORC1 mTORC2	& DMSO	10mM
<b>MK-2206</b>	Cayman Chemical	Akt	DMSO	10mM

Table 2.4 - Concentrations for Rapamycin and Everolimus.

<i>For</i>	<i>Using</i>	<i>Dilution</i>	<i>Dilutant</i>	<i>Final concentration</i>
20 $\mu$ M	20mM stock	None	N/A	20mM
10 $\mu$ M	20mM stock	1 in 2	DMSO	10mM
2 $\mu$ M	10mM stock	1 in 5	DMSO	2mM
0.2 $\mu$ M	2mM stock	1 in 10	DMSO	0.2mM
0.1 $\mu$ M	0.2mM stock	1 in 2	DMSO	0.1mM
0.02 $\mu$ M	0.1mM stock	1 in 5	DMSO	0.02mM

Table 2.5 - Concentrations for AZD2014 and MK-2206.

<i>For</i>	<i>Using</i>	<i>Dilution</i>	<i>Dilutant</i>	<i>Final concentration</i>
10 $\mu$ M	10mM stock	None	N/A	10mM
1 $\mu$ M	10mM stock	1 in 10	DMSO	1mM
0. $\mu$ M	1mM stock	1 in 10	DMSO	0.1mM
0.01 $\mu$ M	0.1mM stock	1 in 10	DMSO	0.01mM
0.001 $\mu$ M	0.01mM stock	1 in 10	DMSO	0.001mM

The initial drug screens (with Rapamycin and Everolimus) were done with 6 different concentration points, however for later drug screens (with AZD2014 and MK-2206) 5 different concentration points were used. Additionally, along with the vehicle control, the initial assays also contained an only-media control without the DMSO. The plate layout was designed in a way to have the wells on the edges of the plate filled with PBS in order to reduce the evaporation from the wells containing media and 3 lines were fitted per plate (Figure 2.1). If more than 3

lines were included in the experiment another plate with corresponding layout was set up for those lines.

A.

PBS	PBS	PBS	PBS	PBS	PBS	PBS	PBS	PBS	PBS	PBS	PBS
0.02	0.02	0.02	0.1	0.1	0.1	0.2	0.2	0.2	2	2	2
10	10	10	20	20	20	v.	v.	v.	media	media	media
0.02	0.02	0.02	0.1	0.1	0.1	0.2	0.2	0.2	2	2	2
10	10	10	20	20	20	v.	v.	v.	media	media	media
0.02	0.02	0.02	0.1	0.1	0.1	0.2	0.2	0.2	2	2	2
10	10	10	20	20	20	v.	v.	v.	media	media	media
PBS	PBS	PBS	PBS	PBS	PBS	PBS	PBS	PBS	PBS	PBS	PBS

B.

PBS	PBS	PBS	PBS	PBS	PBS	PBS	PBS	PBS	PBS	PBS	PBS
PBS	0.001	0.001	0.001	0.01	0.01	0.01	0.1	0.1	0.1	PBS	PBS
PBS	1	1	1	10	10	10	v.	v.	v.	PBS	PBS
PBS	0.001	0.001	0.001	0.01	0.01	0.01	0.1	0.1	0.1	PBS	PBS
PBS	1	1	1	10	10	10	v.	v.	v.	PBS	PBS
PBS	0.001	0.001	0.001	0.01	0.01	0.01	0.1	0.1	0.1	PBS	PBS
PBS	1	1	1	10	10	10	v.	v.	v.	PBS	PBS
PBS	PBS	PBS	PBS	PBS	PBS	PBS	PBS	PBS	PBS	PBS	PBS

Figure 2.1 - Experimental plate layout for drug assays.

Triplicate technical repeats of different conditions were tested. 6 different concentrations of drug were used along with a vehicle control. 3 organoid lines (1, 2, 3) would fit on one plate.

A. The plate layout and concentrations used for screens with Rapamycin and Everolimus. A just media control was used as well in these initial assays.

B. The plate layout and concentrations used for screens with AZD2014 and MK-2206.

For the combination drug with irradiation assays organoids were plated as described in Section 2.3.3.1. Triplicate repeats of each organoid line were plated for each concentration and control on 96-well plates: Drug Only, Irradiation and Drug. Experiments with AZD2014 and MK-2206 would also include an Irradiation Only plate.

#### 2.3.3.4. Viability assay

Organoid viability was measured by a bioluminescent based assay that uses levels of ATP produced by live and metabolically active cells. Equal volume of reagent was added to the media with cells that were sat at room temperature for 30 minutes, and then mixed by pipetting up and down. The plate was covered with aluminium foil and left in the hood for 30 minutes incubation in order to allow the reagent to lyse the cells. Released ATP would then be used in the luciferase reaction and produce luminescence (Figure 2.2). The amount of light produced would correspond to the amount of viable cells.

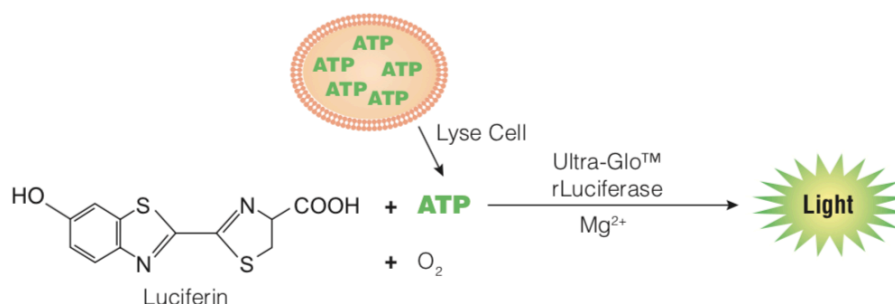


Figure 2.2 - Luciferase reaction.

Luciferin with the presence of ATP from lysed cells releases a light signal. The signal intensity can be measured with a luminescence reader and the viability of cells can be calculated.

The assay works by generating a stable luminescent signal caused by a reaction with ATP released from lysed cells. The intensity of the signal depends on the amount of ATP released from the cells.

The viability assay used for investigating organoid survival was CellTiter-Glo® 3D Cell Viability Assay (Promega, USA), which was used according to the manufacturer's instructions. The luminescence was read with a plate reader (EnSpire® luminescence plate reader, Perkin Elmer Life Science, USA). The viability values were normalised by dividing the luminescence values for the condition by luminescence of the control group. Results were visually represented and analysed using GraphPad Prism 8 software (GraphPad, USA).

#### **2.3.3.5. Fixing of organoids in formalin**

Media from each well was removed and organoids were resuspended in OHS and collected in 15ml falcon tube. Organoids were incubated in OHS on ice for 30 minutes in order to remove Matrigel completely and then centrifuged at 400xg for 5 minutes. The supernatant was removed and discarded. Organoids were resuspended in freshly prepared 4% solution of paraformaldehyde (PFA; made from 16% PFA, Thermo Fisher Scientific, USA) and incubated at room temperature for 1 hour. Suspended organoids were washed with 10ml of PBS and centrifuged at 400xg for 5 minutes. The supernatant was removed and discarded and organoids were resuspended in 1ml of PBS, transferred to a 1.5ml Eppendorf tube and centrifuged at 300xg for 5 minutes. The supernatant was removed, leaving only small amounts of PBS in which the organoids were resuspended initially. Then, organoids were resuspended in 200µl of 2% (w/v)

liquid agarose. Once the agarose with organoids set, they were moved into tissue embedding cassettes. The cassettes were placed overnight in PBS.

Following sections include protocols for paraffin embedding, haematoxylin and eosin staining, and immunohistochemistry. All of these protocols were performed in the assistance of, or alone by, Rachel Wheat – a member of the Beggs laboratory.

#### **2.3.3.6. Paraffin embedding of fixed organoids**

The cassettes containing formalin fixed organoids immersed in agarose were washed with 70% ethanol for 1 hour. This was followed by 1 hour incubation in 90% ethanol and 1 hour incubation in 100% ethanol. Then, the cassettes were incubated in HistoClear (Geneflow, UK) for 2 hours. The HistoClear was replaced twice during the incubation time. Using a HistoSatr paraffin embedding station (Thermo Fisher Scientific, USA) with the oven set to 58°C, fixed organoids were placed in stainless-steel moulds and immersed in molten paraffin for 2 hours. This was followed by the cassettes being immersed in molten paraffin and attached to the top of the stainless-steel moulds. The block was cooled down until solidified. The blocks were removed from the moulds and labelled. Blocks were stored at room temperature until cut into sections. The sections were cut using a microtome. Sections were investigated under a light microscope to find fixed organoids before proceeding to staining. Once sections containing organoids were identified, they were placed on the glass slips and used for staining.

## **2.4. Haematoxylin and Eosin (H&E) staining**

H&E staining was used to highlight the cellular structure of the tissue. The nuclei of cells are stained with blue by the application of hemalum – a complex formed from aluminium ions and oxidised haematoxylin. Following the nuclear staining the other cellular structures were counterstained with eosin, colouring the structures in shades of pink, red, and orange. The protocol used is summarised below.

The sections were immersed in HistoClear for 5 minutes, followed by 5 minute washes with 100% ethanol, then 90% ethanol, and finally 70% ethanol. Sections were placed in purified water for minutes before applying Harris Haematoxylin (Sigma-Aldrich, USA) for 30 seconds (extended to 10 minutes for stronger stain). The stain was then washed under running water for 5 minutes. Following the water wash, the sections were stained with eosin (Sigma-Aldrich, USA) for 3 minutes and washed with purified water for 5 seconds. Then, the 1 minute washes with 70% ethanol, 90% ethanol, and 100% ethanol were performed and finished with a 1 minute HistoClear wash. Stained sections were then mounted with DPX (Sigma-Aldrich, USA) onto glass slides.

## **2.5. Immunohistochemistry (IHC)**

IHC was used to selectively identify pan-Cytokeratin and CDX2 proteins in fixed organoid and primary tumour sections with primary antibodies. The DAKO EnVision™+ System kit (Agilent, USA) was used along with primary antibodies: pan-Cytokeratin (ab27988, Abcam, United Kingdom) and CDX2 (ab157524, Abcam, UK).

The slides were incubated at 60°C overnight in an oven. Following the incubation the slides were de-waxed using a 5 minute Histoclear wash. The slides then were dehydrated with subsequent 5 minute washes of 100%, 90%, and 70% ethanol. The slides were then washed with distilled water for 3 minutes and placed in a pre-heated antigen retrieval solution (Abcam, UK) using a pressure cooker. After the incubation, the slides were brought down to room temperature for approximately 10 minutes and the pressure was released. The pressure cooker was furthered cooled down with tap water for 30 minutes. The slides were removed and rinsed twice with PBS. The staining area was marked using PAP pen (Abcam, UK). The slides were incubated with a DAKO peroxidase block for 10 minutes in the humidified chamber. Subsequently, slides were washed in PBS for 3 minutes. This was repeated two more times. Following the washes, around 100µl of serum block was applied to each slide. The slides were incubated for 30 minutes in the humidified chamber. Any excess wax was removed with tissue paper by blotting. The primary antibodies were diluted in DAKO antibody dilutant; 1:500 for pan-Cytokeratin and 1:100 for CDX2. The slides were incubated with

the antibodies for 1 hour. The slides were washed 4 times with PBS for 3 minutes and then were placed in the humidified chamber for 30 minute incubation in a DAKO labelled polymer. This was followed by DAKO DAB incubation for 5-10 minutes and a distilled water wash. Slides were counterstained with haematoxylin for 30 seconds (or if necessary up to 10 minutes) and rinsed with tap water. The slides were immersed in 1% acid alcohol (HCL in 70% ethanol) and immediately taken out and washed with distilled water for 5 minutes. Slides were then washed with subsequent 1 minute incubations with 70%, 90%, and 100% ethanol followed by a 1 minute wash with HistoClear. Each stained slide was mounted with DPX, ready to be imaged with light microscopy.

## **2.6. Light microscopy**

For light microscopy investigation, an EVOS™ XL Core Microscopy and Imaging System (Thermo Fisher Scientific, USA) was used. Cultured cells and organoids, as well as FFPE organoid sections, were assessed under the microscope. Both 10x and 20x magnification settings were used. The images were taken by the built-in microscope software and exported as .jpg files. For primary tumour sections imaging, an Axio Scan.Z1 Slide Scanner (Zeiss, Germany) was used and the images were exported to Zeiss Zen Blue edition software v. 3.1 (Zeiss, Germany), where they were analysed and exported to .tiff files.

## **2.7. Nucleic acid extraction**

### **2.7.1. Sample disruption and homogenisation**

#### **2.7.1.1. DNA extraction from tissue**

30mg of fresh frozen tissue was cut on a petri dish sitting on a dry ice and immediately placed in a sterile 2ml tube containing RLT buffer with 0.01%  $\beta$ -mercaptoethanol and a 5mm stainless steel bead. The tissue was lysed using TissueLyser II (Qiagen, Germany) at 20Hz for 1 minute, and then the sample plate was rotated and set for another 1 minute at 20Hz.

#### **2.7.1.2. DNA extraction from organoids**

Media surrounding organoids was collected and organoids ( $\sim 10^5$  cells) were resuspended with RLT buffer containing 0.01%  $\beta$ -mercaptoethanol and transferred into a sterile 1.5ml Eppendorf tube. The tube was vortexed for 10 seconds and centrifuged briefly.

### **2.7.2. Nucleic acid extraction**

Both DNA and RNA were extracted and purified using a spin column-based purification. The method for nucleic acid extraction uses a matrix of silica beads that can either bind DNA/RNA for washing or release it during the elution step depending on the solution pH and salt concentration.

Tissue or cells were lysed as described in Section 2.7.1.1. Then, the DNA and RNA were extracted simultaneously using a DNA/RNA AllPrep Mini Kit (Qiagen, Germany) following the manufacturer's protocol from step 4. All of the centrifugations were performed at 8000xg.

DNA from blood was extracted using a Maxwell® RSC Instrument and Maxwell® RSC Buffy Coat DNA Kit (Promega, USA) according to manufacturer's instructions.

DNA was stored at -20°C and RNA was stored at -80°C.

## **2.8. Nucleic acid quantification and quality control**

### **2.8.1. 2.6.1 Qubit™**

Extracted DNA and RNA were quantified with Qubit™ Broad Range DNA and Qubit™ Broad Range RNA assays (Invitrogen, USA) accordingly. Additionally, generated libraries and pooled concentrations were quantified with a Qubit™ High Sensitivity DNA assay. A mix of buffer and a dye included with the kit was freshly prepared with a 200:1 ratio. 1µl of sample (DNA, RNA, or cDNA) was mixed with 199µl buffer-dye mix. Two standards supplied with the manufacturer were also prepared (10µl standard with 190µl buffer-dye mix) to ensure accurate read out. The samples were quantified after 2 minute room temperature incubation using Qubit™ 3.0, a digital luminescence reader.

### **2.8.2. TapeStation**

In addition to nucleic acid quantification, both DNA and RNA quality were checked with TapeStation (Agilent Technologies, USA). For the quality of the DNA and RNA extracts the Genomic DNA ScreenTapes and High Sensitivity RNA ScreenTapes (Agilent Technologies, USA) were used according to the manufacturer's instructions. The DNA integrity number (DIN) and RNA integrity number (RIN) was investigated to establish the quality of extracted nucleic acids, with good quality considered to be between 8 and 10. For quality control of generated libraries, the D1000 ScreenTapes (Agilent Technologies, USA) were used. In addition to DIN and RIN, an average base pair length was calculated. The instrument used for running ScreenTapes was TapeStation2200 (Agilent, USA) and the software to analyse the DIN and RIN values, as well as the average base pair length, was the TapeStation Analysis Software, version A.02.02 (Agilent Technologies, USA).

### **2.9. Sequencing**

All sequencing done for this thesis was next generation sequencing (NGS) using Illumina sequencing instruments. This sequencing method is based on clonal amplification of the sample and sequencing by synthesis chemistry – a process that recognises the nucleic acid bases while combining them into a chain. Each

base can be identified as it emits unique fluorescent signal when it is added to the growing chain, which determines the sequence order.

## **2.9.1. DNA Sequencing**

### **2.9.1.1. Panel Sequencing**

Targeted DNA sequencing was used for investigating organoid mutational profiles. A custom panel (QIAseq Targeted DNA Panel, Qiagen, Germany) of 30 genes that are commonly mutated in colorectal cancer have been used for generating libraries for sequencing. The full list of gene is in Table 2.6.

Table 2.6 - List of genes for the targeted panel sequencing.

<i>Gene name</i>	<i>Chromosome</i>
<i>RPL22</i>	1
<i>ARID1A</i>	1
<i>NRAS</i>	1
<i>ELF3</i>	1
<i>ZFP36L2</i>	2
<i>MSH2</i>	2
<i>MSH6</i>	2
<i>ACVR2A</i>	2
<i>BMPR2</i>	2
<i>MLH1</i>	3
<i>CTNNB1</i>	3
<i>PIK3CA</i>	3
<i>FBXW7</i>	4
<i>APC</i>	5
<i>BRAF</i>	7
<i>PTEN</i>	10
<i>TCF7L2</i>	10
<i>ATM</i>	11
<i>BCL9L</i>	11
<i>KRAS</i>	12
<i>POLE</i>	12
<i>B2M</i>	15
<i>TP53</i>	17
<i>RNF43</i>	17
<i>SOX9</i>	18
<i>TGIF1</i>	18
<i>SMAD2</i>	18
<i>SMAD4</i>	18
<i>POLD1</i>	19
<i>GNAS</i>	20

40ng of DNA from each line was used as an input for the library preparation and the protocol was carried out according to the manufacturer's instruction. When preparing all of the mixes, the amount required for each reagent was multiplied

by the number of samples being processed at the time with 10% additional to account for pipetting error.

#### **2.9.1.1.1. Fragmentation with end-repair and A-tailing**

An enzymatic fragmentation of DNA was carried out in order to fragment the input DNA in the same reaction with end-repair and A-tailing. A fragmentation mix was prepared containing 2.5µl of 10x fragmentation buffer and 0.75µl of FERA solution. 3.25µl of the fragmentation mix was added to each DNA sample (40ng) and the volume was brought up to total of 20µl for each sample. The samples were then placed in the thermocycler with the following cycling conditions (see Table 2.7).

Table 2.7 - Fragmentation, end-repair and A-tailing program.

Step	Incubation temperature	Incubation time
1	4°C	1 min
2	32°C	24 min
3	72°C	30 min
4	4°C	Hold

#### **2.9.1.1.2. Adapter ligation**

The adapter ligation mix was prepared with 10µl of 5x ligation Buffer, 5µl of DNA ligase, 7.2µl of ligation solution, and 2.8µl of IL-N701 adapter per reaction. Then,

25µl of ligation mix was added to each 25µl sample. The reaction was then incubated in the thermal cycler at 20°C for 15 minutes. The adapter-ligated fragments were then cleaned up using SPRI beads according to the manufacturer’s instructions.

### 2.9.1.1.3. Target enrichments

Following the adapter-ligation, the cleaned up DNA fragments were enriched for targeted regions by adding 9.6µl of the enrichment mix (4µl 5x TEPCR buffer, 5µl Qiaseq Targeted DNA Panel, 0.8µl IL-Forward primer, and 0.8µl HotStarTaq DNA Polymerase) to each reaction and using the cycling conditions recommended by the manufacturer based on the number of custom primers in the targeted panel (see Table 2.8).

Table 2.8 - Target enrichment program.

Step	Temperature	Time	Number of cycles
1	95°C	13 min	1 cycle
2	98°C	2 min	1 cycle
3	98°C	15 sec	6 cycles
4	65°C	15 min	
5	72°C	5 min	1 cycle
6	4°C	5 min	1 cycle
7	4°C	Hold	Hold

The enriched products were cleaned up with Solid Phase Reversible Immobilization (SPRI) beads according to manufacturer's instructions.

#### **2.9.1.1.4. PCR amplification**

Cleaned up enriched fragments were barcoded and amplified with a universal PCR. For this step, a primer plate with unique indexes was used and, as instructed by the manufacturer's instructions, the reagents were directly added to the plate containing the dried primers with unique indexes. 13.4µl of cleaned up library product was added to a well containing a unique index. Following this, a PCR mix containing 4µl 5x UPCR buffer, 1µl HotStaTaq Polymerase, and 1.6µl nuclease-free water was added to each reaction. Each reaction was carefully mixed by pipetting up and down at least 10 times. Each reaction was transferred to a fresh plate and a PCR was set up using the following cycling conditions (Table 2.9):

Table 2.9 - PCR amplification program.

Step	Temperature	Time	Number of cycles
1	95°C	13 min	1
2	98°C	2 min	1
3	98°C	15 sec	21
4	60°C	2 min	
5	72°C	5 min	1
6	4°C	5 min	1
7	4°C	Hold	Hold

21 cycles have been selected as per manufacturer's recommendation based on the number of primers. The PCR products were cleaned up using SPRI beads according to the manufacturer's protocol.

Following the clean-up, the quality of the libraries was checked by quantifying the libraries with Qubit and using a high sensitivity D1000 TapeStation (Agilent Technologies) in order to check their quality and average base size.

#### **2.9.1.1.5. Library pooling and sequencing**

Following quality control, the samples were pooled at the same concentration into one final library. A final quality control was performed by quantifying with Qubit DNA Broad Range and running the library with High Sensitivity D1000 TapeStation. After quality control, the library was diluted to 4nM.

The library was processed to be loaded for sequencing with a MiSeq instrument (Illumina, USA) using the manufacturer's protocol. The library was denatured with 20% Sodium Hydroxide and Trizma hydrochloride (Sigma-Aldrich, USA) and furthered diluted with HT1 hybridization buffer according to manufacturer's instructions. A standard 1% PhiX spike in control was added to the final library, which was then loaded onto the MiSeq cartridge. Pooled samples were sequenced with a MiSeq instrument with paired end sequencing on a 300 cycle high output flow cell.

#### **2.9.1.2. Whole genome sequencing**

DNA extracted from irradiated and control organoids, along with DNA extracted from original tumour the organoids were derived from and DNA from matching normal tissue was sent to Novogene for whole genome sequencing. The library preparation and sequencing was performed outside of our laboratory. Samples were quantified in order to ensure 1µg input. Additionally, the integrity of the DNA was checked with TapeStation, ensuring the sample was not fragmented, was of good quality, and the DIN score was above 8 to ensure successful library preparation.

## **2.9.2. RNA Sequencing**

For total RNA sequencing TruSeq Stranded Total RNA library preparation kit (Illumina, USA) was used according to manufacturer's instructions. The workflow for generating the library for RNA sequencing consisted of 6 steps. The summary of each step is described below.

### **2.9.2.1. RiboZero Depletion and RNA fragmentation**

Each sample of RNA was normalised with nuclease-free water for 100ng input in the final volume of 10 $\mu$ l. 5 $\mu$ l of rRNA Binding Buffer and 5 $\mu$ l of rRNA Removal Mix were added to each sample. Samples were then incubated at 68°C for 5 minutes in the thermocycler with heated lid (lid temperature: 100°C). Following the incubation, samples were left at room temperature for 1 minute. Then using rRNA Removal Beads the rRNA was depleted by mixing in 35 $\mu$ l of the beads to each sample. The supernatant was transferred to a fresh PCR plate and cleaned up with SPRI beads according to the manufacturer's instructions. Following the clean up the samples were incubated at 94°C for 8 minutes in the thermocycler with heated lid (lid temperature: 100°C).

### 2.9.2.2. cDNA synthesis

The first strand of cDNA was synthesised by first combining 1µl of SuperScript II with 9µl of First Strand Act D Mix. 8µl of the mix was then added to each sample and was incubated in the thermal cycler with the following conditions (Table 2.10):

Table 2.10 - cDNA synthesis program.

Step	Temperature	Time
1	25°C	10 min
2	42°C	15 min
3	70°C	15 min
4	4°C	Hold

Following the synthesis of the first strand, the second strand was synthesized by adding 5µl of Resuspension Buffer and 20µl of Second Strand Marking Mix to each reaction. Samples were incubated at 16°C for 1 hour in the thermal cycler. Following the incubation, samples were equilibrated to room temperature by being placed on the bench for 5 minutes. A SPRI bead based clean-up was performed according to the protocol instructions before continuing to the next step.

### 2.9.2.3. Adenylation of 3' ends and adapter ligation

3' ends were adenylated by adding 2.5µl of Resuspension buffer and followed by adding 12.5µl of A-tailing to each sample. Samples were incubated in the thermal cycler with heated lid (lid temperature: 100°C) and the following cycling conditions (Table 2.11):

Table 2.11 - Adapter ligation program.

Step	Temperature	Time
1	35°C	30 min
2	70°C	5 min
3	4°C	Hold

Following the incubation, 2.5µl of Resuspension Buffer and 2.5µl of Ligation Mix were added to each sample. Then, 2.5µl of a unique Adapter Index was added to each sample and mixed gently by pipetting up and down 10 times. Samples were incubated at 30°C for 10 minutes. 5µl of Stop Ligation Buffer was added to each sample and a SPRI beads based clean-up was performed following the manufacturer's instructions.

#### 2.9.2.4. PCR amplification

Adapter ligated cDNA strands were amplified by universal PCR. 5µl of PCR Primer Cocktail and 25µl of PCR Master Mix were added to each reaction and run on the thermal cycler with the following conditions (Table 2.12):

Table 2.12 - PCR amplification program.

Step	Temperature	Time	Number of cycles
1	98°C	30 sec	1
2	98°C	10 sec	15
3	60°C	30 sec	
4	72°C	30 sec	
5	72°C	5 min	1
6	4°C	Hold	Hold

The amplified libraries were cleaned up with SPRI beads according to the manufacturer's instructions.

#### 2.9.2.5. Library normalisation and pooling

Each library was quantified with Qubit DNA Broad Range (Thermo Fisher Scientific, USA) and High Sensitivity D1000 TapeStation (Agilent Technologies, USA). When the quality control met the requirements, all samples were normalised and pooled together into one library. The library underwent a final

quality control quantification and TapeStation run. The pooled library was then further diluted to 4nM.

#### **2.9.2.6. Sequencing**

The library was processed to be loaded onto sequencing with NextSeq 550 instrument (Illumina, USA) using the manufacturer's instructions. The library was denatured with 20% Sodium Hydroxide and Trizma hydrochloride (Sigma-Aldrich, USA) and further diluted with HT1 hybridization buffer according to manufacturer's instructions. 1% PhiX spike in control was added to the final library, which was then loaded onto the NextSeq cartridge. Pooled samples were sequenced with NextSeq 550 instrument with paired end sequencing on a 300 cycle high output flow cell.

### **2.9.3. Chromium single cell 3' sequencing**

#### **2.9.3.1. Overview**

Single-cell RNA sequencing utilises NGS technology providing high resolution information of gene expression from individual cells. There are different methods of single cell sequencing available. In this thesis all single cell sequencing was performed using a Chromium Single Cell 3' Gene Expression v2 Kit (10x Genomics). The 10x Chromium solutions allow labelling of each individual cell

with their GEMs (gel beads in emulsion) technology. Oligo barcoded gel beads are combined with individual cells and separated with partitioning oil into GEMs which are then further processed in a library preparation process (see Figure 2.3 A). Each gel bead consists of four parts (see Figure 2.3 B), which include a unique 10x barcode, UMI (unique molecular identifier) – unique for each cell, which will allow accurate quantification of gene expression.

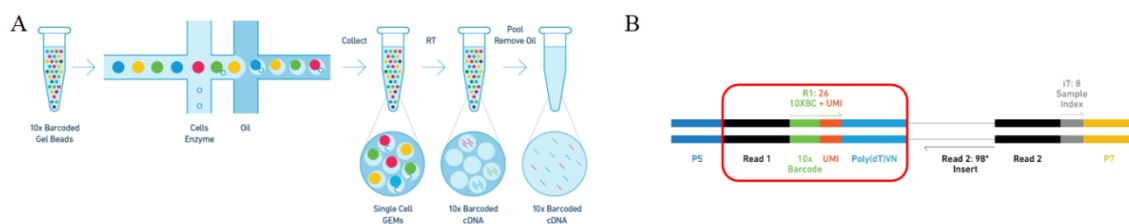


Figure 2.3 - The Principal for the 10x Chromium Single Cell Sequencing.

A) Microfluidic partitioning of reagents and cells into gel beads in emulsion (GEMs). Gel beads flow from left to right and are mixed with cells before being surrounded by the partitioning oil.

B) Final library product with highlighted oligo-barcoded gel beads. Gel beads consisting of 4 main parts – partial Illumina Read 1 sequence, crucial for the library preparation, 10x bead specific barcode, UMI- unique molecular identifier, unique for the, Poly(dT) end, which enables capture of polyadenylated molecules.

### 2.9.3.2. Organoid preparation

Media from wells was removed and organoids were resuspended in ice cold OHS, collected into a sterile 15ml collection tube and left on ice for 30 minutes in order to dissociate Matrigel. Organoids were centrifuged at 300xg and the supernatant was discarded. Organoids were washed with ice cold PBS0 in order to remove any residual Matrigel. The supernatant was discarded and the organoid pellet was resuspended in 1ml TrypLE with 10µM Rho kinase inhibitor

Y-27632 and incubated at 37°C in a water bath for 5 minutes. Following the incubation 5ml of ice cold PBS0 was added to the organoids suspension and additional gentle mechanical disruption was performed in order to ensure the single cell suspension. The cell suspension was washed with PBS0 twice. Lastly, cells were resuspended in 500µl of PBS0 and strained through a Flowmi™ 40µm Cell Strainer. Before progressing to cell labelling, the count and quality (live cell count) was investigated using a cell counter model (BioRad, USA). The expected viability of cells to proceed with the protocol was at 75%, however for organoids post irradiation treatment 70% threshold was accepted (the viability and the live cell counts of samples that proceeded further for the single-cell sequencing can be seen in Table 2.13)

Table 2.13 - Samples viability and cell counts

Sample Name	Viability	Live cell count
<b>S292064</b>	80%	8.50 x10 <sup>6</sup>
<b>S292064 irradiated</b>	81%	3.30 x10 <sup>6</sup>
<b>S302389</b>	75%	2.62 x10 <sup>6</sup>
<b>S302389 irradiated</b>	72%	3.18 x10 <sup>6</sup>

### 2.9.3.3. GEM generation and barcoding

The Chromium Chip B was assembled in a 10x Chip Holder and 50% Glycerol Solution was dispensed into the unused chip wells: 75µl for row labelled 1, 40µl for row labelled 2, and 280µl for row labelled 3. Samples were normalised in order

to achieve 10 000 cell recovery, and mixed with Master Mix for a total volume of 80µl. 75µl of cell suspension mix was loaded into wells in row labelled 1. 40µl of Gel Beads were loaded into the wells in the row labelled 2. Finally, 280µl in two parts (2x 140µl) of Partitioning Oil was dispensed into wells in row labelled 3. 10x Gasket was attached to the Chip Holder, which was then placed in the Chromium Controller and program Chromium Single Cell B was run. 100µl of GEMs were transferred from the wells into a fresh tube strip placed on ice. The recovered GEMs were incubated in the thermal cycler with the following conditions (see Table 2.14). The lid temperature was set to 53°C.

Table 2.14 - Post GEM barcoding incubation.

Step	Temperature	Time
1	53°C	45 min
2	85°C	5 min
3	4°C	Hold

#### 2.9.3.4. cDNA Library Construction

125µl of Recovery Agent was added to each sample and mixing was avoided. Samples were incubated for 2 minutes at room temperature. 125µl of the Recovery Agent/Partitioning Oil from the bottom of the tube was removed and discarded. 200µl of Dynabeads Cleanup Mix was added to each sample and incubated at room temperature for 10 minutes. Tube strip containing samples was placed on a 10x Magnetic Separator set at a High position. Supernatant was

removed and beads were washed with 300µl of ethanol. A second wash with 200µl of ethanol was performed and the samples were moved to a Low position on the magnet. After all ethanol was removed and air dried, samples were eluted in 35.5µl of Elution Solution. 35µl of eluted samples were transferred to a new strip tube and taken to the PCR amplification. The Amplification Mix containing 50µl of Amp Mix and 15µl of cDNA Primers were added to each 35µl sample. The samples were placed in the thermal cycler and run with cycling conditions summarised in Table 2.15. The lid temperature was set to 105°C and the number of cycles was set for the amount recommended by the manufacturer.

Table 2.15 - cDNA library construction program.

Step	Temperature	Time	Number of cycles
1	98°C	3 min	1
2	98°C	15 sec	11
3	63°C	30 sec	
4	72°C	1 min	1
5	72°C	1 min	1
6	4°C	Hold	Hold

The PCR products were cleaned up with SPRI beads and ethanol according to the manufacturer's instructions.

### 2.9.3.5. Fragmentation, end repair, and A-tailing

10µl of purified cDNA samples were taken to the fragmentation, end repair, and A-tailing reaction. 25µl of buffer EB was added to each sample with a Fragmentation Mix containing 5µl of Fragmentation Buffer and 10µl of Fragmentation Enzyme. Samples were transferred to a pre-cooled thermal cycler and further incubated with the conditions listed in the Table 2.16. The lid temperature was set to 65°C.

Table 2.16 - Fragmentation, end repair and A-tailing program.

Step	Temperature	Time
1	4°C	Hold
2	32°C	5 min
3	65°C	30 min
4	4°C	Hold

Following the incubation the samples were cleaned up with SPRI beads and ethanol according to the manufacturer's instructions.

### 2.9.3.6. Adaptor ligation

Adaptor Ligation Mix containing 20µl Ligation Buffer, 10µl DNA Ligase, and 20µl Adaptor Oligos was added to each sample and incubated at 20°C for 15 minutes in the thermal cycler with the lid temperature set to 30°C. Once finished, the

samples were cleaned up with SPRI beads and ethanol according to the manufacturer's instructions.

### 2.9.3.7. Index PCR

Samples were indexed and amplified with universal PCR. 50µl of Amp Mix was added to each sample along with 10µl of SI Primer containing a unique index. Samples were incubated in a thermal cycler with heated lid (lid temperature: 105°C) at the cycling conditions in Table 2.17.

Table 2.17 - Indexing program.

Step	Temperature	Time	Number of cycles
1	98°C	45 sec	1
2	98°C	20 sec	
3	54°C	30 sec	12
4	72°C	20 sec	
5	72°C	60 sec	
6	4°C	Hold	Hold

The number of cycles was adjusted to the cDNA following protocol recommendations. Final PCR product was cleaned up with SPRI beads and ethanol according to the manufacturer's instructions.

### **2.9.3.8. Library normalisation and pooling**

The generated libraries were quantified with Qubit DNA Broad Range and run on a TapeStation with D1000 High Sensitivity ScreenTapes (Agilent Technologies, USA). Libraries that met the quality control were normalised and pooled together. The library pool was further diluted to a 4nM final concentration.

### **2.9.3.9. Sequencing**

The libraries were prepared the same way as described in Section 2.9.2.6 and sequenced with a NextSeq 550 instrument (Illumina, USA) with the paired end sequencing on a 300 cycle high output flow cell (Illumina, USA).

## **2.10. Methylation array**

Methylation arrays provide quantitative examination of selected methylation sites across the genome. Methylation sites were investigated with Illumina technology, utilising the BeadChip platform that generates a genome-wide profile of human methylome. BeadChip technology relies on two different types of beads that detect CpG methylation. The U bead type matches the unmethylated CpG, whereas the methylated site is matched by the M bead type (Figure 2.4).

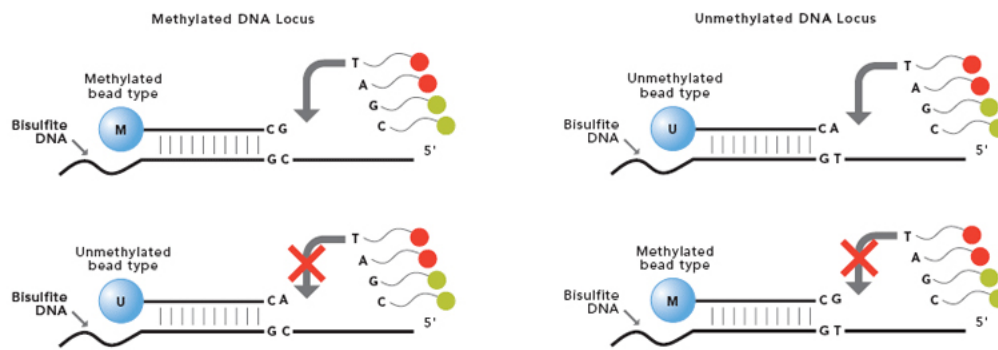


Figure 2.4 - 450k methylation array chemistry.

Two site specific probes designed to catch methylated loci (M bead type) and unmethylated loci (U bead type). The signal is emitted with the fluorescent reagent of the labelled ddNTPs which are incorporated with single-base extension. The methylation levels can be determined by calculating the ratio of the detected signals from the methylated and unmethylated sites.

### 2.10.1. Bisulfite DNA conversion

In order to detect methylation on genomic DNA, first it requires bisulfite conversion. In this process the unmethylated cytosine is converted into uracil, while the methylated cytosine stays unconverted. Bisulfite conversion was performed using an EZ DNA Methylation Kit (Zymo Research, USA) with 500ng DNA input, and the protocol was followed with the following adjustments. 7.5µl of M-Dilution Buffer was added to the normalised DNA sample adjusting the total volume to 50µl with water. Then samples were mixed by pipetting up and down and incubated for 30 minutes at 42°C. Following the incubation 97.6µl of prepared CT Conversion Reagent was added to each sample and mixed. Next steps of the protocol were followed according to the manufacturer's instructions. The efficiency of bisulfite conversion was investigated post array scanning as an array quality control.

## **2.10.2. 450k Arrays**

### **2.10.2.1. DNA amplification**

4µl of bisulfite converted DNA was moved to a MIDI microplate and combined with 20µl of MA1, 4µl of 0.1N sodium hydroxide (NaOH), and incubated for 10 minutes at room temperature. Following the incubation 68µl of RPM and 75µl of MSM were mixed into each reaction and hybridised for 20 hours and 45 minutes at 37°C in the Illumina Hybridisation Oven.

### **2.10.2.2. DNA fragmentation and precipitation**

Following the hybridisation 50µl of FMS was added to each sample and incubated for 1 hour at 37°C. After the incubation the DNA was precipitated with PM1 reagent and 2-propanol and the dried pellet was resuspended with 46µl of RA1 according to the manufacturer's instructions.

### **2.10.2.3. Hybridisation to BeadChip**

The fragmented DNA was incubated at 95°C for 20 minutes followed by incubation at room temperature for 30 minutes. The hybridisation chambers were prepared by putting the BeadChip Hyb Chamber gaskets into the BeadChip Hyb Chambers and 400µl of PB2 was dispensed into humidifying buffer reservoirs in

the Hyb Chambers. The chambers were covered with the lid to prevent evaporation. 12x1 BeadChip was used and 15µl of each DNA sample was loaded onto the appropriate section of the BeadChip. The Hybridisation Chamber with the BeadChips were placed in the Illumina Hybridisation Oven and incubated at 48°C for 17 h and 45 min. Following the incubation the BeadChips were washed with PB1 and Flow-Through Chambers were assembled according to the protocol's instructions.

#### **2.10.2.4. BeadChip extend and stain**

Flow-Through Assembly was in the Chamber rack once equilibrated to 44°C. The following reagents were pipetted into the glass back plate of the reservoir:

1. 150µl RA1 incubated for 30 seconds, repeated for a total of 5 times.
2. 45µl XC1 incubated for 10 minutes.
3. 450µl XC2 incubated for 10 minutes.
4. 200µl TEM incubated for 15 minutes.
5. 450µl 95% formamide/1mM EDTA incubated for 1 minute, repeated for a total of 2 times.

All reagents were then incubated for a further 5 minutes. The chamber rack temperature was ramped up to the temperature indicated on the STM tube. Finally, 450µl of XC3 was added and incubated for 1 minute. The protocol

proceeded immediately to staining the BeadChip, where the following incubations were done using the specified reagents:

1. 250µl STM incubated for 10 minutes.
2. 450µl XC3 incubated for 1 minute, repeated for a total of 2 times.
3. 5 minute incubation.

This 3 step cycle was repeated 4 times and immediately followed with PB1 and XC4 washes. The prepared BeadChip was scanned using an iScan system and the Methylation NXT scan setting was selected according to the manufacturer's instructions.

## **2.11. Data analysis**

### **2.11.1. Panel Sequencing**

The sequencing data was analysed using Biomedical Genomics Workbench software (Qiagen, Germany) using a custom workflow for analysing QIAseq Targeted DNA Panels generated by the manufacturer. The reference genome hg19 was used for aligning the data. The list of variants was produced by the software available as a .csv file. Silent mutations were filtered out and all other variants were referenced using ClinVar and COSMIC databases.

### **2.11.2. Whole Genome Sequencing**

The whole genome analysis was performed by Dr Mohammed Elasrag. The raw data quality was obtained with FastQC tools (Andrews, 2010). Once the data passed the quality control, the sequencing reads were aligned to the reference genome (GRch38) using BWA aligner (Li and Durbin, 2009). Aligned files were sorted with SAMtools (Li et al. 2009) and PCR duplicates were removed with Picard tools. Insertions, deletions and single nucleotide variants were called using the Genomic Variant Call Format (GVCF) using GATK and the Unified Genotyper function. The Integrative Genomics Viewer (IGV; <https://www.broadinstitute.org/igv/>; Robinson et al. 2011) was used for visualisation and interactive exploration of the aligned data files. The variants were annotated using VEP software (McLaren, et al. 2016).

### **2.11.3. RNA Sequencing**

The sequencing data was processed and analysed with the help of a bioinformatician from the Computational Centre of Bioinformatics (CCB) – Grigorios Papatzikas.

Data was aligned and quality control was performed using the Partek Flow computational application. The data was counted for gene counts with the same software. The reads were aligned to human reference genome hg19 cDNA index (Ensemble release 75) with STAR. Gene-level differential expression was

analysed using R (v.3.6.1) and the DESeq2 package (v.1.26.0, Love et al. 2014). Differential analysis compared cases of patients that completely responded to radiotherapy to cases of patient that did not respond to radiotherapy. Differentially expressed genes (DEGs) were calculated with the Wald statistical test, correcting for multiple comparisons with the Benjamini-Hochberg method using an adjusted p-value threshold of 5% ( $p_{adj} < 0.05$ ). Transcripts per million (TPM) expression values were calculated to normalise for sequencing depth and gene length (Li et al, 2010). Principal Component Analysis (PCA) was generated with  $\log_2\text{TPM}+1$  values with the *PCAtools 1.0.0* package (Blighe and Lun, 2021). Additionally, The  $\log_2\text{TPM}+1$  expression values were also used in generating heatmaps and in hierarchical clustering with the Ward method and distance: 1 – Spearman’s rank correlation. For heatmap generation the gplot v.3.0.1.2 R package (Warnes et al. 2009) was used. Finally, rather than focusing only on significant genes, we have used gene set enrichment analysis with the *SetRank v1.1.0* R software package (Simillion et al., 2017) to identify statistically significant pathways (SetRank parameter thresholds:  $\text{setPCutoff} = 0.01$  and  $\text{fdrCutoff} = 0.05$ ).

For organoid irradiation experiments, the same process was done, but heatmaps were generated with gplot v.3.0.1.2 using FPKM normalised values and the hierarchical clustering was performed using the Ward.D2 method with distance: 1- Spearman’s rank correction. The gene set enrichment analysis (GSEA) was performed using the SetRank package (version Simillion et al. 2017). P-values were adjusted using the Benjamini-Hochberg method and unless stated

otherwise, adjusted p-values were used for determining the significance using a cut off value of 0.05.

#### **2.11.4. Single-cell sequencing**

The initial analysis of the data was performed using a 10x Genomics data analysis tool – Loupe Browser (v.2.0.0 10x Genomics, USA). Single-cell sequencing data was analysed by Professor Andrew Beggs and Professor Christopher Yau. For the analysis, Seurat R package v.3 was used (Stuart et al. 2019). In order to analyse the data, all single cell runs were merged into a single *SeuratObject* with metadata indicating line of origin and radiation status. Data was then log transform normalised, scaled, and dimensionality reduction was performed with principal component analysis in order to estimate clusters. Cell clustering was performed by calculating a K-nearest neighbour (KNN) graph then the Louvain algorithm was used to iteratively group cells together. Non-linear dimensional reduction plots were generated to visualise and explore the dataset.

#### **2.11.5. Methylation array**

The methylation array scanning output was processed with Genome Studio (v.2011.1, Illumina, USA), where all internal scanning quality controls have been checked. The data was normalised and analysed using the ChAMP package (v.2.10.2, Tian et al. 2017) on R (version 3.5.1) using the package pipeline. The

p-values were adjusted with the Benjamini-Hochberg method. The GSEA was performed using the Empirical Bayes (eBayes) method and significance was determined using area under curve (AUC) score with cut off at 0.75 score.

## **2.12. Protein analysis**

### **2.12.1. Protein extraction**

Protein was extracted from organoids by first breaking down the Matrigel with ice cold Cultrex® Organoid Harvesting Solution and transferring organoids to 15ml falcon tube. The tube with organoids was kept on ice for 10 minutes and then centrifuged at 400xg for 5 minutes. Supernatant was removed and the organoid pellet was resuspended in RIPA buffer (ThermoFisher Scientific, USA) with 1x Protease/Phosphatase inhibitor cocktail (Cell Signalling Technology); 100µl of the RIPA/inhibitor cocktail solution was used per organoids collected from 3 wells of 24-well plate. The organoids were left to lyse on ice for 30 minutes. Lysates were transferred to a fresh 1.5ml Eppendorf tube and incubated at 100°C for 5 minutes. Further, lysates were sonicated twice for ten seconds and centrifuged at 13000xg for 5 minutes to pellet remaining debris. The supernatant was transferred to a fresh 1.5ml Eppendorf tube. Lysates were stored at -80°C.

### **2.12.2. Protein quantification**

Protein was quantified using the Pierce BCA Protein Assay Kit (Thermo Fisher Scientific, USA). A 50:1 ratio solution of reagent A and reagent B respectively was prepared and 200 $\mu$ l of the solution was added to a 96-well plate per sample and standard. A range of protein standards (0, 25, 125, 500, 750, 1000, 15000, and 2000 $\mu$ l/ml) was prepared with Bovine Serum Albumin (BSA, supplied with the kit) in RIPA. 10 $\mu$ l of sample or standard was added to reagent solution in duplicate and mixed. The plate was incubated at 37°C for 30 minutes. The results were collected by reading the plate at 540nm on a microplate spectrophotometer (EnSpire, PerkinElmer, USA). Average background from the 0 $\mu$ g/ml standard was subtracted from the other readings and a standard curve was graphed from the BSA standard values using Microsoft Excel. Concentrations of the samples were calculated using the standard curve.

### **3. RESULTS CHAPTER 1: METHOD DEVELOPMENT – ESTABLISHING HUMAN COLORECTAL ORGANOID CULTURES**

#### **3.1. Introduction**

Organoids are 3D tissue constructs grown in vitro that can be derived from PSCs or ASCs that are able to self-organise into structures that mimic their corresponding in vivo organ with their microanatomy and organ specific differentiated cell types (Kretzschmar and Clevers, 2016).

Research into the understanding of intestinal stem cell niche over the years was essential for the initial development of 3D cultures. One of the most crucial discoveries that subsequently led to establishing the first organoid culture was defining *Lgr5* as an intestinal stem cell specific marker gene. This discovery allowed purification and characterisation of the intestinal stem cells, which further gave insight into adult intestinal stem cells and the fact that they can be proliferative in vivo (Barker et al. 2007). It was then vital to identify all of the essential niche factors required for maintaining stem cells in an undifferentiated state, as well as allowing stem cell differentiation. The very first organoids were derived from mouse intestines as the intestinal stem cell niche was recreated in vitro. The niche factors discovery was inspired by genetic mouse studies showing EGF and Wnt activity is needed for epithelial proliferation and stem cell renewal, whilst differentiation is controlled through BMP signalling. Consequently, the first organoid media contained a Wnt signalling activator (R-spondin), EGF as a

mitogen, and Noggin – which inhibits BMP activity (Kim, Koo and Knoblich, 2020). For derivation of human organoids the media need to be supplemented with additional factors. It was found that unlike in murine cultures, the human intestinal organoids are not fully functional in secreting Wnt niche, therefore human organoid media had to be supplemented with exogenous Wnt3a. Additionally, it has been found that long-term culture and passaging requires inhibition of the TGF $\beta$  and p38 MAPK pathways, through A 83-01 and SB202190 respectively (Sato et al. 2011). Lastly, in order to support the growth in a 3D manner an identification of an extracellular matrix (ECM) was required. Matrigel, which encourages 3D aggregation and polarisation of cells, was chosen and proven to emulate ECM (Jensen et al. 2010; Kretzschmar and Clevers, 2016).

### **3.2. Aims and Methods**

As for the start of this project, this method was not established in our laboratory and had to be researched and set up from the beginning. The methods for the derivation and expansion of organoids from human gastrointestinal tissues have been described by Sato et al. in 2011 and this protocol was followed for establishing cultures. Inevitably it was found that the methods described in the literature needed adaptation to work within a clinical environment. This chapter sets out our experience with organoid derivation, its method introduction and establishment in our laboratory and what modifications were made to the original

protocol in order to establish successful organoid cultures for modelling radiotherapy in colorectal cancer.

### **3.2.1. Patient recruitment**

Tissue for organoid derivation was obtained from patients undergoing colorectal tumour resection surgery at the Queen Elizabeth Hospital in Birmingham. Due to limited quantities of post-treatment of rectal cancer patients the patient samples were extended to untreated, resected colon cancer tissue. Patients were identified and recruited prospectively between August 2017 and March 2019. All recruited patients consented under the HBRC ethics. The tumour resections along with normal tissue margins were resected and furthered sampled by the pathologists. The paired tumour with matching normal tissue specimens were then passed to Birmingham BioBank where they were anonymised and released to the laboratory on the same day as the patient's surgery. The samples were stored at 4°C until being processed.

### **3.2.2. Method outline**

The protocol published by Sato and his colleagues in Gastroenterology (Sato et al. 2011) was followed in order to establish a patient derived organoids culture in the lab for modelling colorectal cancer radiosensitivity. The protocol consists of four main steps- 1) tissue dissection and washing, 2) tissue digestion, 3)

Collecting released cells and additional washes, and 4) plating and culturing (see Figure 3.1).

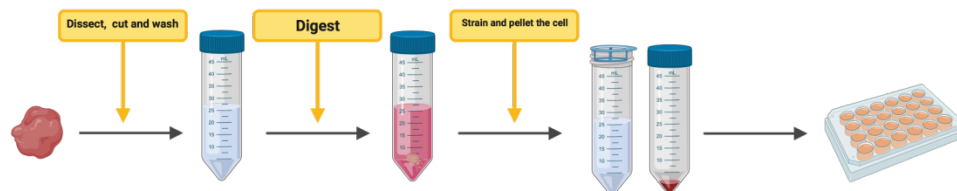


Figure 3.1 - Outline of the protocol for organoids derivation.

Tissue sample is dissected into smaller pieces and washed prior to digestion. The released cells are separated from undigested tissue and washed again. The final pellet of cells is plated on 24 well plates using Matrigel and cultured in specialised organoid media.

Firstly, the tissue fragments were cut into small 5mm pieces and washed 3 times or until the supernatant was clear with PBS without calcium and magnesium (PBS0). Subsequently, the fragments were incubated for 30 minutes in chelation buffer (distilled water with 5.6 mmol/l  $\text{Na}_2\text{HPO}_4$ , 8 mmol/l  $\text{KH}_2\text{PO}_4$ , 96.2 mmol/l sucrose, 54.9 mmol/l D-sorbitol, 0.5 mmol/l DL-dithiothreitol) on ice for crypt isolation from control colorectal tissue and in dissociation buffer (DMEM F-12, 2.5% heat activated Foetal Bovine Serum, 0.1mg/ml primocin, 75 U/ml collagenase IX, 125  $\mu\text{g}/\text{mL}$  dispase II) for 1 hour for cancer samples. Following digestion, the tissue and supernatant were strained through the 50 $\mu\text{m}$  or 20 $\mu\text{m}$  filter (normal tissue and carcinoma tissue respectively) and collected in 50ml falcon tube. As the normal tissue crypts size was expected to be bigger the

size of the straining filter was chosen appropriately not to filter out the crypts. The tumour tissue was dissociated into single cells, hence 20µm size strainer was used. Dissociated cells were pelleted at 300xg for 3 minutes and further washed with ice cold PBS0 twice. Washed pelleted cells were resuspended in Matrigel and seeded in 24 well plates with density of 500 crypts/1000 single cells per 25µl of Matrigel per well). The plate with seeded cells was incubated at 37°C to allow the Matrigel to polymerize and then 500µl of culture medium was added to each well. The plate with seeded cells was then kept in an incubator at 37°C and 5% CO<sub>2</sub>. The culture was maintained with media changes every 2 days and passaging every week.

As the protocol was followed to replicate the method, certain adjustments have been made based on the results.

### **3.3. Results**

#### **3.3.1. Protocol modifications: sample collection and initial washing**

Primarily patients' samples were placed in a small tube containing RPMI media and processed immediately following the sample collection. As in the original protocol, the tissue was washed with PBS0 after being dissected into smaller pieces. At the beginning, despite organoids developing, the culture would not progress further as cells would get infected and quickly die off resulting in culture termination. It was noticed that the infection would more often occur in samples

processed from normal tissue in contrast to cultures derived from tumour tissues. It was concluded that the presence of antibiotics in the dissociation buffer partially protects the culture from infection. The protocol has been modified by adding antibiotics (Primocin 100mg/ml) to the chelation buffer and additionally to PBS0 used for the initial washing steps of the tissue. This protocol modification resulted in a significant drop in infection rate, however not eradicating this issue completely. Following this modification, infection of the culture would affect both tumour and normal tissues equally. In order to limit the infection rate further, tissue resections were collected and placed immediately in the RPMI media supplemented with antibiotics (100mg/ml Primocin) and incubated overnight at 4°C. As the samples weren't processed immediately, the success rate of organoid derivation was lowered, however, the cultures were no longer lost to infection.

In order to mitigate the lowered success rate for organoid derivation, further protocol modifications were considered.

### **3.3.2. Sample dissociation**

#### **3.3.2.1. Buffers**

Firstly, we started incubating the normal tissue at 37°C, same as tumour tissue, in order to increase the efficiency of EDTA in chelation buffer. The incubation time has not been extended from the original protocol. As the organoid culture

started to become more popular, the STEMCell Technologies company started offering media for murine organoid culture as well as dissociation buffers. Since the chelation buffer preparation was time consuming, I decided to try replacing the chelation buffer dissociation with the commercially available Gentle Dissociation Buffer (GDB) from STEMCell Technologies.

The same samples were processed using the described above protocol with different buffers. A control tissue sample has been equally divided into two pieces (A and B) and processed for organoid derivation. Sample A has been dissociated using chelation buffer, whereas sample B with GDB. Following the 30 minute incubation at 37°C, the 20µl sample was taken for visual inspection under a microscope. Following the incubation the solutions were both investigated with the light microscopy by taking 10µl of the crypt suspension and placing it onto the microscope slide and investigated under the light microscope. It was observed that the tissue was successfully dissociated with both buffers. Furthermore, the intestinal crypts were successfully isolated with the use of either chelation buffer or GDB. Moreover, The visual investigation showed that crypts isolated from tissue dissociated with GDB were digested more, and more single cells were observed. It was concluded that the GDB is more efficient at digesting normal tissue than the chelation buffer. The comparison of isolated crypts using both buffers are represented in Figure 3.2.

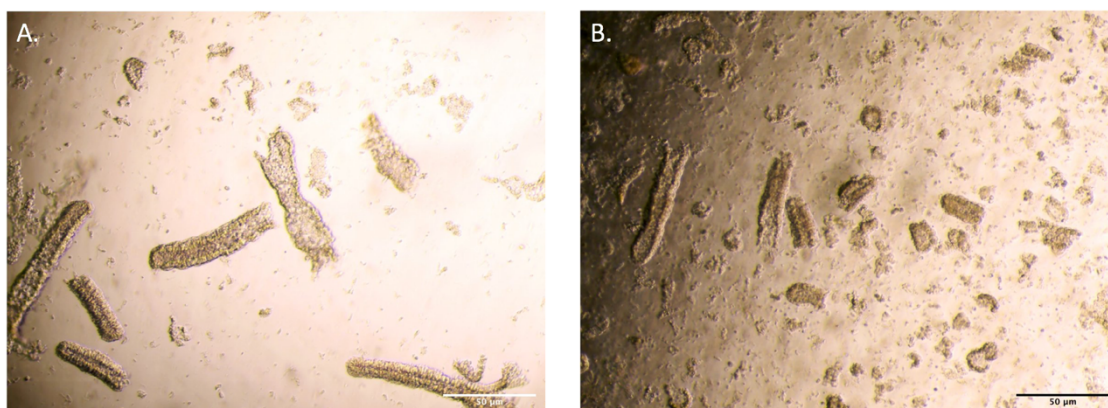


Figure 3.2 - Visual crypt inspection post digestion.

Visible crypts after normal tissue digestion using two different digestion buffers.

A) Visible crypts in the suspension after digestion using chelation buffer.

B) Visible crypts and cell clumps after digestion with Gentle Dissociation Buffer.

After being seeded in Matrigel and left in incubation at 37°C and 5% CO<sub>2</sub>, both samples resulted in formation of organoids and successful derivation. This comparison was performed twice, using two different control tissue samples. As results for the GDB dissociation were satisfactory, the protocol was updated and the chelation buffer was replaced with the commercially available buffer.

### 3.3.2.2. Mechanical fragmentation

When processing tumour tissue it was observed that the majority of tumour samples would not digest efficiently following the 1 hour incubation. The issue would persist despite the incubation time being further extended by 30 minutes. Additionally, extending digestion time was not desirable, as extended incubation was associated with reduction in cell viability. In order to improve the efficiency

of digestion another tissue sectioning step was added. After cutting the tissue into small pieces with a scalpel, it was placed in a 5ml sterile tube containing 1ml of digestion buffer and was subsequently dissected further with Castro-Viejo surgical scissors. This additional step ensured the tissue was cut into pieces smaller than 5mm (see Figure 3.3). Following this, an additional 1ml of tumour dissociation buffer was added to the 5ml tube containing tissue and then placed in the incubator for the 1h incubation period. Examining the supernatant under the microscope, tissue that underwent the additional cutting stage with the surgical scissors was more digested in comparison to the one that did not. This step was therefore implemented for normal tissue processing.

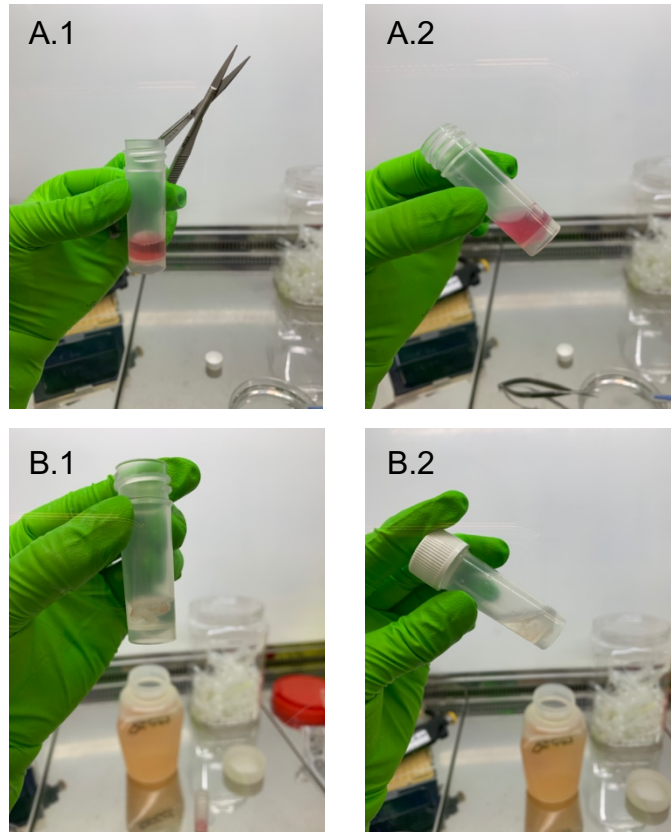


Figure 3.3 - Castro-Viejo surgical scissors fragmentation.

As an additional fragmentation step, cut samples were further dissected with surgical scissors. 'A' figures represent tumour tissue and 'B' figures represent normal tissue. 1 – pre-processing, 2- post-processing.

### 3.3.3. Culturing Media

Media for organoid culture is complex as it contains many specific niche factors without which they cannot grow. The composition of organoid culture medium was followed per the protocol by Sato et al. 2011, Wnt and R-spondin were supplied as conditioning media collected from cell lines expressing those proteins: ATCC® CRL-2647™ for Wnt and Cultrex HA-R-Spondin1-Fc 293T Cells for R-spondin). Furthermore, 50% of conditioning media from L-WRN cell line expressing Wnt, R-spondin and Noggin was also trialled for the organoid

culture medium. Organoid growth would slow down or completely stop when cultured with organoid medium containing L-WRN conditioning medium. Three different batches of medium were prepared, however every time it was found that either organoids would not form or existing cultures would die.

The original organoid medium based on the published protocol was effective, nonetheless it would give inconsistent results due to batch-to-batch differences. This impacted the establishment of new cultures as well as the maintenance of normal tissue cultures. Commercially available media – Human IntestiCult (STEMCell Technologies) became available for trial. It was noticed that organoids cultured in Human IntestiCult would grow consistently, more organoids would form, and the establishment of new cultures was more successful in comparison to the laboratory-made media. Based on these results it was therefore decided to use Human IntestiCult media for culturing organoids.

#### **3.3.4. Normal tissue – trouble shooting**

When establishing organoids from both normal and cancerous tissues, organoids would form within two days of seeding. Towards the seven days after seeding, the organoids would expand and differentiate, forming structures with arms that would resemble intestinal structures (see Figure 3.4). However, the normal tissue organoids once differentiated would be harder to dissociate and often the culture would die off after the first or second passage and 100% of normal tissue cultures would not survive after passage two. This issue was consulted with Hans Clevers'

laboratory during a week-long training course in the Hubrecht Institute, and it was suggested that due to high differentiation the amount of stem cells would significantly drop. This mean that after passaging their numbers would be too low to maintain successful expansion. An additional recommendation was made to seed the crypts and cells more densely as human organoids would expand better in denser conditions. Furthermore, collaborators from the Sanger Institute, Cambridge, advised adding prostaglandin  $1\mu\text{M}$   $\text{PGE}_2$  into culture media. This would maintain the organoids in a less differentiated state (see Figure 3.4 A.3) and help maintain the long term expansion of the culture. After applying these changes, normal colon tissue organoids were successfully established in the laboratory.

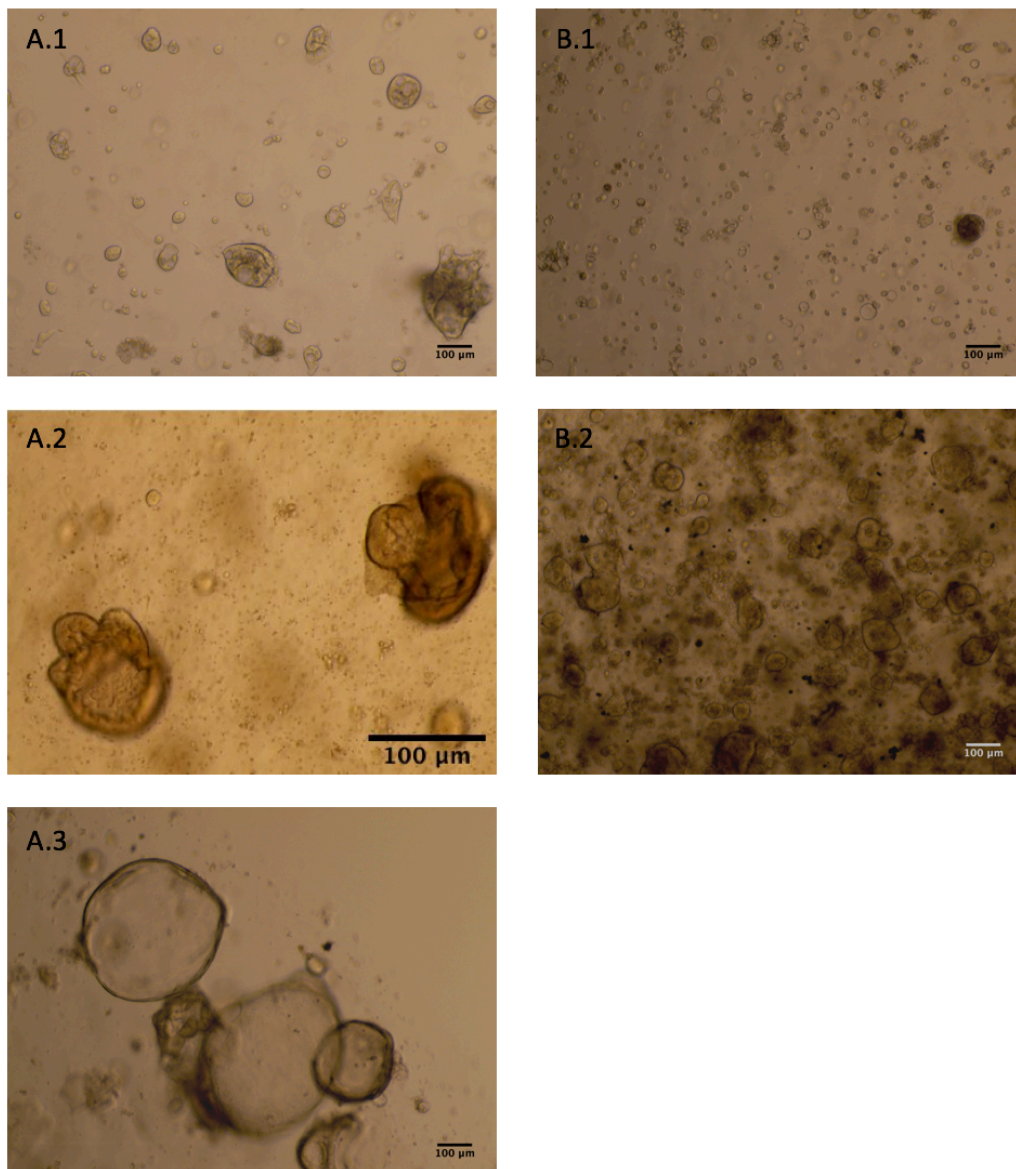


Figure 3.4 - Organoids at different stages of culture.

Pictures of A) normal tissue and B) tumour organoids at certain culture stages – 1) two days after seeding, 2) seven after seeding. A.3 represent normal organoids seven days post seeding after implementing the protocol changes (adding prostaglandin and seeding more crypts per well).

### 3.3.5. Passaging

For passaging, Sato et al. instructions were followed. However, certain modifications were applied to optimise the method for the laboratory. In the

original protocol, passaging was achieved by mechanical disruption using a P1000 pipette (as seen in Figure 3.5), with further mechanical dissociation being achieved with a fire-polished Pasteur pipette. This was followed by a washing process using basal medium.

The fire-polished Pasteur pipette disruption could not be implemented in our laboratory, so an alternative method was employed consisting of mechanical disruption by pipetting up and down around 20 times using a P1000 pipette with a P10 tip stacked on top of the standard P1000 tip.

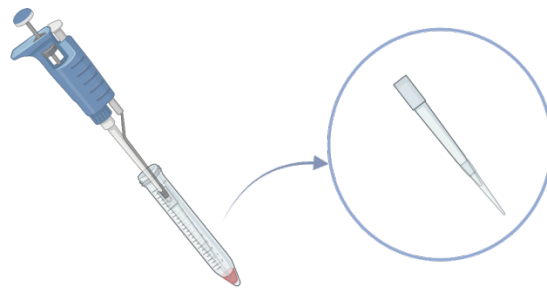


Figure 3.5 - Mechanical disruption.

An illustration showing the method of mechanical disruption. The 1ml suspension of organoids was disrupted by pipetting up and down with a P1000 pipette with an additional P10 tip on top of the P1000 tip.

Although a good level of disruption of organoids was achieved, this technique would put the cells under increased stress and also would extend the time required for passaging. Therefore, prior to washing, pelleted organoids were resuspended in 1ml of TrypLE (Thermo Fisher Scientific) and incubated for three

minutes at 37°C in a water bath. Following the incubation, organoids were further disrupted with P1000 and P10 combined tips by pipetting up and down three to five times (depending on the amount of wells being passaged).

Lastly, after changing the house-made organoid media to commercial Human IntestiCult, all the washes were performed with ice cold PBS0.

### **3.3.6. Freezing**

All lines were passaged at least four times before being frozen, as it allowed the line to become established and have a sufficient organoid count for cryopreservation. It was noted that often lines frozen after first or second passage would die off after thawing. It was also found that the success of the organoid cryopreservation was maximised when organoids were collected for freezing two to three days after being passaged. Furthermore, an additional step of removing Matrigel was introduced to the organoid freezing process. Following media removal, organoids were resuspended in ice cold OHS and left on ice for 30 minutes in order to fully dissociate Matrigel, as leftover Matrigel would often impact the efficiency of cryopreservation. Lastly, the pelleted organoids were gently resuspended in Advanced DMEM/F12 media, and an equal volume of DMSO/FBS (20:80 ratio) was slowly added to the Eppendorf containing resuspended organoids; drop by drop while gently tapping on the tube. The suspension was then transferred to cryovial and stored in a Mr. Frosty at -80°C

for the first 24 hours, and subsequently moved to liquid nitrogen for long term storage. The protocol followed for thawing was the same as that for cells (a detailed description of the protocol can be found in Materials and Methods; see Section 2.3.2.3).

### **3.3.7. Matrigel**

While culturing established organoids lines with many formed organoid colonies, it was observed that the Matrigel would often dissociate partially and become loose. This would result in losing parts of organoids cultures during media changes. After closer investigation and consultation with the Corning technical team, it was suggested that this could be the result of low protein concentration in the Matrigel batch. A new batch of Matrigel with protein concentration above 10 mg/ml was used from that point forward, and the issue of loose Matrigel while culturing organoids was no longer observed.

### **3.4. Protocol summary**

In order to establish the final version of the protocol for organoid derivation and culture, nine sample pairs (normal and tumour) were processed. The final derivation protocol steps included same four main steps as the main protocol. The summary of the protocol with the implemented changes is as follows.

First, the tissue was dissected into smaller pieces and washed using PBS0 with 100mg/ml Primocin until the supernatant was clear (Figure 3.6 B1-B3). The cleaned tissue was then moved into a 5ml sterile collection tube containing 1ml of appropriate digestion buffer (tumour digestion buffer for tumour samples or GDB for normal tissue samples). Then, additional mechanical fragmentation was performed using Castro-Viejo surgical scissors, dissecting the tissue into much smaller pieces. Samples were then incubated at 37°C and 5% CO<sub>2</sub> for a duration of 30 minutes for normal tissue, or 1 hour for tumour tissue. After visual inspection of digestion effectiveness, the samples were either further incubated or strained and washed with PBS0. Cells were pelleted and resuspended in 100% ice cold Matrigel and plated on 24-well plates. Cells/organoids were cultured in Human IntestiCult; the media was supplemented with 100mg/ml Primocin for the first two days after seeding. Subsequent media changes were carried out every two days using media without antibiotics. Organoids were passaged every seven days in either 1:5 or 1:6 ratios depending on the organoid line. Protocol steps along with microscope pictures of samples immediately after seeding and seven days after seeding are presented in Figure 3.6. A detailed standard operating procedure (SOP) can be found in Appendix A.

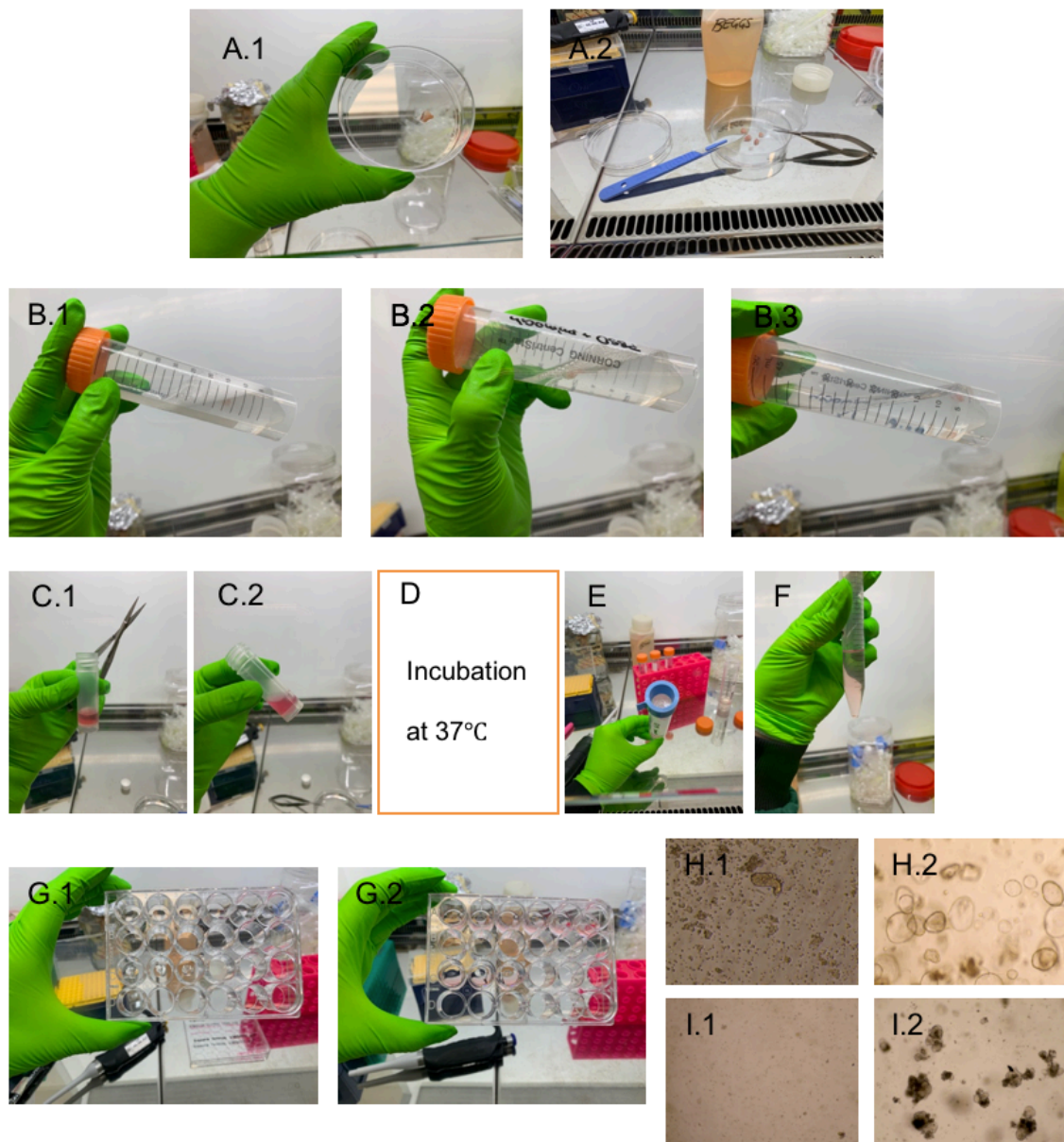


Figure 3.6 - Organoids derivation steps.

A.1 and A.2 – samples being cut into smaller pieces on a sterile petri dish with a scalpel.

B.1 – first wash with PBS0 supplemented with 100mg/ml Primocin.

B.2 and B.3 – second and third washes of samples, with noticeable clearer supernatant.

C – additional mechanical dissection using scissors 1- before and 2- after.

D- Incubation of sample to allow the enzymatic digestion of the tissue, 30 minute incubation for normal tissue or 1 hour incubation for the tumour tissue.

E – straining the sample to collect only digested cells.

F – pelleting cells after washing them with PBS0.

G.1 – plating cells suspended in Matrigel onto 24-well plates.

G.2 – media added into each well with plated samples after allowing the Matrigel to polymerise.

H.1 – normal tissue sample on the day of seeding.

H.2 – normal tissue sample seven days after seeding.

I.1 – tumour tissue sample on the day of seeding.

I.2 – tumour tissue seven days after seeding.

### **3.5. Discussion**

In this chapter I present the adaptations that I had to make to successfully carry out organoid derivation and expansion from human colorectal samples by making modifications to the original Sato et al. 2011 protocol. Since the method was first published, more studies have been published improving the method. Therefore, it is natural to adjust the protocol to meet the needs of the study and laboratory. In this thesis, the modifications to the original method varied from simple changes, such as use of GDB instead of a chelation buffer, to more elaborate ones, such as troubleshooting the culturing conditions for normal tissue organoids. One key problem that had to be solved was the infections the cultures suffered after processing the tissue for organoid derivation. This was particularly problematic as it would result in organoids dying. It is known that the human gastrointestinal tract's microbiome is rich and diverse, containing bacteria and fungi as well as other microorganisms (Barko et al. 2018). Therefore, while working with primary tissue samples, the tissue would contain these microorganisms. Adding an antibiotic treatment helped to reduce their levels significantly in order to avoid cultures becoming contaminated. The additional use of Primocin as an antibiotic for media collection, washes, and culturing instead of

Penicillin-Streptomycin protected the cultures against a wider range of contaminants. Primocin is active against bacteria, mycoplasma, and fungi, whereas Penicillin-Streptomycin, which is more commonly used in cell cultures, is effective only against bacteria. Microbiome interactions were not studied as part of the scope of this thesis. Therefore the use of an antibiotic with such a wide range of effectiveness was not harmful for the method, and simply ensured contamination of the organoid cultures was minimised. Furthermore, changing to a commercially available organoid culture media minimised batch-to-batch variation as well as increased efficiency in the laboratory.

Another important step added to the protocol that improved the effectiveness of the method was the additional mechanical dissociation of tissue. Tumours are known to be challenging to digest while maintaining integrity of the cells. In order to get a single cell suspension, a lengthy process is often required, and longer incubation periods have been linked to a reduction in cell viability (Garaud et al. 2014). Thus, ensuring the tumours are digested without extending the incubation time protected the sample's cell viability and further maximised chances for successful culture derivation.

It is not known why organoids derived from normal tissue once differentiated into mature budding structures would lose their stem cell-like properties and would not expand after passaging. The addition of PGE<sub>2</sub> kept organoids in a circular spheroid-like form and allowed long-term culturing. Recent studies have shown that prostaglandin PGE<sub>2</sub> upon the irradiation damage acts as a key mediator

between intestinal epithelium and the mesenchyme (Roulis et al. 2020). This study was in line with another study that identified the involvement of PGE<sub>2</sub> in mediating the expansion of transfer repair wound-associated epithelial cells upon wounding (Miyoshi et al. 2017). Organoids when damaged transform into circular form (Sprangers, Zaalberg and Marice, 2020). This supports the addition of PGE<sub>2</sub> into the normal tissue culture for maintaining the less differentiated state of organoids.

To summarise, the Sato et al. (2011) protocol alone was sufficient to establish a preliminary method in our laboratory. With the aforementioned changes, it was possible to optimise and standardise the protocol as well as establish and maintain long term organoid lines that were suitable for disease modelling. Although not all changes improved the effectiveness of the method, they all certainly made it more efficient for the laboratory.

## **4. RESULTS CHAPTER 2: CHARACTERISATION OF ESTABLISHED ORGANOID LINES FOR MODELLING IRRADIATION RESPONSE**

### **4.1. Introduction**

Studying cancer would not be possible without appropriate and representative models which give researchers insight into disease complexities from different angles – from molecular changes driving disease progression to tumour microenvironment interactions. Along with studying the driving mechanisms of carcinogenesis, a large part of research focuses on studying novel therapies and patients' response to it. Hence, the choice of an appropriate pre-clinical model that accurately reflects patients' pathological attributes and biological response to treatment is crucial (Kim, Koo and Knoblich, 2020).

Radiotherapy still forms part of the main treatment regimen prescribed to patients with cancer (Miller et al. 2016). All rectal cancer patients presenting with advanced stage of the disease will receive neo-adjuvant radiotherapy. However, despite great advancements in technology and radiobiology, there is still a high percentage of patients that will not have any response to irradiation. In order to tackle this problem, more extensive research is required that can identify the mechanisms behind resistance to irradiation treatment as well as radiosensitivity. Although two-dimensional (2D) monolayer cell cultures provide crucial insight into basic tumour biology and radiobiology, due to lack of tissue architecture of the original organ and lack of heterogeneity, they are not representative of solid

tumours (Kim, Koo and Knoblich, 2020). Studies on radiotherapy response that have been conducted on cell lines do not fully represent the tumour biology and therefore, might not replicate the actual response. Murine models – particularly patient-derived xenograft mouse models – have been extensively utilised in this area (see summary of use of mouse models as pre-clinical models in radiobiology research in Figure 4.1, Butterworth, 2019). Scientific advancements such as genome editing have allowed modelling of the disease with mice at a more precise angle. Furthermore, the development of small animal irradiators which allow small beam delivery under image guidance widen the precision of radiobiological studies (Dow, 2015).

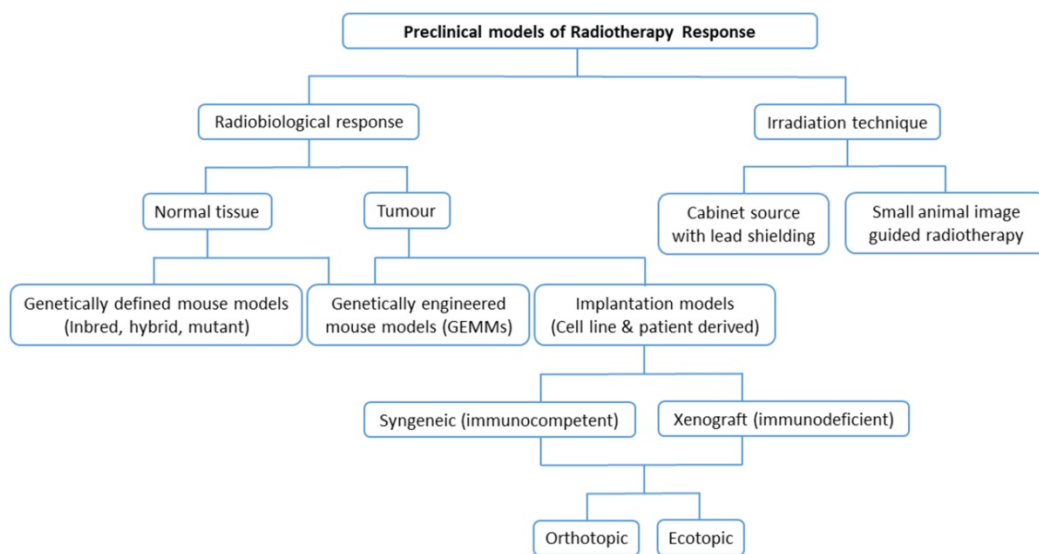


Figure 4.1 - Summary of murine based pre-clinical models for studying tumour and normal tissue response to irradiation used in radiobiology research.

Figure taken from Butterworth, 2019.

Although studying irradiation using mouse models has a lot of advantages and is used as standard in radiobiological research, it also has certain disadvantages.

The main two drawbacks of murine models are their cost and the fact that they are not practical for large drug screens. Additionally, in the overall context of radiosensitivity there are significant differences between mice and human. Human bodies are more radiosensitive to total body irradiation in comparison to mice – up to twice as sensitive (Butterworth, 2019). Therefore, emerging new 3D organoid models have shown promise to the future of radiobiology research and response modelling. 3D models have been utilised more and more to replace both cell lines and mouse models across different aspects of cancer research, including therapy response studies. Organoids pose as a good alternative to murine models as they are cheaper, can be scaled for large drug screen, and yet are equally representative of patients' genetic profiles and tumour heterogeneity with 3D tissue architecture, in contrast to cell lines (Yang et al. 2018).

At the beginning of this study, there weren't many studies published utilising organoids as models for studying radiotherapy response and only just recently more studies have emerged in which organoids have been utilised for studying radiotherapy (Venhatachalam, Schmidt and Heiden, 2018; Martin et al. 2020). One notable study utilised 3D spheroid cultures to develop a novel system of irradiation (Tesei et al. 2013). Nevertheless, the majority of studies are still conducted using murine models, therefore highlighting the need to develop suitable in vitro models that enable studying response to irradiation. Being aware of the potential of organoids, we have sought to establish patient-derived organoid lines that would pose as models for colorectal cancer and radiotherapy response.

## **4.2. Aims and methods**

The main aim of this chapter is to obtain an accurate organoid model for studying radiotherapy of colorectal cancer. With the objectives of the chapter being as follows:

1. Select and characterise organoid lines that would pose as colorectal cancer models for radiobiological research and compare their characteristics to the tumour origin.
2. Establish a robust and effective method of irradiation delivery that replicates the clinical regime.
3. Choose an accurate method of measuring cell viability following a course of radiotherapy.

Four suitable lines have been selected for this study using the established derivation protocol, described in Chapter 3. We have used a variety of techniques in order to characterise the selected organoid lines and compared them to the tumour tissue they have been derived from. The organoids and the tumour tissue were characterised visually with a light microscope for the pathological features. Additionally, we have used immunohistochemistry to stain both organoids and their corresponding tumour tissues for common tumour and epithelial markers. We have also performed DNA sequencing with targeted sequencing panel on

organoid lines to investigate their mutational profiles. Once the organoids were characterised we exposed them to irradiation and investigated their viability. In this chapter we also describe how we chose an appropriate method of irradiating cells and accurately measuring their response.

### **4.3. Results**

#### **4.3.1. Establishing lines for the disease modelling**

Once the organoid derivation and maintenance protocols were optimised and established in the laboratory, patient-derived lines were expanded with the purpose of creating a bank of colorectal organoids.

Organoid lines had to meet the following requirements in order to be used as models for studying the irradiation response in colorectal cancer. Firstly, organoids need to grow and expand. For example, many organoids would form within two days after seeding and the majority of those would grow into bigger structures. In some cases, very few small organoids would form and would not expand initially. These organoids would usually die after passage 1 or 2. However, following the passage the organoids would start to grow comparably well and further expand, allowing the number of organoids to increase. This was important as a large number of organoids is required for viability experiments with multiple replicates or sequencing and simultaneous culture maintenance. Additionally, in order to call the line established, it needed to be able to be

successfully passaged at least 5 times. It was found that the organoid cultures could still die after passage 3. It was noticed that all organoid lines that still expanded well after passage 5 would carry on as a reliable culture. Finally, expanded organoids were cryopreserved and thawed after a week to see if they would successfully expand after cryopreservation. In order to have a robust and reliable model it was essential for the lines to be able to successfully expand after freezing. Lines that were too fragile to survive cryopreservation did not have sufficient organoid numbers and therefore were not appropriate to serve as models.

From lines that met the described requirements, three tumour organoid lines were initially selected: rectal, sigmoid and colon cancer. Another rectal line (S345653) was also selected and included in ongoing experiments as it became available. As this line was not available at the beginning of this study, certain experiments were not conducted using these organoids.

Since only a limited number of rectal tumour samples were available it was decided that all colorectal tumours should be included. What is more, it was decided that in order to model the radiosensitivity and irradiation response in colorectal cancer it was important to have a wide representation of colorectal tumours that would differ in their characteristics and were subjected to different or no treatments prior to resection. All rectal tumour samples came from surgical resections, and therefore came from patients that have received neo-adjuvant therapy. Although it was thought that establishing and expanding organoids from

tissue that has been subjected to radiotherapy can be problematic, the organoid lines derived from patients that have received radiotherapy prior to resection have been established successfully and expanded well. Lines derived from tumours that have been subjected to irradiation have been seen as a valuable tool for studying radioresistance and radiosensitivity. However, in order to model tumour response to radiation it was desired to also have naïve lines, that originated from cells that were not previously exposed to irradiation. As the current clinical treatment recommendations are neo-adjuvant radiotherapy, rectal samples available for organoid derivation would consist of cells that have been exposed to irradiation already. For these reasons, samples of colon and sigmoid origin were included in this study. Selected lines included sigmoid tumour (S292064), colon tumour (S302389), and two rectal tumours (S309884 and S345653); Patients with rectal cancer received neo-adjuvant treatment, one patient received short course radiotherapy and one long course radiotherapy combined with chemotherapy prior to surgery. Based on the Tumour Regression Score (TRS) measuring the pathological response to neo-adjuvant treatment, the patient who received long course radiotherapy combined with chemotherapy had a partial pathological response, whereas the patient who received short course radiotherapy preceding the surgery had poor or no response to the treatment. The patient information is summarised in Table 4.1.

**Table 4.1 - Summary of patients' tumour information.**

Tumour information that includes localisation (rectum, sigmoid colon, colon), stage (using TNM system), MMR status, and what therapy the patient had received prior to surgery as well as its

outcome. Additionally, a RAS mutation status is included where investigated. pMMR – proficient mismatch repair; TRS- tumour regression score, WT- wild type

ID	Tissue Type	Stage	MMR status	Neo-adjuvant therapy	Pathological response (TRS)	RAS mutation status	BRAF V600E status
S292064	Sigmoid Tumour	T3 N0 M0	pMMR	No	N/A	WT	negative
S302389	Colon Tumour	T3 N1 M0	pMMR	No	N/A	WT	negative
S309884	Rectal Tumour	T3 N1 M0	pMMR	Radiotherapy (short course)	TRS-3	NRAS mutant	negative
S345653	Rectal Tumour	T2 N0 M0	pMMR	Radio/chemotherapy (long course)	TRS-2	KRAS mutant	negative

#### 4.3.2. Characterisation of organoid lines

We started by characterising pathological features of the primary tumour section. H&E stained sections were examined under the microscopy with a pathologist. We also performed ICH staining for pan-Cytokeratin and CDX2, epithelial and intestinal markers. Then we examined the pathological features of organoids as well as the expression of pan-Cytokeratin and CDX2 to compare to the original tumour sections. Finally, we performed panel sequencing in order to characterise the molecular profiles of the organoid lines.

#### **4.3.2.1. Light microscopy characterisation: tumour tissue**

Along organoids lines, paraffin embedded sections of the original formalin fixed tumours were obtained from biobank and investigated for pathological features. Firstly, sections were stained with H&E to look at the histological characteristics of the tumours (Figure 4.2). All sections displayed features of aggressive colorectal adenocarcinoma with irregular growth of epithelial tissue within the colorectal tissue. With help of a clinical pathologist, certain features of these tumours were highlighted. S292064 section displayed a profusion of cancerous cells invading the muscle layer. The H&E staining of S302389 showed abundant extracellular mucin that indicated that the tumour is a mucinous adenocarcinoma. Lastly, in sections coming from both S309882 and S345653, a necrosis was found. This was a likely result of the radiation treatment that both patients received. The necrosis was more pronounced in a tumour from a patient that had have received short course therapy.

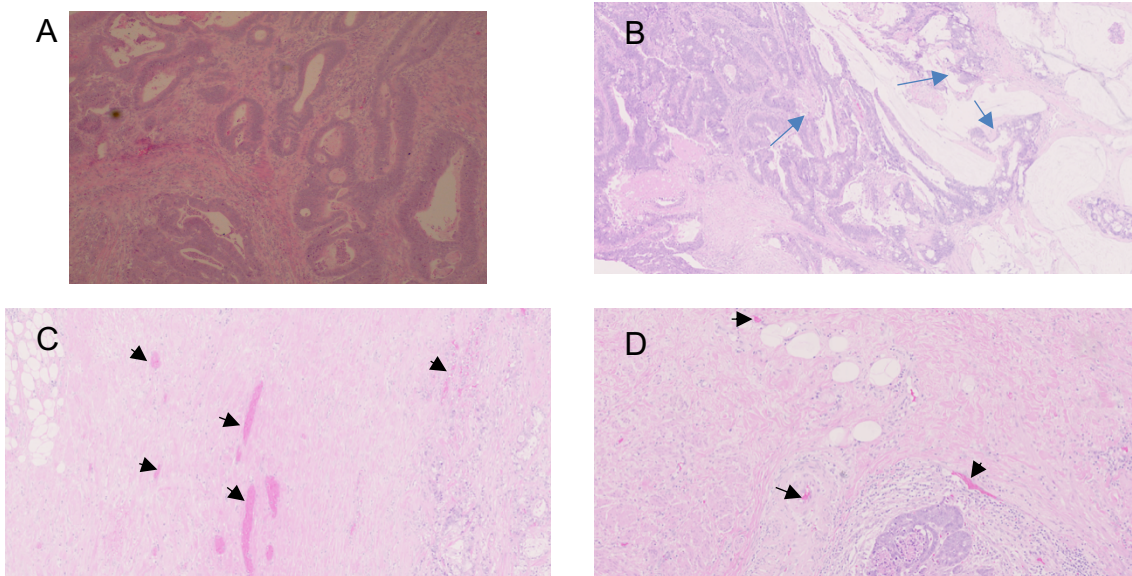


Figure 4.2 - H&E staining of original tumour tissue sections.

A) S292064- sigmoid adenocarcinoma, B) S302389- colon adenocarcinoma, blue arrows highlight the abundance of mucin, C) S309884- rectal adenocarcinoma, D) S345653- rectal carcinoma, black arrow highlights the necrosis

After histopathological examination of H&E stained sections, the original tumour sections were stained for pan-Cytokeratin and CDX2 markers using immunohistochemistry. Both markers are used in clinical pathology to aid with diagnosis. Pan-Cytokeratin marks epithelial cells, whereas the CDX2 is a marker for adenocarcinoma of intestinal origin. The tumours were stained for those markers as they were expected to express them based on diagnosis. This would then show whether or not the organoid lines grew from these tissues and retained these markers and features. All tumours stained positive for both markers as expected (Figure 4.3).

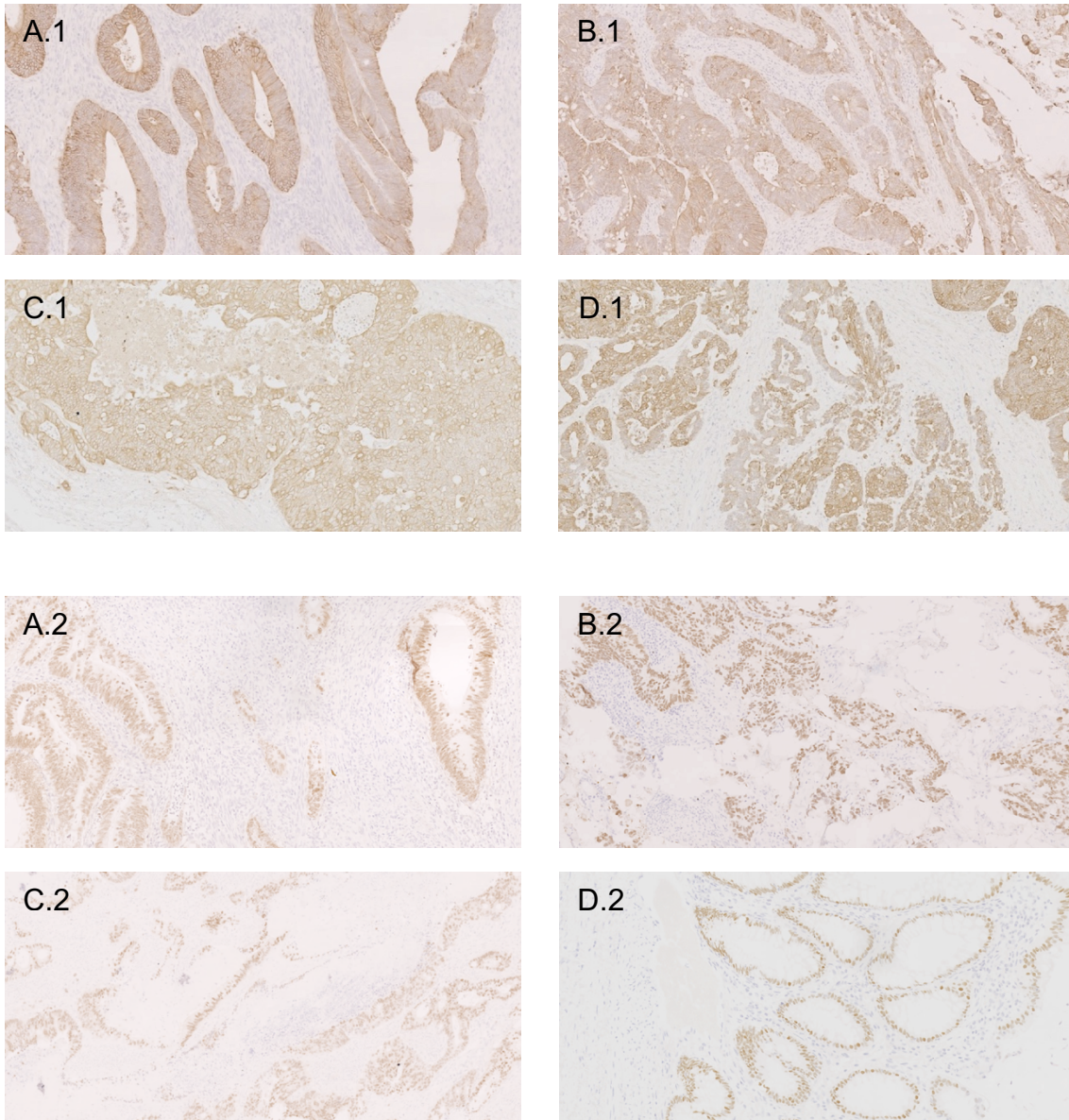


Figure 4.3 - Immunohistochemistry of original tumour sections.

Stains of tumour sections for Pan-Cytokeratin (A.1-D.1) and CDX2 (A.2-D.2). A) S292064, B) S302389, C) S309884, D) S345653.

#### 4.3.2.2. Light microscopy characterisation: organoid lines

As a next step before modelling the irradiation response with the selected organoids, the lines were characterised and examined in order to investigate the

resemblance to the original tumour. Firstly, when looking at the organoids' morphology and growth, it was determined that the lines derived from these tumours were exhibiting a good growth rate and morphology characteristic for organoids of tumour origin (Figure 4.4). Organoids for all lines had an irregularly rounded shape and expanded rapidly. The growth of lines S292064, S302389, and S309884 was aggressive as organoids would expand rapidly and had to be passaged in high split ratios (1:5 or 1:6) every 7 days. In contrast, line S345653 would grow less aggressively with the organoids developing more slowly and had to be passaged every 10 days in 1:3 or 1:4 split ratios. The growth of the organoids would correspond with original tumour properties. Patients S292064, S302389, and S309884 all presented with aggressive stage T3 tumours, with S302389 and S309884 tumours also invading the lymph nodes. The S345653 tumour was detected at stage T2 and did not invade the lymph nodes. Furthermore, the S345653 tumour was the only one that was chromosomally stable while the other tumours displayed chromosomal instability.

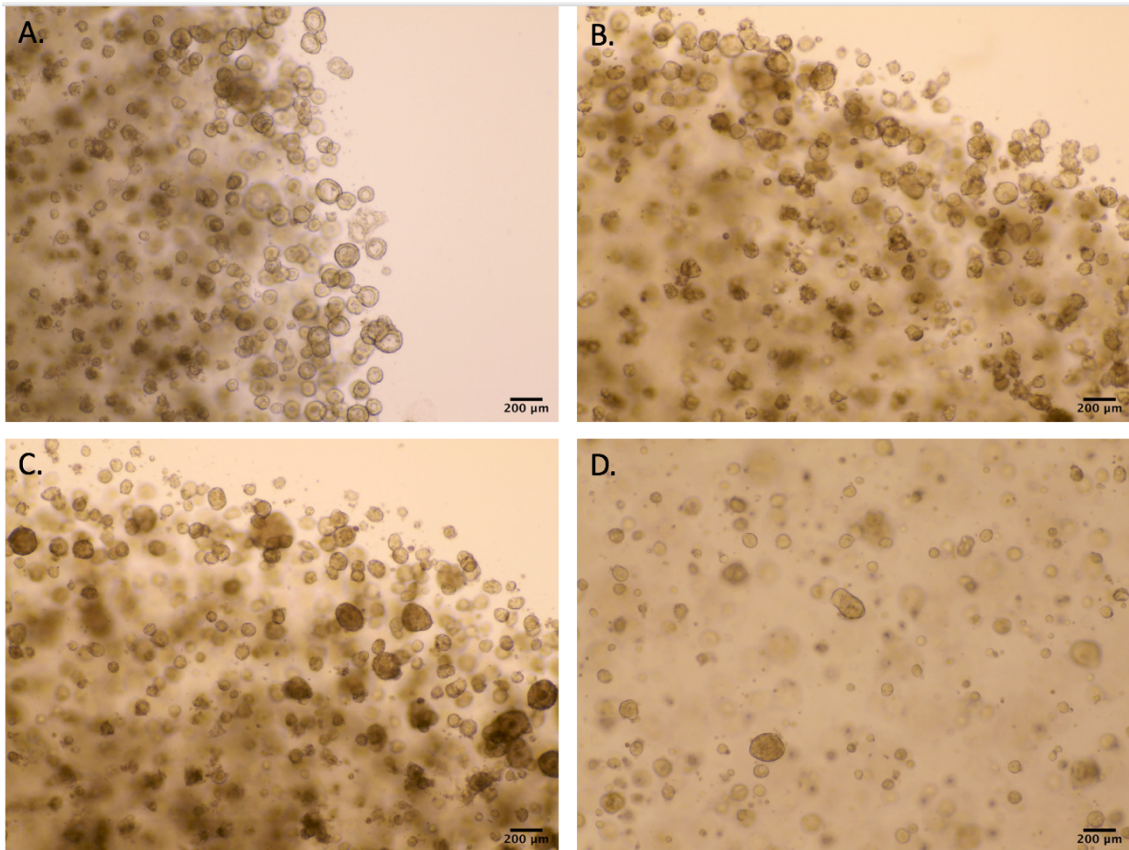


Figure 4.4 - Organoid lines' morphology.

Microscope taken images showing selected organoid lines on day 3 after being passaged. A) S292064, B) S302389, C) S309884, D) S345653.

Next, the organoids from each line were fixed in paraffin and stained for the same immunohistochemistry markers as the original tumour sections. This staining was performed in order to investigate whether the organoids grown would also express pan-Cytokeratin and CDX2 markers ensuring the organoids are derived from colorectal tumour cells. Organoids of all lines stained positive for pan-Cytokeratin (Figure 4.5 A.1-D.1), confirming epithelial origin of the organoids. The CDX2 marker was present in 3 out of 4 lines – S292064, S302389, and S309884, whereas the S345653 staining was CDX2 negative (Figure 4.5 A.2-D.2). As the

original tumour stained positive for CDX2 marker it was further investigated whether the organoids derived from the tumour were in fact cancer.

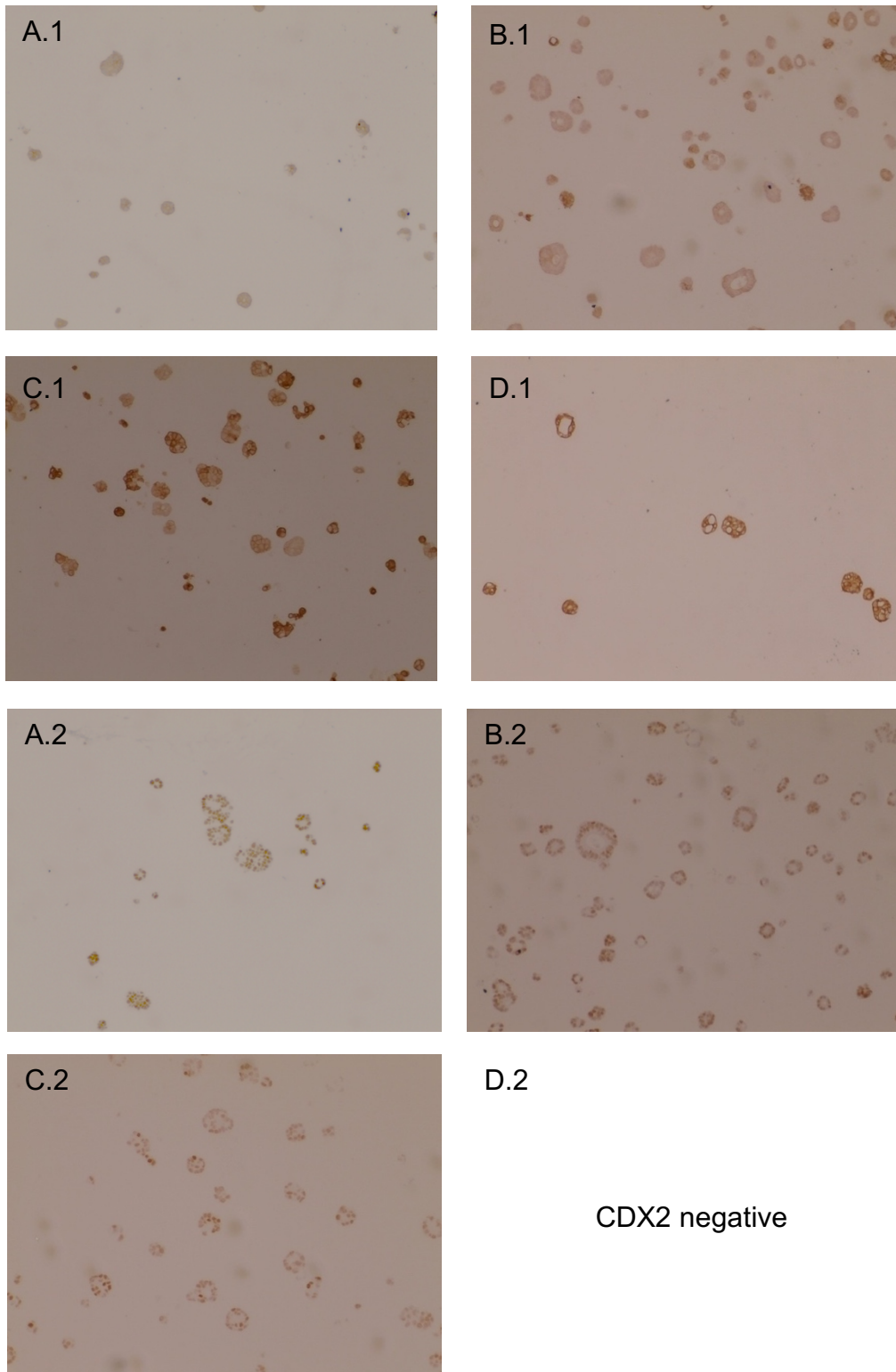


Figure 4.5 - Immunohistochemistry stains of organoids.

Stains of organoids for Pan-Cytokeratin (A.1-D.1) and CDX2 (A.2-D.2). A) S292064, B) S302389, C) S309884, D) S345653. S2345653 lines were not stained for CDX2.

### **4.3.3. Mutational profile**

To further characterise selected organoid lines, a molecular profile of genetic mutations was created. This was done with a custom targeted panel sequencing (Qiagen). A list of 30 genes (full list can be found in Section 2.9.1.1, Table 2.6) commonly mutated in colorectal cancer was selected and organoid DNA was enriched for selected genes to investigate the mutations present in the organoids. As this was performed when the S345653 line was not yet available, the matched mutational profiles have been analysed using whole genome sequencing data that was performed for a different experiment (Chapter 5). A simplified schematic of the most significant mutations is summarised in Figure 4.6.

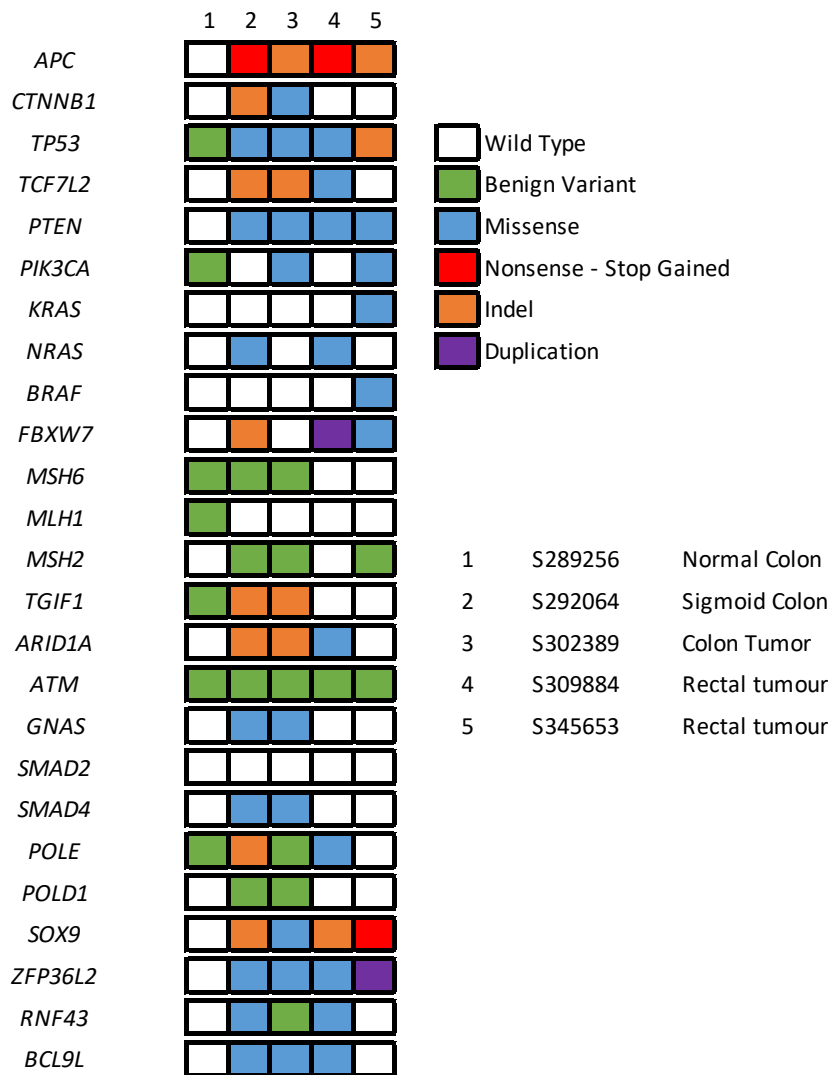


Figure 4.6 - The results of the panel sequencing.

An overview of mutations of selected organoid lines (4 lines selected for this study and a normal tissue organoid as a control). Indel- Insertion/Deletion mutation.

The figure shows the types of mutations found in the most commonly mutated genes in colorectal cancer. More than one variant was found in some cases, however then the variant that was thought to be more impactful was chosen to be presented in the figure.

For sample S345653 this data was extracted from whole genome sequencing to match the genetic profiles obtained for the other samples with panel sequencing.

As expected, all lines had mutations of the *APC* gene. A stop gain mutation was found in sigmoid line, whereas an insertion in exon 17 resulting in frameshift was detected in colon organoids. In rectal line S309884 a stop gain mutation was detected, however, frameshift mutations were also found resulting in multiple stop gains. A deletion in exon 16 causing frameshift and early termination was detected in another rectal line (S345653). Additionally, lesions of Wnt pathway associated genes such as *CTNNB1* and *RNF43* were also detected with missense variants present in all tested lines. Furthermore, missense mutations known to be involved in colorectal carcinogenesis such as *TP53* and *SMAD4* were also present with *TP53* being mutated in all of the lines. *SMAD4* mutations were found in sigmoid and colon organoids lines. Furthermore, alterations of *SOX9* were found in all tumour lines. Indel mutations of *SOX9* were detected in S292064 and S309884 whereas missense and nonsense mutations were found in S302389 and S345653 respectively. Furthermore, mutations of *POLE* were also detected, whereas for colon organoids it was identified as a benign mutation. *KRAS* and *BRAF* missense mutations (p.Gly12Asp and p.Asp594Gly respectively) were found only in the S345653 line. Although, *KRAS* alterations were not present in the remaining 3 tumour lines, missense variants of the *NRAS* gene were found in the S292064 line and S309884 organoids. *FBXW7* was found to be duplicated in rectal S309884 organoids and in sigmoid organoids. These also had indel mutations in coding regions with one insertion resulting in a stop

gain. Lastly, two *PIK3CA* mutations were found, a missense mutation in the S292064 line resulting in possible splice site disruption and another missense mutation in the S345653 line. We have noted a low count of the *PIK3CA* variant in the S302389 line; however it had good coverage and quality score. A normal tissue organoid line was also sequenced to confirm the organoids in the culture are indeed derived from normal tissue and there was no contamination. No non-benign variants were found confirming the non-tumour origin of the organoids.

As the rectal line S345653 was available later in this study, it was not sequenced with the custom panel initially with the other samples. The sample was whole genome sequenced and using the panel gene list we investigated the line variants. The following mutations were identified: a nonsense mutation in *APC*, and a point mutation of *KRAS* (p.Gly12Asp) and *BRAF* (p.Asp594Val). Furthermore, missense mutations of *FBXW7* (p.Arg385His) and *PIK3CA* (p.Cys378Arg) were identified. The remaining variants can be seen in Figure 4.6.

The available patient information showed that both S292064 and S302389 had no Ras mutations, nor BRAF V600E. The S309884 patient had a mutant NRAS and S345653 had a mutant KRAS. This matched with the mutations found in corresponding organoids, with the exception of S292064 organoids having mutant NRAS (a frameshift mutation which would not have been detected by the SOC assays from the primary tumour which could only detect single base changes).

Additionally, a whole genome sequencing analysis was performed to compare the original tumour with the corresponding organoid line and the preliminary data showed >99% similarity in detected mutations (data not shown as still under analysis).

#### **4.3.4. Irradiating organoids**

Once the organoids were well characterised and expanded it was important to determine the best method of irradiating lines to model the response of cells to clinical radiation dose. Firstly, it was decided that due to time limitations of the study, the lines are going to receive only short-course therapy – 25Gy dose delivered in 5 x 5Gy fractions. Next, an appropriate time for the cultures to be irradiated was chosen. As the organoid cultures were derived from adult stem cells/patient tumour cells, the ongoing cultures were expanding and required passaging. Furthermore, for certain experiments the organoid cultures had to be further expanded to test the long term effects of irradiation. Results of treatment of organoids freshly formed shortly after passaging could have been impacted due to cultures being still fragile after splitting. Furthermore, newly formed organoids were too small and therefore would not replicate the 3D tumour conditions too closely, where the bigger structures had more uneven access to the oxygen and nutrients, which plays a big role in radiation response. On the other hand, when the cultures were too mature they would start to die off if not passaged, therefore the effects of irradiation could not be explicit. After observing the cultures, 3<sup>rd</sup> day after plating organoids after passaging was chosen as the

most appropriate time to start irradiation treatment. The organoids would form mature enough structures, but wouldn't have started accumulating dead cells. An example of culture 3 days after being plated for the irradiation experiment can be seen in Figure 4.7.

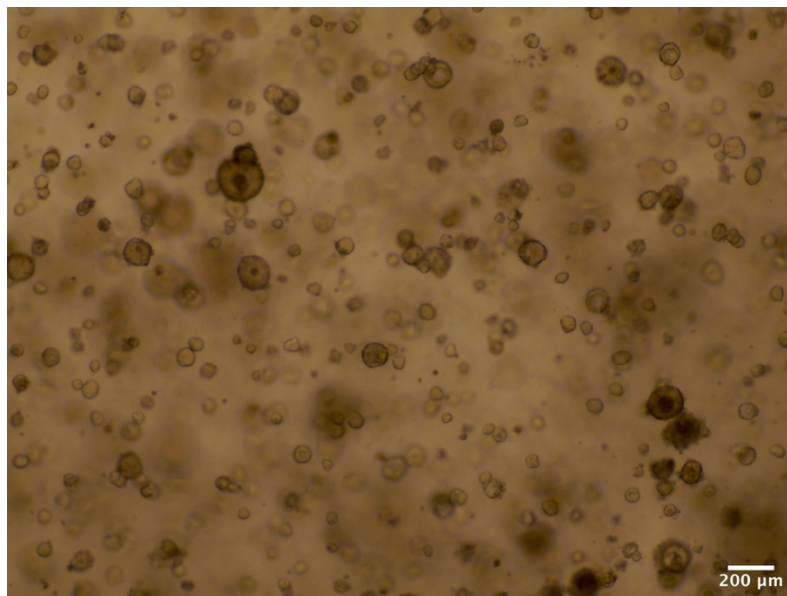


Figure 4.7 - Organoids ready for the irradiation experiment.

A microscope image showing organoids plated for the irradiation experiment ready for the first dose delivery at 3 days after passaging. The image shows organoids from the S302389 line.

Initially, the irradiator available for delivering treatment to cells was the IBL 437C irradiator (CIS Biointernational) that would deliver gamma radiation from a caesium source. However, technical issues were encountered due to certain machine features. The diameter of the cylinder holding samples for the radiation delivery was smaller than the plates with organoid cultures. In order to overcome this issue different solutions were tested (Figure 4.8).

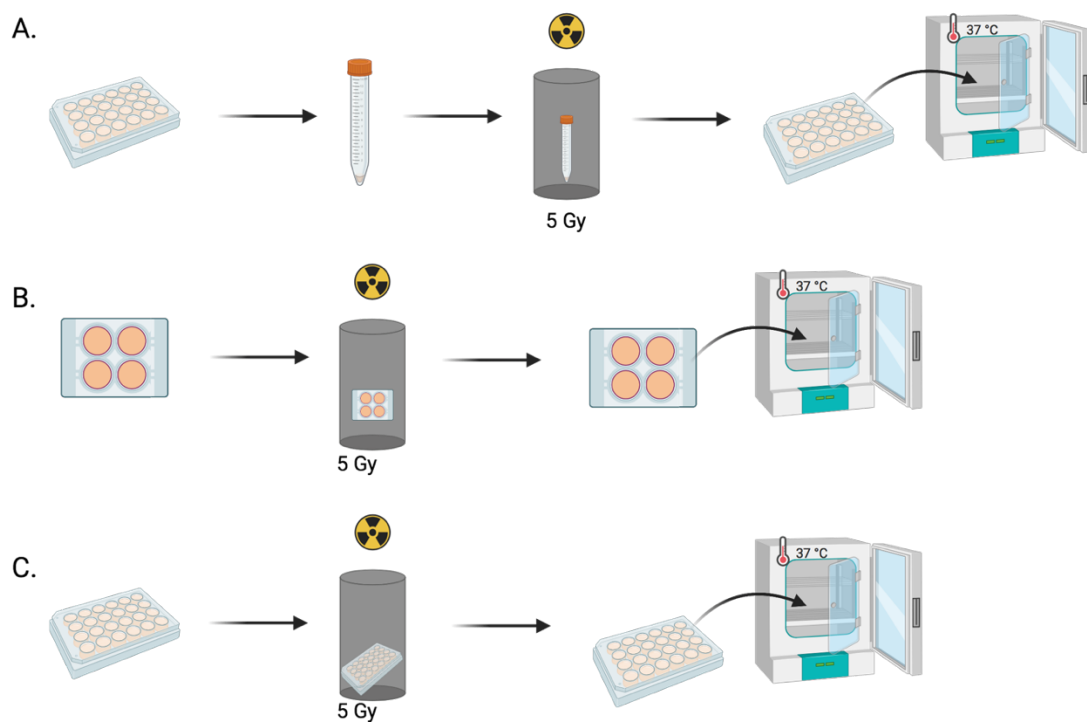


Figure 4.8 - Schematic of irradiation delivery with IBL 437C irradiator.

A. Plated organoids were resuspended with PBS0 and collected into a sterile 15ml falcon tube and transported to the caesium source irradiator. The organoid containing tube was placed in the irradiator's cylinder and single 5Gy dose was delivered. The organoids were then transported back to the tissue culture lab and re-plated on a new, sterile 24-well plate and put into culturing incubator. This process was repeated daily until the final dose of 25Gy was delivered.

B. Organoids were plated and cultured on sterile IVF 4-well Nunc plates. The plates were then transported to the caesium source irradiator, placed in the irradiator's cylinder and irradiated with a single dose of 5Gy. The organoids were transported back to the incubator.

C. Organoids were plated for the experiment on 24-well or 96-well plates in preparation to the experiment. The plates were transported to the caesium source irradiator and placed in the cylinder. In order to fit the plates in the cylinder they had to be tilted. The single dose of 5Gy was delivered and the organoids were transported back to the incubator.

Created with Biorender.com

Firstly, plated organoids were collected with ice cold PBS0 into sterile 15 ml falcon tubes, which were kept on ice while transported to the machine and tubes were then further placed in the cylinder and irradiated. The organoids were re-plated onto a fresh plate until the next dose. This method was not suitable for studying the delivery of clinical dose in 5 fractions, as repeated re-plating of

organoids after irradiation treatment was thought to introduce too much variation and putting organoids under additional stress. To overcome this particular issue, we searched for smaller plates for culturing organoids. As smaller culturing plates were not available, we have chosen sterile Nunc IVF dishes (Thermo Fisher Scientific, USA). These dishes would fit into the irradiator cylinder, however as the dishes were not manufactured specifically for cell culture, the organoids would often get infected due to compromised sterile conditions caused by the loose lid. Furthermore, cultures would get compromised during transport to the irradiator located in a different building. Finally, organoid lines were cultured on 24-well plates or if prepared for the viability assay on 96-well clear bottom plates. For the dose delivery, plates were wrapped with parafilm and transported to the irradiator. Then, one plate at the time was put into cylinder by tilting it in order to fit. It was found that by tilting the plates the media would not spill or cross to a different well. However, in order to avoid any contamination, each line was cultured on separate plates with multiple replicates. Nevertheless, this method was not ideal therefore an X-ray irradiator was acquired which would fit plates without compromising the experiment. From this point onwards, the organoids were plated for the experiment and cultured for 3 days prior to starting the irradiation course. At day 3 after being passaged, plates with organoids were sealed with parafilm, transported into the X-ray irradiator and a 5Gy dose was delivered. Immediately after irradiation, the organoids were transported back to the incubator where they were placed without the protective parafilm until delivery of the next dose (see Figure 4.9). This was process was repeated four more times

to replicate a 5x5Gy short course radiotherapy treatment resulting in a total dose of 25Gy. The media was changed every 2 days as with any other organoid culture. This method was used for all following experiments, apart from irradiating lines for single-cell sequencing due to the time limitations of the study. Lastly, for all of the irradiation experiments there was a separate control plate for each organoid line that was treated exactly the same (including securing with parafilm, transporting to the irradiator room, and media changes) apart from receiving irradiation treatment.

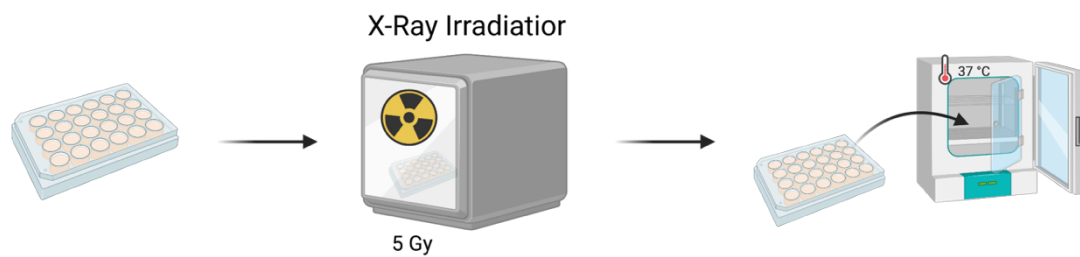


Figure 4.9 - Irradiation method schematic.

Organoids cultured on plates were irradiated with 5Gy single dose X-ray irradiator and then placed back into the culturing incubator. This process was repeated daily until the total dose of 25Gy was delivered.

Created with Biorened.com

#### 4.3.5. Measuring organoids' viability after irradiation treatment

For the next step in determining the modelling of irradiation response with organoid lines was measuring the effects of the treatment – with the question of what is the best way of measuring the response and after what time it is best to investigate it. Firstly, visual investigation was performed, where morphology of control organoids was compared to irradiated organoids under microscope 3

hours after delivery of the last dose. As it can be seen in Figure 4.10, all lines responded to irradiation as more dead cells can be observed in irradiated lines than in the control counterparts. Furthermore, from visual inspection the most dead cells were seen in the line S302389 that was irradiated. What is more, the least difference was observed between the control and treated S309884 organoids.

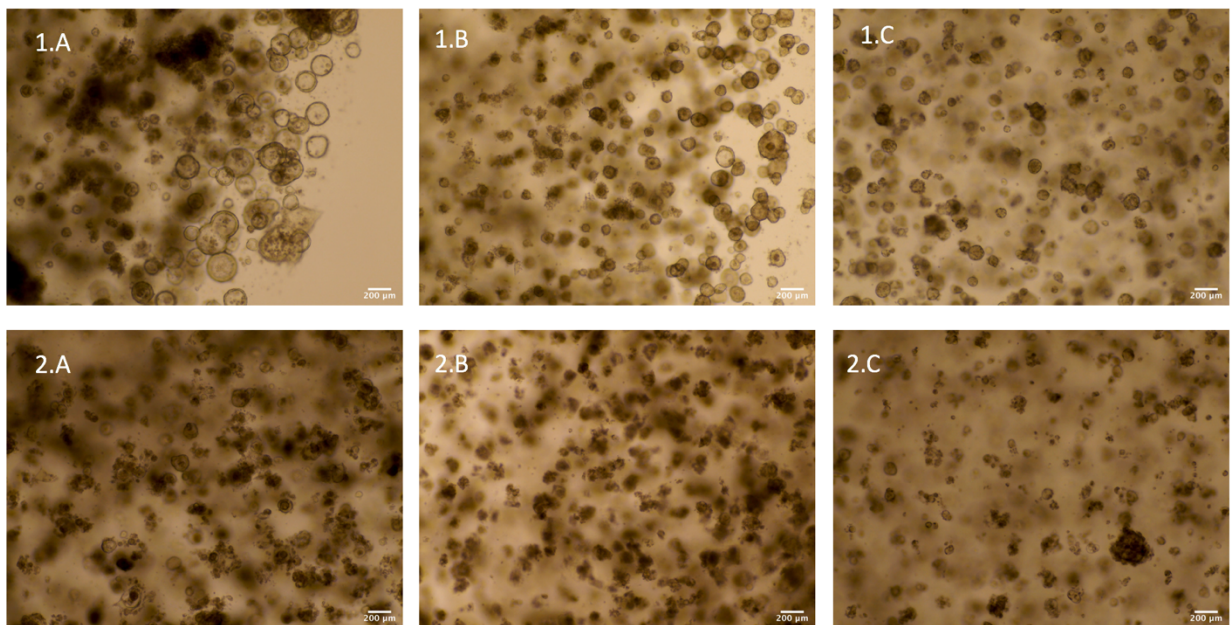


Figure 4.10 - Irradiation effect on organoid lines.

A visual comparison of control organoids (1.A-1.C) with organoids that have received an equivalent of short course radiotherapy -25Gy in 5 fractions (2.A-2.C).

Although, the microscope examination of organoids and their growth following the irradiation treatment would show that all lines respond to irradiation, with a line to line variation, it would not give quantitative results that would allow the

response to be measured more accurately. Therefore, in order to measure cell death, a viability assay was performed from this point onward, which would measure cell activity by utilising released ATP in the luminescence reaction. The chosen viability assay was a 3D cell dedicated kit – a CellTiter-Glo 3D from Promega. The line S345653 wasn't available when the initial irradiation experiments were performed, so there is no visual comparison for these organoids. When treated with irradiation the viability of S345653 organoids was measured solely with the viability assay.

After choosing an appropriate viability assay, it was decided not to test the viability on the same day as the last dose of irradiation is delivered. It is known that the effects of radiation on tissue take time and in the clinic the interval between treatment and surgery is between 4 to 8 weeks. We could not introduce this interval between the treatment and the measurement of viability due to culture limitations, as much time as possible was allowed before the appearance of cell death related to space limitations occurred. The cell viability assays were performed 96 hours after the last dose of irradiation was delivered. We have also investigated the long terms effects of irradiation by expanding the cultures after irradiation, however, for the majority of experiments this was a standardised protocol.

The viability assay performed 96 hours after irradiation showed that each line responds to irradiation with a big reduction in cell viability. Furthermore, the differences between each line response were also visible (see Figure 4.11),

confirming the initial visual investigation. The rectal line (S309884) displayed the lowest reduction in viability after irradiation treatment. Both sigmoid and colon lines' viability was reduced a lot and at similar level. Further analysis of the irradiation response of the lines is described in the next results chapters.

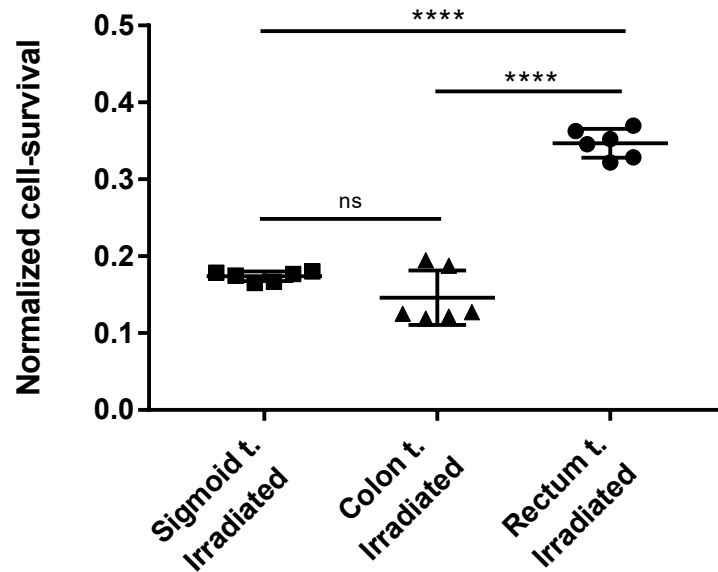


Figure 4.11 - Irradiation response.

A comparison of response to irradiation for three lines: S292064 (Sigmoid tumour), S302389 (Colon tumour) and S309884 (Rectum tumour). Organoids received 25Gy in 5 fractions using X-ray irradiator. t- tumour. The response was measured with normalised viability.

## 4.4. Discussion

### 4.4.1. Organoid pathology

To summarise, three organoid lines were initially selected as models for studying the radiotherapy response. Those lines all came from three different patients with advanced T3 stage colorectal cancer with proficient MMR. Each line represented

a different part of colorectal tissue – colon (S302389), sigmoid (S292064) and rectum (S309884). The rectal line was established from the tumour of a patient that had received neo-adjuvant short- course radiotherapy. Another line established from a rectal tumour (S345653) was added to the study due to its contrast relative to the other lines' characteristics. First of all, the patient the line was established from had received long-course neo-adjuvant radiotherapy before the resection, and the tumour was classified as chromosomally stable. The S302389 tumour was classified as a mucinous subtype of CRC. Mucinous adenocarcinoma comprises of only 10-15% of all CRC cases and has been linked to a higher rate of *KRAS* and *BRAF* mutations and *MSI* (Li et al. 2020), interestingly neither *BRAF* nor *KRAS* mutations were detected in the S302389 line, and what is more it was classified with pMMR. All derived lines have expressed pan-Cytokeratin, an epithelial marker present in the intestinal tissue, validating that the established organoids were derived from epithelial tissue. Furthermore, when stained for the CDX2, a marker of intestinal phenotype found in CRC (Graule et al. 2018). CDX2 has been shown to serve as a prognostic marker as the reduced expression of CDX2 in CRC has been correlated with cancer progression, metastasis, and poor prognosis (Zhang et al. 2016). All lines apart from the S345653 rectal cancer line stained positive for the marker. The tumours from which the organoids were derived stained positive for both markers. The loss of CDX2 can occur with the exposure to radiotherapy treatment, with a potentially reduced amount of CDX2 present in tumour tissue, the selected cells and clones for the organoid derivation could result in the complete loss of CDX2.

The advanced state of the S234563 tumour could account for the low expression of CDX2 and when deriving organoids, subclonal populations of cells that do not express the marker, due to their aggressive nature, were selected and expanded in culture.

#### **4.4.2. Genomic characterisation of organoids**

Many studies have been conducted in order to investigate the mutational profiles of colorectal cancer tumours and to identify the most commonly mutated genes occurring in CRC. Mutational profiles investigated with DNA sequencing have shown the presence of mutations which corresponded with current findings of common genetic alterations found in CRC. As expected, genes involved in the Wnt signalling pathway such as *APC*, *CTTNB1*, and *RNF143* were found to be mutated in organoids. *APC* mutations were detected in all organoid lines, and the alterations included nonsense mutations and frameshift mutations resulting in a truncated protein. It has been shown that in CRC patients the majority of mutations in the *APC* gene leads to truncated protein and 30% of those are a result of a nonsense or point mutation, whereas the majority (68%) is caused by a frameshift mutation (Bèroud and Soussi, 1996). Although a small population of organoids were characterised, we have found more frameshift mutations, as they were detected in 3 out of 4 organoid lines, and nonsense mutation were present in 50% of the lines. This correlates well with the known literature, considering the small sample size. Furthermore, *SOX9* and *TP53* alterations were found in all

organoid lines, whereas *SMAD4*, and *ARID1A*, *FBXW7*, and *PIK3CA* lesions were found in some organoid lines. These lesions, along with *APC* and Wnt mutations, were found to be of the most commonly mutated in a TCGA study that looked at a large population of colorectal cancer samples in order to characterise mutational profiles of CRC patients (The Cancer Genome Atlas Network, 2012). More recent studies that characterised CRC genetic profiles also found the mentioned mutations along with *BCL9L* and *KIT* alterations (Giannakis et al. 2016, Stodolna et al. 2021). The *BCL9L* mutations were detected in 3 organoid lines, whereas the *KIT* gene was not in the targeted panel gene list, so it is not known if mutations of this gene were present in the organoid lines. Interestingly, a *KRAS* mutation was only detected in S345653 rectal line, whereas *KRAS* has been shown to be one of the top mutated genes in CRC (The Cancer Genome Atlas Network, 2012; Dinu et al. 2014). Although not all tumours carry mutant *KRAS*, we expected to see more lines with mutations in this gene. The established organoid lines carry the mutation characteristics for colorectal cancer. Furthermore, the Ras and BRAF V600E status of patients clinical data matched the organoids status for those mutations, with the exception of the S292064 organoid line. The panel sequencing showed that the sigmoid organoids have NRAS frameshift mutation. The clinical data suggest a wild-type variant, however the particular mutation that was detected with our panel could possibly be missed in the clinical assay, and therefore not reported. Additionally, the preliminary WGS data that compared tumour resection with the organoids

showed over 99% similarity in the mutational profiles (data not shown as still under analysis).

The mutation profiles of the organoid lines are characteristic of non-hypermutated tumours (The Cancer Genome Atlas Network, 2012), which would correlate with patient information stating that all patients recruited to this study were pMMR.

Based on the sequencing results and patient information, we are confident that the organoid lines have similar mutational profiles as the CRC patients. Furthermore, the normal tissue organoid line exhibited only benign mutations, confirming the organoids derived from patients have been established appropriately and are representative of the patients' tissue of origin. Finally, certain gene mutations such as *PIK3CA* were found in low counts but with good quality scores, supporting the evidence that organoids are highly heterogeneous such as primary tumours, with different clone subpopulations. With this finding we were confident that the established organoid lines were accurate and representative models for CRC tumours.

#### **4.4.3. Organoid irradiation**

As previously mentioned, one of the aims of this study was to establish a method of delivering short course radiotherapy to the organoids. The method we developed involved minimising external factors that could impact the response of cells to the treatment, and the dose regimen was chosen to replicate clinical

conditions. The clonogenic assay method is a “gold standard” for researching radiotherapy response using cell lines (Matsui et al. 2019). However, this method has not been chosen in this thesis. As organoids grow into small cell colonies that can self-organise into 3D structures we speculated this assay is not essential to measure the endpoint survival. The viability assay was chosen to quantify the level of cell death instead. Furthermore, the irradiated organoids were subsequently expanded into resistant lines by down-selecting the viable cells. Although, irradiation studies utilising organoids were not available at the start of this project, in the last couple of years more and more publications which use organoid models to predict response to radiotherapy have emerged (Ganesh et al. 2019; Martin et al. 2020; Yao et al. 2020). We have noted that similar methods of delivery of irradiation and assessing organoid viability were chosen. Ganesh et al. in their study would plate approximately 10 000 cells per well. Both Ganesh et al. Yao et al used X-rays as a source of radiation. Furthermore, a chemiluminescence assay for measuring viability was chosen as the method for accurately determining the response to radiotherapy.

In this study, in order to allow cells to recover and take the effects of irradiation after delivery of the last dose, the viability was measured 96 hours after the last dose of treatment was delivered. This is similar to the methods that have been published where the viability was assessed at least 3 days post irradiation in all of studies, ranging from 3 to 11 days from the dose delivery (Ganesh et al. 2019; Martin et al. 2020; Yao et al. 2020). It is known that irradiation induces long term effects, and to fully see the results of the radiotherapy a longer period for cell

recovery is needed (Shiff et al. 1990; Glimelius, 2014). Nevertheless, with a relatively short (but still considered extended) recovery period we have observed a response to the treatment and differences in response between the different lines. This suggests the chosen time for measuring viability is appropriate and informative enough to study the lines' response to irradiation.

#### **4.5. Conclusions**

In conclusion, the selected lines for studying irradiation response pose as a good representation of colorectal cancer and resemble the original tumour tissue from which they have been derived. Therefore, we believe they can model a truthful response to irradiation treatment. Additionally, a method of delivering short-course radiotherapy has been successfully established which enables studying the response to treatment using these patient derived organoids as models.

## **5. RESULTS CHAPTER 3: EFFECTS OF IRRADIATION TREATMENT ON COLORECTAL ORGANOID AND THEIR GENOMICS**

### **5.1. Introduction**

Radiotherapy as a part of rectal cancer therapy is a standard in the current clinical setting and it plays an important role in the overall treatment. Radiotherapy was first used to treat rectal cancer in 1973, where Papillon used a specialised proctoscope to deliver radiation directly to the tumour. As the tube that would deliver the X-rays had to be in direct contact with the tumour, the treatment was possible only for early stage rectal cancers. The treatment was well tolerated by patients, even the elder and frail ones, and had good outcomes (Papillon, 1973). In case of advanced rectal cancer the treatment included surgery only until the mid 1980s. However, consequent to this was that the rate of local recurrence was high and the overall survival was poor (Tseng et al. 2019). With the introduction of an improved surgical method – total mesorectal excision (TME) – local recurrence rates reduced significantly to around 5-10%. Furthermore, at the time several clinical trials have investigated introducing radiotherapy or chemo-radiotherapy treatment that would follow the surgical excision for the advanced rectal cancers (T3/4, N+). It was clear from all trials that the adjuvant RT improves local recurrence rates; however it does not have a significant impact on overall survival (Gastrointestinal Tumour Study Group, 1985; Fisher et al. 1988; Krook et al. 1991; Colorectal Cancer Collaboration Group, 2001). Despite having no

impact on the overall survival rates, the reduction in local recurrence was still very important.

Adjuvant chemotherapy has been shown to improve overall survival, hence the National Health Institute has officially recommended adjuvant chemo-radiotherapy as a standard of care (NIH consensus conference, 1990). This quickly became a standard in clinical care for advanced rectal cancer patients (Tseng et al. 2019). Further randomised trials looked into adjuvant vs. neoadjuvant radio-chemotherapy. A German CAO/ARO/AIO 94 phase III trial has studied the comparison of pre- and postoperative chemo-radiotherapy in 823 patients with locally advanced rectal cancer. The results showed significant advantage for the preoperative chemo-radiotherapy as the cumulative 5-year local recurrence rates were only 6% in preoperative group in comparison to 13% for the postoperative group. The acute and chronic toxicity rates were also lower with the preoperative chemo-radiation (Sauer et al. 2004). What is more, the 10-year cumulative local recurrence rates were investigated and were 7.1% and 10.1% for pre- and postoperative groups respectively. No significant difference in the 10 year disease-free survival was noted (Sauer et al. 2012). Another influential trial (NSABP-R-03), that also compared chemo-radiotherapy administration before and after surgery in locally advanced rectal cancer patients, showed advantage of preoperative chemo-radiation over the postoperative. The disease-free survival was 64.7% in the preoperative cohort in contrast to 53.4% in the postoperative cohort. The rates for the 5-year overall survival were 74.5% vs. 65.6% (in the same order) and 15% of patients had a complete pathological

response to treatment in the preoperative cohort (Roh et al. 2009). In addition to this, another trial has been conducted before TME became standard practice. The Swedish rectal cancer trial has randomised patients with T1-3 rectal cancer and compared the short-course radiotherapy administered prior to surgery with surgery alone. A significant decrease in local recurrence was observed - 12% vs. 27% for neoadjuvant radiotherapy administration vs. surgery alone. In addition, the 5-year overall survival was better for patients treated with short course radiotherapy prior to surgery (58%) in comparison to the cohort treated with surgery only (48%; Cedermark et al. 1997). A follow up was performed after 13 years, noting that the overall survival was still better for the group treated with radiotherapy prior to surgery – 30% vs. 38% (Folkesson et al. 2005). A fourth trial that deserves consideration looked at the neo-adjuvant administration of short-course radiotherapy but employing the TME surgical method. This trial found that although there was no difference in overall survival, the local recurrence rates were significantly lower for the irradiation treated patients (Kapitejin et al. 2001). Lastly, another trial looked into the difference between short-course radiotherapy delivered before surgery and postsurgical delivery of chemo-radiation, finding that the local recurrence rates were significantly decreased in the preoperative cohort (Sebag-Montefiore et al. 2009).

As some of the trials run in parallel, there are two treatment routes in rectal cancer treatment – short course radiotherapy or long course chemo-radiotherapy. Both of these are delivered prior to surgery as the data clearly showed more favourable outcomes for the patients receiving radiotherapy in such a setting. These trials

have shown the significance radiotherapy in rectal cancer treatment and its effect on reduced local recurrence which is crucial in the management of rectal cancer (Tseng et al. 2019).

It is understood that a big role in the poor response to radiation treatment is tumour resistance. In an ideal scenario, within the delivery of treatment the irradiation effects act onto cancerous cells and result in their death. However, with irradiation treatment the tumour cells can potentially acquire resistance through the clonality of the resistant subclone (Laurent-Puig et al. 2015).

Rectal tumours have been shown to be resistant to radiotherapy as 40% of patients will have no significant response to the treatment, and only 10% of patients will have complete pathological response (Geng and Wang, 2016). In order to improve the treatment outcomes it is necessary to understand why certain patients respond completely, some partially, and the majority very little to the radiotherapy. It has been shown that cancer stem cells (CSCs) play a role in both acquired and native resistance to radiotherapy (Galez, Totis and Bisio, 2021). They have shown resistance to cytotoxic effects of reactive oxygen species and have a higher DNA repair potential (Diehn et al. 2009; Maugerri-Saccá, Vingerri and De Maria. 2011). In addition to CSCs and their role in radioresistance, an epithelial-to-mesenchymal transition (EMT) has also been proposed to play a role in acquired radioresistance (Sato, Shimokawa and Imai, 2019). The EMT results in upregulation of mesenchymal markers and cancer cells that are invasive and have migratory properties that have been associated

with poor prognosis (Wu et al. 2018; Zhang et al. 2020; Cheng et al. 2021). Different studies that have exposed cell lines to small doses of X-ray irradiation over a long period of time have shown that exposure to irradiation promotes EMT or disrupts pathways such the DNA repair, Akt signalling pathway, and mTOR signalling pathway (Shimura et al. 2010; Shintani et al. 2011; Shimura et al. 2014; Shimura et al. 2017).

Although different studies have been done in order to understand resistance to radiotherapy and potential targets have been suggested, there is still no identified marker for radiosensitivity. Furthermore, all mentioned studies have been done on cell lines which, as discussed in Chapter 1, have been shown not to be representative of heterogeneous tumours. In this chapter we describe how we have used organoids derived from colorectal cancer patients as models and subjected them to short-course radiotherapy in order to study the impact of irradiation on CRC tumour cells. We have also taken a multiomics approach to analyse the control and irradiated organoids in order to see if we can identify and confirm initial findings of new radioresistance and radiosensitivity markers.

## **5.2. Aims and Methods**

The main aim for this chapter is to make use of organoid models to characterise changes to the genome and gene expression that arise after short-course radiotherapy in order to identify potential biomarkers for either radioresistance or radiosensitivity.

The objectives for this chapter are as follows:

1. Investigate the response to irradiation for each of the organoid lines.
2. Investigate changes that irradiation causes to DNA after short-course therapy.
3. Investigate the changes that occur in gene expression in organoids that are treated and not treated with short-course radiotherapy.

Using established colorectal organoid lines we planned to investigate their response to irradiation with a cell viability investigation, DNA sequencing, methylation arrays and RNA sequencing (see Figure 5.1).

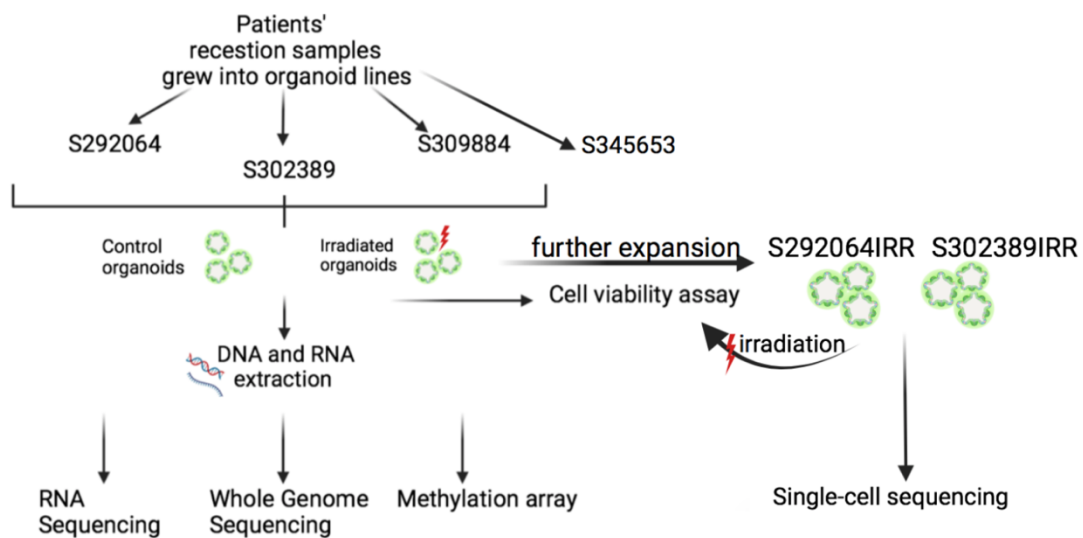


Figure 5.1 - Experimental plan schematic.

Established organoid lines from 4 different patients were subjected to short-course radiotherapy equivalent; control organoids were grown in parallel but were not subjected to treatment. The cell viability was performed to investigate the response. Nucleic acids were extracted from the remaining organoids (line S345653 was not subjected to RNA/DNA extraction and genomic analysis). 6 technical repeats were used for DNA and RNA extraction. Extracted DNA and RNA was used for whole genome sequencing, total RNA sequencing, and DNA methylation arrays. All

lines were further expanded after the radiation treatment and grew into resistant lines. Two lines were established this way: S292064IRR and S302389IRR. The response to irradiation was investigated for these IRR lines and single-cell sequencing was performed to understand the radioresistance driving mechanisms.

The irradiation therapy delivered to the organoid lines was equivalent to clinical short-course therapy – 25Gy delivered over the course of 5 days in 5Gy fractions. At first all of the organoid model lines have been investigated for their individual response to irradiation, a short course radiotherapy equivalent. Newly passaged organoids were plated on 96-well clear bottom plates in triplicate technical repeats. On day 3 after plating, short course radiotherapy was delivered and the viability measured 96 hours after the last dose was delivered (the detailed protocol for irradiation method is described in Chapter 2 Sections 2.3.3.1 – 2.3.3.2).

In parallel we cultured the organoid lines and also subjected them to short course radiotherapy. We then extracted DNA and RNA from the treated and control untreated organoids 96 hours after delivery of the last dose. The DNA was studied for methylation changes with 450k Methylation Arrays and whole genome sequencing analysis, whereas the extracted RNA was investigated with total RNA sequencing.

The experiments investigating genomic changes have been performed only on 3 lines (S292064, S302389, and S309884) due to certain organoid lines only becoming available later in the study. However, response to irradiation has been tested on all of the lines and is presented in this chapter.

## **5.3. Results**

### **5.3.1. Irradiation response**

Initially, three organoid lines were subjected to irradiation and their response was measured as briefly mentioned in the previous chapter (see Figure 4.11). A significant drop in viability was observed in organoids after irradiation. Furthermore, it was noticed that the survival of rectal (S309884) organoids after irradiation was higher than colon and sigmoid organoids after irradiation. The irradiation response was then re-measured for all lines available and the control vs. irradiated responses were plotted as well as just the irradiation response (see Figure 5.2). As in the initial irradiation response experiment, a significant response and a drop in organoid viability was observed in all lines after irradiation treatment. Lines S292064 and S302389 had similar responses to the first experiment and there was no significant difference in response between these lines. Over 90% of organoids from both of these lines lost their viability after irradiation treatment. Moreover, rectal line S309884 had consistently responded significantly less to irradiation in comparison to the other two lines, but with the majority of organoids still dying following irradiation treatment. Response to irradiation of another rectal line (S345653) was also significantly poorer in comparison to other lines and had the lowest response out of all lines subjected to radiotherapy.

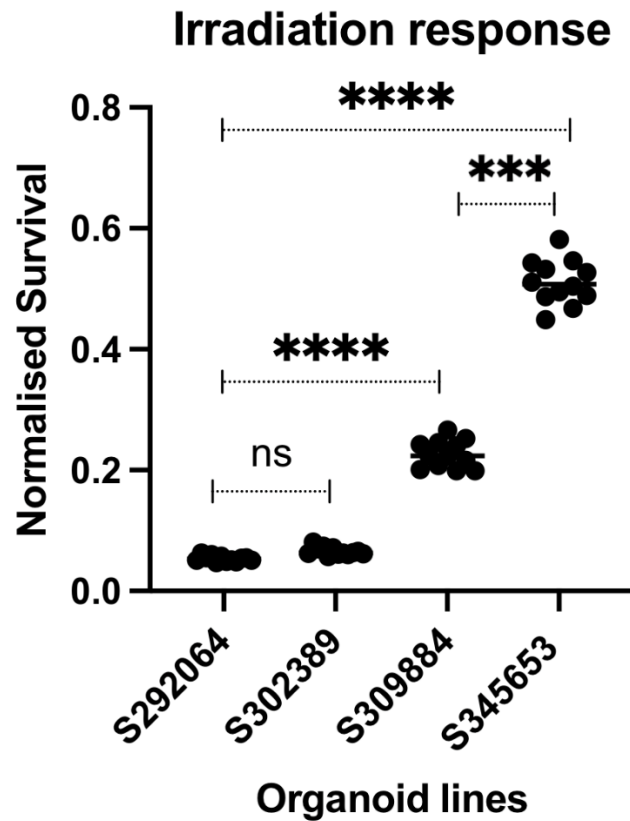


Figure 5.2 - Organoid response to irradiation.

All organoid lines and their response to irradiation. The normalised survival rate was calculated for each line. S292064 and S302389 responded well to irradiation, whereas S302884 had a moderate response and S34564 had a poor response. Significant differences between the line responses were calculated with paired t-tests.

Along with the organoids plated for the viability experiment, the same lines were plated on 24-well plates and treated with short course therapy for other experiments. A proportion of the organoids were kept, passaged, and further expanded in order to create corresponding irradiated lines for studying long term effects of irradiation. Both of the rectal lines did not further expand following passaging despite repeated attempts, however lines S292064 and S302389 both needed 5 gentle passages (with 2:1 ratio) before starting to expand again. The

new lines were referred to as S292064IRR and S302389IRR. The irradiated lines were exposed to short course radiotherapy and their viability was measured and compared against their corresponding original naïve lines as well as rectal organoids which come from tumours previously exposed to irradiation. The S292064IRR line was generated first before the S302389IRR expanded. Therefore only this line was initially compared to its naïve counterpart and rectal line S309884 (other rectal lines were also not yet available). The results of that experiment are shown in the Figure 5.3 A. There was a significantly lower response to irradiation for the irradiated line in comparison to the naïve line. Additionally, there was no significant difference between the rectal line (previously exposed to irradiation since the patient received radiotherapy) and the S292064IRR line. The experiment was repeated once line S302389IRR was generated and another rectal line (S345653) was available (Figure 5.3 B). Again, it was observed that the S292064IRR line had a poorer response to irradiation in comparison to its naïve analogue, whereas in S302389IRR there was no significant difference in response to irradiation since both naïve and irradiated lines responded well to the treatment, having very low cell viability. Furthermore, the S292064IRR line's response was similar to the S345653 line's response, which was noted as the poorest response to irradiation out of all subjected lines.

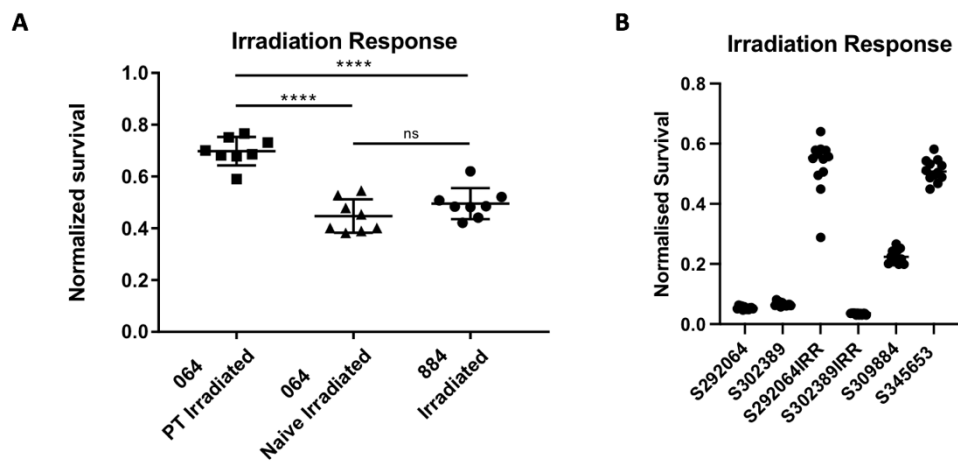


Figure 5.3 - Organoid irradiation response.

A) Comparison of in vitro made resistant lines with their naïve counterparts and with line from a patient that had received radiotherapy. 064 – S292064, 884- S309884, PT – post treatment, 064 PT- referred to as S292064IRR.

B) Response to irradiation for all of the lines including the resistant lines that were created in the lab.

Below is a table summarising all the lines, their origins, and their response to irradiation (see Table 5.1).

Table 5.1 - Summarised irradiation response information for organoids.

A summary of response outcome to irradiation treatment for each line along with clinical information for the patient the line was derived from. N/A – not applicable for patients that have not received radiotherapy.

Line ID	Origin	Organoids response	Patient's clinical response
S292064	Sigmoid tumour	Good	N/A
S302389	Colon tumour	Good	N/A
S309884	Rectal tumour	Partial	Poor
S345653	Rectal tumour	Poor	Poor
S292064IRR	Irradiated S292064	Poor	N/A
S302389IRR	Irradiated S302389	Good	N/A

To further investigate the effects of irradiation on cells, both DNA and RNA were extracted from control and treated organoids 96 hours after the last dose of irradiation was delivered. A series of investigations were performed to see whether we could identify drivers of radioresistance and radiosensitivity on a molecular level.

Firstly, we performed whole genome sequencing using the extracted DNA. For this experiment lines S345653, S292064IRR, and S302389IRR were not yet established. Therefore the results for this experiment and the following 2 experiments (methylation arrays and RNA sequencing) represent only 3 organoid lines: S292064, S302389 and S309884.

### 5.3.2. Whole genome sequencing

For the whole genome analysis, data for control organoid samples was merged and the same was done for irradiated organoid samples. The analysis was performed in order to observe the effects of irradiation on the whole genome and resulting patterns were investigated for copy number variations (CNVs) and single nucleotide variations (SNVs).

The results showed that irradiation treatment causes changes to the whole genome as we have observed multiple alterations (both deletions and duplications) across the whole genome (see Figure 5.4)

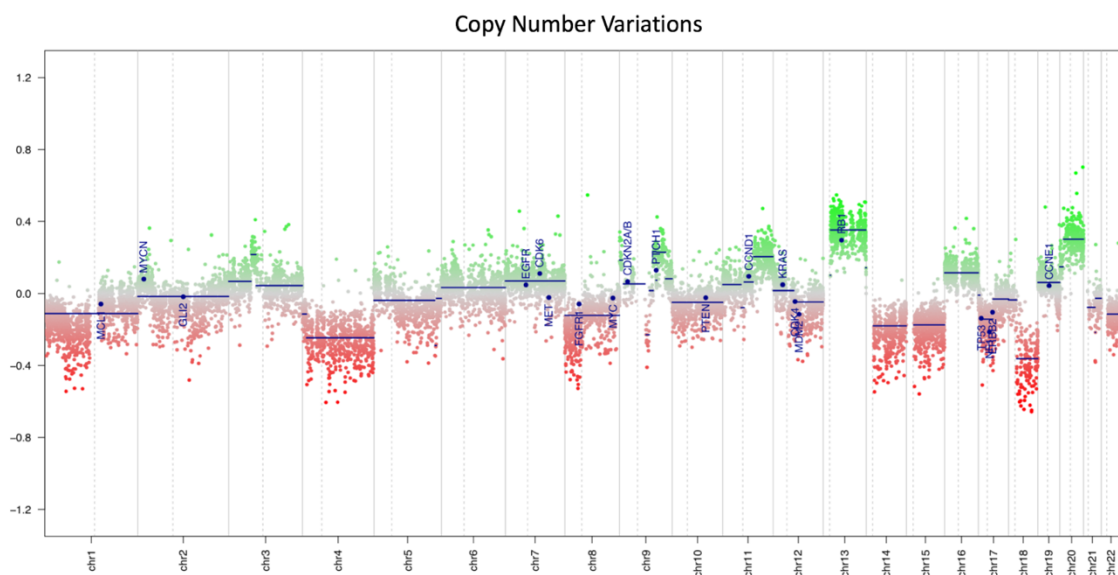


Figure 5.4 - Copy number variations (CNVs) scatter plot for irradiated samples. CNVs across the whole genome found in the irradiated organoid dataset.

Among the alterations caused by irradiation, we observed a gain of *MYCN*, *EGFR*, *CDKN2A/B* and a loss of *TP53*, *PTEN*, and *FGFR*. Deletions posed as the majority of detected CNVs and most of the deletions were large with >20bp.

In addition to patterns in CNVs, we have looked at patterns of SNVs across the irradiated samples. 1681 common variants were found after subtracting variants present in control samples. The nonsense mutations and variants in non-coding regions have been filtered out. In addition, we have filtered out any mutations with CADD score lower than 15 in order to have a list of mutations with pathogenic consequences and obtained a list of alterations of 78 genes. For simplifying reasons, we have filtered one alteration per gene, based on the highest CADD score. The list of top 10 mutations based on the CADD score are listed in Table 5.2.

Table 5.2 - Top 10 SNVs in irradiated organoids.

<i>Gene Name</i>	<i>Consequence</i>	<i>Variant</i>	<i>CADD score</i>
<i>SPINK5</i>	Stop gained	p.Cys646*	47
<i>ARAP2</i>	Stop gained	p.Glu1617*	43
<i>ZNF568</i>	Stop gained	p.Lys474*	41
<i>FXR1</i>	Stop gained	p.Arg291*	40
<i>PITX2</i>	Stop gained	p.Lys51*	39
<i>APC</i>	Stop gained	p.Arg1460*	37
<i>KIAA1324L</i>	Stop gained	p.Glu114*	37
<i>ACVR2B</i>	Splice acceptor variant	-	35
<i>ACVR2A</i>	Frameshift variant	p.Gly473fs	34
<i>KCNMA1</i>	Missense variant	p.Arg854Trp	33

Furthermore, we have found missense mutations in the *NRAS*, *RAF1*, and *HERC2* genes that have been shown to often be mutated in cancer and to be involved in cell signalling and DNA repair pathways. The details of mutations in those genes are in Table 5.3. The full list of genes can be found in Appendix B.

Table 5.3 - Highlighted SNVs.

<i>Gene Name</i>	<i>Consequence</i>	<i>Variant</i>	<i>CADD score</i>
<i>NRAS</i>	Missense variant	p.Gly12Cys	31
<i>RAF1</i>	Missense variant	p.Ser176Leu	24.6
<i>HERC2</i>	Missense variant	p.Lys3336Lys	24.6
<i>PIK3CA</i>	Missense variant	p.Thr1052Lys	23.2

### **5.3.3. Methylation array results**

After examining the irradiation effects on the genome we have also performed methylation arrays in order to examine any changes in methylation caused by irradiation treatment. Two technical repeats of each sample were processed. DNA extracted from control organoids and irradiated organoids was used for examining the methylome of the organoids with 450k microarrays (Illumina, USA). The results showed only thirteen significant differentially methylated positions (see Table 5.4). The p-value for each of the significant genes was below the 0.05 cut off value, however the adjusted p-values (adjustment method: Benjamini-Hochberg) suggested non-significance. The base factor for the majority of highlighted genes was greater than or equal to 4, suggesting the lack of significance in the adjusted p-values could be a result of the small sample population. The bar plots for each of the significant genes were investigated in order to assess the differential methylation. We observed a big difference in between two cohorts, suggesting the significance of these genes (all plots can be found in Appendix C). The heatmap for the significant genes is represented in the Figure 5.5.

Table 5.4 - List of all significant differentially methylated regions in treated and control organoids.

<b>CG ID</b>	<b>GENE NAME</b>	<b>P-VALUE</b>	<b>ADJUSTED P-VALUE</b>	<b>BASE FACTOR</b>	<b>REGION</b>
<b>CG22355463</b>	<i>ZNF827</i>	1.36x10 <sup>-6</sup>	0.21	5.87	Body-island
<b>CG03169527</b>	<i>C3orf31</i>	1.48x10 <sup>-6</sup>	0.21	5.79	TSS1500-shore
<b>CG14121014</b>	<i>NUP107</i>	1.83x10 <sup>-6</sup>	0.21	5.57	1stExon-island
<b>CG03390569</b>	<i>LOC100302652</i>	2.10x10 <sup>-6</sup>	0.21	5.44	Body-island
<b>CG05957736</b>	<i>PHLDB2</i>	2.85x10 <sup>-6</sup>	0.23	5.14	5'UTR-shore
<b>CG04861640</b>	<i>ZNF187</i>	4.41x10 <sup>-6</sup>	0.30	4.70	TSS200-shore
<b>CG17662034</b>	<i>RDH10</i>	5.65x10 <sup>-6</sup>	0.30	4.46	1stExon-island
<b>CG17438055</b>	<i>COX7A2</i>	6.42x10 <sup>-6</sup>	0.30	4.33	TSS200-opensea
<b>CG10213457</b>		6.69x10 <sup>-6</sup>	0.30	4.29	IGR-shelf
<b>CG04108612</b>	<i>PAFAH2</i>	9.53x10 <sup>-6</sup>	0.39	3.93	5'UTR-island
<b>CG01882498</b>	<i>LIN54</i>	1.12x10 <sup>-6</sup>	0.40	3.77	TSS1500-shore
<b>CG01358551</b>	<i>AP2S1</i>	1.23x10 <sup>-6</sup>	0.40	3.68	Body-island
<b>CG08081407</b>	<i>ARF4</i>	1.28x10 <sup>-6</sup>	0.40	3.63	TSS1500-shore

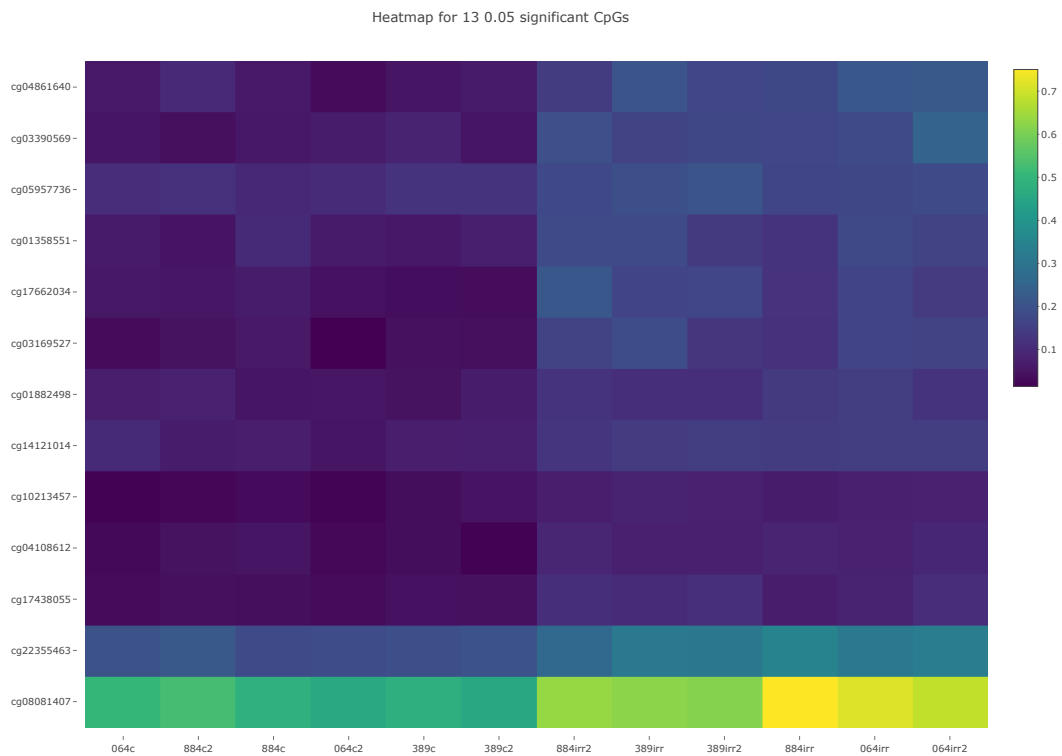


Figure 5.5 - Heatmap representing significant differentially methylated genes between irradiated and control organoids.

The data analysis did not reveal any differences in methylation pattern between control and treated organoids. Although there were no differences between irradiated and control samples, there was a clear pattern difference between the samples; most particularly the difference in S309884 organoids and the remaining two lines (see Figure 5.6).

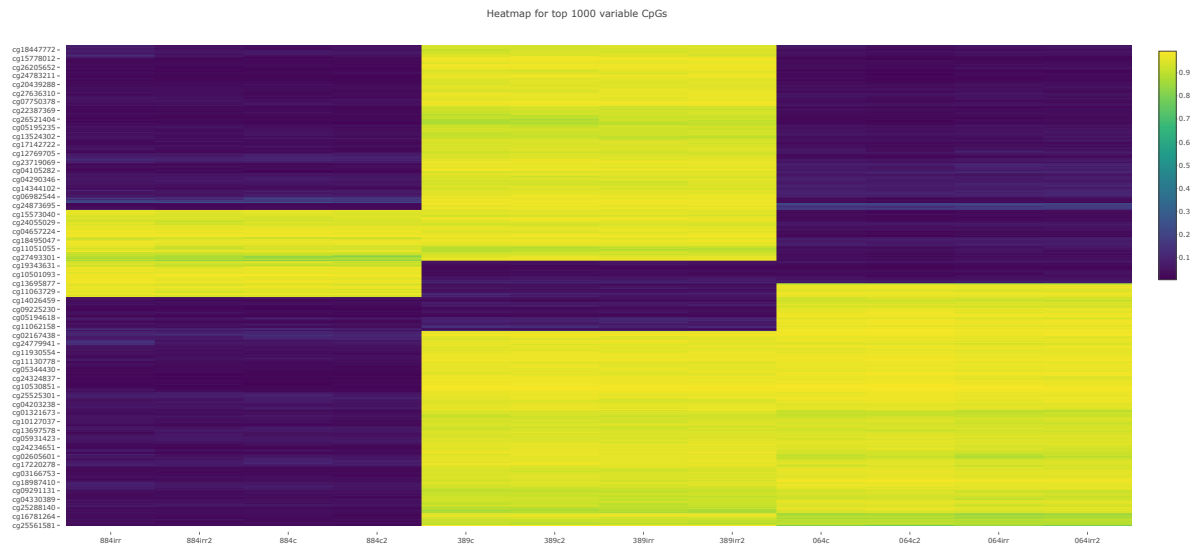


Figure 5.6 - Heatmap representing methylation across all samples.

Lastly, we performed a gene set enrichment analysis to see whether or not we could identify dysregulation in pathways. Initial results showed no significant pathways, however this could have been a result of non-significant adjusted p-values. Using the eBayes method, a list of enriched pathways has been generated. Using an area under cover (AUC) cut-off of 0.75 we identified 119 enriched pathways. The top enriched pathway in the analysis is the “Zerbini response to sulindac dn” pathway that is involved in cell cycle signalling and mitotic regulation. Another pathway, “Reactome nfkb activation through fadd rip1 pathway mediated by caspase 8 and 10”, was shown to be differentially methylated in irradiated organoids. The genes in this pathway are involved in TNF signalling and in inducing apoptosis. The top 10 enriched pathways are listed in the Table 5.5

Table 5.5 - GSEA for differentially methylated regions in irradiated organoids.

<b>PATHWAY</b>	<b>nREP</b>	<b>AUC</b>
ZERBINI RESPONSE TO SULINDAC DN	6	0.92
MIPS TFIID COMPLEX B CELL SPECIFIC	11	0.86
MIPS TFIID COMPLEX	11	0.85
MIPS TFIID BETA COMPLEX 1	10	0.85
REACTOME NFKB ACTIVATION THROUGH FADD RIP1 PATHWAY MEDIATED BY CASPASE 8 AND 10	11	0.84
KUMAMOTO RESPONSE TO NUTLIN 3A DN	9	0.83
MIPS 26S PROTEASOME	22	0.82
MIPS TFIID BETA COMPLEX	11	0.82
GNF2 MBD4	22	0.82
MIPS HISTONE H3.1 COMPLEX	8	0.81

### 5.3.4. Total RNA Sequencing

#### 5.3.4.1. Retrospective patients

After we investigated the DNA changes, we then went to investigate the changes in gene expression. However, before performing RNA sequencing on the control and irradiated organoids, we looked into the expression data for a retrospective study where we compared tumour gene expression from 36 patients, 10 of which had a complete pathological response and 26 which had no response. This was done in order to see whether or not we could identify any genes or pathways that are dysregulated in patients after receiving radiotherapy, as well as to look for

potential radiosensitivity and radioresistance markers so we could later compare against the organoid experiments.

This data was a part of a larger data set prepared by another lab PhD candidate (Kasun Wanigasooriya) who shared total RNASeq data for purpose of this study. A retrospective cohort of locally advanced rectal cancer patients who received neoadjuvant chemoradiotherapy was identified. FFPE blocks from patients' pre-therapy biopsies and post therapy resections were obtained through Human Biomaterials Resource Centre (HBRC), Birmingham under the same ethical approval as the samples for the organoid derivation project (Ref: 15/NW/0079). 4x 8  $\mu$ m scrolls were obtained per block. The RNA extraction, library preparation, and sequencing were performed by Kasun Wanigasooriya. The sequencing output was shared for this thesis and analysed with the help of the Centre for Computational Biology, Birmingham.

The principal component analysis showed that both complete responders and non-responders cluster together and without any clear separation with the exception of 4 outliers (Figure 5.7). We ran principal component analysis excluding patient 9, and the variance was still above 60%. Therefore, we decided not to exclude the outliers from the analysis.

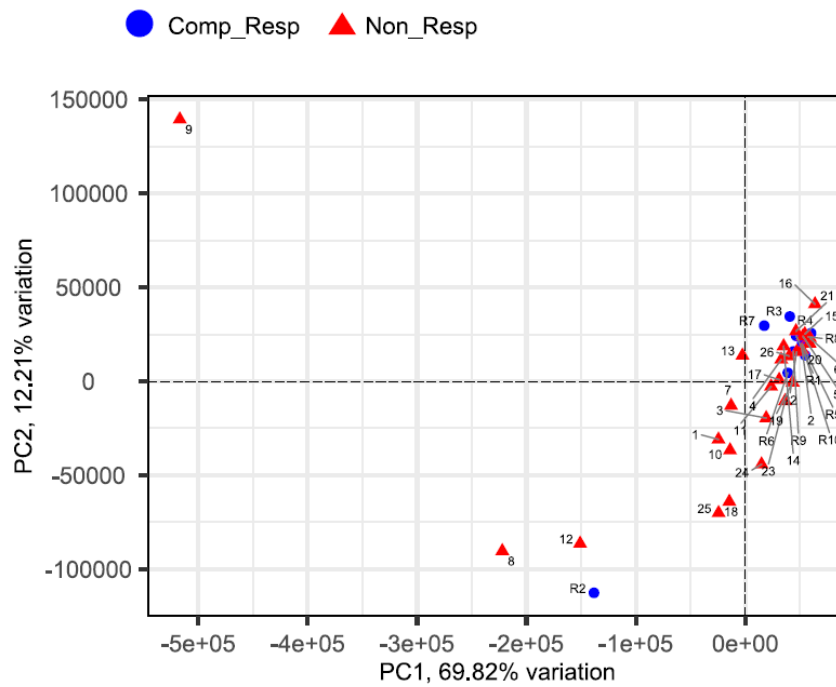


Figure 5.7 - PCA plot for retrospective RNASeq data.  
 Comp\_Resp – Complete responders; Non\_Resp- Non-responders

The differential expression analysis showed expression of 13046 genes of which 778 genes were significant. Furthermore, the gene set enrichment analysis (GSEA) identified 153 significant gene sets out of 976 KEGG gene sets (using setPCutoff= 0.01 and fdrCutOff= 0.05) with 35 significant pathways. The top 10 pathways are listed in Table 5.6.

Table 5.6 - List of top 10 enriched pathways.

<i>Pathway</i>	<i>SetRank</i>	<i>pSetRank</i>	<i>Adjusted p-value</i>
<i>Pathways in cancer</i>	0.126	$4.66 \times 10^{-58}$	$6.07 \times 10^{-37}$
<i>Endocytosis</i>	0.021	$3.07 \times 10^{-13}$	$6.07 \times 10^{-37}$

<i>HTLV-I infection</i>	0.05	$6.23 \times 10^{-31}$	$6.07 \times 10^{-37}$
<i>Alzheimer's disease</i>	0.01	0.001	$6.07 \times 10^{-37}$
<i>Epstein-Barr virus infection</i>	0.03	$9.91 \times 10^{-20}$	$6.07 \times 10^{-37}$
<i>MAPK signalling pathway</i>	0.026	$6.96 \times 10^{-17}$	$6.07 \times 10^{-37}$
<i>Cytokine-cytokine receptor interaction</i>	0.005	1	$6.07 \times 10^{-37}$
<i>Purine metabolism</i>	0.003	1	$6.07 \times 10^{-37}$
<i>RNA transport</i>	0.003	1	$6.07 \times 10^{-37}$
<i>mTOR signalling</i>	0.009	0.009	$6.07 \times 10^{-37}$

From the top 10 significantly enriched pathways we selected the following pathways: Pathways in cancer, Endocytosis, HTLV-I infection, MAPK signalling, and mTOR signalling. These pathways have been selected for closer investigation as they (or the genes in those pathways) have been linked to radiation resistance in the literature. Many genes that were found to be differentially expressed between two investigated groups would be highlighted in multiple pathways. Those genes were *PIK3CB* and *PIK3R3* from the Phosphoinositide 3-kinases family, which were consistently seen upregulated in

the non-responder cohort among the enriched pathways. However, the *PIK3R2* was seen to be upregulated in patients with complete response. Furthermore *FZD6*, *MAP2K1*, and *CCNB2* were also found to be upregulated in the patients that have not responded to radiotherapy. From individual pathways we have seen overexpression of *BRCA2*, *MSH3*, *DDIT4*, *VEGFA*, *EPN3*, and *ERBB3* in non-responders. The Venn diagram below shows the all significant genes in those top 5 pathways (Figure 5.8).

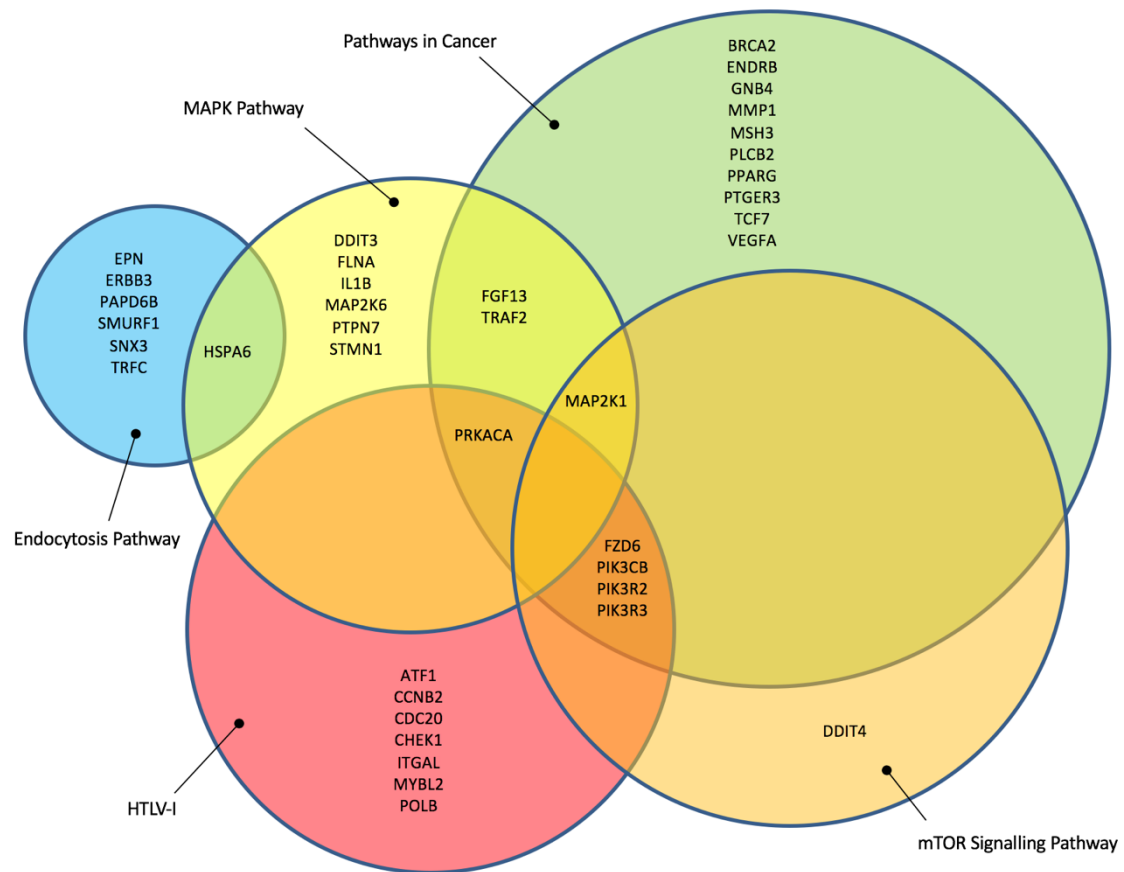


Figure 5.8 - Overlap of significant pathways. Venn diagram representing the top 5 significant pathways and their significant gene overlap.

The summary of the mentioned genes and their p-values can be found in Table 5.7. Additionally, heatmaps were generated for visual representation of differentially expressed genes between the two cohorts (see Figure 5.9).

Table 5.7 - Selected differentially expressed genes.

<i>Gene name</i>	<i>p-value</i>	<i>Adjusted p-value</i>
<i>BRCA2</i>	2.49x10 <sup>-03</sup>	0.062
<i>CCNB2</i>	2.71 x10 <sup>-03</sup>	0.056
<i>DDIT4</i>	5.64 x10 <sup>-05</sup>	0.007
<i>EPN3</i>	5.23 x10 <sup>-03</sup>	0.093
<i>ERBB3</i>	6.31 x10 <sup>-04</sup>	0.028
<i>FZD6</i>	3.42 x10 <sup>-05</sup>	0.006
<i>MAP2K1</i>	5.10 x10 <sup>-03</sup>	0.09
<i>MSH3</i>	1.31 x10 <sup>-06</sup>	0.0007
<i>PIK3CB</i>	1.84 x10 <sup>-04</sup>	0.015
<i>PIK3R2</i>	5.95 x10 <sup>-03</sup>	0.051
<i>PIK3R3</i>	1.81 x10 <sup>-03</sup>	0.01
<i>VEGFA</i>	1.99 x10 <sup>-03</sup>	0.053

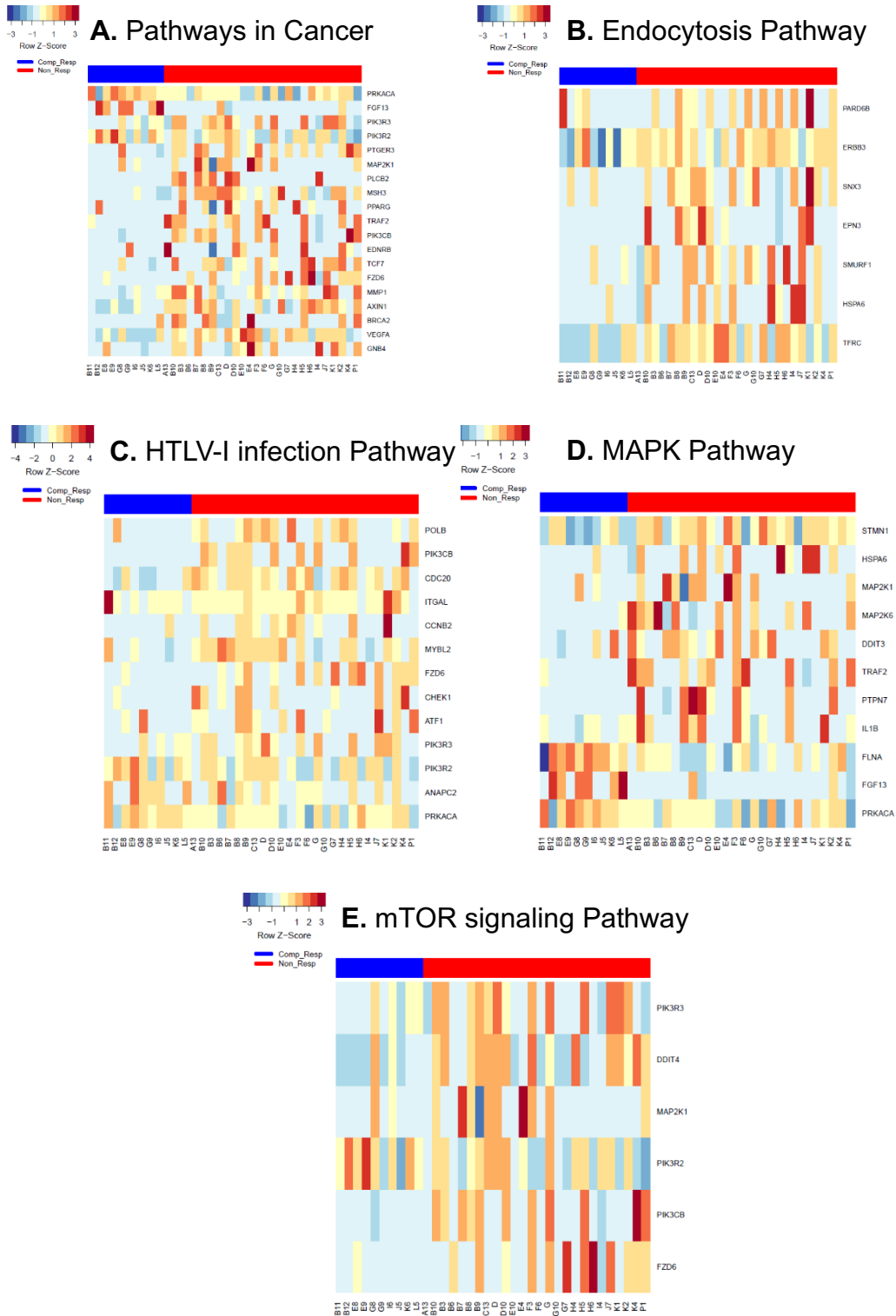


Figure 5.9 - Visual representation of differentially expressed genes in the top 5 significantly enriched pathways.

To match the patients from the PCA plot to sample names in the heatmaps please refer to Appendix D.

Moreover, there were 3 other significantly enriched pathways that were not in the top 10 enriched pathways but had differentially expressed genes and have either been previously linked to resistance or included *PIK3CA* related genes. Those pathways were the apoptosis, Ras signalling, and FoxO signalling pathways. The same genes as mentioned with the top 5 enriched pathways were highlighted in those pathways. Additionally, higher expression of *PARP4* (adjusted p-value = 0.026) was also found in the non-responder group (see Figure 5.10).

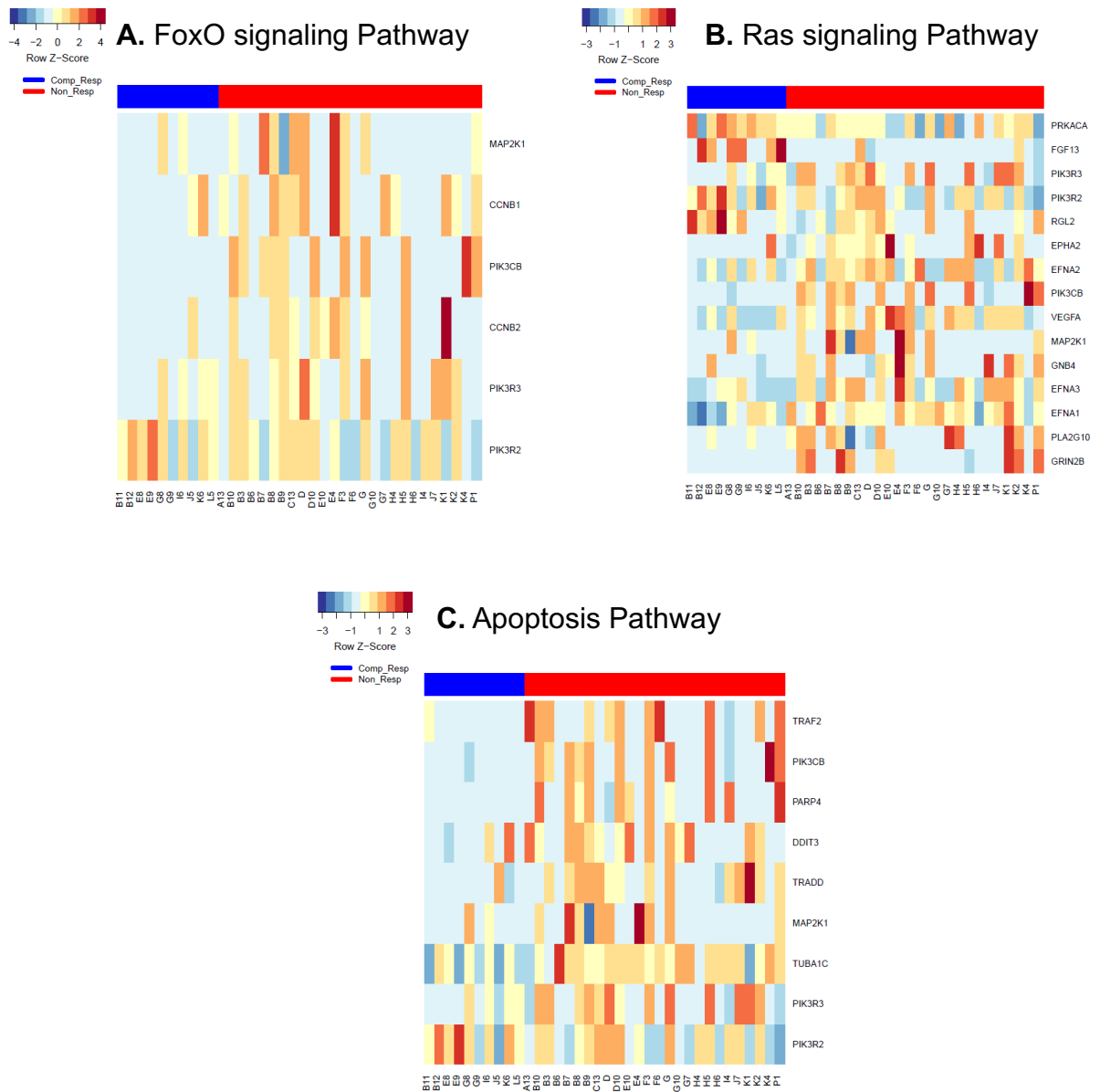


Figure 5.10 - Visual representation of differentially significant genes for remaining pathways.

*PIK3CB*, *PIK3R2*, *PIK3R3*, and *MAP2K1* were commonly present across almost all significant pathways of interest, suggesting that they could play a major role in the different responses to treatment. We have looked closely at the differential expression of these genes in between the cohorts, see Figure 5.11.

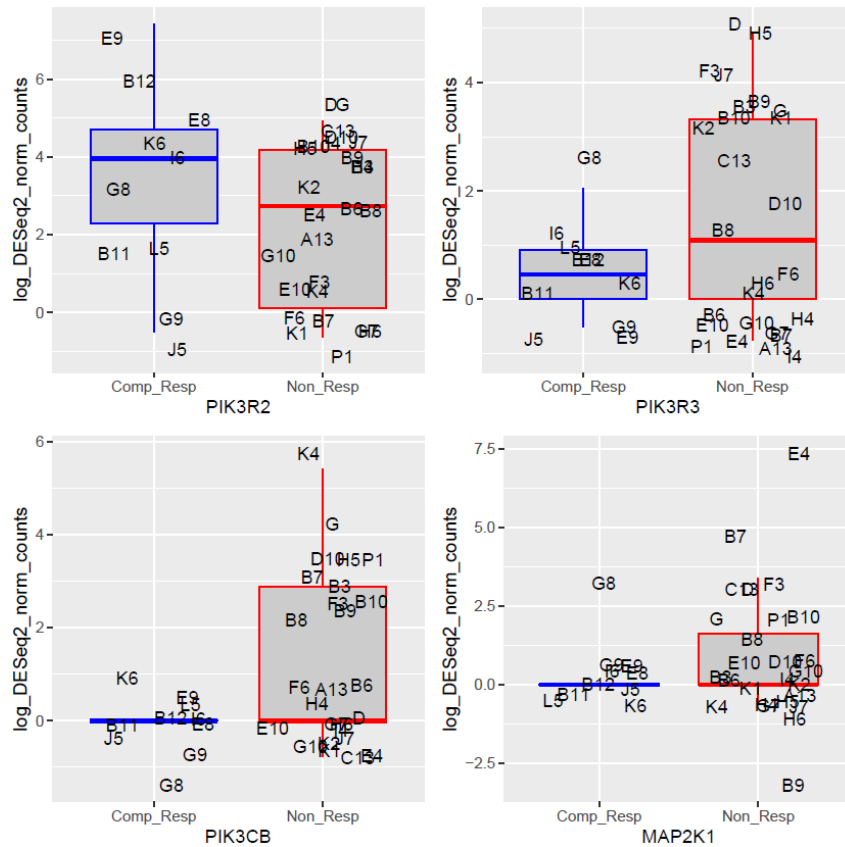


Figure 5.11 - Differential expression comparison for individual genes from the mTOR pathway.

Boxplots represent the differential expression between the two cohorts. Complete responders (blue) and Non-responders (Red).

Additionally, the mTOR pathway was particularly interesting as there was big significance in the differential expression in the pathway genes (*DDIT4* and *FZD6*). We have also compared the expression of mTOR itself (see Figure 5.12).

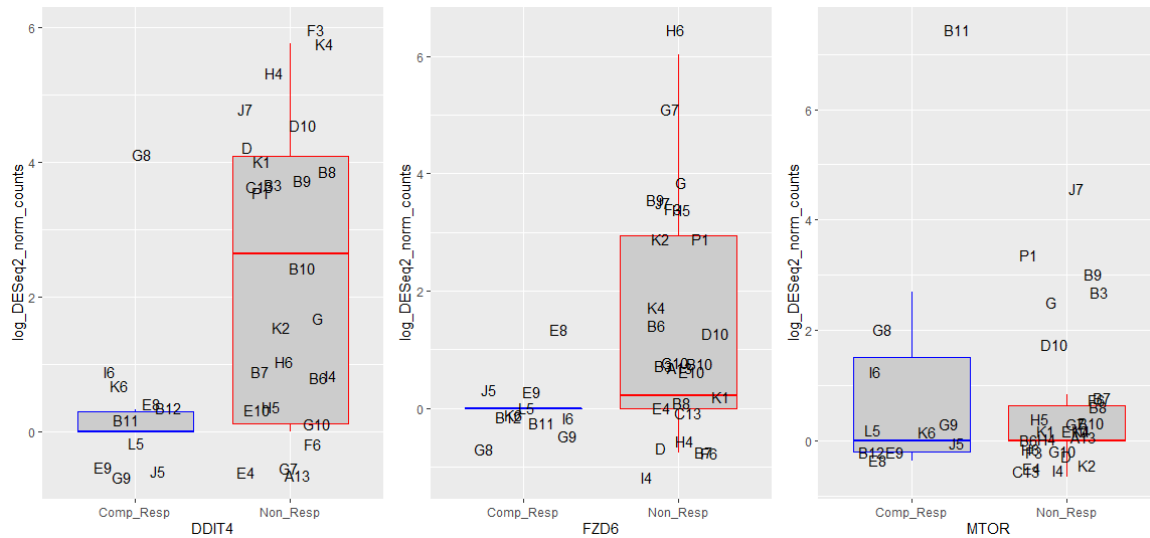


Figure 5.12 - Differential expression comparison for the remaining individual genes from mTOR pathway.

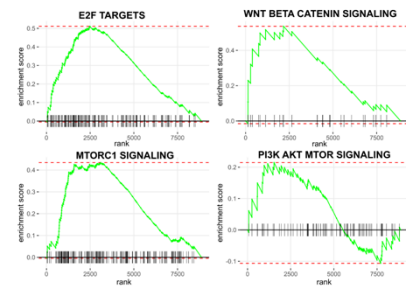
Boxplots represent the differential expression between two cohorts, Complete responders (blue) and Non-responders (Red).

Enrichment scores of the GSEA analysis were also produced (Figure 5.13) which showed again many pathways that were enriched in the non-responder cohort. Of particular interest was the fact that we found that MTORC1 signalling, Wnt Beta Catenin signalling, and E2F targets have been significantly increased in the non-responders. We have also observed that PIK3CA/Akt/mTOR signalling was also mostly increased in this group (see Figure 5.13 B). In the group of complete responders we have only seen 3 pathways of which only one was significant, indicating that the myogenesis is reduced in those patients (see Figure 5.13 C).

A.

Pathway	Gene ranks	NES	pval	padj
E2F_TARGETS		1.69	2.0e-04	1.0e-02
SPERMATOGENESIS		1.50	2.0e-02	2.0e-01
WNT_BETA_CATENIN_SIGNALING		1.46	3.8e-02	3.2e-01
G2M_CHECKPOINT		1.45	3.7e-03	4.6e-02
MTORC1_SIGNALING		1.45	3.4e-03	4.6e-02
ANGIOGENESIS		1.41	6.4e-02	4.0e-01
MYC_TARGETS_V2		1.37	6.1e-02	4.0e-01
HEDGEHOG_SIGNALING		1.35	1.0e-01	5.6e-01
APICAL_SURFACE		1.28	1.5e-01	7.4e-01
NOTCH_SIGNALING		1.25	1.8e-01	7.4e-01
ANDROGEN_RESPONSE		1.16	2.3e-01	9.0e-01
MYC_TARGETS_V1		1.16	1.7e-01	7.4e-01
INFLAMMATORY_RESPONSE		1.09	3.2e-01	9.7e-01
PANCREAS_BETA_CELLS		1.09	3.7e-01	9.7e-01
CHOLESTEROL_HOMEOSTASIS		1.04	4.2e-01	9.7e-01
ALLOGRAFT_REJECTION		1.04	4.2e-01	9.7e-01
GLYCOLYSIS		1.03	4.3e-01	9.7e-01
KRAS_SIGNALING_UP		1.03	4.4e-01	9.7e-01
REACTIVE_OXYGEN_SPECIES_PATHWAY		1.02	4.4e-01	9.7e-01
XENOTOXIC_METABOLISM		1.02	4.6e-01	9.7e-01
COAGULATION		1.02	4.6e-01	9.7e-01
UNFOLDED_PROTEIN_RESPONSE		0.99	5.2e-01	9.7e-01
IL2_STATS_SIGNALING		0.99	5.3e-01	9.7e-01
PEROXISOME		0.98	5.3e-01	9.7e-01
HYPOXIA		0.97	5.6e-01	9.7e-01
COMPLEMENT		0.96	5.8e-01	9.7e-01
MITOTIC_SPINDLE		0.95	5.8e-01	9.7e-01
IL6_JAK_STATS_SIGNALING		0.95	5.8e-01	9.7e-01
APICAL_JUNCTION		0.93	6.6e-01	9.9e-01
BILE_ACID_METABOLISM		0.91	6.3e-01	9.9e-01
PSD_PATHWAY		0.89	7.3e-01	9.9e-01
APOPTOSIS		0.84	8.0e-01	9.9e-01
EPITHELIAL_MESENCHYMAL_TRANSITION		0.82	8.5e-01	9.9e-01
KRAS_SIGNALING_DN		0.82	7.5e-01	9.9e-01
ESTROGEN_RESPONSE_LATE		0.81	8.5e-01	9.9e-01
TGF_BETA_SIGNALING		0.79	8.0e-01	9.9e-01
DNA_REPAIR		0.78	8.7e-01	9.9e-01
PROTEIN_SECRETION		0.75	8.7e-01	9.9e-01
TNF_SIGNALING_VIA_NFKB		0.73	9.4e-01	9.9e-01
ESTROGEN_RESPONSE_EARLY		0.73	9.4e-01	9.9e-01
OXIDATIVE_PHOSPHORYLATION		0.73	9.5e-01	9.9e-01
FATTY_ACID_METABOLISM		0.71	9.4e-01	9.9e-01
PRK_AKT_MTOR_SIGNALING		0.68	9.4e-01	9.9e-01
UV_RESPONSE_DN		0.67	9.6e-01	9.9e-01
HEME_METABOLISM		0.65	9.8e-01	9.9e-01
INTERFERON_GAMMA_RESPONSE		0.63	9.9e-01	9.9e-01
UV_RESPONSE_UP		0.62	9.9e-01	9.9e-01
INTERFERON_ALPHA_RESPONSE		-0.79	9.3e-01	9.9e-01
ADIPOGENESIS		-0.98	5.0e-01	9.7e-01
MYOGENESIS		-1.73	3.2e-03	4.6e-02

B.



C.

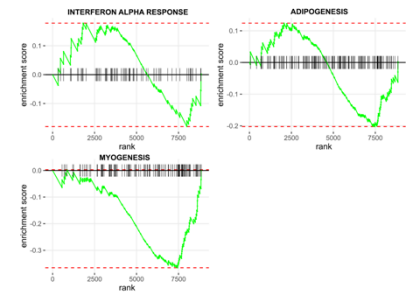


Figure 5.13 - Gene Set Enrichment Analysis and enrichment scored.

- A) A list of significantly enriched pathways with gene ranks.
- B) GSEA Enrichment scores for non-responder cohort.
- C) GSEA Enrichment scores for complete responder cohort.

As the mTOR pathway got particularly highlighted in the analysis, the summarised pathway shown with gene up- and downregulation is presented in

Figure 5.14.

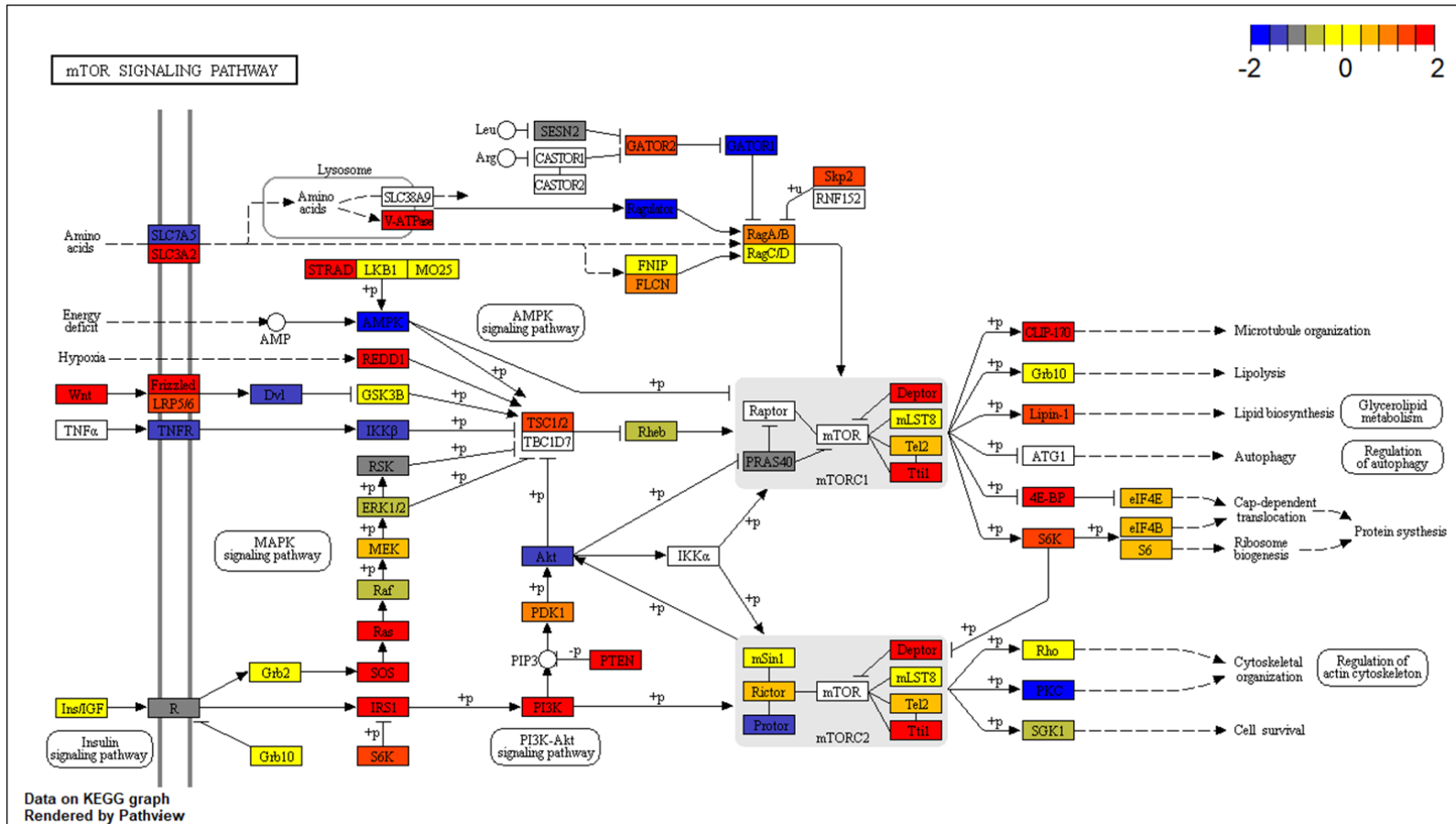


Figure 5.14 - mTOR signalling pathway in responders vs. non-responders.

A visual representation of mTOR pathway differential expression in patients that had complete pathological response (blue) and patients that did not respond to radiotherapy (red).

### 5.3.4.2. Irradiated organoids

The extracted RNA of control and irradiated organoids was sequenced and the differential analysis of these revealed expression differences caused by irradiation shortly after treatment delivery. The analysis of the total RNA sequencing was performed by Grigorios Papatzikas.

The principal component analysis showed that irradiated samples clustered together overlapping with the control organoids cluster (Figure 5.15). However, due to small sample size it was hard to define whether there were two separate clusters.

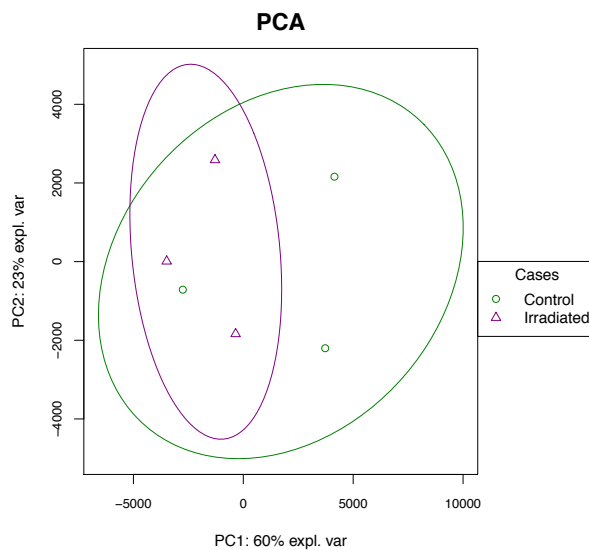


Figure 5.15 - Principal Component Analysis plot for organoid RNASeq data.

Firstly, out of the differentially expressed genes we have identified 17 genes that are known to be commonly mutated in colorectal cancer. As the shift in expression could be noticed between irradiated and control samples there was no clear pattern. The biggest differences between control and irradiated organoids were an increased expression of the *SMAD4* (adjusted p-value = 0.0117) gene in control samples and increased expression of *SMAD7* (p-value = 0.0001) in irradiated samples (see Figure 5.16).

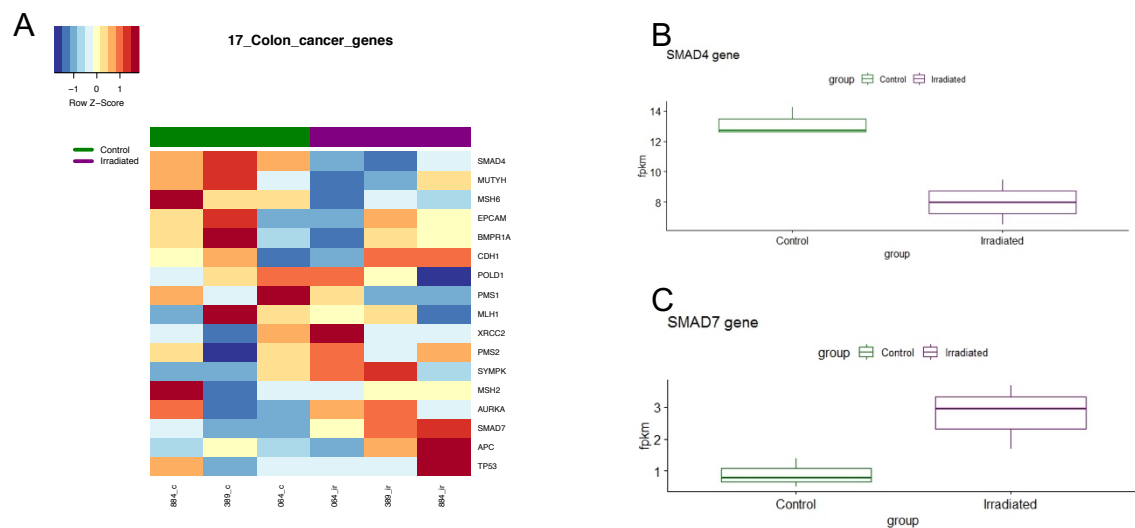


Figure 5.16 - Differentially expressed gene in Colon Cancer Pathway.

A) Heatmap representing differentially expressed gene between control (green) and irradiated (purple).

B) Differential expression of SMAD4 between two groups.

C) Differential expression of SMAD7 between two groups.

Next we have investigated genes with higher expression in irradiated samples and identified 26 genes with significantly increased expression (Figure 5.17 A). Among these we saw *NDRG1* and *CDCA7*, a N-Myc family member and a direct target gene of c-Myc. We also identified genes involved in the apoptosis pathway

such as *BCL2L14* and *TRIB3*. Furthermore, genes linked to hypoxia and the HIF1A pathway (*VEGFA* and *ALDOC*) were also found upregulated in irradiated samples. We also found *SCD*, a gene responsible for metabolic control, and *CCDC121*, a gene whose function is not yet clearly described, to be upregulated in the samples that have received radiotherapy. Additionally, increased gene expression was more pronounced for the S302389 irradiated sample than the other two lines. This was particularly true of *VEGFA*, *ALDOC*, *SCD*, *TRIB3*, and *NDR1*. See Table 5.8 for the list of genes.

Table 5.8 - List of genes upregulated in irradiated organoids.

<i>Gene name</i>	<i>p-value</i>	<i>Adjusted p-value</i>
<i>ALDOC</i>	5.78x10 <sup>-07</sup>	8.22 x10 <sup>-04</sup>
<i>BCL2L14</i>	2.18 x10 <sup>-04</sup>	5.60 x10 <sup>-02</sup>
<i>CCDC121</i>	1.95 x10 <sup>-04</sup>	5.09 x10 <sup>-02</sup>
<i>CDCA7</i>	4.89 x10 <sup>-04</sup>	8.95 x10 <sup>-02</sup>
<i>NDRG1</i>	1.20 x10 <sup>-06</sup>	1.44 x10 <sup>-03</sup>
<i>SCD</i>	2.80 x10 <sup>-05</sup>	1.40 x10 <sup>-02</sup>
<i>TRIB3</i>	3.07 x10 <sup>-04</sup>	6.97 x10 <sup>-02</sup>
<i>VEGFA</i>	3.71 x10 <sup>-04</sup>	7.85 x10 <sup>-02</sup>

We have also investigated genes with higher expression in control samples and the analysis highlighted 68 significant genes (Figure 5.17 B). Among the genes with elevated expression in the control sample population were genes involved in cell metabolism, cell differentiation, cell cycle progression, and apoptosis. All

samples had high expression of *ZCCHC12* (a downstream effector of BMP signalling), *LBH* (which is a regulator of the Wnt pathway), and *MSH4*. Furthermore, we also identified *WDR49*, *BIRC3*, and *TNFAIP3* genes, which are involved in apoptosis.

As previously seen, the colon organoids' expression was found to be more distinct in comparison to the other organoid samples. Finally, it was observed that there was higher expression in certain genes, particularly in sample S302389. Among these genes we have highlighted *MUC4*, *MMP7*, *CXCL1*, *NGFR*, *TM4SF20*, and *MUC17*. See Table 5.9 for the list of genes.

Table 5.9 - List of genes upregulated in control organoids.

<i>Gene name</i>	<i>p-value</i>	<i>Adjusted p-value</i>
<i>BIRC3</i>	4.51 x10 <sup>-06</sup>	4.15 x10 <sup>-03</sup>
<i>CXCL1</i>	4.27 x10 <sup>-04</sup>	8.35 x10 <sup>-02</sup>
<i>LBH</i>	4.09 x10 <sup>-08</sup>	1.28 x10 <sup>-04</sup>
<i>MMP7</i>	8.19 x10 <sup>-06</sup>	6.10 x10 <sup>-03</sup>
<i>MSH4</i>	5.86 x10 <sup>-04</sup>	9.95 x10 <sup>-02</sup>
<i>MUC17</i>	2.57 x10 <sup>-04</sup>	6.32 x10 <sup>-02</sup>
<i>MUC4</i>	2.24 x10 <sup>-05</sup>	1.25 x10 <sup>-02</sup>
<i>NGFR</i>	2.97 x10 <sup>-05</sup>	1.40 x10 <sup>-02</sup>
<i>TM4SF20</i>	9.10 x10 <sup>-07</sup>	1.19 x10 <sup>-03</sup>
<i>TNFAIP3</i>	1.94 x10 <sup>-07</sup>	3.75 x10 <sup>-04</sup>
<i>WDR49</i>	4.73 x10 <sup>-05</sup>	2.00 x10 <sup>-02</sup>



Table 5.10 - Top 10 enriched pathways for organoid RNA experiment.

<i>Pathway</i>	<i>pSetRank</i>	<i>Adjusted p-value</i>
<i>Lysosome</i>	0.001	2.58 x10 <sup>-18</sup>
<i>Cell adhesion molecules (CAMs)</i>	1.000	2.58 x10 <sup>-18</sup>
<i>Ras signalling pathway</i>	0.015	2.58 x10 <sup>-18</sup>
<i>Cholinergic synapse</i>	0.000	2.58 x10 <sup>-18</sup>
<i>MAPK signalling pathway</i>	1.000	2.58 x10 <sup>-18</sup>
<i>Phosphatidylinositol signalling system</i>	1.000	2.58 x10 <sup>-18</sup>
<i>Biosynthesis of unsaturated fatty acids</i>	1.000	2.58 x10 <sup>-18</sup>
<i>Insulin signalling pathway</i>	1.000	2.58 x10 <sup>-18</sup>
<i>Rap1 signalling pathway</i>	1.000	2.58 x10 <sup>-18</sup>
<i>Progesterone-mediated oocyte maturation</i>	1.000	2.58 x10 <sup>-18</sup>

## 5.4. Single-cell sequencing

### 5.4.1. Short term effects of irradiation

We went on to investigate the changes in expression caused by the irradiation treatment with single-cell RNA Sequencing. We first selected one line of organoids to test. We took a control sample from the S292064 line, and a sample from the same line that had received 25Gy irradiation in 5 fractions over 5 days. The cells were processed 96 hours after the delivery of the last irradiation dose as in the other irradiation experiments. The initial data exploration was performed by looking at the t-distributed stochastic neighbour embedding (t-SNE) plots for control and irradiated cells. The control organoid cell population consisted of

1380 cells, and we have distinguished 5 different clusters of cells. In contrast, only irradiated organoids data consisted of 465 cells that would cluster into two different populations (see Figure 5.18).

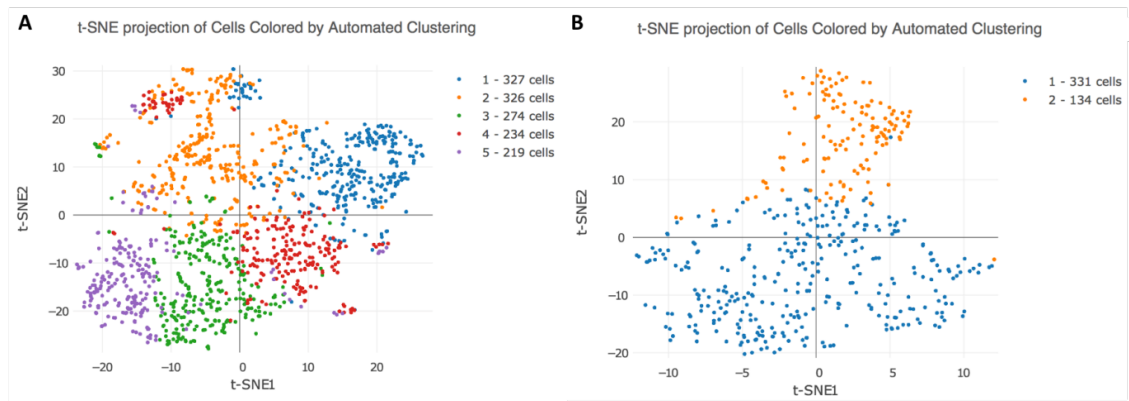


Figure 5.18 - t-SNE plots of single-cell sequencing data for short-term irradiation effects exploration.

A) Population of cells in the control organoids show 5 different cell population clusters, B) Population of cells in the irradiated organoids show two different cell population clusters

The first cluster of cells (blue) in the irradiated organoids sample characterised with the expression of mitochondrial DNA genes associated with cell death. In comparison, the second cluster markers were only two genes: *MALAT1* and *FTH1*. As the results of the short time effects were not insightful and for the irradiated cells we could observe the populations of dying cells and recovering cells, we did not perform any further analysis and modified this experiment.

#### **5.4.2. Long term effects of irradiation**

RNA sequencing analysis from organoid data did not highlight the driving mechanisms of radioresistance; however the retrospective study data was indicative of radioresistance drivers. Therefore, we tried to replicate the long term effects of irradiation with organoids, as we maintained the organoids in culture after their short course radiotherapy treatment. S292064 organoids were irradiated with short course therapy and further expanded after the treatment. Then, both the control line (S292064) and the new, expanded irradiated line (S292064IRR) were processed for single-cell sequencing. This was also done for remaining lines: S302389, S309884, and S345653. Note, however, that only the S302389 line further expanded after irradiation treatment – establishing the S302389IRR line. Due to not being able to expand the S309884 and S34563 lines after irradiation treatment, we did not perform single-cell sequencing on those samples. The output sequencing data was analysed by Professor Chris Yau and Professor Andrew Beggs.

Firstly, the analysis of both control organoid lines were compared with the “IRR” lines to see the differential expression at the single-cell level. The Uniform Manifold Approximation and Projection (UMAP) plot in Figure 5.19 shows the different cell population clusters for control and irradiated organoids. As expected, the clusters overlap as the cells come from the same patient lines. However, we also observed a few differences. Organoids that had received

irradiation treatment and continued to grow had less dead cells, and showed cell clusters that consist of dying tumour cells.

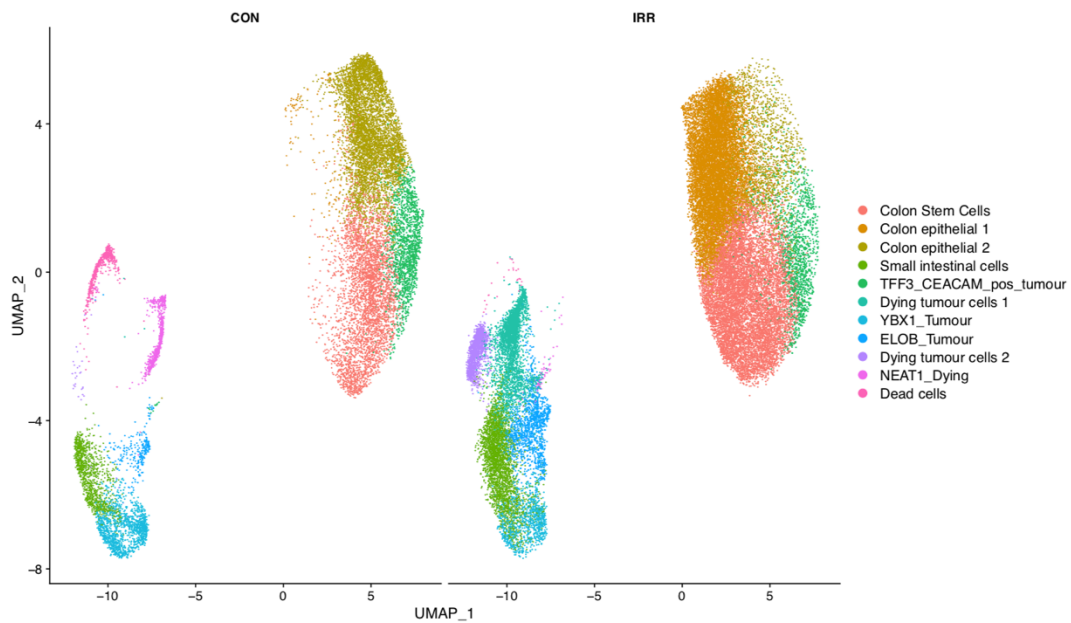


Figure 5.19 - UMAP representing difference in cell populations between control and irradiated organoid cells.

Additionally, from Dr Yau's data analysis we were able to conclude that organoids that received and survived the irradiation treatment displayed an upregulation in DNA repair activity and arrested cell cycle (see Figure 5.20 A). Furthermore, when comparing the resistant line to its naïve counterpart the mTOR activity is upregulated in the S292064IRR line (see Figure 5.20 B).

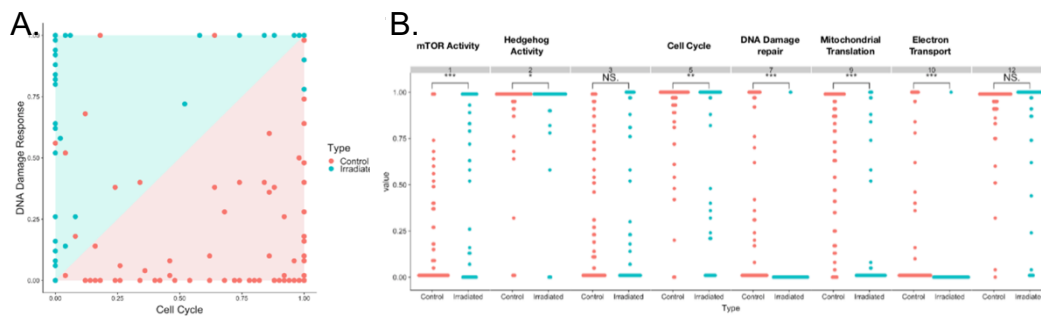


Figure 5.20 - Differential Pathway Analysis results for S292064IRR organoid line.

A) Plot representing two pathways that have been differentially expressed between control and treated organoids.

B) A differential expression between control and treated cells for significantly differentiated pathways.

## 5.5. Discussion

### 5.5.1. Irradiation response

We have shown that all of the generated organoid lines respond to irradiation. Moreover, there are differences in response between individual lines. It was observed that lines established from cells that have not been previously exposed to irradiation have responded significantly better in comparison to the lines that have been previously irradiated, with the exception of the S302389IRR line. Both of the rectal lines used for this study came from patients that have received neo-adjuvant radiotherapy, therefore the organoid lines came from cells that have been previously exposed to irradiation. Both of these lines responded less to irradiation compared to the lines that came from sigmoid and colon cancer patients (which have not received irradiation prior to tumour resection). This was expected as previous cell exposure to radiation therapy would select for a population of cells that are resistant to the treatment (Sato, Shimokawa and Imai,

2019). Interestingly, the S292064IRR line – a new line generated in the laboratory by irradiating the sigmoid line (S292064) – showed similar resistance to radiotherapy treatment as the rectal lines. Though this significant difference between the naïve S292064 and S292064IRR lines was observed, there was no significant difference in the response between the S292064IRR line and the rectal lines, suggesting that the lab generated resistant line has a similar response when compared to patient resistant lines and therefore being clinically relevant posing as a good model for studying radiation response. On the other hand, the response of the “resistant” S302389 line (S302389IRR) did not significantly change in comparison to its naïve analogue. We believe that the lack of shift in treatment response could be due to the specific genetic profile of the line. The colon line has a *PIK3CA* missense mutation, which is one of the proposed candidates for radiosensitivity markers. Alteration of this gene has not been detected in S292064 organoids further supporting this hypothesis. Nevertheless, the S345653 line also has a *PIK3CA* mutation, yet has a poor response to the treatment (both organoids and patient responded to neo-adjuvant long-course radiotherapy). However, it also has a *KRAS* mutation which has been linked to driving radioresistance (Yang et al. 2021) – it is possible this could overcome the potential radiosensitivity caused by the missense mutations of *PIK3CA*.

### 5.5.2. Irradiation causes changes to DNA

The whole genome analysis of the control and irradiated organoids showed that the equivalent of short-course radiotherapy has an effect on the whole genome. We have found CNVs across all chromosomes. It is known that radiation causes double strand breaks in DNA and results in DNA damage (Vignard, Mirey and Salles, 2013). It has been shown that exposure to irradiation treatment causes copy number variation burden with duplications and deletions. Both large (>20bp) and small (<20bp) deletions have been found in the analysis of post irradiated DNA, and the unique deletion signature has been associated with the irradiated samples (Kodaira, Asakawa and Nakamura, 2017; Kocakavuk et al. 2021). In this chapter we demonstrate that irradiation of cells results in whole genome alterations and a large number of deletions.

In addition to CNVs we have also found mutation patterns, where the same SNVs were detected in all irradiated samples. The mutations were found in genes involved in main cell signalling pathways. *SPINK5* is involved in the cell adhesion pathway and contributes to cell integrity. We have also detected mutations in *ACVR2B*, *ACVR2A*, and *KIAA1324L* genes, that all play role in BMP signalling. *ACVR2A* and *ACVR2B* are type II receptors that with type I receptors form a transmembrane heterotetrametric receptor complex that can bind ligands such as BMPs or activin. It has been shown that type II receptors can phosphorylate type I receptors which can activate SMAD signal transduction as well as PI3K, Rho or p38 (Valer et al. 2019). *KIAA1324L* regulates the BMP signalling pathway

(NCBI, 2022) although not much information regarding this gene exists in the literature. Additionally, pathogenic mutation of *RAF1* was also found. *RAF1* plays an important role in ERK1/2 signalling, where it can cause growth arrest and differentiation (Reusch et al. 2001). Furthermore, *RAF1* has been known to interact with *Akt*, where it can be inhibited by *Akt* phosphorylation (Moelling et al. 2002). Affected genes have been involved in TGF- $\beta$  signalling which has been shown to mediate EMT, which in turn has been proposed to drive radioresistance (Xu, Lamouille and Derynck, 2009; Farhood et al. 2020; Sato, Shimokawa and Imai, 2019).

### **5.5.3. Short-course radiotherapy causes cell cycle arrest**

Several studies have looked at the effects of radiation therapy on DNA methylation. Kim et al. (2010) compared methylation patterns in two cancer cell lines (resistant and non-resistant) and identified methylation differences in 1091 genes. Antwih et al. (2013) investigated DNA methylation patterns at different time points following treatment and found that DNA methylation patterns change, where cell cycle arrest was observed 24 hours post-irradiation and cell senescence was significant 72 hours post irradiation. Other studies showed that irradiation can result in either hypomethylation or hypermethylation depending on the organ (Miousse, Kutanzi and Koturbash, 2017). In this chapter we have shown that organoids did not display major changes in methylation patterns after irradiation treatment. Only 13 genes have been shown to be differentially

methyated in irradiated organoids. The GSEA showed enrichment in the growth arrest and apoptosis related pathways; similar enriched pathways were found in the aforementioned methylation studies.

#### **5.5.4. *PI3K* genes are upregulated in patients that do not respond to radiotherapy**

Retrospective RNA sequencing of patients that completely responded or did not respond to radiotherapy revealed differential expression in multiple pathways. The main genes that have been found to be upregulated in non-responders were the *PIK3CB* and *PIK3R3* genes from the *PI3K* family. In addition, *FZD6* and *DDIT4* from the mTOR signalling pathway and *CCNB2* were found to be upregulated in the cohort that did not respond to irradiation. The Akt/mTOR pathway has been described in literature to be upregulated in colorectal cancer and also has been linked to resistance to radiotherapy (Toulany and Rodemann, 2013; Sato, Shimokawa and Imai, 2019). PI3K/Akt/mTOR has also been linked to radioresistance in prostate cancer (Chang et al. 2014; Chang et al. 2015). Additionally, *DDIT4* has been shown to be expressed under stress situations triggered by mTOR (Shoshani et al. 2002). *DDIT4* has also been described to have the ability to drive treatment resistance in cancer. What is more, patients with overexpression of *DDIT4* have been shown to have a poorer survival rate (Tirad-Hurtado, Fajardo and Pinto, 2018). The fact we have observed upregulation of *DDIT4* in the non-responder cohort correlates with the worse

survival predictions. Lastly, *CCNB2* overexpression in non-responders links the radioresistance to TGF- $\beta$  signalling, which as mentioned before has also been linked to radioresistance. Interestingly, *PIK3R2* was upregulated in patients with pathCR.

#### **5.5.5. Irradiated organoids overexpress *SMAD7***

Following retrospective RNA analysis, the impact of short-course therapy on organoids and their transcriptome was investigated. With differential analysis we have observed that irradiated organoids have upregulated *SMAD7* expression. *SMAD7* is a key regulator of TGF- $\beta$ , where it inhibits the activity of this gene and has been shown to drive tumorigenesis in multiple studies (Zhu, Chen and Chen, 2011). TGF- $\beta$  has been shown to have a dual role in cancer progression, as at early stages it acts as a tumour suppressor gene, but its ability to drive EMT at later stages makes it pro oncogenic (Massague, 2008). Here we speculate that overexpressed *SMAD7* is inhibiting the tumour suppressing activity of TGF- $\beta$  and driving the survival of irradiated cells. In addition to *SMAD7* and 4 dysregulation we have observed differential expression in irradiated and control organoids. The upregulated genes were in irradiated population and were linked to the apoptosis pathway and hypoxia. Two genes (*NDRG1* and *CDCA7*) that were overexpressed in irradiated samples have been linked to Myc signalling. *NDRG1* is a member of the N-myc family and is involved in stress response and apoptosis activation (Ellen et al. 2008). As irradiation causes a lot of stress on the cells we

expected to see upregulation of genes involved in apoptosis and growth arrest. For the control samples we have observed that the differentially expressed genes are particularly pronounced in S302389. Interestingly, the lines that best responded to irradiation were those of colon organoids as well as the S302389IRR line – a “resistant” line created from the S302389 line. We have found upregulation of *MUC4*, *MMP7*, and *ZCCHC12* in control samples. As the S302389 line is derived from a mucinous colorectal tumour it explains the elevated expression of mucin. The mucinous subtypes of colorectal cancer have been linked in the literature to TGF- $\beta$  signalling (Fessler et al. 2016). This could explain the elevated *MMP7* and *ZCCHC12* genes involved in TGF- $\beta$  signalling. Interestingly, in irradiated samples the gene particularly pronounced in S302389 was *TRIB3*. This gene has been shown to negatively regulate cell survival. What is more, it has been shown to disrupt insulin signalling as it can directly bind Akt and block its activation and subsequently inhibit cell survival. This result suggests that Akt plays a key role in radioresistance. Supporting evidence has been shown in the literature, where studies showed Akt can drive radioresistance and by targeting Akt/cyclin D cells can be sensitised to irradiation (Shimura et al 2014; Shimura et al. 2017).

### **5.5.6. Single-cell sequencing reveals mTOR as potential driver of radioresistance**

As final analysis in this chapter we have investigated single-cell RNA expression of irradiated organoids. Initially, we have performed single-cell sequencing on organoids shortly after the last dose of irradiation has been delivered. We have not been able to identify radioresistance or radiosensitivity drivers and we could only distinguish two cell populations in irradiated organoids – dying cells and metabolically active cells. The control organoids were shown to be heterogeneous as we found 5 different cell populations. We suggest that the experiment was performed too soon after delivery of the last dose. Hence, we have repeated the experiment for *in vitro* made resistant organoid lines. The results showed that organoids after 4-5 weeks of irradiation treatment have a shift in expression. We have observed differences in cell populations and gene expression. The main finding is that we identified upregulation of the mTOR pathway in S292064IRR organoids. Furthermore, we did not observe elevated mTOR or a related pathway in S302389IRR organoids. With this evidence we speculate that the mTOR pathway can drive resistance to radiotherapy. Finally, the single-cell sequencing showed that organoids are heterogeneous with different cell populations. What is more, we observed changes in the cells expression and cell populations after the irradiation treatment. Chen et al. 2018 investigated the organoids after chemotherapy treatment with single-cell sequencing and observed similar heterogeneity of organoids and a shift in expression of clusters with exposure to treatment.

Unfortunately, line S345653 did not expand further after irradiation and we could not obtain single cell sequencing data. Due to time limitations we also couldn't obtain the post irradiation WGS and RNASeq for this line to see whether it would show any dysregulation in the mTOR pathway as well.

## 5.6. Conclusions

Irradiation causes major disruption to the whole genome and impacts gene expression. Although, irradiation also has an effect on DNA methylation we did not observe major pattern changes or disruption to methylation levels in irradiated cells. Furthermore, with the above evidence we conclude that the upregulation of mTOR drives resistance to radiotherapy and poses as a potential target for sensitising cells for irradiation. In our analysis we have also identified TGF- $\beta$  to play a role in radioresistance, however with the dual nature of the gene we suggest that mTOR is an easier target for improving radioresistance. Finally, we also showed that *Akt* and *PI3K* genes play a key role in response to irradiation. Based on the described results we suggest that inactivation of Akt favours the response to irradiation and patients with non-functioning mutant *PIK3CA* can rescue the mTOR driven radioresistance. Lastly, although the initial findings prior to this study suggested *FBXW7* played a role in radioresistance, the results of this chapter showed no evidence that *FBXW7* influences radiation response. Therefore, this line of investigation was not further pursued.

## **6. RESULTS CHAPTER 4: SENSITISING CELLS TO IRRADIATION WITH MTOR AND AKT INHIBITORS**

### **6.1. Introduction**

Radiotherapy has been used as one of the main non-surgical treatments for cancer for over a century. Despite being one of the oldest treatments of malignancies, it is still relevant in current treatment strategies. With time, it has evolved with more precise dose and delivery (Abshire and Lang, 2018). However, radiotherapy alone often has not been sufficient as a treatment, and what is more a lot of tumours become resistant to treatment. Thus, chemotherapeutic agents have been gradually taking more of a key role in treating cancer. More and more agents have become available to treat cancer and chemotherapy has taken one of the main roles in cancer treatments. However, it is often linked to high cytotoxicity and also treatment resistance has been observed. Hence, the key to improve therapeutic outcome is a multimodal approach of combination therapy. Radiotherapy was first combined with a chemotherapeutic agent in the 1970s for Ewing's sarcoma treatment and already then the results suggested better outcome with such approach than radiotherapy or chemotherapy alone (Jaffe et al. 1976). Since then, with more precise radiation delivery and targeted chemotherapeutic agents, combination therapy started emerging as a key treatment strategy for certain types of cancers such as rectal cancer. Current combination therapy regimens for rectal cancer use chemotherapeutic drugs that

do not selectively sensitise the tumour to radiation, but with their toxicity combined with radiotherapy can result in a bigger impact killing cancerous cells (Brunner et al. 2016). Those kinds of agents are referred to in the literature as radiation modifiers. However, lately there has been a search for radiation sensitisers – chemotherapeutic agents that on their own will not be toxic, but will enhance radiation induced cell death of tumour cells once combined with radiotherapy. Both radiation modifiers and sensitisers are the backbone of combination therapy as the agent effect on enhancing the results of radiation benefits the overall therapeutic outcome and can increase the patient's overall survival rate (Citrin and Mitchel, 2014).

Knowing that a small proportion of rectal cancer patients do indeed have a complete pathological response to radiotherapy is encouraging, and with further research it may be possible to induce the same response in the rest of patients with poorer response to irradiation. Hence, with the gained knowledge of the results described in the previous chapter we wanted to see whether combining certain chemotherapeutic agents could cause the appropriate conditions for better or complete pathological response for colorectal cancer tumours.

## **6.2. Aims and methods**

Both RNA and DNA sequencing data investigating the effects of irradiation on cells have highlighted two pathways that appear to play a key role in response to radiotherapy: the mTOR signalling pathway and the PI3K signalling pathway. As

chemotherapeutic agents are available that target both of these pathways, we have tried to test our hypothesis by trying to sensitise cells to irradiation by inhibiting chosen pathways with a selection of drugs. In this chapter we have performed drug screens with and without combined radiotherapy and measured the resulting organoids' viability. We have tested different concentrations of mTOR inhibitors: Rapamycin, Everolimus, AZD2014, and an Akt inhibitor – MK-2206.

## **6.3. Results**

### **6.3.1. Targeting mTOR**

#### **6.3.1.1. Rapamycin and Everolimus**

As a first inhibition target we have chosen mTOR as there are two drugs that inhibit its activity that are already used in the clinic: Rapamycin (also known as Sirolimus) and Everolimus. Rapamycin and its 40-O-(2 hydroxyethyl) derivative, Everolimus, are known to be used in preventing rejection of transplanted organs. Furthermore, both of the drugs have been trialled for the treatment of several cancers. Additionally, Everolimus has been approved as part of breast cancer, pancreatic cancer, and kidney cancer treatment.

Firstly, we have cultured organoids in Everolimus for the duration of a short course radiotherapy treatment (5 days) as we wanted to investigate the impact of chemotherapy on response to irradiation. Following 3 days after passaging, the

organoids were plated on 96-well plates laid with Matrigel and suspended in media containing Everolimus or vehicle for control. Another plate for testing just irradiation contained just media. The culture media containing fresh concentration of the therapeutic agent was replaced after 72 hours from starting the experiment. Organoids were then subjected to short course radiation (5x5Gy). The viability assay was performed 72 hours after the last dose of irradiation was delivered. The results have shown that despite increasing concentrations of mTOR inhibitor there was no decline in cell survival and what is more, cells that were irradiated while being cultured in media containing drug were shown to have a higher survival rate in comparison to the vehicle control (Figure 6.1). The results indicated that inhibiting mTOR with Everolimus would increase the survival of cells subjected to irradiation based on the increased cell viability. As those results were the opposite of the initial hypothesis we then decided to perform kill curves with both Everolimus and Rapamycin and see the organoids' response to those mTOR inhibitors without irradiation.

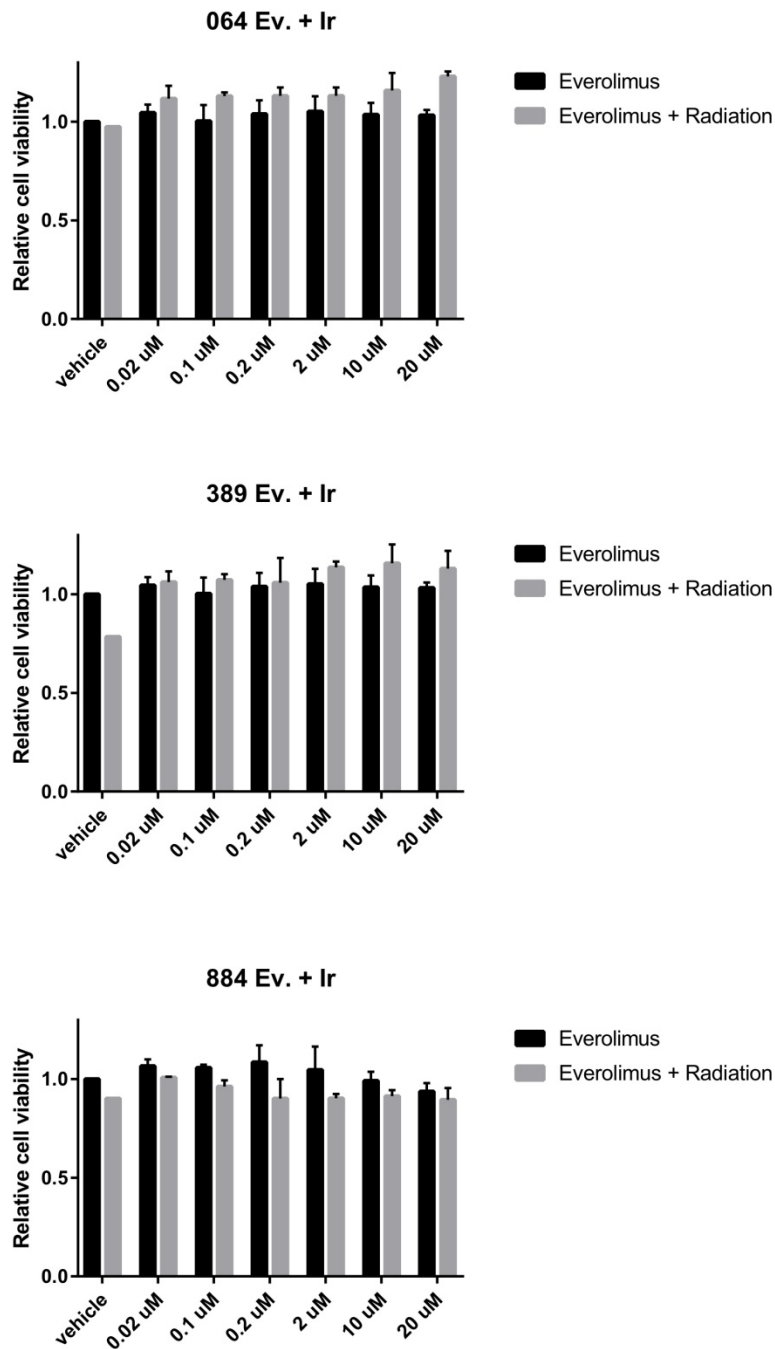


Figure 6.1 - Comparison of chemotherapy with combination therapy on organoids.

Organoids were treated with different concentrations of Everolimus (0.02 $\mu$ M - 20 $\mu$ M) as well as combination of Everolimus and short-course radiotherapy. Organoid viability was compared after two treatment approached. 064- S292064, 389- S302389, 884- S309884; Ev- Everolimus treatment; Ir- Irradiation treatment.

We have investigated the response of organoid lines to different concentrations of Rapamycin and Everolimus performing a drug screen assay in which organoid lines were cultured in media containing increasing concentrations of therapeutic agent for 72 hours. Organoids were passaged 3 days prior to the experiment, and then an equal amount of organoids was plated onto 96-well clear bottom plates that were laid with Matrigel and resuspended in media containing Rapamycin or Everolimus in different concentrations (drug concentrations tested: 0.02 $\mu$ M, 0.1 $\mu$ M, 0.2 $\mu$ M, 2 $\mu$ M, 10 $\mu$ M and 20 $\mu$ M). Each concentration was tested in triplicate technical repeats. After 72 hours, the effects of the chemotherapeutic agents were investigated with a viability assay measuring ATP with chemiluminescence.

For both Everolimus and Rapamycin there was no decline in viability observed for all of the lines, where in fact the viability did not significantly decrease and stayed the same across the different drug concentrations (Figure 6.2). This experiment was repeated 3 times and with each assay we would see that both Rapamycin and Everolimus are not toxic to organoids. Furthermore, we would speculate that they might improve their viability.

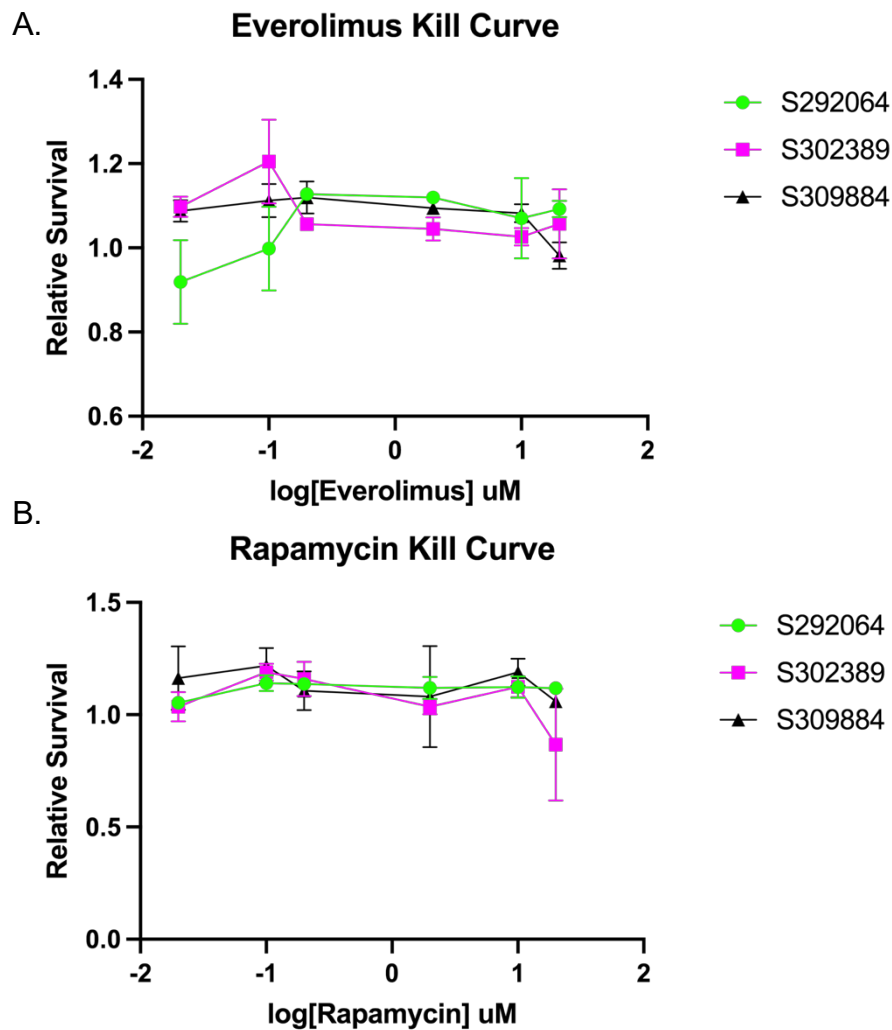


Figure 6.2 - Everolimus and Rapamycin kill curves.

A dose dependent response of organoid to different concentration of A) Everolimus (0.02 $\mu$ M - 20 $\mu$ M). and B) Rapamycin (0.02 $\mu$ M - 20 $\mu$ M). The organoids tested were 3 original lines: sigmoid S292064, colon S302389, and rectal S309884.

We then investigated whether chemotherapy can sensitise the cells to irradiation by combing the two treatments. As this was a novel approach we have tested both 1) culturing the organoids in chemotherapeutic agents before irradiation and 2) adding the drug after the last dose of the short course therapy was delivered. We then compared the responses to see if any of the approaches resulted in a

better response. For this experiment, we have used the same culturing approach where organoids that were passaged 3 days prior to the start of the experiment were plated on 96-well clear-bottom plates laid with Matrigel. In the first condition, organoids were cultured in Rapamycin for 72 hours followed by replacing the media with just a culture media and then delivering 25Gy in 5Gy fractions over the course of 5 days. In the second condition, the 25Gy were delivered first and then organoid culture media was changed to media containing Rapamycin. For each condition there was a control plate in which organoids were not subjected to radiotherapy, but were cultured in Rapamycin for 72 hours. For each condition the control plate had the Rapamycin added at the same time as the tested condition, using the concentrations described in Section 2.3.3.3 Table 2.4. The viability of all organoids was measured and compared.

The results showed that in both conditions, as in the kill curve experiment, organoid viability was not greatly affected by the increasing concentrations of the Rapamycin. Furthermore, the viability was not decreased successfully with delivery of the drug only. However, the combination of drug and irradiation treatment resulted in lowered viability of the organoids. When comparing the relative survival rates for both of the experiments, the response to irradiation was better in the second condition in which Rapamycin was delivered after the irradiation treatment. However, when the irradiated only control vehicle was plotted across the graphs as a reference point for each drug concentration, there was minimal to no difference between radio- and combination therapy in both cases. The response to only irradiation baseline was applied to the graph after

reanalysing data a few weeks after the experiment. Without looking at the irradiation only response, the strategy of delivering irradiation followed by the drug treatment seemed to have better results. Also, when comparing against the baseline, it we concluded that there was no clear difference for either condition. For these reasons, we selected the irradiation followed by drug treatment method of delivery for future drug screen experiments. See Figure 6.3 for the results.

In addition to the initial experiment's results we considered the fact that the combination treatment employed short course therapy as opposed to a clinical regimen of long-course radiotherapy combined with chemotherapy. We hypothesised that the agents might have a better effect on the lasting effects of irradiation post-treatment and prevent cells developing resistance as they are being sensitised with therapeutic agents.

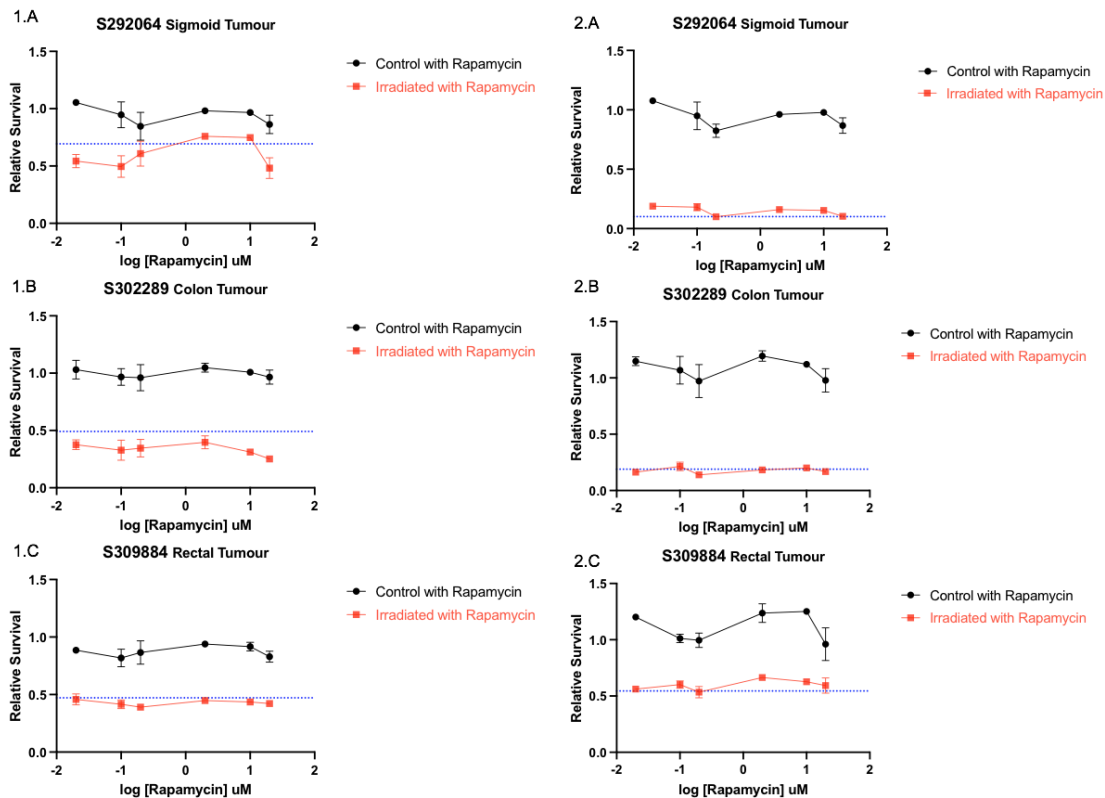


Figure 6.3 - Approach comparison of sensitising cells to irradiation with Rapamycin

- 1) Organoids treated with combination of irradiation and chemotherapy with drug being delivered prior to radiation.
- 2) Organoids treated with combination of irradiation and chemotherapy with drug being delivered after the irradiation treatment.

The plots show the effects of treatment on organoid viability. The effects of drug only are represented by the black control line, whereas the effects of the combination of chemoradiotherapy is represented by the red line. The blue dashed line represents a baseline of response to irradiation only. The organoids subjected to treatments were 3 original lines: sigmoid S292064, colon S302389, and rectal S309884.

We then investigated the organoids' response once again to radiotherapy combined with mTORC1 inhibitor treatment using the chosen approach of delivering short course radiotherapy followed by a 72 hour culture in Rapamycin or Everolimus (see Figure 6.4). Organoids were prepared and plated the same way as described before. The results showed consistently that inhibiting mTOR

with either Rapamycin or Everolimus does not change the survival of organoids when exposed to the agents. Additionally, organoids cultured in media containing Rapamycin or Everolimus after irradiation did not display worsened survival, and in certain cases inhibiting mTOR with the mentioned drugs would desensitise the cells to irradiation effects, as the observed survival was higher in comparison to the irradiation only control. Lastly, no difference was observed between organoid responses to treatments that used Everolimus instead of Rapamycin.

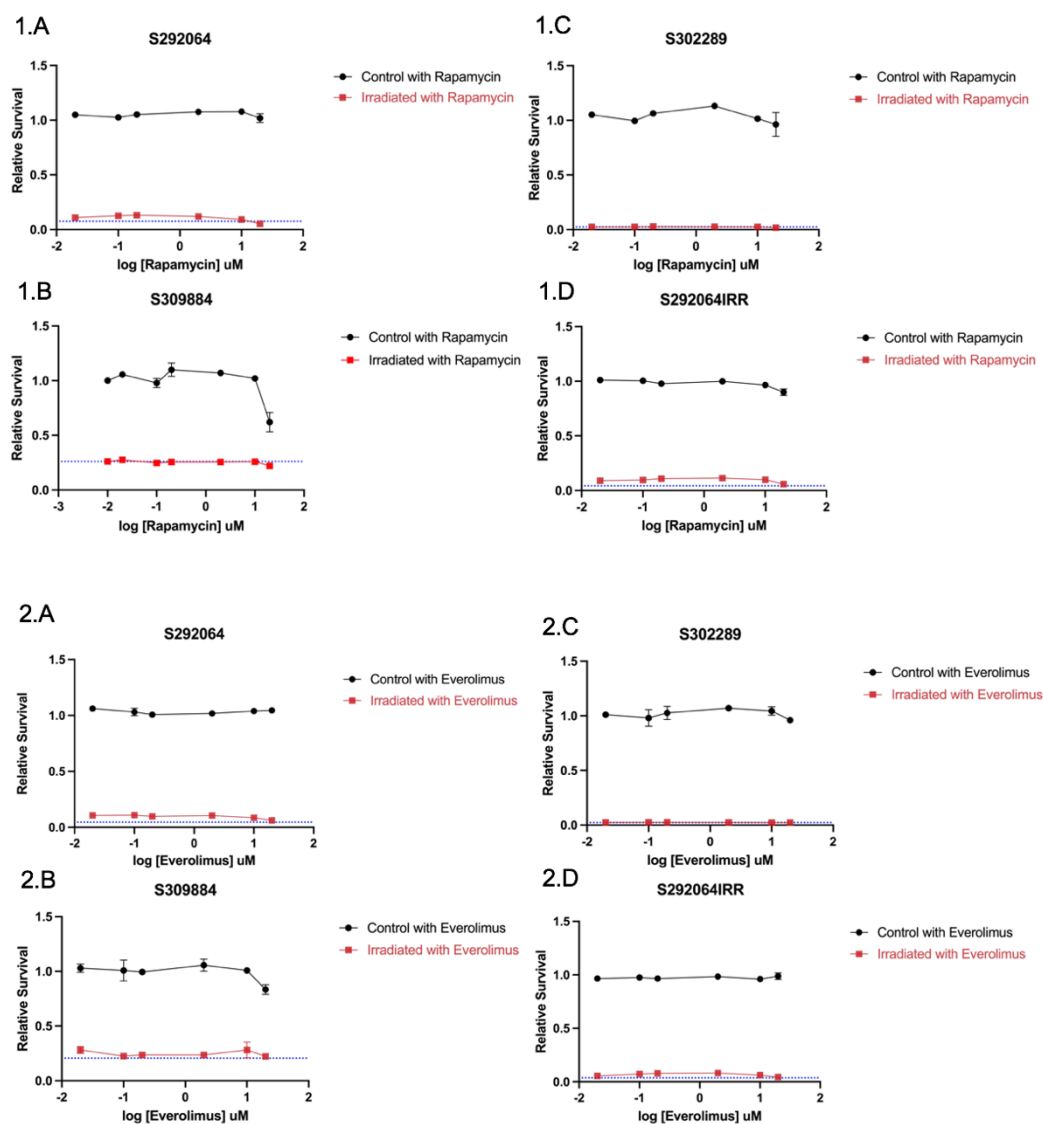


Figure 6.4 - Sensitising cells to irradiation with Rapamycin and Everolimus.

The plots show the effects of chemoradiation treatment with 1.A – 1.D Rapamycin or 2.A – 2.D Everolimus. Viability of organoids treated with drug only is represented by the black control line, whereas the effects of the combination of chemoradiotherapy are represented by the red line. The blue dashed line represents a baseline of response to irradiation only. The organoids subjected to treatments were lines: sigmoid S292064, colon S302389, rectal S309884, and S292064IRR.

### **6.3.1.2. AZD2014**

Drug screen combined with irradiation treatment of organoids we have showed that inhibiting mTOR with Rapamycin or Everolimus is not effective in sensitising cells to irradiation, and what is more it is possibly makes them more resistant to the treatment. As both of the drugs inhibit mTOR through blocking mTORC1 only, this leads to hyperactivation of mTORC2 and Akt phosphorylation that can drive cell survival. We speculated that for this reason the organoids' survival was better with the drug when exposed to irradiation. Therefore we decided to see whether blocking mTOR through inhibition of both mTORC1 and mTORC2 would result in cells being sensitised to irradiation. We have used another chemotherapeutic drug AZD2014 (Vistusertib), an ATP-competitive inhibitor of mTOR kinase in order to test the new hypothesis, which was dual blocking of mTORC1 and mTORC2 will sensitise cells to irradiation.

Before investigating the impact of AZD2014 on the irradiation effect we have performed a kill curve experiment, where at the time available organoid model lines (S292064, S302389 and S309884) were cultured in media containing increasing concentrations of AZD2014 (0.005 $\mu$ M, 0.01 $\mu$ M, 0.1 $\mu$ M, 1 $\mu$ M), see Figure 6.5 A. The results showed that with increased drug concentration the viability of organoids would also increase. However, the S292064 organoid line displayed a decreasing trend. When other lines (S292064IRR, S302389IRR and S345653) became established and available they have also been subjected to a kill curve experiment to investigate their response. In contrast to the results for

the original lines, the viability of the organoids decreased with the increase of the AZD2014 concentrations (Figure 6.5 B).

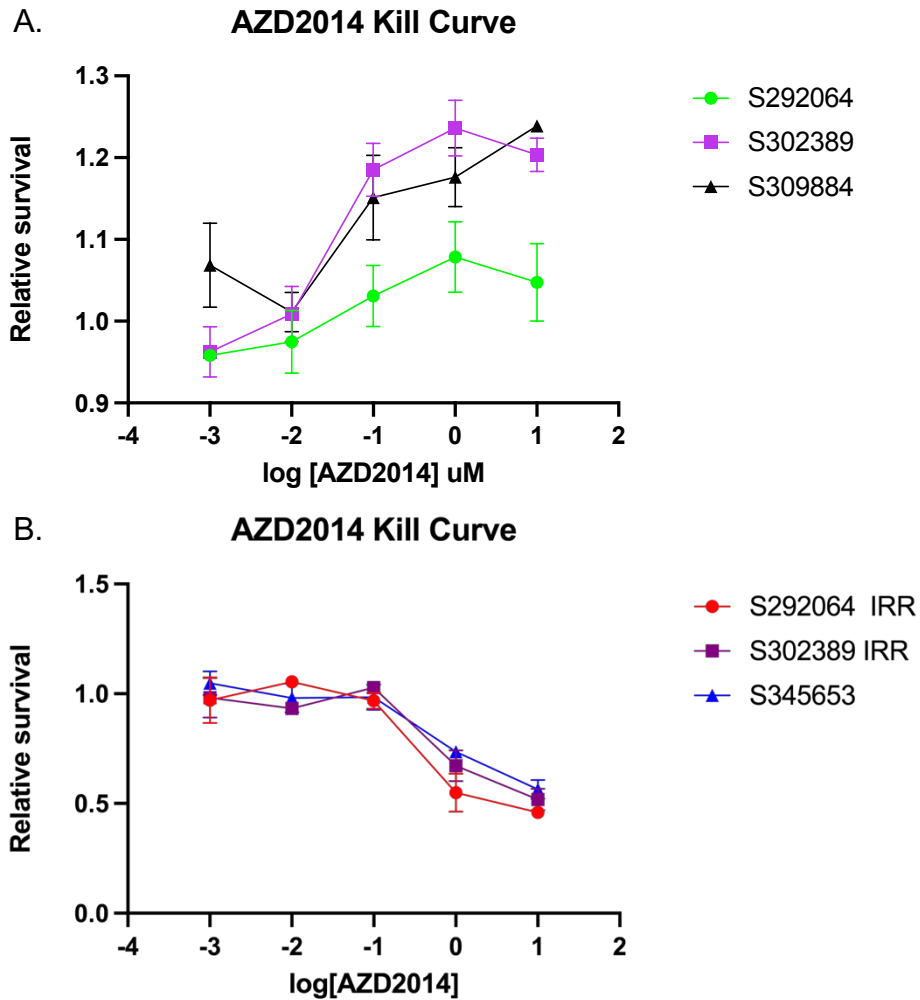


Figure 6.5 - AZD2014 Kill curve.

A dose dependent response of organoid to different concentration of AZD2014 (0.001 - 1 $\mu$ M). A) Kill curve for 3 original organoid lines, B) Kill curve for the remaining, resistant lines.

As the next step, we have investigated the impact of AZD2014 on irradiation response of the organoids. We have used the same approach for combining radiotherapy with chemotherapy for organoids as in the previous experiment,

where we have irradiated organoids with 25Gy in 5 fractions and then cultured organoids in chemotherapeutic agent for 72 hours after which their viability was investigated with an ATP luminescence assay; see Figure 6.6 for viability curves.

Exposing organoids to dual mTOR inhibitor after irradiation treatment showed a promising result of decreased cell viability for all of the lines. When compared to irradiated only controls, lines S292064, S302389, and S309884 exhibited better response to treatment with the combination therapy as their viability was significantly lowered. S292064 organoids viability was lowered by around 20% across all of the concentration points. For the S302389 colon line we have observed a decreasing trend in viability together with increasing concentration of AZD2014 with the highest concentration resulting in 20% decrease in cell viability. Similarly to the colon organoids, the rectal line (S309884) displayed a decreasing trend and improved response to treatment varied between 10-20% depending on drug concentration. The smallest dose of AZD2014 combined with irradiation was enough for the viability to reduce in comparison to irradiated control, apart from the S302389 organoids, for which we saw a lowered viability from the second lowest tested concentration. We have also investigated the response of the other three lines (S292064IRR, S302389IRR and S345653) to irradiation combined with the AZD2014 (Figure 6.6 D, E and F). Rectal line S345653, which displays the resistance traits and was shown to have the poorest response to irradiation out of all of the model lines, showed improved response to combination treatment at 0.1 $\mu$ M and 1 $\mu$ M of AZD2014 in comparison to irradiation only. For the S292064IRR line the response to combination therapy

was better than irradiation only, whereas for the S302389IRR the viability was lower than for the irradiation, but only for the last two highest concentration points. For better visualisation, the control plots were excluded from the graphs. The viability of all organoid lines cultured in the drug for 72 hours without irradiation were significantly higher than the viability of organoids that were irradiated only or irradiated and then exposed to AZD2014.

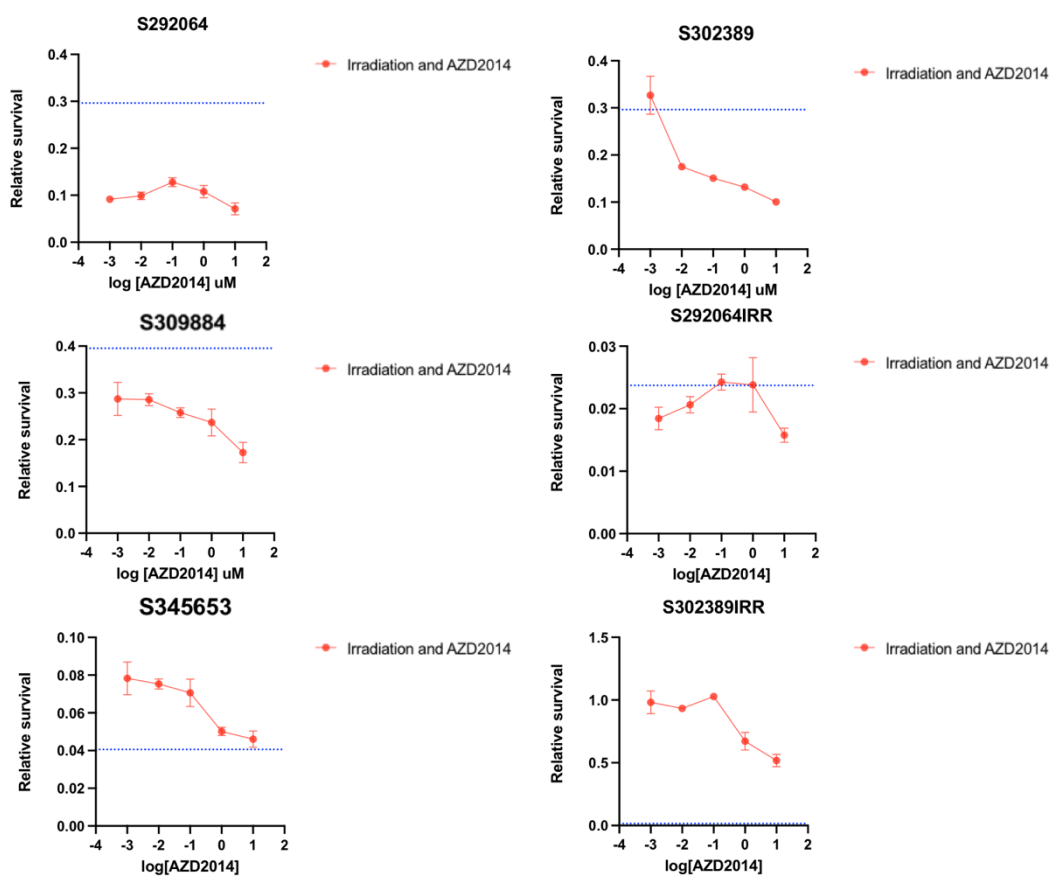


Figure 6.6 - Sensitising cells to irradiation with AZD2014.

Organoids treated with combination of irradiation and AZD2014. The viability of treated organoids with combination of chemoradiotherapy is represented by the red line. The blue dashed line represents a baseline of response to irradiation only. The organoids subjected to treatments were: sigmoid S292064, colon S302389, rectal S309884, S292064IRR, S345653, and S302389IRR.

### **6.3.2. Targeting Akt**

As Akt is a part of mTOR signalling and PIK3CA was highlighted multiple times during our initial biomarker search analysis we have also decided to see the impact of inhibiting Akt. We have chosen a selective allosteric Akt inhibitor (MK-2206) to see whether combining it with irradiation will help sensitise organoids to irradiation.

Before doing combination therapy experiments, we have examined the impact of MK-2206 alone on organoid lines by performing the kill curve experiment (Figure 6.7). We have observed that small concentrations of the Akt inhibitor would make the organoids more viable in comparison to the control and then with higher concentration exposure their viability would decline. However, the viability would not drop below the relative 100% viability. Once the “resistant” lines became available, the kill curve was also done to examine the response of those organoid lines to the Akt inhibitor at different concentrations. Despite no gradual declining tendency in survival was observed, all of the lines’ survival lowered significantly and equally with all tested concentration. Due to materials and time constraints only 4 different concentration points were tested for this kill curve.

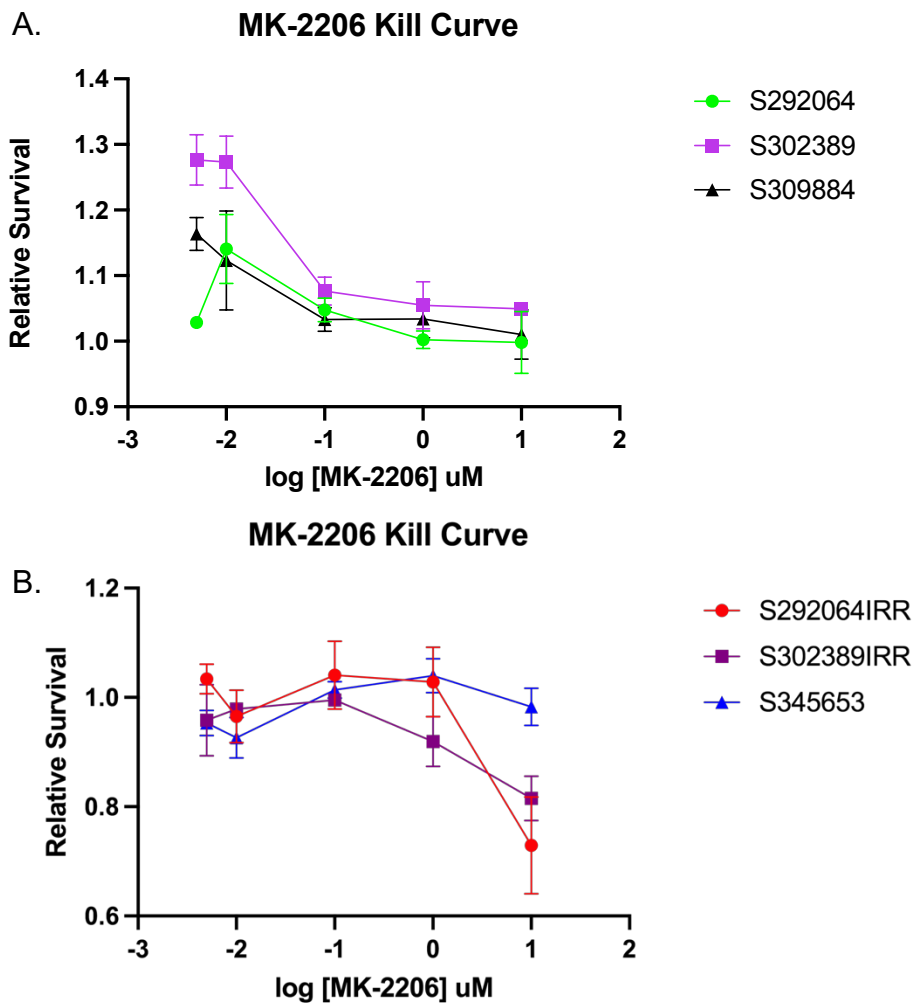


Figure 6.7 - MK-2206 Kill curve.

A dose dependent response of organoid to different concentration of MK-2206 (0.005 - 10 $\mu$ M). A) Kill curve for 3 original organoid lines, B) Kill curve for the remaining, resistant lines

We have then proceeded with combination therapy experiments with irradiation and MK-2206 (Figure 6.8). Response to irradiation of lines S292064, S302389 and S309884 was improved with the combination of MK-2206 treatment after short course radiotherapy in comparison to irradiation only. When comparing the variance in viability between combination of irradiation and MK-2206 treatment with irradiation only the most distinct difference was line S292064 with a slight

decline in viability with increased drug concentration. S302389 organoids also had a better response to the treatment when combined with the Akt inhibitor, but with no change in response with different drug concentrations. The rectal organoids (S309884) also had a better response to irradiation combined with MK-2206; however the viability would increase with the increased concentration of the drug in the organoid culture.

Organoids from rectal line S345653 would show a decreasing trend in viability with the increase of the drug concentration with only the two highest concentration points causing better response than irradiation only. The S292064IRR and S302389IRR lines responded better to irradiation treatment only in comparison to the irradiation with the drug.

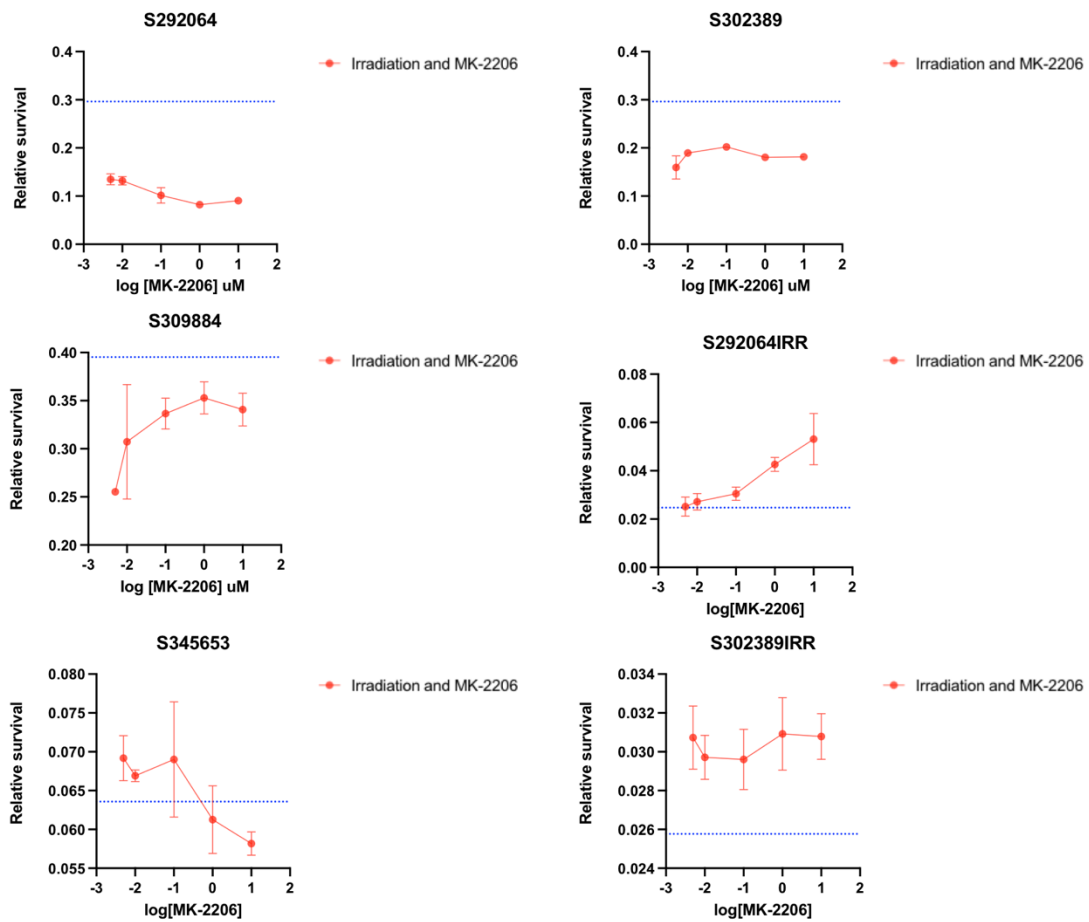


Figure 6.8 - Sensitising cells to irradiation with MK-2206.

Organoids treated with combination of irradiation and MK-2206. The viability of treated organoids with combination of chemoradiotherapy is represented by the red line. The blue dashed line represents a baseline of response to irradiation only. The organoids subjected to treatments were: sigmoid S292064, colon S302389, rectal S309884, S292064IRR, S345653, and S302389IRR.

## 6.4. Discussion

Dysregulation of PI3K/Akt/mTOR signalling pathways has been widely reported in many cancers, including colorectal cancer, and as a result influences processes that are directly involved with and drive tumorigenesis (Bahrami et al.

2017). What is more, it has been often highlighted that such dysregulation of this pathway is correlated to both chemotherapy and radiotherapy resistance (Shimura et al. 2014; Sato, Shimokawa and Imai, 2019). Consequently, using Akt or mTOR inhibitors seems like a promising next step for finding the answer to cancer treatment resistance. In this chapter we have demonstrated the effects of several mTOR and Akt inhibitors on colorectal organoids and their response to radiotherapy.

#### **6.4.1. Inhibition of mTORC1 is not sufficient to sensitise cells to irradiation**

Everolimus and Rapamycin are two established drugs that are already used in the clinic for several treatment regimens including cancer treatment (Royce and Osman, 2015; Xie, Wang and Proud, 2016). Additionally, those mTORC1 inhibitors have been in studies on cell line radioresistance, where different cell lines were subjected to combined treatment of rapamycin and irradiation (Nagata et al. 2010; Nam et al. 2013; Sato et al. 2017). All of the mentioned studies have shown promising results of Rapamycin sensitising cells to irradiation. When we subjected organoids to a wide range of different concentrations of Rapamycin and Everolimus to investigate the effects of the drug alone on organoid viability, neither of the drugs had negative effects on organoid survival. The lack of toxicity on organoids could have been caused by the nature of the tested organoids, which consisted of tumour cells. The effects of Rapamycin and Everolimus can differ depending on the cell type (Nyfeler et al. 2011), therefore the often seen

toxicity in patients that have received mTORC1 inhibitor is caused by the effects of the drug on different cell types and also on non-cancerous cells (Tee, 2018). The treatment on its own is not effective against colorectal cancer organoids. Therefore, we hoped that in combination with irradiation, cells would respond better to radiotherapy being sensitised by the mTOR inhibition initiated by Rapamycin/Everolimus. However, we have observed the opposite effect, where the survival was better or at worst no different to irradiation only. In the previous studies that have tried using Rapamycin in order to sensitise cell lines to irradiation, that effect was not observed. In fact there have been reports of reduced viability of cells after exposure to the drug and irradiation. We speculate that the different results might be due to the differences between organoids and cell lines, as 3D structures more closely recapitulate the tumour microenvironment and hypoxic conditions, which play a key role in treatment resistance and mTORC1 signalling (Wouters and Koritzinsky, 2008). We speculate that the observed increase in survival and slight protection from irradiation effects could be caused by the hyper-activation of the kinase Akt. Both Everolimus and Rapamycin work through inhibiting mTORC1 which can then through a negative feedback loop lead to the hyperactivation of Akt, while not inhibiting mTORC2. This then results in longer cell survival (Kim et al. 2014). Additionally, it has been shown that hypoxic conditions drive radioresistance through the inhibition of mTORC1 (Wouters and Koritzinsky, 2008), which supports our hypothesis about Rapamycin and Everolimus driving cell survival.

We acknowledge that when comparing the delivery of the drug before and after irradiation we did not initially plot the irradiation only response, and made conclusions without considering this base line. We have chosen to deliver the drug after irradiation, although it might not have been the best approach concluding from the replotted data. A clinical trial that examined chemoradiotherapy concluded that the timing of chemotherapy did not determine the benefit to patients, but the addition of chemotherapy itself was more important (Bosset et al. 2016). We therefore believe that choosing this approach did not have a significant effect on our analysis and conclusions.

#### **6.4.2. Dual inhibition of mTORC1 and mTORC2 results in partial sensitisation of cells to irradiation**

As mTORC1 inhibition was not sufficient to have an effect on combination treatment, another mTOR inhibiting agent was trialled. We selected a highly selective ATP-competitive inhibitor of mTOR - AZD2014. This therapeutic agent that is at the clinical trial stage serves to block the mTOR pathway through inhibiting both mTORC1 and mTORC2 (Eyre et al. 2014). The S292064, S302389, and S309884 organoid lines did not display a decrease in viability when incubated for 72 hours with different concentrations of the drug. In fact, with higher drug concentrations the viability was shown to increase. As the relative viability was over 1, this would suggest the addition of the drug would promote proliferation for these colorectal organoid lines. However, for the S292064IRR,

S302389IRR, and S3456534 lines, the trend was the opposite and a gradual decrease in viability was indeed observed. These findings are important as they validate the hypothesis that the resistant lines have dysregulated mTOR/Akt pathway and by targeting it with mTOR inhibitor we can rescue the resistance to treatment. When organoids were treated with a combination of radiotherapy followed by the AZD2014 treatment we observed improved treatment response for the S292064, S302389, and S309884 lines whereas the rest of the lines did not have better response than to irradiation only. For the S302389IRR line, which would respond fully to irradiation only, the AZD2014 treatment caused the resistance to radiotherapy. The lack of effect from AZD2014 on the rectal line could be caused by the presence of a *KRAS* mutation in the G12 codon (mutation p.Gly12Asp). Ali et al. (2017) showed that AZD2014 is not effective against the *KRAS* mutant cells, particularly displaying the G12 or G13 alterations. In this study, the effect of other mTOR inhibitors on tumours with *KRAS* driven therapeutic resistance were investigated. In contrast to the ineffective AZD2014, the results showed that Rapamycin would result in resistant clones' growth inhibition (Ali et al. 2017). Although the line was not available when the initial Everolimus and Rapamycin screens were performed, we carried out a 2 week screen of Rapamycin and AZD2014 for the rectal lines and the S292064IRR resistant line where we observed the effect of reduced viability after exposure to Rapamycin in S345653 rectal organoids. The remaining lines did not reduce in viability. The results for these experiments did not provide any further insight over the results captured in Section 6.3, and therefore this line of investigation was not

further pursued. Full results can be found in Appendix E. Furthermore, AZD2014 did also result in a decrease in viability in these organoids, as well as the remaining lines. This kind of effect on the line was partially concordant with the findings of Ali et al. (2017). AZD2014 showed no significant effects on *KRAS* mutated cells in the Ali et al. study, but the organoids have had a decrease in cell viability. This could have been caused by the 2 week exposure to the drug; however the 72 hour assay showed a similar viability decrease in the S34563 line. Due to study time limitations and a lack of more organoid lines with *KRAS* mutations, we were not able to investigate the effects of adding radiation. However, this would be an interesting study to pursue in the future.

#### **6.4.3. Inhibition of Akt partially sensitises cells to irradiation**

Organoids treated with increasing concentrations of MK-2206 did not display a reduction in viability, and for the “non-resistant” lines the viability seemed to increase within lower drug concentrations and stayed unchanged for the resistant lines. However, when combined with irradiation similar results to combination therapy with AZD2014 were observed. For lines S292064, S302389, and S309884 there was clear evidence that the cells’ viability decreased more once the drug had been added after the last dose of irradiation. For certain lines the effect would reduce with an increase of drug concentration which could suggest that dosing may play a critical role in the combination treatment. Although, the

response did not improve for line S302389IRR with combination of MK-2206 and irradiation, no drug-induced radioresistance was observed.

Inhibiting Akt with MK-2206 showed similar results as to using AZD2014 when combining those agents with irradiation, where we were able to sensitise certain lines to irradiation with combination therapy. With those results we speculate that blocking one pathway is not sufficient to fully sensitise cells to irradiation.

## **6.5. Conclusions**

We conclude that combining Everolimus or Rapamycin with radiotherapy as a treatment is not effective and does not result in better response to irradiation. The results show that both mTOR and Akt plays a key role in driving short term (and possibly long term) resistance to radiotherapy and pose as a good target for therapy. We also speculate that in order to sensitise the cells to irradiation effects and overcome the anti-apoptotic behaviour of cells driven by the dysregulation of mTOR/Akt pathway, a simultaneous inhibition of both Akt and mTORC1/2 is required. However, more research needs to be carried out looking into combining mTOR and Akt inhibitors and studying the expression to understand further whether certain lines respond differently.

## **7. DISCUSSION AND CONCLUSIONS**

### **7.1. Organoids pose as a good model for studying irradiation and modelling patients' response to treatment**

Prior to this study, organoids had started to emerge as a new and promising model that could be utilised for studying cancer and other human diseases. However, not many studies had been made available with organoids being used to model response to radiotherapy. In this thesis I described how we have used organoid derivation methods in order to establish organoids in our laboratory and use them to model response to irradiation. Furthermore, I have demonstrated that organoids are representative of patients' tumours as their pathological and molecular characteristics match those of the colorectal tumour. With the molecular characterisation of the derived organoid lines, we have demonstrated that derived organoid lines carry a mutations burden that is typical for colorectal cancer. What is more, using single-cell sequencing we have demonstrated that organoids are heterogeneous, just like primary tumours. Finally, we have showed that lines are different and when exposed to irradiation display an individual response.

Since the start of this project, studies utilising organoids for modelling radiotherapy and patients' response have been published and they demonstrated the same as we have in this thesis – that organoids are representative models

for predicting patients' response to radiotherapy (Driehuis et al. 2019; Yao et al. 2020).

## **7.2. mTOR/Akt pathway plays a key role in driving radioresistance**

The wide variety of sequencing experiments performed in support of this thesis, including whole genome sequencing, total RNA sequencing, and single-cell RNA sequencing, revealed that the PI3K/Akt/mTOR pathway is dysregulated in treatment resistant samples. Furthermore, we have also correlated that to a retrospective RNASeq analysis that also highlighted *mTOR* and *PI3K* genes to be upregulated in patients that did not respond to radiotherapy. With this evidence we have used a range of mTOR inhibitors in order to sensitise cells to irradiation. A single inhibition of mTORC1 with Rapamycin or Everolimus was not effective and did not sensitise cells to irradiation, as we proposed this resulted in Akt-driven cell survival. The inhibition of mTORC1 and mTORC2 through AZD2014 showed that cells partially get sensitised to irradiation. The *KRAS* mutant line did not get sensitised with AZD2014, which suggest that the presence of a *KRAS* mutation further drives resistance. The literature supports this, as *KRAS* has been linked to radioresistance (Yang et al. 2021; Zhao et al 2021).

As the sequencing results also showed the dysregulation of *PI3K* and *Akt* genes, the organoids have been subjected to chemoradiotherapy using MK-2206, an Akt inhibitor. We have observed sensitisation to radiotherapy in selected lines following this method, but the resistant lines did not exhibit an improved

response. We speculate that the inhibition of mTOR or Akt alone is not sufficient for sensitising cells to radiotherapy. We believe using a combined mTOR and Akt inhibition approach would result in improved response. Another PhD candidate in the laboratory has been able to demonstrate with his preliminary results that using Dactolisib, a dual mTOR and PI3K inhibitor, results in radiosensitivity of organoids, though this work is not yet published. In the literature, we have found studies that showed increased radiosensitivity after inhibition of both mTOR and PI3K (Zhu, Fu and Hu, 2013, Kuger et al. 2014; Miyasaka et al. 2015; Chen et al. 2019). Additionally, many clinical studies are being conducted with dual mTOR/PI3K inhibitors as they show promise to tackling the resistance mechanisms (Yang et al. 2019).

### **7.3. Radiosensitivity markers**

One of the main aims of this study was to identify radiosensitivity biomarkers that would help with patient stratification. When starting this study we had two potential candidates for radiosensitivity markers: inactivating mutations of *PIK3CA* or *FBXW7*. Our results did not reveal *FBXW7* as a potential candidate; therefore we did not proceed with it and suggest that the mutations could occur with *PIK3CA*. However, we have observed in the analysis an upregulation of *PI3K* genes in the non-responder cohort, as well as upregulation of the Akt pathway in organoids. The combination assays of Akt inhibitor MK-2206 and radiotherapy showed partial radiosensitivity of the non-resistant lines. We have showed more

supporting evidence that inactivating mutations in the *PIK3CA* gene can be good candidate for predicting favourable response to radiotherapy. Nevertheless, more studies need to be done in order to validate this.

#### **7.4. Study limitations**

There have been a number of limitations in this study. Firstly, radiotherapy is applicable only to rectal cancer tumours, and it is not administered for colon or sigmoid tumours due to their anatomical position. In this study we wanted to investigate the effects of radiotherapy on rectal cancer cells, but due to limited sample availability we have expanded the patient recruitment to all colorectal resections for organoid derivation. Furthermore, the sample size for the experiments performed was small, which particularly had an impact on RNA sequencing analysis and methylation array analysis. Due to the small sample size, we only had one organoid with *KRAS* mutation, which has limited our ability to conclude the effects of mutated *KRAS* on mTOR-driven radioresistance.

Although we showed that organoids are representative models for studying cancer and modelling response to irradiation, we are aware of the limitations of organoids. The microenvironment component of tumours where immune cells and blood vessels are present are important to tumour biology, and consequently can play a role in treatment response.

Finally, one of the main study limitations was time. Though western blot analysis was attempted, due to time limitations it was not possible to finish troubleshooting the method in time to run protein analysis.

Finally, in this thesis we have explored the irradiation effects 96h after the last dose was delivered to organoids, with the exception of the single-cell sequencing experiments. Clinical data suggests that the long intervals between the radiotherapy and surgery is beneficial for the patient as irradiation effects can take long period of times (Francois et al. 1999; Tseng et al. 2019). Due to the nature of organoids derived from adult stem cells/ cancer cells and time constraints of this PhD we have not fully explored the long term effects that radiotherapy has on organoids.

## **7.5. Future direction**

In this study we have used 3 organoid lines for sequencing analysis and 4 lines for chemoradiotherapy response investigation. Although the organoid lines were different, only one line had a mutant *KRAS*. The responses of the *KRAS* mutant line S345653 show that more research needs to be done to understand whether or not mutations in this gene can further drive radioresistance and cause the inhibition of the mTOR pathway. This could be investigated with recruiting patients with wild type *KRAS* and patients with mutant *KRAS* and performing a combination of chemoradiotherapy assays.

In this thesis I have mainly investigated the short-term effects of irradiation on organoids. However, resistance mechanisms have been detected with sequencing analyses that have been performed on established radioresistant samples (retrospective data and single-cell sequencing 5 weeks post irradiation). Total RNA sequencing of the larger organoid cohort 5 weeks from delivery of the last dose would be beneficial and insightful. By establishing each organoid line's response to radiotherapy, it would be possible to compare against the retrospective data to validate our findings.

Finally, CRISPR/Cas9 gene editing could be employed in order to validate our speculation about inactivating mutations of *PIK3CA*. This could be achieved by performing a series of assays with a knocked out *PIK3CA* gene in organoids and subjecting them to irradiation and chemoradiation. In addition to this, drug assays with mTOR or mTOR/Akt inhibitors could be done on the knock out and WT lines to see if the effects are enhanced.

## **7.6. Final Conclusions**

To summarise we have found patient-derived organoids to be a representative model of patients with colorectal cancer as they displayed characteristics of patient tumours. What is more we conclude that organoids serve as an appropriate model for modelling patient's response to radiotherapy and combine radio-chemotherapy. We also conclude that dysregulation of mTOR and Akt

driver to radioresistance. Finally, we suggest that inactivation of PIK3CA can be indicative of good response to irradiation

## 8. BIBLIOGRAPHY

Abshire, D. and Lang, M., 2018. The Evolution of Radiation Therapy in Treating Cancer. *Seminars in Oncology Nursing*, 34(2), pp.151-157.

Ali, M., Kaltenbrun, E., Anderson, G., Stephens, S., Arena, S., Bardelli, A., Counter, C. and Wood, K., 2017. Codon bias imposes a targetable limitation on KRAS-driven therapeutic resistance. *Nature Communications*, 8(1).

Amado, R., Wolf, M., Peeters, M., Van Cutsem, E., Siena, S., Freeman, D., Juan, T., Sikorski, R., Suggs, S., Radinsky, R., Patterson, S. and Chang, D., 2008. Wild-Type KRAS Is Required for Panitumumab Efficacy in Patients With Metastatic Colorectal Cancer. *Journal of Clinical Oncology*, 26(10), pp.1626-1634.

Andrews, S., 2010. *Babraham Bioinformatics - FastQC A Quality Control tool for High Throughput Sequence Data*. [online] Bioinformatics.babraham.ac.uk. Available at: <<http://www.bioinformatics.babraham.ac.uk/projects/fastqc/>> [Accessed 28 January 2022].

Antwih, D., Gabbara, K., Lancaster, W., Ruden, D. and Zielske, S., 2013. Radiation-induced epigenetic DNA methylation modification of radiation-response pathways. *Epigenetics*, 8(8), pp.839-848.

Aoki, K. and Taketo, M., 2007. Adenomatous polyposis coli (APC): a multi-functional tumor suppressor gene. *Journal of Cell Science*, 120(19), pp.3327-3335.

Asati, V., Mahapatra, D. and Bharti, S., 2016. ChemInform Abstract: PI3K/Akt/mTOR and Ras/Raf/MEK/ERK Signaling Pathways Inhibitors as

Anticancer Agents: Structural and Pharmacological Perspectives. *ChemInform*, 47(13), p.no-no.

Bahrami, A., Khazaei, M., Hasanzadeh, M., ShahidSales, S., Joudi Mashhad, M., Farazestanian, M., Sadeghnia, H., Rezayi, M., Maftouh, M., Hassanian, S. and Avan, A., 2017. Therapeutic Potential of Targeting PI3K/AKT Pathway in Treatment of Colorectal Cancer: Rational and Progress. *Journal of Cellular Biochemistry*, 119(3), pp.2460-2469.

Baker, S., Fearon, E., Nigro, J., Hamilton, S., Preisinger, A., Jessup, J., vanTuinen, P., Ledbetter, D., Barker, D., Nakamura, Y., White, R. and Vogelstein, B., 1989. Chromosome 17 Deletions and p53 Gene Mutations in Colorectal Carcinomas. *Science*, 244(4901), pp.217-221.

Baker, S., Preisinger, A., Paraskeva, C., Markowitz, S., Willson, J., Hamilton, S. and Vogelstein, B., 1990. p53 gene mutations occur in combination with 17p allelic deletions as late events in colorectal tumorigenesis. *Cancer Research*, 50(23), pp.7717-22.

Barbi, S., Cataldo, I., De Manzoni, G., Bersani, S., Lamba, S., Mattuzzi, S., Bardelli, A. and Scarpa, A., 2010. The analysis of PIK3CA mutations in gastric carcinoma and metanalysis of literature suggest that exon-selectivity is a signature of cancer type. *Journal of Experimental & Clinical Cancer Research*, 29(1).

Bardelli, A., Corso, S., Bertotti, A., Hobor, S., Valtorta, E., Siravegna, G., Sartore-Bianchi, A., Scala, E., Cassingena, A., Zecchin, D., Apicella, M., Migliardi, G., Galimi, F., Lauricella, C., Zanon, C., Perera, T., Veronese, S., Corti, G., Amatu, A., Gambacorta, M., Diaz, L., Sausen, M., Velculescu, V., Comoglio, P., Trusolino, L., Di Nicolantonio, F., Giordano, S. and Siena, S., 2013. Amplification of the MET Receptor Drives Resistance to Anti-EGFR Therapies in Colorectal Cancer. *Cancer Discovery*, 3(6), pp.658-673.

Barker, N., van Es, J., Kuipers, J., Kujala, P., van den Born, M., Cozijnsen, M., Haegebarth, A., Korving, J., Begthel, H., Peters, P. and Clevers, H., 2007. Identification of stem cells in small intestine and colon by marker gene Lgr5. *Nature*, 449(7165), pp.1003-1007.

Barko, P., McMichael, M., Swanson, K. and Williams, D., 2017. The Gastrointestinal Microbiome: A Review. *Journal of Veterinary Internal Medicine*, 32(1), pp.9-25.

Baron, J. and Sandler, R., 2000. Nonsteroidal Anti-Inflammatory Drugs and Cancer Prevention. *Annual Review of Medicine*, 51(1), pp.511-523.

Bartfeld, S., Bayram, T., van de Wetering, M., Huch, M., Begthel, H., Kujala, P., Vries, R., Peters, P. and Clevers, H., 2015. In Vitro Expansion of Human Gastric Epithelial Stem Cells and Their Responses to Bacterial Infection. *Gastroenterology*, 148(1), pp.126-136.e6.

Benvenuti, S., Frattini, M., Arena, S., Zanon, C., Cappelletti, V., Coradini, D., Grazia Daidone, M., Pilotti, S., Pierotti, M. and Bardelli, A., 2008. PIK3CA cancer mutations display gender and tissue specificity patterns. *Human Mutation*, 29(2), pp.284-288.

Beroud, C. and Soussi, T., 1996. APC gene: database of germline and somatic mutations in human tumors and cell lines. *Nucleic Acids Research*, 24(1), pp.121-124.

Blanco-Calvo, M., Concha, Á., Figueroa, A., Garrido, F. and Valladares-Ayerbes, M., 2015. Colorectal Cancer Classification and Cell Heterogeneity: A Systems Oncology Approach. *International Journal of Molecular Sciences*, 16(12), pp.13610-13632.

Blighe, K. and Lun, A., 2021. PCAtools: PCAtools: Everything Principal Components Analysis. R package version 2.6.0. [online] Available at: <<https://github.com/kevinblighe/PCAtools>> [Accessed 28 January 2022].

Bodmer, W., Bailey, C., Bodmer, J., Bussey, H., Ellis, A., Gorman, P., Lucibello, F., Murday, V., Rider, S., Scambler, P., Sheer, D., Solomon, E. and Spurr, N., 1987. Localization of the gene for familial adenomatous polyposis on chromosome 5. *Nature*, 328(6131), pp.614-616.

Body, A., Prenen, H., Latham, S., Lam, M., Tipping-Smith, S., Raghunath, A. and Segelov, E., 2021. The Role of Neoadjuvant Chemotherapy in Locally Advanced Colon Cancer. *Cancer Management and Research*, Volume 13, pp.2567-2579.

Bosset, J., Collette, L., Calais, G., Mineur, L., Maingon, P., Radosevic-Jelic, L., Daban, A., Bardet, E., Beny, A. and Ollier, J., 2006. Chemotherapy with Preoperative Radiotherapy in Rectal Cancer. *New England Journal of Medicine*, 355(11), pp.1114-1123.

Brunner, T., 2016. The rationale of combined radiotherapy and chemotherapy – Joint action of Castor and Pollux. *Best Practice & Research Clinical Gastroenterology*, 30(4), pp.515-528.

Buckley, A., Lynam-Lennon, N., O'Neill, H. and O'Sullivan, J., 2020. Targeting hallmarks of cancer to enhance radiosensitivity in gastrointestinal cancers. *Nature Reviews Gastroenterology & Hepatology*, 17(5), pp.298-313.

Bujko, K., Nowacki, M., Nasierowska-Guttmejer, A., Michalski, W., Bebenek, M. and Kryj, M., 2006. Long-term results of a randomized trial comparing preoperative short-course radiotherapy with preoperative conventionally fractionated chemoradiation for rectal cancer. *British Journal of Surgery*, 93(10), pp.1215-1223.

Butterworth, K., 2019. Evolution of the Supermodel: Progress in Modelling Radiotherapy Response in Mice. *Clinical Oncology*, 31(5), pp.272-282.

Byrne, A., Alférez, D., Amant, F., Annibaldi, D., Arribas, J., Biankin, A., Bruna, A., Budinská, E., Caldas, C., Chang, D., Clarke, R., Clevers, H., Coukos, G., Dangles-Marie, V., Eckhardt, S., Gonzalez-Suarez, E., Hermans, E., Hidalgo, M., Jarzabek, M., de Jong, S., Jonkers, J., Kemper, K., Lanfrancone, L., Mælandsmo, G., Marangoni, E., Marine, J., Medico, E., Norum, J., Palmer, H., Peeper, D., Pelicci, P., Piris-Gimenez, A., Roman-Roman, S., Rueda, O., Seoane, J., Serra, V., Soucek, L., Vanhecke, D., Villanueva, A., Vinolo, E., Bertotti, A. and Trusolino, L., 2017. Interrogating open issues in cancer precision medicine with patient-derived xenografts. *Nature Reviews Cancer*, 17(4), pp.254-268.

Calon, A., Lonardo, E., Berenguer-Llargo, A., Espinet, E., Hernando-Momblona, X., Iglesias, M., Sevillano, M., Palomo-Ponce, S., Tauriello, D., Byrom, D., Cortina, C., Morral, C., Barceló, C., Tosi, S., Riera, A., Attolini, C., Rossell, D., Sancho, E. and Batlle, E., 2015. Stromal gene expression defines poor-prognosis subtypes in colorectal cancer. *Nature Genetics*, 47(4), pp.320-329.

Cancer Research UK. 2022. *Bowel cancer survival statistics*. [online] Available at: <<https://www.cancerresearchuk.org/health-professional/cancer-statistics/statistics-by-cancer-type/bowel-cancer/survival#heading-Zero>> [Accessed 27 January 2022].

Cao, R., Wang, L., Wang, H., Xia, L., Erdjument-Bromage, H., Tempst, P., Jones, R. and Zhang, Y., 2002. Role of Histone H3 Lysine 27 Methylation in Polycomb-Group Silencing. *Science*, 298(5595), pp.1039-1043.

Cedermark, 1997. Improved Survival with Preoperative Radiotherapy in Resectable Rectal Cancer. *New England Journal of Medicine*, 336(14), pp.980-987.

Chang, L., Graham, P., Hao, J., Ni, J., Bucci, J., Cozzi, P., Kearsley, J. and Li, Y., 2013. Acquisition of epithelial–mesenchymal transition and cancer stem cell phenotypes is associated with activation of the PI3K/Akt/mTOR pathway in prostate cancer radioresistance. *Cell Death & Disease*, 4(10), pp.e875-e875.

Chang, L., Graham, P., Hao, J., Ni, J., Bucci, J., Cozzi, P., Kearsley, J. and Li, Y., 2014. PI3K/Akt/mTOR pathway inhibitors enhance radiosensitivity in radioresistant prostate cancer cells through inducing apoptosis, reducing autophagy, suppressing NHEJ and HR repair pathways. *Cell Death & Disease*, 5(10), pp.e1437-e1437.

Chang, L., Graham, P., Ni, J., Hao, J., Bucci, J., Cozzi, P. and Li, Y., 2015. Targeting PI3K/Akt/mTOR signaling pathway in the treatment of prostate cancer radioresistance. *Critical Reviews in Oncology/Hematology*, 96(3), pp.507-517.

Chatterjee, N. and Walker, G., 2017. Mechanisms of DNA damage, repair, and mutagenesis. *Environmental and Molecular Mutagenesis*, 58(5), pp.235-263.

Chen, K., Srinivasan, T., Lin, C., Tung, K., Gao, Z., Hsu, D., Lipkin, S. and Shen, X., 2018. Single-Cell Transcriptomics Reveals Heterogeneity and Drug Response of Human Colorectal Cancer Organoids. *2018 40th Annual International Conference of the IEEE Engineering in Medicine and Biology Society (EMBC)*,.

Chen, Y., Wang, C., Wei, M., Tzeng, Y., Lan, K., Cheng, A. and Kuo, S., 2019. Maintenance BEZ235 Treatment Prolongs the Therapeutic Effect of the Combination of BEZ235 and Radiotherapy for Colorectal Cancer. *Cancers*, 11(8), p.1204.

Cheng, H., Zhou, L., Long, Y., Xiang, J. and Chen, L., 2021. MACC1 Is Associated With Epithelial–Mesenchymal Transition and Can Predict Poor Prognosis in Nasopharyngeal Carcinoma. *Frontiers in Oncology*, 11.

Cheng, Y. and Li, G., 2012. Role of the ubiquitin ligase Fbw7 in cancer progression. *Cancer and Metastasis Reviews*, 31(1-2), pp.75-87.

Ciccia, A. and Elledge, S., 2010. The DNA Damage Response: Making It Safe to Play with Knives. *Molecular Cell*, 40(2), pp.179-204.

Citrin, D. and Mitchell, J., 2014. Altering the Response to Radiation: Sensitizers and Protectors. *Seminars in Oncology*, 41(6), pp.848-859.

Colorectal Cancer Collaborative Group, 2001. Adjuvant radiotherapy for rectal cancer: a systematic overview of 8507 patients from 22 randomised trials. *The Lancet*, 358(9290), pp.1291-1304.

Cox, A. and Der, C., 2010. Ras history. *Small GTPases*, 1(1), pp.2-27.

Davies, R., Miller, R. and Coleman, N., 2005. Colorectal cancer screening: prospects for molecular stool analysis. *Nature Reviews Cancer*, 5(3), pp.199-209.

Diehn, M., Cho, R., Lobo, N., Kalisky, T., Dorie, M., Kulp, A., Qian, D., Lam, J., Ailles, L., Wong, M., Joshua, B., Kaplan, M., Wapnir, I., Dirbas, F., Somlo, G., Garberoglio, C., Paz, B., Shen, J., Lau, S., Quake, S., Brown, J., Weissman, I. and Clarke, M., 2009. Association of reactive oxygen species

levels and radioresistance in cancer stem cells. *Nature*, 458(7239), pp.780-783.

Dinu, D., Dobre, M., Panaitescu, E., Birla, R., Iosif, C., Hoara, P., Caragui, A., Boeriu, M., Constantinoiu, S. and Ardeleanu, C., 2014. Prognostic significance of KRAS gene mutations in colorectal cancer - preliminary study. *Journal of Medical Science*, 7(4), pp.581-589.

Dow, L., 2015. Modeling Disease In Vivo With CRISPR/Cas9. *Trends in Molecular Medicine*, 21(10), pp.609-621.

Drew, D., Cao, Y. and Chan, A., 2016. Aspirin and colorectal cancer: the promise of precision chemoprevention. *Nature Reviews Cancer*, 16(3), pp.173-186.

Driehuis, E., Kolders, S., Spelier, S., Löhmußaar, K., Willems, S., Devriese, L., de Bree, R., de Ruiter, E., Korving, J., Begthel, H., van Es, J., Geurts, V., He, G., van Jaarsveld, R., Oka, R., Muraro, M., Vivié, J., Zandvliet, M., Hendrickx, A., Iakobachvili, N., Sridevi, P., Kranenburg, O., van Boxtel, R., Kops, G., Tuveson, D., Peters, P., van Oudenaarden, A. and Clevers, H., 2019. Oral Mucosal Organoids as a Potential Platform for Personalized Cancer Therapy. *Cancer Discovery*, 9(7), pp.852-871.

Drost, J. and Clevers, H., 2018. Organoids in cancer research. *Nature Reviews Cancer*, 18(7), pp.407-418.

Drost, J., van Jaarsveld, R., Ponsioen, B., Zimmerlin, C., van Boxtel, R., Buijs, A., Sachs, N., Overmeer, R., Offerhaus, G., Begthel, H., Korving, J., van de Wetering, M., Schwank, G., Logtenberg, M., Cuppen, E., Snippert, H., Medema, J., Kops, G. and Clevers, H., 2015. Sequential cancer mutations in cultured human intestinal stem cells. *Nature*, 521(7550), pp.43-47.

Ellen, T., Ke, Q., Zhang, P. and Costa, M., 2008. NDRG1, a growth and cancer related gene: regulation of gene expression and function in normal and disease states. *Carcinogenesis*, 29(1), pp.2-8.

Eyre, T., Collins, G., Goldstone, A. and Cwynarski, K., 2014. Time now to TORC the TORC? New developments in mTOR pathway inhibition in lymphoid malignancies. *British Journal of Haematology*, 166(3), pp.336-351.

Falasca, M. and Maffucci, T., 2012. Regulation and cellular functions of class II phosphoinositide 3-kinases. *Biochemical Journal*, 443(3), pp.587-601.

Farhood, B., khodamoradi, E., Hoseini-Ghahfarokhi, M., Motevaseli, E., Mirtavoos-Mahyari, H., Elejo Musa, A. and Najafi, M., 2020. TGF- $\beta$  in radiotherapy: Mechanisms of tumor resistance and normal tissues injury. *Pharmacological Research*, 155, p.104745.

Fearon, E. and Vogelstein, B., 1990. A genetic model for colorectal tumorigenesis. *Cell*, 61(5), pp.759-767.

Fearon, E., 2011. Molecular Genetics of Colorectal Cancer. *Annual Review of Pathology: Mechanisms of Disease*, 6(1), pp.479-507.

Feeney, G., Sehgal, R., Sheehan, M., Hogan, A., Regan, M., Joyce, M. and Kerin, M., 2019. Neoadjuvant radiotherapy for rectal cancer management. *World Journal of Gastroenterology*, 25(33), pp.4850-4869.

Fessler, E., Drost, J., Hooff, S., Linnekamp, J., Wang, X., Jansen, M., De Sousa E Melo, F., Prasetyanti, P., IJspeert, J., Franitza, M., Nürnberg, P., Noesel, C., Dekker, E., Vermeulen, L., Clevers, H. and Medema, J., 2016. TGF $\beta$  signaling directs serrated adenomas to the mesenchymal colorectal cancer subtype. *EMBO Molecular Medicine*, 8(7), pp.745-760.

Fisher, B., Wolmark, N., Rockette, H., Redmond, C., Deutsch, M., Wickerham, D., Fisher, E., Caplan, R., Jones, J., Lerner, H., Gordon, P., Feldman, M., Cruz, A., Legault-Poisson, S., Wexler, M., Lawrence, W. and Robidoux, A., 1988. Postoperative Adjuvant Chemotherapy or Radiation Therapy for Rectal Cancer: Results From NSABP Protocol R-011. *JNCI Journal of the National Cancer Institute*, 80(1), pp.21-29.

Fodde, R., Smits, R. and Clevers, H., 2001. APC, Signal transduction and genetic instability in colorectal cancer. *Nature Reviews Cancer*, 1(1), pp.55-67.

Folkesson, J., Birgisson, H., Pahlman, L., Cedermark, B., Glimelius, B. and Gunnarsson, U., 2005. Swedish Rectal Cancer Trial: Long Lasting Benefits From Radiotherapy on Survival and Local Recurrence Rate. *Journal of Clinical Oncology*, 23(24), pp.5644-5650.

Francois, Y., Nemoz, C., Baulieux, J., Vignal, J., Grandjean, J., Partensky, C., Souquet, J., Adeleine, P. and Gerard, J., 1999. Influence of the Interval Between Preoperative Radiation Therapy and Surgery on Downstaging and on the Rate of Sphincter-Sparing Surgery for Rectal Cancer: The Lyon R90-01 Randomized Trial. *Journal of Clinical Oncology*, 17(8), pp.2396-2396.

Frouws, M., Bastiaannet, E., Langley, R., Chia, W., van Herk-Sukel, M., Lemmens, V., Putter, H., Hartgrink, H., Bonsing, B., Van de Velde, C., Portielje, J. and Liefers, G., 2017. Effect of low-dose aspirin use on survival of patients with gastrointestinal malignancies; an observational study. *British Journal of Cancer*, 116(3), pp.405-413.

Fugger, K. and West, S., 2016. Keeping homologous recombination in check. *Cell Research*, 26(4), pp.397-398.

Galez, C., Totis, C. and Bisio, A., 2021. Radiation Resistance: A Matter of Transcription Factors. *Frontiers in Oncology*, 11.

Ganesh, K., Wu, C., O'Rourke, K., Szeglin, B., Zheng, Y., Sauvé, C., Adileh, M., Wasserman, I., Marco, M., Kim, A., Shady, M., Sanchez-Vega, F., Karthaus, W., Won, H., Choi, S., Pelossof, R., Barlas, A., Ntiamoah, P., Pappou, E., Elghouayel, A., Strong, J., Chen, C., Harris, J., Weiser, M., Nash, G., Guillem, J., Wei, I., Kolesnick, R., Veeraraghavan, H., Ortiz, E., Petkovska, I., Cercek, A., Manova-Todorova, K., Saltz, L., Lavery, J., DeMatteo, R., Massagué, J., Paty, P., Yaeger, R., Chen, X., Patil, S., Clevers, H., Berger, M., Lowe, S., Shia, J., Romesser, P., Dow, L., Garcia-Aguilar, J., Sawyers, C. and Smith, J., 2019. A rectal cancer organoid platform to study individual responses to chemoradiation. *Nature Medicine*, 25(10), pp.1607-1614.

Gao, C. and Chen, Y., 2010. Dishevelled: The hub of Wnt signaling. *Cellular Signalling*, 22(5), pp.717-727.

Garaud, S., Gu-Trantien, C., Lodewyckx, J., Boisson, A., De Silva, P., Buisseret, L., Migliori, E., Libin, M., Naveaux, C., Duvillier, H. and Willard-Gallo, K., 2014. A Simple and Rapid Protocol to Non-enzymatically Dissociate Fresh Human Tissues for the Analysis of Infiltrating Lymphocytes. *Journal of Visualized Experiments*, (94).

Garcez, P., Loiola, E., Madeiro da Costa, R., Higa, L., Trindade, P., Delvecchio, R., Nascimento, J., Brindeiro, R., Tanuri, A. and Rehen, S., 2016. Zika virus impairs growth in human neurospheres and brain organoids. *Science*, 352(6287), pp.816-818.

Geng, L. and Wang, J., 2017. Molecular effectors of radiation resistance in colorectal cancer. *Precision Radiation Oncology*, 1(1), pp.27-33.

Giannakis, M., Mu, X., Shukla, S., Qian, Z., Cohen, O., Nishihara, R., Bahl, S., Cao, Y., Amin-Mansour, A., Yamauchi, M., Sukawa, Y., Stewart, C., Rosenberg, M., Mima, K., Inamura, K., Nosho, K., Nowak, J., Lawrence, M., Giovannucci, E., Chan, A., Ng, K., Meyerhardt, J., Van Allen, E., Getz, G., Gabriel, S., Lander, E., Wu, C., Fuchs, C., Ogino, S. and Garraway, L., 2016. Genomic Correlates of Immune-Cell Infiltrates in Colorectal Carcinoma. *Cell Reports*, 15(4), pp.857-865.

Glimelius, B., 2014. Optimal Time Intervals between Pre-Operative Radiotherapy or Chemoradiotherapy and Surgery in Rectal Cancer?. *Frontiers in Oncology*, 4.

Grana, T., Rusyn, E., Zhou, H., Sartor, C. and Cox, A., 2002. Ras mediates radioresistance through both phosphatidylinositol 3-kinase-dependent and Raf-dependent but mitogen-activated protein kinase/extracellular signal-regulated kinase kinase-independent signaling pathways. *Cancer Research*, 62(14), pp.4142-4150.

Graule, J., Uth, K., Fischer, E., Centeno, I., Galván, J., Eichmann, M., Rau, T., Langer, R., Dawson, H., Nitsche, U., Traeger, P., Berger, M., Schnüriger, B., Hädrich, M., Studer, P., Inderbitzin, D., Lugli, A., Tschan, M. and Zlobec, I., 2018. CDX2 in colorectal cancer is an independent prognostic factor and regulated by promoter methylation and histone deacetylation in tumors of the serrated pathway. *Clinical Epigenetics*, 10(1).

Greene, F., Stewart, A. and Norton, H., 2002. A New TNM Staging Strategy for Node-Positive (Stage III) Colon Cancer. *Annals of Surgery*, 236(4), pp.416-421.

Grusch, M., Petz, M., Metzner, D., Ozturk, D., Schneller, D. and Mikulits, W., 2010. The Crosstalk of RAS with the TGF- $\beta$  Family During Carcinoma

Progression and its Implications for Targeted Cancer Therapy. *Current Cancer Drug Targets*, 10(8), pp.849-857.

Gu, M., Nishihara, R., Chen, Y., Li, W., Shi, Y., Masugi, Y., Hamada, T., Kosumi, K., Liu, L., da Silva, A., Nowak, J., Twombly, T., Du, C., Koh, H., Li, W., Meyerhardt, J., Wolpin, B., Giannakis, M., Aguirre, A., Bass, A., Drew, D., Chan, A., Fuchs, C., Qian, Z. and Ogino, S., 2017. Aspirin exerts high anti-cancer activity in PIK3CA-mutant colon cancer cells. *Oncotarget*, 8(50), pp.87379-87389.

Guinney, J., Dienstmann, R., Wang, X., de Reyniès, A., Schlicker, A., Soneson, C., Marisa, L., Roepman, P., Nyamundanda, G., Angelino, P., Bot, B., Morris, J., Simon, I., Gerster, S., Fessler, E., De Sousa E Melo, F., Missiaglia, E., Ramay, H., Barras, D., Homicsko, K., Maru, D., Manyam, G., Broom, B., Boige, V., Perez-Villamil, B., Laderas, T., Salazar, R., Gray, J., Hanahan, D., Tabernero, J., Bernardis, R., Friend, S., Laurent-Puig, P., Medema, J., Sadanandam, A., Wessels, L., Delorenzi, M., Kopetz, S., Vermeulen, L. and Tejpar, S., 2015. The consensus molecular subtypes of colorectal cancer. *Nature Medicine*, 21(11), pp.1350-1356.

Handy, D., Castro, R. and Loscalzo, J., 2011. Epigenetic Modifications. *Circulation*, 123(19), pp.2145-2156.

Hernando-Herraez, I., Garcia-Perez, R., Sharp, A. and Marques-Bonet, T., 2015. DNA Methylation: Insights into Human Evolution. *PLOS Genetics*, 11(12), p.e1005661.

Huang, R. and Zhou, P., 2020. DNA damage response signaling pathways and targets for radiotherapy sensitization in cancer. *Signal Transduction and Targeted Therapy*, 5(1).

Huch, M., Gehart, H., van Boxtel, R., Hamer, K., Blokzijl, F., Verstegen, M., Ellis, E., van Wenum, M., Fuchs, S., de Ligt, J., van de Wetering, M., Sasaki, N., Boers, S., Kemperman, H., de Jonge, J., Ijzermans, J., Nieuwenhuis, E., Hoekstra, R., Strom, S., Vries, R., van der Laan, L., Cuppen, E. and Clevers, H., 2015. Long-Term Culture of Genome-Stable Bipotent Stem Cells from Adult Human Liver. *Cell*, 160(1-2), pp.299-312.

Isella, C., Brundu, F., Bellomo, S., Galimi, F., Zanella, E., Porporato, R., Petti, C., Fiori, A., Orzan, F., Senetta, R., Boccaccio, C., Ficarra, E., Marchionni, L., Trusolino, L., Medico, E. and Bertotti, A., 2017. Selective analysis of cancer-cell intrinsic transcriptional traits defines novel clinically relevant subtypes of colorectal cancer. *Nature Communications*, 8(1).

Isella, C., Terrasi, A., Bellomo, S., Petti, C., Galatola, G., Muratore, A., Mellano, A., Senetta, R., Cassenti, A., Sonetto, C., Inghirami, G., Trusolino, L., Fekete, Z., De Ridder, M., Cassoni, P., Storme, G., Bertotti, A. and Medico, E., 2015. Stromal contribution to the colorectal cancer transcriptome. *Nature Genetics*, 47(4), pp.312-319.

Issa, J., 2002. Epigenetic Variation and Human Disease. *The Journal of Nutrition*, 132(8), pp.2388S-2392S.

Jackson, S. and Bartek, J., 2009. The DNA-damage response in human biology and disease. *Nature*, 461(7267), pp.1071-1078.

Jaffe, N., Paed, D., Traggis, D., Salian, S. and Cassady, J., 1976. Improved outlook for Ewing's sarcoma with combination chemotherapy (vincristine, actinomycin D and cyclophosphamide) and radiation therapy. *Cancer*, 38(5), pp.1925-1930.

Jančík, S., Drábek, J., Radzioch, D. and Hajdúch, M., 2010. Clinical Relevance of KRAS in Human Cancers. *Journal of Biomedicine and Biotechnology*, 2010, pp.1-13.

Jass, J., 2007. Classification of colorectal cancer based on correlation of clinical, morphological and molecular features. *Histopathology*, 50(1), pp.113-130.

Jensen, K., Driskell, R. and Watt, F., 2010. Assaying proliferation and differentiation capacity of stem cells using disaggregated adult mouse epidermis. *Nature Protocols*, 5(5), pp.898-911.

Jiang, Y., Kimchi, E., Staveley-O'Carroll, K., Cheng, H. and Ajani, J., 2009. Assessment of K-ras mutation. *Cancer*, 115(16), pp.3609-3617.

Jin, B., Li, Y. and Robertson, K., 2011. DNA Methylation: Superior or Subordinate in the Epigenetic Hierarchy?. *Genes & Cancer*, 2(6), pp.607-617.

Jiricny, J., 2006. The multifaceted mismatch-repair system. *Nature Reviews Molecular Cell Biology*, 7(5), pp.335-346.

John, T., Kohler, D., Pintilie, M., Yanagawa, N., Pham, N., Li, M., Panchal, D., Hui, F., Meng, F., Shepherd, F. and Tsao, M., 2011. The Ability to Form Primary Tumor Xenografts Is Predictive of Increased Risk of Disease Recurrence in Early-Stage Non-Small Cell Lung Cancer. *Clinical Cancer Research*, 17(1), pp.134-141.

Jung, B., Staudacher, J. and Beauchamp, D., 2017. Transforming Growth Factor  $\beta$  Superfamily Signaling in Development of Colorectal Cancer. *Gastroenterology*, 152(1), pp.36-52.

Kapiteijn, E., Marijnen, C., Nagtegaal, I., Putter, H., Steup, W., Wiggers, T., Rutten, H., Pahlman, L., Glimelius, B., van Krieken, J., Leer, J. and van de Velde, C., 2001. Preoperative Radiotherapy Combined with Total Mesorectal Excision for Resectable Rectal Cancer. *New England Journal of Medicine*, 345(9), pp.638-646.

Kaplan, D., Whitman, M., Schaffhausen, B., Pallas, D., White, M., Cantley, L. and Roberts, T., 1987. Common elements in growth factor stimulation and oncogenic transformation: 85 kd phosphoprotein and phosphatidylinositol kinase activity. *Cell*, 50(7), pp.1021-1029.

Karthaus, W., Iaquinta, P., Drost, J., Gracanin, A., van Boxtel, R., Wongvipat, J., Dowling, C., Gao, D., Begthel, H., Sachs, N., Vries, R., Cuppen, E., Chen, Y., Sawyers, C. and Clevers, H., 2014. Identification of Multipotent Luminal Progenitor Cells in Human Prostate Organoid Cultures. *Cell*, 159(1), pp.163-175.

Kaur, G. and Dufour, J., 2012. Cell lines. *Spermatogenesis*, 2(1), pp.1-5.

Kawakami, H., Zaanani, A. and Sinicrope, F., 2015. Microsatellite Instability Testing and Its Role in the Management of Colorectal Cancer. *Current Treatment Options in Oncology*, 16(7).

Kim, E., Kim, A., Kim, S., Kim, H., Chang, J., Ahn, C. and Chang, Y., 2014. Inhibition of mTORC1 induces loss of E-cadherin through AKT/GSK-3 $\beta$  signaling-mediated upregulation of E-cadherin repressor complexes in non-small cell lung cancer cells. *Respiratory Research*, 15(1).

Kim, E., Park, A., Dong, S., Ahn, J. and Park, W., 2010. Global analysis of CpG methylation reveals epigenetic control of the radiosensitivity in lung cancer cell lines. *Oncogene*, 29(33), pp.4725-4731.

Kim, J., Koo, B. and Knoblich, J., 2020. Human organoids: model systems for human biology and medicine. *Nature Reviews Molecular Cell Biology*, 21(10), pp.571-584.

Kim, L., Cook, R. and Chen, J., 2016. mTORC1 and mTORC2 in cancer and the tumor microenvironment. *Oncogene*, 36(16), pp.2191-2201.

Kocakavuk, E., Anderson, K., Varn, F., Johnson, K., Amin, S., Sulman, E., Lolkema, M., Barthel, F. and Verhaak, R., 2021. Radiotherapy is associated with a deletion signature that contributes to poor outcomes in patients with cancer. *Nature Genetics*, 53(7), pp.1088-1096.

Kodaira, M., Asakawa, J. and Nakamura, N., 2017. Radiation-Induced Deletions in Mouse Spermatogonia are Usually Large (over 200 kb) and Contain Little Sequence Similarity at the Junctions. *Radiation Research*, 187(6), p.722.

Korphaisarn, K., Morris, V., Overman, M., Fogelman, D., Kee, B., Pratap Singh Raghav, K., Manuel, S., Shureiqi, I., Wolff, R., Eng, C., Menter, D., Hamilton, S., Kopetz, S. and Dasari, A., 2017. FBXW7 missense mutation: a novel negative prognostic factor in metastatic colorectal adenocarcinoma. *Oncotarget*, 8(24), pp.39268-39279.

Koyama, F., Lopes Ramos, C., Ledesma, F., Alves, V., Fernandes, J., Vailati, B., São Julião, G., Habr-Gama, A., Gama-Rodrigues, J., Perez, R. and Camargo, A., 2018. Effect of Akt activation and experimental pharmacological inhibition on responses to neoadjuvant chemoradiotherapy in rectal cancer. *British Journal of Surgery*, 105(2), pp.e192-e203.

Kretzschmar, K. and Clevers, H., 2016. Organoids: Modeling Development and the Stem Cell Niche in a Dish. *Developmental Cell*, 38(6), pp.590-600.

Krook, J., Moertel, C., Gunderson, L., Wieand, H., Collins, R., Beart, R., Kubista, T., Poon, M., Meyers, W., Mailliard, J., Twito, D., Morton, R., Veeder, M., Witzig, T., Cha, S. and Vidyarthi, S., 1991. Effective Surgical Adjuvant Therapy for High-Risk Rectal Carcinoma. *New England Journal of Medicine*, 324(11), pp.709-715.

Kuger, S., Cörek, E., Polat, B., Kämmerer, U., Flentje, M. and Djuzenova, C., 2014. Novel PI3K and mTOR Inhibitor NVP-BEZ235 Radiosensitizes Breast Cancer Cell Lines under Normoxic and Hypoxic Conditions. *Breast Cancer: Basic and Clinical Research*, 8, p.BCBCR.S13693.

Kuipers, E., Grady, W., Lieberman, D., Seufferlein, T., Sung, J., Boelens, P., van de Velde, C. and Watanabe, T., 2015. Colorectal cancer. *Nature Reviews Disease Primers*, 1(1).

Lam, K., Pan, K., Linnekamp, J., Medema, J. and Kandimalla, R., 2016. DNA methylation based biomarkers in colorectal cancer: A systematic review. *Biochimica et Biophysica Acta (BBA) - Reviews on Cancer*, 1866(1), pp.106-120.

Lancaster, M. and Knoblich, J., 2014. Generation of cerebral organoids from human pluripotent stem cells. *Nature Protocols*, 9(10), pp.2329-2340.

Lao, V. and Grady, W., 2011. Epigenetics and colorectal cancer. *Nature Reviews Gastroenterology & Hepatology*, 8(12), pp.686-700.

Laurent-Puig, P., Pekin, D., Normand, C., Kotsopoulos, S., Nizard, P., Perez-Toralla, K., Rowell, R., Olson, J., Srinivasan, P., Le Corre, D., Hor, T., El Harrak, Z., Li, X., Link, D., Bouché, O., Emile, J., Landi, B., Boige, V., Hutchison, J. and Taly, V., 2015. Clinical Relevance of KRAS-Mutated Subclones Detected with Picodroplet Digital PCR in Advanced Colorectal

Cancer Treated with Anti-EGFR Therapy. *Clinical Cancer Research*, 21(5), pp.1087-1097.

Lee, S., Hu, W., Matulay, J., Silva, M., Owczarek, T., Kim, K., Chua, C., Barlow, L., Kandoth, C., Williams, A., Bergren, S., Pietzak, E., Anderson, C., Benson, M., Coleman, J., Taylor, B., Abate-Shen, C., McKiernan, J., Al-Ahmadie, H., Solit, D. and Shen, M., 2018. Tumor Evolution and Drug Response in Patient-Derived Organoid Models of Bladder Cancer. *Cell*, 173(2), pp.515-528.e17.

Levine, S., King, I. and Kingston, R., 2004. Division of labor in Polycomb group repression. *Trends in Biochemical Sciences*, 29(9), pp.478-485.

Li, H. and Durbin, R., 2009. Fast and accurate short read alignment with Burrows-Wheeler transform. *Bioinformatics*, 25(14), pp.1754-1760.

Li, H., Handsaker, B., Wysoker, A., Fennell, T., Ruan, J., Homer, N., Marth, G., Abecasis, G. and Durbin, R., 2009. The Sequence Alignment/Map format and SAMtools. *Bioinformatics*, 25(16), pp.2078-2079.

Li, N., Lorenzi, F., Kalakouti, E., Normatova, M., Babaei-Jadidi, R., Tomlinson, I. and Nateri, A., 2015. FBXW7-mutated colorectal cancer cells exhibit aberrant expression of phosphorylated-p53 at Serine-15. *Oncotarget*, 6(11), pp.9240-9256.

Li, X., Sun, K., Liao, X., Gao, H., Zhu, H. and Xu, R., 2020. Colorectal carcinomas with mucinous differentiation are associated with high frequent mutation of KRAS or BRAF mutations, irrespective of quantity of mucinous component. *BMC Cancer*, 20(1).

Li, Y., Tang, P., Cai, S., Peng, J. and Hua, G., 2020. Organoid based personalized medicine: from bench to bedside. *Cell Regeneration*, 9(1).

Liao, X., Lochhead, P., Nishihara, R., Morikawa, T., Kuchiba, A., Yamauchi, M., Imamura, Y., Qian, Z., Baba, Y., Shima, K., Sun, R., Nosho, K., Meyerhardt, J., Giovannucci, E., Fuchs, C., Chan, A. and Ogino, S., 2012. Aspirin Use, Tumor PIK3CA Mutation, and Colorectal-Cancer Survival. *New England Journal of Medicine*, 367(17), pp.1596-1606.

Lindahl, T. and Barnes, D., 2000. Repair of Endogenous DNA Damage. *Cold Spring Harbor Symposia on Quantitative Biology*, 65(0), pp.127-134.

Linnemann, J., Miura, H., Meixner, L., Irmeler, M., Kloos, U., Hirschi, B., Bartsch, H., Sass, S., Beckers, J., Theis, F., Gabka, C., Sotlar, K. and Scheel, C., 2015. Quantification of regenerative potential in primary human mammary epithelial cells. *Development*,.

Liu, G. and Sabatini, D., 2020. mTOR at the nexus of nutrition, growth, ageing and disease. *Nature Reviews Molecular Cell Biology*, 21(4), pp.183-203.

Liu, S., Chen, S. and Zeng, J., 2017. TGF- $\beta$  signaling: A complex role in tumorigenesis (Review). *Molecular Medicine Reports*,.

Loomans, C., Williams Giuliani, N., Balak, J., Ringnalda, F., van Gurp, L., Huch, M., Boj, S., Sato, T., Kester, L., de Sousa Lopes, S., Roost, M., Bonner-Weir, S., Engelse, M., Rabelink, T., Heimberg, H., Vries, R., van Oudenaarden, A., Carlotti, F., Clevers, H. and de Koning, E., 2018. Expansion of Adult Human Pancreatic Tissue Yields Organoids Harboring Progenitor Cells with Endocrine Differentiation Potential. *Stem Cell Reports*, 10(3), pp.712-724.

Lorimer, P., Motz, B., Kirks, R., Boselli, D., Walsh, K., Prabhu, R., Hill, J. and Salo, J., 2017. Pathologic Complete Response Rates After Neoadjuvant Treatment in Rectal Cancer: An Analysis of the National Cancer Database. *Annals of Surgical Oncology*, 24(8), pp.2095-2103.

Love, M., Huber, W. and Anders, S., 2014. Moderated estimation of fold change and dispersion for RNA-seq data with DESeq2. *Genome Biology*, 15(12).

Lucey, B., Nelson-Rees, W. and Hutchins, G., 2009. Henrietta Lacks, HeLa Cells, and Cell Culture Contamination. *Archives of Pathology & Laboratory Medicine*, 133(9), pp.1463-1467.

Lynch, H. and de la Chapelle, A., 2003. Hereditary Colorectal Cancer. *New England Journal of Medicine*, 348(10), pp.919-932.

Martin, M., Adileh, M., Hsu, K., Hua, G., Lee, S., Li, C., Fuller, J., Rotolo, J., Bodo, S., Klingler, S., Haimovitz-Friedman, A., Deasy, J., Fuks, Z., Paty, P. and Kolesnick, R., 2020. Organoids Reveal That Inherent Radiosensitivity of Small and Large Intestinal Stem Cells Determines Organ Sensitivity. *Cancer Research*, 80(5), pp.1219-1227.

Martini, M., De Santis, M., Braccini, L., Gulluni, F. and Hirsch, E., 2014. PI3K/AKT signaling pathway and cancer: an updated review. *Annals of Medicine*, 46(6), pp.372-383.

Massagué, J., 2008. TGF $\beta$  in Cancer. *Cell*, 134(2), pp.215-230.

Matano, M., Date, S., Shimokawa, M., Takano, A., Fujii, M., Ohta, Y., Watanabe, T., Kanai, T. and Sato, T., 2015. Modeling colorectal cancer using CRISPR-Cas9-mediated engineering of human intestinal organoids. *Nature Medicine*, 21(3), pp.256-262.

Matsui, T., Nuryadi, E., Komatsu, S., Hirota, Y., Shibata, A., Oike, T. and Nakano, T., 2019. Robustness of Clonogenic Assays as a Biomarker for Cancer Cell Radiosensitivity. *International Journal of Molecular Sciences*, 20(17), p.4148.

Maugeri-Saccà, M., Bartucci, M. and De Maria, R., 2012. DNA Damage Repair Pathways in Cancer Stem Cells. *Molecular Cancer Therapeutics*, 11(8), pp.1627-1636.

Maugeri-Saccà, M., Vigneri, P. and De Maria, R., 2011. Cancer Stem Cells and Chemosensitivity: Figure 1. *Clinical Cancer Research*, 17(15), pp.4942-4947.

McCauley, H. and Wells, J., 2017. Pluripotent stem cell-derived organoids: using principles of developmental biology to grow human tissues in a dish. *Development*, 144(6), pp.958-962.

McLaren, W., Gil, L., Hunt, S., Riat, H., Ritchie, G., Thormann, A., Flicek, P. and Cunningham, F., 2016. The Ensembl Variant Effect Predictor. *Genome Biology*, 17(1).

McVey, M. and Lee, S., 2008. MMEJ repair of double-strand breaks (director's cut): deleted sequences and alternative endings. *Trends in Genetics*, 24(11), pp.529-538.

Miller, K., Siegel, R., Lin, C., Mariotto, A., Kramer, J., Rowland, J., Stein, K., Alteri, R. and Jemal, A., 2016. Cancer treatment and survivorship statistics, 2016. *CA: A Cancer Journal for Clinicians*, 66(4), pp.271-289.

Miousse, I., Kutanzi, K. and Koturbash, I., 2017. Effects of ionizing radiation on DNA methylation: from experimental biology to clinical applications. *International Journal of Radiation Biology*, 93(5), pp.457-469.

Miyasaka, A., Oda, K., Ikeda, Y., Sone, K., Fukuda, T., Inaba, K., Makii, C., Enomoto, A., Hosoya, N., Tanikawa, M., Uehara, Y., Arimoto, T., Kuramoto, H., Wada-Hiraike, O., Miyagawa, K., Yano, T., Kawana, K., Osuga, Y. and Fujii, T., 2015. PI3K/mTOR pathway inhibition overcomes radioresistance via

suppression of the HIF1- $\alpha$ /VEGF pathway in endometrial cancer. *Gynecologic Oncology*, 138(1), pp.174-180.

Miyoshi, H., VanDussen, K., Malvin, N., Ryu, S., Wang, Y., Sonnek, N., Lai, C. and Stappenbeck, T., 2016. Prostaglandin E2 promotes intestinal repair through an adaptive cellular response of the epithelium. *The EMBO Journal*, 36(1), pp.5-24.

Moelling, K., Schad, K., Bosse, M., Zimmermann, S. and Schweneker, M., 2002. Regulation of Raf-Akt Cross-talk. *Journal of Biological Chemistry*, 277(34), pp.31099-31106.

Molinari, C., Marisi, G., Passardi, A., Matteucci, L., De Maio, G. and Ulivi, P., 2018. Heterogeneity in Colorectal Cancer: A Challenge for Personalized Medicine?. *International Journal of Molecular Sciences*, 19(12), p.3733.

Moore, L., Le, T. and Fan, G., 2012. DNA Methylation and Its Basic Function. *Neuropsychopharmacology*, 38(1), pp.23-38.

Nagata, 2010. Effect of rapamycin, an mTOR inhibitor, on radiation sensitivity of lung cancer cells having different p53 gene status. *International Journal of Oncology*, 37(4).

Nam, H., Han, M., Chang, H., Lee, Y., Lee, M., Lee, H., Lee, B., Lee, H., Lee, K., Jung, M., Jeon, H., Choi, S., Park, N., Kim, S. and Kim, S., 2013. Radioresistant Cancer Cells Can Be Conditioned to Enter Senescence by mTOR Inhibition. *Cancer Research*, 73(14), pp.4267-4277.

Ncbi.nlm.nih.gov. 2022. *ELAPOR2 endosome-lysosome associated apoptosis and autophagy regulator family member 2 [Homo sapiens (human)]* - Gene - NCBI. [online] Available at: <<https://www.ncbi.nlm.nih.gov/gene/222223>> [Accessed 25 January 2022].

Ngan, S., Burmeister, B., Fisher, R., Solomon, M., Goldstein, D., Joseph, D., Ackland, S., Schache, D., McClure, B., McLachlan, S., McKendrick, J., Leong, T., Hartopecanu, C., Zalcborg, J. and Mackay, J., 2012. Randomized Trial of Short-Course Radiotherapy Versus Long-Course Chemoradiation Comparing Rates of Local Recurrence in Patients With T3 Rectal Cancer: Trans-Tasman Radiation Oncology Group Trial 01.04. *Journal of Clinical Oncology*, 30(31), pp.3827-3833.

Nguyen, H. and Duong, H., 2018. The molecular characteristics of colorectal cancer: Implications for diagnosis and therapy (Review). *Oncology Letters*,.

Nichols, C., Gibson, W., Brown, M., Kosmicki, J., Busanovich, J., Wei, H., Urbanski, L., Curimjee, N., Berger, A., Gao, G., Cherniack, A., Dhe-Paganon, S., Paoletta, B. and Beroukhir, R., 2020. Loss of heterozygosity of essential genes represents a widespread class of potential cancer vulnerabilities. *Nature Communications*, 11(1).

NIH consensus conference, 1990. Adjuvant Therapy for Patients With Colon and Rectal Cancer. *JAMA: The Journal of the American Medical Association*, 264(11), p.1444.

Nyfeler, B., Bergman, P., Triantafellow, E., Wilson, C., Zhu, Y., Radetich, B., Finan, P., Klionsky, D. and Murphy, L., 2011. Relieving Autophagy and 4EBP1 from Rapamycin Resistance. *Molecular and Cellular Biology*, 31(14), pp.2867-2876.

O'Brown, N., Pfau, S. and Gu, C., 2018. Bridging barriers: a comparative look at the blood–brain barrier across organisms. *Genes & Development*, 32(7-8), pp.466-478.

Papillon, J., 1973. Radiotherapy and Chemotherapy for Colorectal Cancer [Abridged]. *Proceedings of the Royal Society of Medicine*, 66(12), pp.1179-1181.

Parry, L. and Clarke, A., 2011. The Roles of the Methyl-CpG Binding Proteins in Cancer. *Genes & Cancer*, 2(6), pp.618-630.

Pennati, M., Folini, M. and Zaffaroni, N., 2008. Targeting survivin in cancer therapy. *Expert Opinion on Therapeutic Targets*, 12(4), pp.463-476.

Pino, M. and Chung, D., 2010. The Chromosomal Instability Pathway in Colon Cancer. *Gastroenterology*, 138(6), pp.2059-2072.

Polakis, P., 2007. The many ways of Wnt in cancer. *Current Opinion in Genetics & Development*, 17(1), pp.45-51.

Porru, M., Pompili, L., Caruso, C., Biroccio, A. and Leonetti, C., 2018. Targeting KRAS in metastatic colorectal cancer: current strategies and emerging opportunities. *Journal of Experimental & Clinical Cancer Research*, 37(1).

Puschhof, J., Pleguezuelos-Manzano, C., Martinez-Silgado, A., Akkerman, N., Saftien, A., Boot, C., de Waal, A., Beumer, J., Dutta, D., Heo, I. and Clevers, H., 2021. Intestinal organoid cocultures with microbes. *Nature Protocols*, 16(10), pp.4633-4649.

Ray, K., Sibson, N. and Kiltie, A., 2015. Treatment of Breast and Prostate Cancer by Hypofractionated Radiotherapy: Potential Risks and Benefits. *Clinical Oncology*, 27(7), pp.420-426.

Reusch, H., Zimmermann, S., Schaefer, M., Paul, M. and Moelling, K., 2001. Regulation of Raf by Akt Controls Growth and Differentiation in Vascular

Smooth Muscle Cells. *Journal of Biological Chemistry*, 276(36), pp.33630-33637.

Rich, J., 2007. Cancer Stem Cells in Radiation Resistance: Figure 1. *Cancer Research*, 67(19), pp.8980-8984.

Robinson, J., Thorvaldsdóttir, H., Winckler, W., Guttman, M., Lander, E., Getz, G. and Mesirov, J., 2011. Integrative genomics viewer. *Nature Biotechnology*, 29(1), pp.24-26.

Rödel, C., Haas, J., Groth, A., Grabenbauer, G., Sauer, R. and Rödel, F., 2003. Spontaneous and radiation-induced apoptosis in colorectal carcinoma cells with different intrinsic radiosensitivities: Survivin as a radioresistance factor. *International Journal of Radiation Oncology\*Biophysics*, 55(5), pp.1341-1347.

Roeder, F., Meldolesi, E., Gerum, S., Valentini, V. and Rödel, C., 2020. Recent advances in (chemo-)radiation therapy for rectal cancer: a comprehensive review. *Radiation Oncology*, 15(1).

Roh, M., Colangelo, L., O'Connell, M., Yothers, G., Deutsch, M., Allegra, C., Kahlenberg, M., Baez-Diaz, L., Ursiny, C., Petrelli, N. and Wolmark, N., 2009. Preoperative Multimodality Therapy Improves Disease-Free Survival in Patients With Carcinoma of the Rectum: NSABP R-03. *Journal of Clinical Oncology*, 27(31), pp.5124-5130.

Rothwell, P., Fowkes, F., Belch, J., Ogawa, H., Warlow, C. and Meade, T., 2011. Effect of daily aspirin on long-term risk of death due to cancer: analysis of individual patient data from randomised trials. *The Lancet*, 377(9759), pp.31-41.

Roulis, M., Kaklamanos, A., Scherthanner, M., Bielecki, P., Zhao, J., Kaffe, E., Frommelt, L., Qu, R., Knapp, M., Henriques, A., Chalkidi, N., Koliaraki, V., Jiao, J., Brewer, J., Bacher, M., Blackburn, H., Zhao, X., Breyer, R., Aidinis, V., Jain, D., Su, B., Herschman, H., Kluger, Y., Kollias, G. and Flavell, R., 2020. Paracrine orchestration of intestinal tumorigenesis by a mesenchymal niche. *Nature*, 580(7804), pp.524-529.

Royce, M. and Osman, D., 2015. Everolimus in the Treatment of Metastatic Breast Cancer. *Breast Cancer: Basic and Clinical Research*, 9, p.BCBCR.S29268.

Sachs, N. and Clevers, H., 2014. Organoid cultures for the analysis of cancer phenotypes. *Current Opinion in Genetics & Development*, 24, pp.68-73.

Sagaert, X., Vanstapel, A. and Verbeek, S., 2018. Tumor Heterogeneity in Colorectal Cancer: What Do We Know So Far?. *Pathobiology*, 85(1-2), pp.72-84.

Saitoh, M., Endo, K., Furuya, S., Minami, M., Fukasawa, A., Imamura, T. and Miyazawa, K., 2015. STAT3 integrates cooperative Ras and TGF- $\beta$  signals that induce Snail expression. *Oncogene*, 35(8), pp.1049-1057.

Samouelian, V., Maugard, C., Jolicoeur, M., Bertrand, R., Arcand, S., Tonin, P., Provencher, D. and Mes-Masson, A., 2004. Chemosensitivity and radiosensitivity profiles of four new human epithelial ovarian cancer cell lines exhibiting genetic alterations in BRCA2, TGF $\beta$ -RII, KRAS2, TP53 and/or CDNK2A. *Cancer Chemotherapy and Pharmacology*, 54(6), pp.497-504.

Samowitz, W., Curtin, K., Wolff, R., Tripp, S., Caan, B. and Slattery, M., 2009. Microsatellite instability and survival in rectal cancer. *Cancer Causes & Control*, 20(9), pp.1763-1768.

Samuels, Y., Wang, Z., Bardelli, A., Silliman, N., Ptak, J., Szabo, S., Yan, H., Gazdar, A., Powell, S., Riggins, G., Willson, J., Markowitz, S., Kinzler, K., Vogelstein, B. and Velculescu, V., 2004. High Frequency of Mutations of the PIK3CA Gene in Human Cancers. *Science*, 304(5670), pp.554-554.

San Filippo, J., Sung, P. and Klein, H., 2008. Mechanism of Eukaryotic Homologous Recombination. *Annual Review of Biochemistry*, 77(1), pp.229-257.

Sánchez-Pérez, E., Villanueva-Herrero, J., Sandoval-Martínez, M. and Jiménez-Bobadilla, B., 2017. Complete pathological response after neoadjuvant therapy in patients with rectal adenocarcinoma. *Revista Médica del Hospital General de México*, 80(4), pp.212-217.

Sato, K., Azuma, R., Imai, T. and Shimokawa, T., 2017. Enhancement of mTOR signaling contributes to acquired X-ray and C-ion resistance in mouse squamous carcinoma cell line. *Cancer Science*, 108(10), pp.2004-2010.

Sato, K., Shimokawa, T. and Imai, T., 2019. Difference in Acquired Radioresistance Induction Between Repeated Photon and Particle Irradiation. *Frontiers in Oncology*, 9.

Sato, T., Stange, D., Ferrante, M., Vries, R., van Es, J., van den Brink, S., van Houdt, W., Pronk, A., van Gorp, J., Siersema, P. and Clevers, H., 2011. Long-term Expansion of Epithelial Organoids From Human Colon, Adenoma, Adenocarcinoma, and Barrett's Epithelium. *Gastroenterology*, 141(5), pp.1762-1772.

Sato, T., Vries, R., Snippert, H., van de Wetering, M., Barker, N., Stange, D., van Es, J., Abo, A., Kujala, P., Peters, P. and Clevers, H., 2009. Single Lgr5 stem cells build crypt-villus structures in vitro without a mesenchymal niche. *Nature*, 459(7244), pp.262-265.

Sauer, R., Becker, H., Hohenberger, W., Rödel, C., Wittekind, C., Fietkau, R., Martus, P., Tschmelitsch, J., Hager, E., Hess, C., Karstens, J., Liersch, T., Schmidberger, H. and Raab, R., 2004. Preoperative versus Postoperative Chemoradiotherapy for Rectal Cancer. *New England Journal of Medicine*, 351(17), pp.1731-1740.

Sauer, R., Liersch, T., Merkel, S., Fietkau, R., Hohenberger, W., Hess, C., Becker, H., Raab, H., Villanueva, M., Witzigmann, H., Wittekind, C., Beissbarth, T. and Rödel, C., 2012. Preoperative Versus Postoperative Chemoradiotherapy for Locally Advanced Rectal Cancer: Results of the German CAO/ARO/AIO-94 Randomized Phase III Trial After a Median Follow-Up of 11 Years. *Journal of Clinical Oncology*, 30(16), pp.1926-1933.

Sauvageau, M. and Sauvageau, G., 2010. Polycomb Group Proteins: Multi-Faceted Regulators of Somatic Stem Cells and Cancer. *Cell Stem Cell*, 7(3), pp.299-313.

Schiff, P., Harrison, L., Strong, E., Fass, D., Shah, J., Spiro, R., Sessions, R., Gerold, F., Vikram, B. and Fuks, Z., 1990. Impact of the time interval between surgery and postoperative radiation therapy on locoregional control in advanced head and neck cancer. *Journal of Surgical Oncology*, 43(4), pp.203-208.

Schlaermann, P., Toelle, B., Berger, H., Schmidt, S., Glanemann, M., Ordemann, J., Bartfeld, S., Mollenkopf, H. and Meyer, T., 2014. A novel human gastric primary cell culture system for modelling *Helicobacter pylori* infection in vitro. *Gut*, 65(2), pp.202-213.

Schwank, G., Koo, B., Sasselli, V., Dekkers, J., Heo, I., Demircan, T., Sasaki, N., Boymans, S., Cuppen, E., van der Ent, C., Nieuwenhuis, E., Beekman, J. and Clevers, H., 2013. Functional Repair of CFTR by CRISPR/Cas9 in

Intestinal Stem Cell Organoids of Cystic Fibrosis Patients. *Cell Stem Cell*, 13(6), pp.653-658.

Sebag-Montefiore, D., Stephens, R., Steele, R., Monson, J., Grieve, R., Khanna, S., Quirke, P., Couture, J., de Metz, C., Myint, A., Bessell, E., Griffiths, G., Thompson, L. and Parmar, M., 2009. Preoperative radiotherapy versus selective postoperative chemoradiotherapy in patients with rectal cancer (MRC CR07 and NCIC-CTG C016): a multicentre, randomised trial. *The Lancet*, 373(9666), pp.811-820.

Seymour, M. and Morton, D., 2019. FOxTROT: an international randomised controlled trial in 1052 patients (pts) evaluating neoadjuvant chemotherapy (NAC) for colon cancer. *Journal of Clinical Oncology*, 37(15\_suppl), pp.3504-3504.

Shimura, T., 2017. Targeting the AKT/cyclin D1 pathway to overcome intrinsic and acquired radioresistance of tumors for effective radiotherapy. *International Journal of Radiation Biology*, 93(4), pp.381-385.

Shimura, T., Kakuda, S., Ochiai, Y., Nakagawa, H., Kuwahara, Y., Takai, Y., Kobayashi, J., Komatsu, K. and Fukumoto, M., 2010. Acquired radioresistance of human tumor cells by DNA-PK/AKT/GSK3 $\beta$ -mediated cyclin D1 overexpression. *Oncogene*, 29(34), pp.4826-4837.

Shimura, T., Noma, N., Sano, Y., Ochiai, Y., Oikawa, T., Fukumoto, M. and Kunugita, N., 2014. AKT-mediated enhanced aerobic glycolysis causes acquired radioresistance by human tumor cells. *Radiotherapy and Oncology*, 112(2), pp.302-307.

Shimura, T., Noma, N., Sano, Y., Ochiai, Y., Oikawa, T., Fukumoto, M. and Kunugita, N., 2014. AKT-mediated enhanced aerobic glycolysis causes

acquired radioresistance by human tumor cells. *Radiotherapy and Oncology*, 112(2), pp.302-307.

Shintani, Y., Okimura, A., Sato, K., Nakagiri, T., Kadota, Y., Inoue, M., Sawabata, N., Minami, M., Ikeda, N., Kawahara, K., Matsumoto, T., Matsuura, N., Ohta, M. and Okumura, M., 2011. Epithelial to Mesenchymal Transition Is a Determinant of Sensitivity to Chemoradiotherapy in Non-Small Cell Lung Cancer. *The Annals of Thoracic Surgery*, 92(5), pp.1794-1804.

Shoshani, T., Faerman, A., Mett, I., Zelin, E., Tenne, T., Gorodin, S., Moshel, Y., Elbaz, S., Budanov, A., Chajut, A., Kalinski, H., Kamer, I., Rozen, A., Mor, O., Keshet, E., Leshkowitz, D., Einat, P., Skaliter, R. and Feinstein, E., 2002. Identification of a Novel Hypoxia-Inducible Factor 1-Responsive Gene, RTP801, Involved in Apoptosis. *Molecular and Cellular Biology*, 22(7), pp.2283-2293.

Simillion, C., Liechti, R., Lischer, H., Ioannidis, V. and Bruggmann, R., 2017. Avoiding the pitfalls of gene set enrichment analysis with SetRank. *BMC Bioinformatics*, 18(1).

Sprangers, J., Zaalberg, I. and Maurice, M., 2020. Organoid-based modeling of intestinal development, regeneration, and repair. *Cell Death & Differentiation*, 28(1), pp.95-107.

Stockton, J., Tee, L., Whalley, C., James, J., Dilworth, M., Wheat, R., Nieto, T., Geh, I., Barros-Silva, J. and Beggs, A., 2021. Complete response to neoadjuvant chemoradiotherapy in rectal cancer is associated with RAS/AKT mutations and high tumour mutational burden. *Radiation Oncology*, 16(1).

Stodolna, A., He, M., Vasipalli, M., Kingsbury, Z., Becq, J., Stockton, J., Dilworth, M., James, J., Sillo, T., Blakeway, D., Ward, S., Ismail, T., Ross, M. and Beggs, A., 2021. Clinical-grade whole-genome sequencing and 3'

transcriptome analysis of colorectal cancer patients. *Genome Medicine*, 13(1).

Stuart, T., Butler, A., Hoffman, P., Hafemeister, C., Papalexi, E., Mauck, W., Hao, Y., Stoeckius, M., Smibert, P. and Satija, R., 2019. Comprehensive Integration of Single-Cell Data. *Cell*, 177(7), pp.1888-1902.e21.

Tee, A., 2018. The Target of Rapamycin and Mechanisms of Cell Growth. *International Journal of Molecular Sciences*, 19(3), p.880.

Tesei, A., Sarnelli, A., Arienti, C., Menghi, E., Medri, L., Gabucci, E., Pignatta, S., Falconi, M., Silvestrini, R., Zoli, W., D'Errico, V., Romeo, A., Parisi, E. and Polico, R., 2013. In vitro irradiation system for radiobiological experiments. *Radiation Oncology*, 8(1).

The Cancer Genome Atlas Network, 2012. Comprehensive molecular characterization of human colon and rectal cancer. *Nature*, 487(7407), pp.330-337.

The Gastrointestinal Tumour Study Group, 1985. Prolongation of the Disease-Free Interval in Surgically Treated Rectal Carcinoma. *New England Journal of Medicine*, 312(23), pp.1465-1472.

Thiboeau, S., French, A., Cunningham, J., Tester, D., Burgart, L., Roche, S., McDonnel, S., Schaid, D., Vockley, C., Michels, V., Farr Jr, G. and O'Connell, M., 1998. Microsatellite instability in colorectal cancer: different mutator phenotypes and the principal involvement of hMLH1. *Cancer Research*, 58(8), pp.1713-8.

Tian, Y., Morris, T., Webster, A., Yang, Z., Beck, S., Feber, A. and Teschendorff, A., 2017. ChAMP: updated methylation analysis pipeline for Illumina BeadChips. *Bioinformatics*, 33(24), pp.3982-3984.

Tirado-Hurtado, I., Fajardo, W. and Pinto, J., 2018. DNA Damage Inducible Transcript 4 Gene: The Switch of the Metabolism as Potential Target in Cancer. *Frontiers in Oncology*, 8.

Tong, J., Tan, S., Zou, F., Yu, J. and Zhang, L., 2016. FBW7 mutations mediate resistance of colorectal cancer to targeted therapies by blocking Mcl-1 degradation. *Oncogene*, 36(6), pp.787-796.

Toolan, H., 1953. Growth of human tumors in cortisone-treated laboratory animals: the possibility of obtaining permanently transplantable human tumors. *Cancer Research*, 3(4-5), pp.389-94.

Toulany, M. and Rodemann, P., 2013. Potential of Akt mediated DNA repair in radioresistance of solid tumors overexpressing erbB-PI3K-Akt pathway. *Translational Cancer Research*, 2(3).

Toyota, M., Ahuja, N., Ohe-Toyota, M., Herman, J., Baylin, S. and Issa, J., 1999. CpG island methylator phenotype in colorectal cancer. *Proceedings of the National Academy of Sciences*, 96(15), pp.8681-8686.

Tseng, M., Soon, Y., Vellayappan, B., Ho, F. and Tey, J., 2019. Radiation therapy for rectal cancer. *Journal of Gastrointestinal Oncology*, 10(6), pp.1238-1250.

Valer, Sánchez-de-Diego, Pimenta-Lopes, Rosa and Ventura, 2019. ACVR1 Function in Health and Disease. *Cells*, 8(11), p.1366.

Van Emburgh, B., Sartore-Bianchi, A., Di Nicolantonio, F., Siena, S. and Bardelli, A., 2014. Acquired resistance to EGFR-targeted therapies in colorectal cancer. *Molecular Oncology*, 8(6), pp.1084-1094.

Vanhaesebroeck, B., Guillermet-Guibert, J., Graupera, M. and Bilanges, B., 2010. The emerging mechanisms of isoform-specific PI3K signalling. *Nature Reviews Molecular Cell Biology*, 11(5), pp.329-341.

Vasen, H., Tomlinson, I. and Castells, A., 2015. Clinical management of hereditary colorectal cancer syndromes. *Nature Reviews Gastroenterology & Hepatology*, 12(2), pp.88-97.

Venkatachalam, V., Schmidt, D. and Heiden, M., 2018. Development of a Method to Characterize the Effects of Radiation on Growth and Morphology of Organoids in 3D Culture. *International Journal of Radiation Oncology\*Biological\*Physics*, 102(3), pp.e154-e155.

Venkatesan, S., Swanton, C., Taylor, B. and Costello, J., 2017. Treatment-Induced Mutagenesis and Selective Pressures Sculpt Cancer Evolution. *Cold Spring Harbor Perspectives in Medicine*, 7(8), p.a026617.

Vértessy, B. and Tóth, J., 2009. Keeping Uracil Out of DNA: Physiological Role, Structure and Catalytic Mechanism of dUTPases. *Accounts of Chemical Research*, 42(1), pp.97-106.

Vignard, J., Mirey, G. and Salles, B., 2013. Ionizing-radiation induced DNA double-strand breaks: A direct and indirect lighting up. *Radiotherapy and Oncology*, 108(3), pp.362-369.

Virag, P., Fischer-Fodor, E., Perde-Schrepler, M., Brie, I., Tatomir, C., Balacescu, L., Berindan-Neagoe, I., Victor, B. and Balacescu, O., 2013. Oxaliplatin induces different cellular and molecular chemoresistance patterns in colorectal cancer cell lines of identical origins. *BMC Genomics*, 14(1), p.480.

Vodenkova, S., Buchler, T., Cervena, K., Veskrnova, V., Vodicka, P. and Vymetalkova, V., 2020. 5-fluorouracil and other fluoropyrimidines in colorectal cancer: Past, present and future. *Pharmacology & Therapeutics*, 206, p.107447.

Vogelstein, B., Fearon, E., Hamilton, S., Kern, S., Preisinger, A., Leppert, M., Smits, A. and Bos, J., 1988. Genetic Alterations during Colorectal-Tumor Development. *New England Journal of Medicine*, 319(9), pp.525-532.

Vousden, K. and Prives, C., 2009. Blinded by the Light: The Growing Complexity of p53. *Cell*, 137(3), pp.413-431.

Wang, W., Qin, J., Voruganti, S., Nag, S., Zhou, J. and Zhang, R., 2015. Polycomb Group (PcG) Proteins and Human Cancers: Multifaceted Functions and Therapeutic Implications. *Medicinal Research Reviews*, 35(6), pp.1220-1267.

Wang, Z., Inuzuka, H., Zhong, J., Wan, L., Fukushima, H., Sarkar, F. and Wei, W., 2012. Tumor suppressor functions of FBW7 in cancer development and progression. *FEBS Letters*, 586(10), pp.1409-1418.

Warnes, G., Bolker, B. and Bonebakker, L., 2009. gplots: various R programming tools for plotting data. *ScienceOpen.com*,.

Waters, A. and Der, C., 2017. KRAS: The Critical Driver and Therapeutic Target for Pancreatic Cancer. *Cold Spring Harbor Perspectives in Medicine*, 8(9), p.a031435.

Weidlich, S., Walsh, K., Crowther, D., Burczynski, M., Feuerstein, G., Carey, F., Steele, R., Wolf, C., Miele, G. and Smith, G., 2011. Pyrosequencing-based methods reveal marked inter-individual differences in oncogene mutation

burden in human colorectal tumours. *British Journal of Cancer*, 105(2), pp.246-254.

WHO, 2022. *Cancer Statistics*. [online] Who.int. Available at: <<https://www.who.int/news-room/fact-sheets/detail/cancer>> [Accessed 28 January 2022].

Willers, H., Azzoli, C., Santivasi, W. and Xia, F., 2013. Basic Mechanisms of Therapeutic Resistance to Radiation and Chemotherapy in Lung Cancer. *The Cancer Journal*, 19(3), pp.200-207.

Williams, T., Yang, L., Estrada, A., Chatterjee, M. and Robb, R., 2016. KRAS Oncogenic Mutations Induce Intrinsic Resistance to Radiation Through Up-Regulation of DNA Repair Pathways. *International Journal of Radiation Oncology\*Biography\*Physics*, 96(2), p.S238.

Wolpin, B. and Mayer, R., 2008. Systemic Treatment of Colorectal Cancer. *Gastroenterology*, 134(5), pp.1296-1310.e1.

Wouters, B. and Koritzinsky, M., 2008. Hypoxia signalling through mTOR and the unfolded protein response in cancer. *Nature Reviews Cancer*, 8(11), pp.851-864.

Wu, S., Du, Y., Beckford, J. and Alachkar, H., 2018. Upregulation of the EMT marker vimentin is associated with poor clinical outcome in acute myeloid leukemia. *Journal of Translational Medicine*, 16(1).

Xie, J., Wang, X. and Proud, C., 2016. mTOR inhibitors in cancer therapy. *F1000Research*, 5, p.2078.

Xie, Y., Chen, Y. and Fang, J., 2020. Comprehensive review of targeted therapy for colorectal cancer. *Signal Transduction and Targeted Therapy*, 5(1).

Xu, J., Lamouille, S. and Derynck, R., 2009. TGF- $\beta$ -induced epithelial to mesenchymal transition. *Cell Research*, 19(2), pp.156-172.

Yang, H., Sun, L., Liu, M. and Mao, Y., 2018. Patient-derived organoids: a promising model for personalized cancer treatment. *Gastroenterology Report*, 6(4), pp.243-245.

Yang, J., Nie, J., Ma, X., Wei, Y., Peng, Y. and Wei, X., 2019. Targeting PI3K in cancer: mechanisms and advances in clinical trials. *Molecular Cancer*, 18(1).

Yang, L., Shen, C., Estrada-Bernal, A., Robb, R., Chatterjee, M., Sebastian, N., Webb, A., Mo, X., Chen, W., Krishnan, S. and Williams, T., 2021. Oncogenic KRAS drives radioresistance through upregulation of NRF2-53BP1-mediated non-homologous end-joining repair. *Nucleic Acids Research*, 49(19), pp.11067-11082.

Yao, Y., Xu, X., Yang, L., Zhu, J., Wan, J., Shen, L., Xia, F., Fu, G., Deng, Y., Pan, M., Guo, Q., Gao, X., Li, Y., Rao, X., Zhou, Y., Liang, L., Wang, Y., Zhang, J., Zhang, H., Li, G., Zhang, L., Peng, J., Cai, S., Hu, C., Gao, J., Clevers, H., Zhang, Z. and Hua, G., 2020. Patient-Derived Organoids Predict Chemoradiation Responses of Locally Advanced Rectal Cancer. *Cell Stem Cell*, 26(1), pp.17-26.e6.

Young, M. and Reed, K., 2016. Organoids as a Model for Colorectal Cancer. *Current Colorectal Cancer Reports*, 12(5), pp.281-287.

Zhang, B., Jones, J., Briggler, A., Hubbard, J., Kipp, B., Sargent, D., Dixon, J. and Grothey, A., 2017. Lack of Caudal-Type Homeobox Transcription Factor 2 Expression as a Prognostic Biomarker in Metastatic Colorectal Cancer. *Clinical Colorectal Cancer*, 16(2), pp.124-128.

Zhang, D., Bi, J., Liang, Q., Wang, S., Zhang, L., Han, F., Li, S., Qiu, B., Fan, X., Chen, W., Jiao, H., Ye, Y. and Ding, Y., 2020. VCAM1 Promotes Tumor Cell Invasion and Metastasis by Inducing EMT and Transendothelial Migration in Colorectal Cancer. *Frontiers in Oncology*, 10.

Zhang, Q., Zhang, Y., Parsels, J., Lohse, I., Lawrence, T., Pasca di Magliano, M., Sun, Y. and Morgan, M., 2016. Fbxw7 Deletion Accelerates KrasG12D-Driven Pancreatic Tumorigenesis via Yap Accumulation. *Neoplasia*, 18(11), pp.666-673.

Zhang, Y., Toneri, M., Ma, H., Yang, Z., Bouvet, M., Goto, Y., Seki, N. and Hoffman, R., 2016. Real-Time GFP Intravital Imaging of the Differences in Cellular and Angiogenic Behavior of Subcutaneous and Orthotopic Nude-Mouse Models of Human PC-3 Prostate Cancer. *Journal of Cellular Biochemistry*, 117(11), pp.2546-2551.

Zhao, Y., Murciano-Goroff, Y., Xue, J., Ang, A., Lucas, J., Mai, T., Da Cruz Paula, A., Saiki, A., Mohn, D., Achanta, P., Sisk, A., Arora, K., Roy, R., Kim, D., Li, C., Lim, L., Li, M., Bahr, A., Loomis, B., de Stanchina, E., Reis-Filho, J., Weigelt, B., Berger, M., Riely, G., Arbour, K., Lipford, J., Li, B. and Lito, P., 2021. Diverse alterations associated with resistance to KRAS(G12C) inhibition. *Nature*, 599(7886), pp.679-683.

Zhou, Y., Liu, J., Li, J., Zhang, J., Xu, Y., Zhang, H., Qiu, L., Ding, G., Su, X., Mei-Shi and Guo, G., 2011. Ionizing Radiation Promotes Migration and Invasion of Cancer Cells Through Transforming Growth Factor-Beta-

Mediated Epithelial–Mesenchymal Transition. *International Journal of Radiation Oncology\*Biology\*Physics*, 81(5), pp.1530-1537.

Zhu, L., Chen, S. and Chen, Y., 2011. Unraveling the biological functions of Smad7 with mouse models. *Cell & Bioscience*, 1(1).

Zhu, W., Fu, W. and Hu, L., 2013. NVP-BEZ235, Dual Phosphatidylinositol 3-Kinase/Mammalian Target of Rapamycin Inhibitor, Prominently Enhances Radiosensitivity of Prostate Cancer Cell Line PC-3. *Cancer Biotherapy and Radiopharmaceuticals*, 28(9), pp.665-673.

## 9. APPENDIX A

### Standard Operating Procedure: Organoid Derivation

1. Place the resection tissue on the sterile Petri dish
2. Cut tissue into small (approximately 1cm) pieces with sterile scalpel
3. Using forceps, place the small section of the tissue into the 50ml falcon tube containing 20ml of ice cold PBS0 supplemented with 0.1mg/ml Primocin
4. Wash tissue by vigorous shaking of the falcon tube
5. Repeat the wash steps with fresh PBS0/Primocin solution until the supernatant is clear
6. Using forceps, move the tissue pieces to sterile 5ml tube containing 1ml appropriate dissociation solution (Gentle Dissociation Buffer with 0.1mg/ml Primocin for normal healthy tissue; Tumour Dissociation Buffer for tumour tissue)
7. Using Castro-Viejo scissors cut the tissue into very small pieces
8. Incubate at 37°C in the organoid culture incubator for 30 minutes (if normal healthy tissue) or 1 hour (if tumour tissue) (mix by inverting the 5ml tube up and down every 15 minute during the incubation)
9. Take 10-20µl of the suspension and pipette onto glass slide and investigate the digestion level under light microscope. If single cell digestion for tumour cells have been achieved or crypts are visible proceed to next step, if not extend the incubation for 10 minutes.

10. Pass the suspension through 50 $\mu$ M strainer (for normal healthy tissue suspension) or 20 $\mu$ M (for tumour tissue suspension)
11. Move to 15ml Falcon tube
12. Add 5ml of ice cold PBS0
13. Centrifuge at 300xg for 5 minutes
14. Remove and discard supernatant
15. Wash with 5ml of PBS0
16. Centrifuge at 300xg for 5 minutes
17. Remove and discard supernatant
18. Resuspend the pellet in 100% Matrigel (estimate the volume of Matrigel based on the pellet size)
19. Plate 50 $\mu$ l of cell-Matrigel suspension into each well of preheated 24-well plates
20. Place the plate inverted at 37°C in the organoid culture incubator and incubate until the Matrigel polymerises (5-15 minutes)
21. Add 500 $\mu$ l of Human IntestiCult with 0.1mg/ml Primocin into each well with plated cells
22. Place in the organoid incubator at 37°C and 5% CO<sub>2</sub>

## 10.APPENDIX B

Table with list of all filtered SNVs for the whole genome sequencing data

<i>Gene Name</i>	<i>Consequence</i>	<i>Protein Position Amino Acid Change</i>	<i>Amino Acids</i>	<i>CADD score</i>
<i>SPINK5</i>	Stop gained	646	C/*	47
<i>ARAP2</i>	Stop gained	1617	E/*	43
<i>ZNF568</i>	Stop gained	538	K/*	41
<i>FXR1</i>	Stop gained	376	R/*	40
<i>PITX2</i>	Stop gained	51	K/*	39
<i>NCKAP5</i>	Stop gained	1654	C/*	38
<i>APC</i>	Stop gained	1450	R/*	37
<i>KIAA1324L</i>	Stop gained	114	E/*	37
<i>KCNMA1</i>	Missense variant	855	R/W	33
<i>SYNDIG1</i>	Missense variant, splice region variant	206	E/D	33
<i>RGS6</i>	Missense variant	463	R/C	32
<i>SMAD2</i>	Missense variant	321	R/Q	32
<i>FBN2</i>	Frameshift variant	2832	I/X	32
<i>MMAB</i>	Missense variant	190	R/H	30
<i>DLGAP1</i>	Missense variant	38	R/Q	29.7
<i>PTPRK</i>	Missense variant	1202	A/V	29.6
<i>PCDH10</i>	Missense variant	34	V/M	29.3

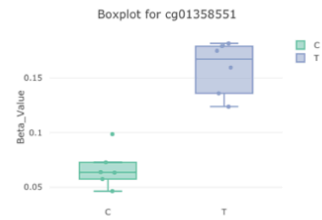
<i>MPPED1</i>	Missense variant	91	R/C	29.2
<i>DCX</i>	Missense variant	144	R/H	29
<i>RNF169</i>	Missense variant	339	S/L	28.7
<i>TTC37</i>	Missense variant	474	D/V	28.4
<i>KRT76</i>	Missense variant	432	A/D	28.3
<i>GRIK1</i>	Missense variant	862	R/W	28.2
<i>ACTR2</i>	Missense variant	177	G/S	27.4
<i>ENDOU</i>	Missense variant	299	F/L	27.2
<i>PLA1A</i>	Missense variant	176	A/T	27
<i>TRPM7</i>	Missense variant	720	T/I	26.9
<i>SLC18A3</i>	Missense variant	310	P/S	26.7
<i>NRXN1</i>	Missense variant	578	V/L	26.4
<i>ZNF793</i>	Missense variant	307	G/R	25.8
<i>GRAMD2</i>	Missense variant	174	R/G	25.6
<i>PAPPA2</i>	Missense variant	320	G/R	25.4
<i>MYF5</i>	Missense variant	85	R/W	25.1
<i>RPAIN</i>	Missense variant	2	A/V	24.9
<i>CDCA2</i>	Frameshift variant	503-504	EE/EX	24.9
<i>C2CD3</i>	Missense variant	533	A/T	24.8
<i>DLC1</i>	Missense variant	667	P/S	24.8
<i>SALL1</i>	Missense variant	648	T/M	24.7
<i>ANK1</i>	Missense variant	256	R/Q	24.7
<i>HERC2</i>	Missense variant	3336	E/K	24.6
<i>RAF1</i>	Missense variant	257	S/L	24.6

<i>KIAA1644</i>	Missense variant	154	R/W	24.5
<i>LRRC52</i>	Missense variant	162	L/F	24.3
<i>KCNH2</i>	Missense variant	547	A/T	24.2
<i>C8B</i>	Missense variant	428	R/Q	23.6
<i>VRK3</i>	Missense variant	275	A/S	23.6
<i>TRDN</i>	Missense variant	93	R/C	23.6
<i>ABCA5</i>	Missense variant	48	L/F	23.4
<i>PABPC4L</i>	Missense variant	125	L/I	23.4
<i>TRPS1</i>	Missense variant	421	I/L	23.3
<i>OR6N1</i>	Missense variant	154	A/D	23.2
<i>HSP90B1</i>	Missense variant	608	R/H	23.2
<i>DDX27</i>	Missense variant	474	K/R	23.2
<i>BCHE</i>	Missense variant	587	N/K	23.2
<i>PIK3CA</i>	Missense variant	1052	T/K	23.2
<i>RPS23</i>	Missense variant	85	V/L	23.2
<i>EPHA4</i>	Missense variant	306	S/L	23
<i>TMEM51</i>	Missense variant	84	S/C	22.6
<i>GLRX3</i>	Missense variant	277	E/G	22.6
<i>TTN</i>	Missense variant	30321	N/Y	22.6
<i>MUC13</i>	Missense variant	467	L/R	22.6
<i>TCHH</i>	Missense variant	685	L/Q	22.2
<i>ZDHHC15</i>	Missense variant	31	V/I	22.2
<i>PKD2L2</i>	Missense variant	343	L/I	20.9
<i>WDR43</i>	Missense variant	182	M/V	20.3
<i>AFAP1L2</i>	Missense variant	760	T/S	19.53

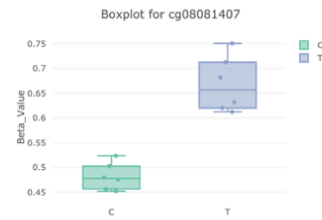
<i>FAT4</i>	Missense variant	2077	P/T	19.43
<i>FLG</i>	Missense variant	935	G/W	19.24
<i>DMXL1</i>	Missense variant	1431	T/M	19.17
<i>YIPF7</i>	Missense variant	200	F/V	18.4
<i>ZNF429</i>	Missense variant	392	T/N	17.51
<i>WDR19</i>	Missense variant	409	D/E	16.8
<i>PRAG1</i>	Missense variant	776	S/L	16.62
<i>CTBP2</i>	Missense variant	537	P/S	16.39
<i>OR56B1</i>	Missense variant	83	A/S	16.24
<i>POMT1</i>	Missense variant	145	A/S	16
<i>HECTD3</i>	Missense variant	201	A/T	15.84
<i>TBC1D28</i>	Missense variant	187	G/R	15.58

## 11.APPENDIX C

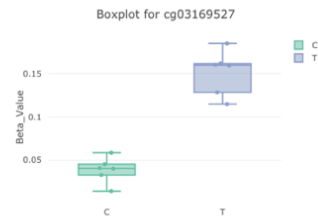
### 1. AP2S1



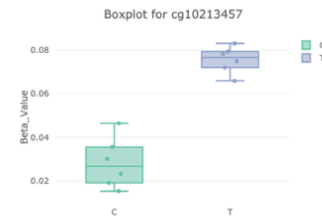
### 2. ARF4



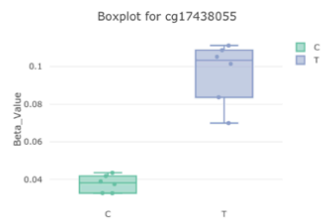
### 3. C3orf31



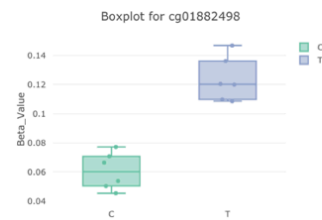
### 4. cg10213457



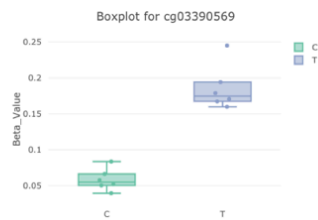
### 5. COX7A2



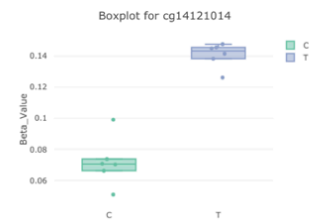
### 6. LIN54



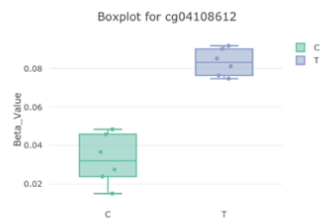
### 7. LOC100302652



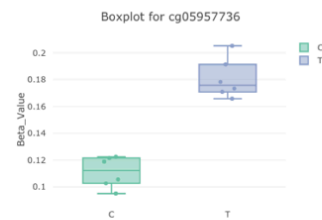
### 8. NUP107



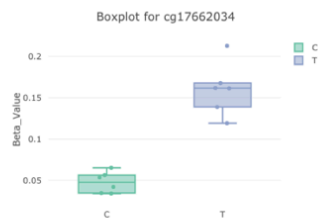
### 9. PFAH2



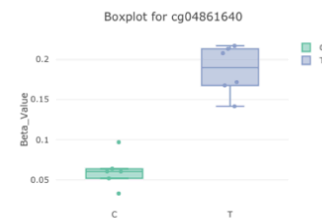
### 10. PHLDB2



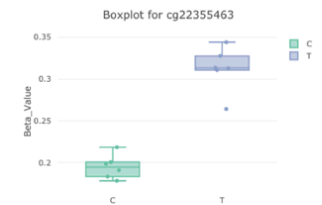
### 11. RDH10



### 12. ZNF187



### 13. ZNF827



Box plot diagrams for significant differentially methylated genes. Individual diagrams for each significant differentially methylated gene from the methylation array analysis. C – control organoids, T- irradiated organoids

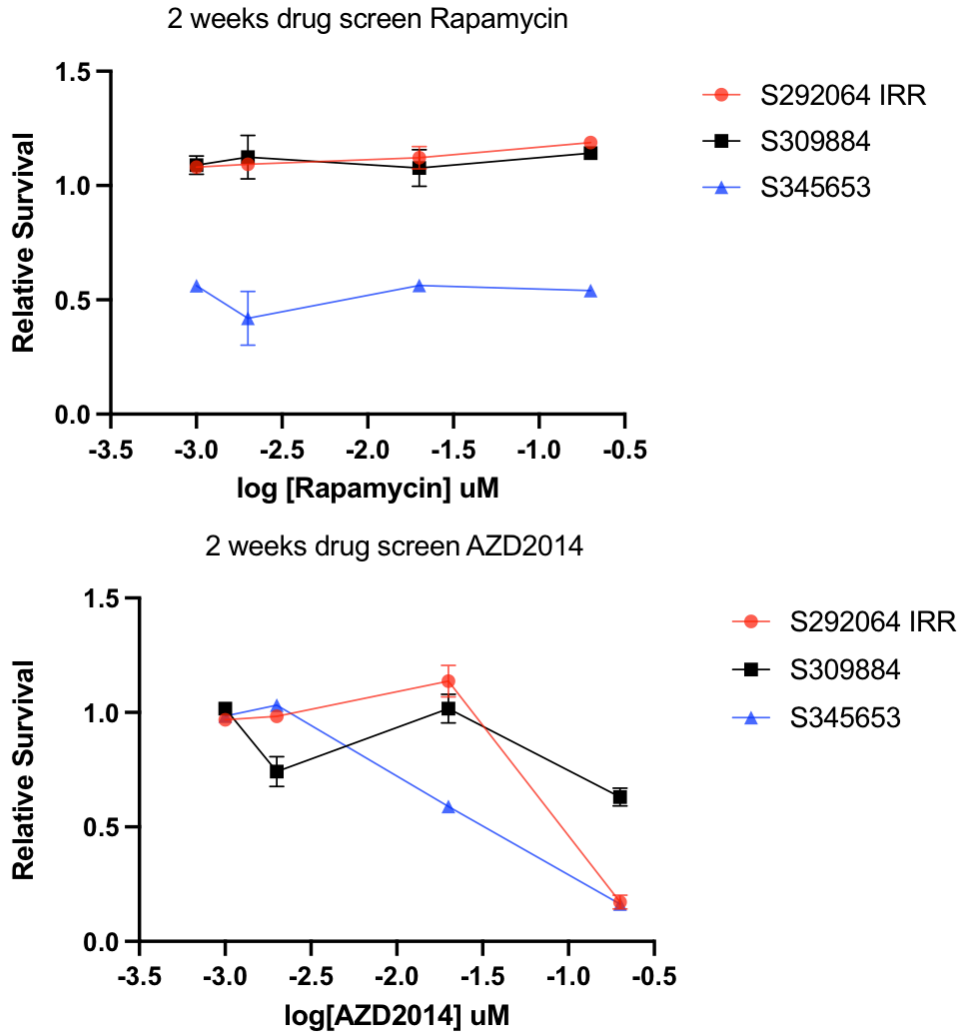
## 12. APPENDIX D

### Retrospective RNA Sequencing Sample Information

#	Sample_name	NCRT_Response	Patient	Source
1	B11	Comp_Resp	R2	Tumour
2	B12	Comp_Resp	R6	Tumour
3	E8	Comp_Resp	R3	Tumour
4	E9	Comp_Resp	R7	Tumour
5	G8	Comp_Resp	R4	Tumour
6	G9	Comp_Resp	R8	Tumour
7	I6	Comp_Resp	R9	Tumour
8	J5	Comp_Resp	R5	Tumour
9	K6	Comp_Resp	R10	Tumour
10	L5	Comp_Resp	R1	Tumour
11	A13	Non_Resp	22	Tumour
12	B10	Non_Resp	13	Tumour
13	B3	Non_Resp	11	Tumour
14	B6	Non_Resp	18	Tumour
15	B7	Non_Resp	6	Tumour
16	B8	Non_Resp	8	Tumour
17	B9	Non_Resp	7	Tumour
18	C13	Non_Resp	23	Tumour
19	D	Non_Resp	14	Tumour

20	D10	Non_Resp	1	Tumour
21	E10	Non_Resp	10	Tumour
22	E4	Non_Resp	4	Tumour
23	F3	Non_Resp	16	Tumour
24	F6	Non_Resp	19	Tumour
25	G	Non_Resp	5	Tumour
26	G10	Non_Resp	25	Tumour
27	G7	Non_Resp	20	Tumour
28	H4	Non_Resp	21	Tumour
29	H5	Non_Resp	2	Tumour
30	H6	Non_Resp	17	Tumour
31	I4	Non_Resp	3	Tumour
32	J7	Non_Resp	26	Tumour
33	K1	Non_Resp	9	Tumour
34	K2	Non_Resp	12	Tumour
35	K4	Non_Resp	15	Tumour
36	P1	Non_Resp	24	Tumour

### 13.APPENDIX E



2 week drug assay kill curves. Resistant organoid lines have been subjected to two week drug screen with decreasing concentrations of A) Rapamycin or B) AZD2014. The concentrations used for both of the drugs were 0.001, 0.002, 0.02 and 0.2  $\mu$ M.